



Synthèse catalytique et décomposition des acides peroxycarboliques

Sébastien Leveneur

► To cite this version:

Sébastien Leveneur. Synthèse catalytique et décomposition des acides peroxycarboliques. Génie des procédés. INSA de Rouen; Åbo akademi, 2009. Français. NNT : 2009ISAM0005 . tel-00560883

HAL Id: tel-00560883

<https://theses.hal.science/tel-00560883>

Submitted on 31 Jan 2011

HAL is a multi-disciplinary open access archive for the deposit and dissemination of scientific research documents, whether they are published or not. The documents may come from teaching and research institutions in France or abroad, or from public or private research centers.

L'archive ouverte pluridisciplinaire **HAL**, est destinée au dépôt et à la diffusion de documents scientifiques de niveau recherche, publiés ou non, émanant des établissements d'enseignement et de recherche français ou étrangers, des laboratoires publics ou privés.

Sébastien Leveneur



Laboratoire de Sécurité des Procédés Chimiques
Institut National des Sciences Appliquées de Rouen



À taille humaine,
à l'échelle du monde





Sébastien Leveneur

b. 1979 in Le Port, Réunion island, France

M. Sc. (Chem. Eng.) 2004

INSA de Rouen

TkL (Chem. Eng.) 2008

Faculty of Chemical Engineering

Åbo Akademi

Catalytic synthesis and decomposition of peroxycarboxylic acids

Sébastien Leveneur

Academic Dissertation

Thesis for the degree of Doctor of Technology to be presented with due permission of the Faculty of Technology at Åbo Akademi University for public criticism in the Salin Auditorium of the Axelia II building, Biskopgatan 8, on Friday the 23rd of October 2009 at 12 p.m.

The opponent appointed by the Faculty of Technology is Professor Jean-Claude Charpentier from the Chemical Engineering Laboratory of Nancy, France

**Laboratoriet för teknisk kemi och reaktionsteknik
Kemisk-tekniska avdelningen
Tekniska fakulteten vid Åbo Akademi**

**Laboratoire de Sécurité des Procédés Chimiques
Institut National des Sciences Appliquées de Rouen**

2009

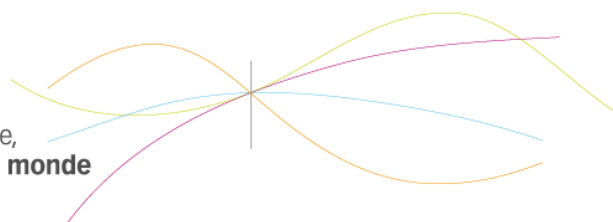
Catalytic synthesis and decomposition of peroxycarboxylic acids

- Green catalytic synthesis of green compounds

Sébastien Leveneur



À taille humaine,
à l'échelle du monde



**Laboratoriet för teknisk kemi och reaktionsteknik
Kemisk-tekniska avdelningen
Tekniska fakulteten vid Åbo Akademi**

**Laboratoire de Sécurité des Procédés Chimiques
Institut National des Sciences Appliquées de Rouen**

2009

Preface

The present work is a collaboration between the Laboratory of Industrial Chemistry and Reaction Engineering, Department of Chemical Engineering, Faculty of Technology at Åbo Akademi University; and the Laboratoire de Sécurité des Procédés Chimiques of INSA de Rouen during the years 2005-2009.

The research is part of the activities performed at Åbo Akademi Process Chemistry Centre (PCC) within the Finnish Centre of Excellence Program (2000-2011) by the Academy of Finland.

First of all, I would like to thank all the people at both laboratories. I am grateful to Professors Lionel Estel (INSA), Dmitry Yu. Murzin (ÅA), and Tapio Salmi (ÅA). Their supervision, availability, and scientific knowledge, were essential to give the credibility to the project and facilitate its progress. Particular thanks go to all the co-authors of the articles; Pr. Johan Wärnå (ÅA) for his contribution in the computational modelling; Docent Kari Eränen (ÅA) for his help with the experimental setup; Docent Narendra Kumar (ÅA) for providing the aluminosilicate materials; Dr. Jean-Pierre Hébert and Dr. Laurent Balland (INSA) for their help with the calorimetric measurements; Docent Päivi Mäki-Arvela (ÅA) for correcting the licentiate thesis; Pr. Jyri-Pekka Mikkola for the social activities.

Stiftelsen för Åbo Akademis forskningsinstitut, Laboratoriet för teknisk kemi och reaktionsteknik, and the Finnish Graduate School in Chemical Engineering (GSCE) are gratefully acknowledged for trusting the project by providing financial support.

Les paragraphes suivants seront en français car même une traduction rigoureuse enlèverait du sens à mes propos. Durant mes études, j'ai eu l'opportunité de rencontrer des personnes qui m'ont aidé et une simple énumération de leurs noms serait insuffisante. Mon intérêt pour la chimie a commencé sur le tard, quand je suis entré en faculté de pharmacie à Marseille. Au début, les matières telles que la chimie organique, la chimie minérale, la thermodynamique ou la cinétique m'effrayaient plus qu'elles ne m'intéressaient. Par chance, ces matières furent enseignées par des professeurs et maîtres de conférences passionnés et intéressants. Je pense entre autre au Pr. Jacques Barbe qui ajoutait des anecdotes à ses cours de chimie minérale pour les rendre plus intéressants. C'est à partir de là que j'ai porté un regard différent sur cette science et commencé à l'étudier.

Ce nouveau centre d'intérêt m'a conduit à la faculté des sciences de Luminy, nichée dans les calanques, pour effectuer une maîtrise de chimie. Ce fût une merveilleuse période pour moi tant sur le plan humain que scientifique. Et je tiens à remercier feu le Pr. Pierre Brun et le Dr. Alain Méou pour m'avoir transmis leur rigueur ainsi que leur passion pour la chimie organique, le Pr. Evelyne Rauzzy qui a réussi la gageure d'avoir rendue accessible et intéressante la mécanique quantique, et le Pr. Evelyne Neau pour avoir valorisé l'aspect pratique de la thermodynamique.

Ayant obtenu ma maîtrise, et après avoir étudié la partie théorique de la chimie, je me sentais chimiste avec quelques connaissances pratiques. Je voulus compléter ma formation en faisant une école d'ingénieur pour avoir une meilleure connaissance des procédés chimiques. Le choix de l'INSA de Rouen se fit presque immédiatement car elle proposait une palette d'enseignements de chimie ainsi qu'une formation sur le risque chimique. Cet intérêt pour le risque chimique avait commencé à Luminy où des cours étaient dispensés par des intervenants. En effet, le seul et unique bénéfice de l'accident d'AZF à Toulouse en 2001 fut de pousser les établissements à considérer le risque chimique comme un enseignement à part entière comme la chimie fine ou le génie des procédés. Très rapidement, je vis que cette matière ne se limitait pas uniquement à l'étude calorimétrique d'une réaction, à des consignes telles que « produits toxiques » ou encore à des recommandations « ne pas rajouter d'eau dans l'acide ». Cette matière englobe aussi une approche juridique, une étude des comportements, l'étude des matériaux utilisés, les normes à respecter. Cette école m'a réellement aidé à « grandir », les projets scientifiques ou sociaux, l'enseignement de sciences sociales, la mise en contact avec des intervenants industriels, ou encore l'enseignement pratique de l'anglais m'ont fait découvrir un monde nouveau.

Fini les cours d'ingénieurs, place au stage, le fameux stage qu'il faut bien choisir...J'avais toujours regretté de ne pas avoir fait une période à l'étranger, même si comme beaucoup de Réunionnais, voyager en métropole est vécu comme un déracinement, ou comme beaucoup de Marseillais partir au nord de Marseille est une entreprise qui nécessite un dictionnaire franco-marseillais, un passeport et un visa. C'est le Dr. Alain Ledoux qui le premier me parla de la Finlande, et plus précisément d'Åbo Akademi. Pourquoi pas ? Même si le stage ne se ferait pas en industrie, il est toujours passionnant de découvrir des pays exotiques.

Arrivé au laboratoire de « Teknisk kemi », un nouveau champ sémantique chimique s'ouvrit devant moi : « chimie verte », « zéolithes », « catalyseur hétérogène », « caractérisation des catalyseurs » ou « désactivation des catalyseurs ». Ces mots ne m'étaient pas complètement inconnus mais soudainement ont remplacé « mesure calorimétrique », « substitution nucléophile », « analyse des risques » ou « emballement thermique ». Faire une thèse dans ce laboratoire semblait excitant ! Non pas pour obtenir le titre ronflant de Docteur ès science en génie des procédés, non pas par crainte d'intégrer le monde industriel....Les raisons furent diverses telles que vivre à l'étranger et avoir une connaissance plus large en chimie. Je tiens à remercier les collègues finlandais : José, Mats K., Pasi V., Henrik pour leurs camaraderies.

Comme tout changement, cela implique des moments difficiles. J'ai eu de la chance, l'immense chance d'avoir été supporté. Malgré tous les efforts d'écriture qu'il m'est possible de faire, les gens nommés, pourraient avoir l'impression d'être cités comme dans une banale liste de remerciements. En dire plus, c'est le risque de frôler la sensiblerie, mais il est dur d'y échapper quand on parle de ce qui vous marque.

Je voudrais remercier Aymé, Christophe, Gilbert, Johanne, Lionel le maître Djanbedlo, Michelle, Monique, Olga, Pasiola, Sophie, Xavier, qui durant ces longues années m'ont donné leurs supports et réconforts quand j'en avais le plus besoin. Même si les Sudistes de cette liste m'ont traité de fada quand je leur ai dit que je partais sur Rouen, et de malade mental quand j'ai décidé de partir en Finlande.

Ce dernier paragraphe de remerciement va à ma Famille. J'ai une pensée particulière pour Gaby qui m'a apporté tout et plus, pendant de longues années ; ainsi que Tonton Pierre dont les rires et le « boute-en-trainisme » étaient le remède de beaucoup de maux. Papa, Maman, La Sœur, Lili, Mishka, Magali et Poupoune, je ne saurais jamais trouver les mots pour vous remercier...tant vos présences sont indissociables à mon existence.

Åbo, September, 2009

Sébastien Leveneur

Referat

Sébastien Leveneur

Katalytisk syntes och sönderfall av perkarboxylsyror

Doktorsavhandling i samarbete av

Laboratoriet för teknisk kemi och reaktionsteknik

Kemisk-tekniska avdelningen

Tekniska fakulteten vid Åbo Akademi, 2009

&

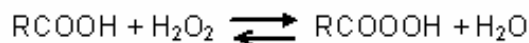
Laboratoire de Sécurité des Procédés Chimiques

Institut des Science Nationales Appliquées de Rouen, 2009

108 sidor

Nyckelord: kinetik, homogena och heterogena katalysatorer, matematisk modellering, massöverföring, linjär fri energi, kalorimetri

Perkarboxylsyror är viktiga ur industriell synvinkel. De används för vattenrening, desinfektering, blekning av cellulosa samt för framställning av finkemikalier. Syntes av en perkarboxylsyra utgående från en karboxylsyra och väteperoxid beskrivs av den reversibla reaktionen



P.g.a. att reaktionens kinetik är långsam, behövs antingen en homogen eller heterogen syrakatalysator för att påskynda reaktionens hastighet.

Detta doktorsarbete beskriver en ett kinetiskt studium av karboxylsyror perhydrolys med svavelsyra vid olika molära förhållanden av reaktanter, olika reaktionstemperaturer (från 30°C till 60°C) samt olika katalysator-koncentrationer. Vattnets och syrakatalysatorernas inverkan på reaktionshastigheten och –jämvikten beaktades, då en kinetisk modell för systemet utvecklades. Systemet är icke-idealt, huvudsakligen p.g.a. närvaron av en stark elektrolyt, svavelsyra; därför introducerades en parameter (δ) för att beskriva avvikelserna från ideala betingelser. Kinetiska och termodynamiska parametrar som bestämdes med hjälp av icke-linjär regressionsanalys var statistiskt väldefinierade.

En 'grönare' reaktionsväg för syntes av perkarboxylsyror utgående från karboxylsyror och väteperoxid undersöktes. Metoden baserar sig på användningen av fasta syror som heterogena katalysatorer. Katjonbytarhartser visade sig vara överlägset aktivare heterogena katalysatorer än aluminosilikater under jämförbara experimentella betingelser.

En allmängiltig matematisk modell utvecklades för systemet; modellen omfattar både kinetiska och massöverföringseffekter i porösa partiklar (t.ex. jonbytarhartsen Amberlite IR-120), vilka fungerar som katalysatorer i satsreaktorer. Storleksfördelningen av katalysatorpartiklarna inkluderades i modellen. En numerisk algoritm och mjukvara utvecklades för att lösa modellen med tanke på simulering och parameterestimering. Med tanke på potentiella industriella tillämpningar fokuserades det aktuella arbetet på perhydrolys av ättiksyra och propionsyra. Koncentrationerna i vätskans huvudmassa och inne i katalysatorpartiklarna kan förutspås av modellen. Det visade sig att de minsta katalysatorpartiklarna arbetade under kinetiska betingelser, medan de största partiklarna (större än 300 mikrometer) påverkas av diffusionshastigheten inne i katalysatorporerna. Detta innebär att den sammansatta effekten av reaktion och diffusion samt partikelsorleksfördelningen blir väsentliga ingredienser i modellen.

Perkarboxylsyras stabilitet undersöktes för att uppskatta riskerna i processen. Perkarboxylsyror sönderfaller i vätskefasen, men huvudprodukterna av sönderfallet, koldioxid och syre överförs till gasfasen. En analytisk metod utvecklades för att bestämma sönderfallet av perkarboxylsyror i vätskefasen genom automatiserad kemisk analys av gasfasen. Metoden är baserad på direkt on line –masspektrometri (MS). En matematisk modell utvecklades för att kunna bestämma de parametrar, som påverkar sönderfallsprocessen i ett halvkontinuerligt gas-vätskesystem. Modellen inkluderade både kinetiska effekter och massöverföringseffekter. En jämförelse av experimentella resultat med resultat som predikteras av den matematiska modellen avslöjade att den modellen förmår beskriva de väsentliga effekterna av sönderfallskinetiken. Tillämpningen av denna metod antydde att perpropionsyra är stabilare än perättiksyra.

I projektets sista fas, efter undersökning av möjligheten att utnyttja heterogena katalysatorer och bestämning av perkarboxylsyrorens stabilitet, konstruerades en kontinuerlig packad bäddreaktor. Syntes av perättiksyra och perpropionsyra genomfördes i reaktorn och det visade sig var möjligt att syntetisera dessa peroxidkomponenter via ett kontinuerligt förfarande.

Abstract

Sébastien Leveneur

Catalytic synthesis and decomposition of peroxycarboxylic acids

Doctoral Thesis in collaboration between

Laboratory of Industrial Chemistry and Reaction Engineering

Department of Chemical Engineering

Faculty of Technology, Åbo Akademi University, 2009

&

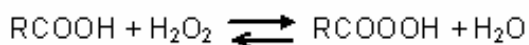
Laboratoire de Sécurité des Procédés Chimiques

Institut des Sciences Nationales Appliquées de Rouen, 2009

108 pages

Keywords: Kinetics, homogeneous and heterogeneous catalysts, mathematical modelling, mass transfer, linear free energy relationships, calorimetry

Peroxycarboxylic acids are widely used in industry for disinfection and bleaching as well as fine chemistry. The synthesis of peroxycarboxylic acid from carboxylic acid and hydrogen peroxide is described by the reversible reaction,



Due to the slow kinetics of this reaction, acid catalysts are needed, either in homogeneous or heterogeneous form.

This thesis describes a kinetic study of carboxylic acids perhydrolysis in the presence of sulphuric acid at various molar reactant ratios, reaction temperatures (from 30°C to 60°C) and catalyst concentrations. The influence of water and acidic catalysts were taken into account to develop a plausible kinetic model. The system is non-ideal, mainly due to the presence of the strong electrolyte (i.e. sulphuric acid), and a parameter (δ) was introduced to describe the non-ideality. The kinetic and thermodynamic parameters determined by non-linear regression analysis were statistically well-identified.

A “greener” way of peroxycarboxylic acid synthesis from carboxylic acid and hydrogen peroxide using solid acid catalysts was investigated. Cation exchange resins showed a higher catalytic activity than aluminosilicates under comparable experimental conditions.

A general model was developed, comprising the kinetic and mass transfer effects in porous catalyst particles (i.e., Amberlite IR-120) in batch reactors. The catalyst particle size distribution was included in the model. Numerical algorithms and software were developed to solve the model for simulation and parameter estimation purposes. Due to the potential industrial applications, the present study was mainly focused on the acetic and propionic acid perhydrolysis. The concentrations in the bulk phase and inside the catalyst particles were predicted by the model. It turned out that the smallest ion-exchange resin particles operate under kinetic control, whereas the largest particles (larger than 300 μm) are influenced by diffusional limitation. Thus the combined effect of reaction and diffusion along with the particle size distribution are essential ingredients in the model.

The stability of peroxycarboxylic acid was investigated to evaluate the risk of the process. Decomposition of peroxycarboxylic acid takes place in the liquid phase, but the main products of decomposition, carbon dioxide and oxygen are transferred to gas phase. An analytical method was developed to determine the decomposition of the peroxycarboxylic acid in the liquid phase by means of chemical analysis of the gas phase. The method is based on on-line mass spectroscopy (MS). A mathematical model for the semi-batch gas-liquid system was developed. The model comprised both kinetic and mass transfer effects. A comparison between experimental results and results predicted from the mathematical model revealed that the model can describe the essential effects of the decomposition kinetics. By this method, it appears that peroxypropionic acid is more stable than peroxyacetic acid.

After confirming the possibility of using heterogeneous catalysts and the stability of peroxycarboxylic acids, a fixed bed reactor was built. Synthesis of peroxypropionic and peroxyacetic acids was carried out, and it was demonstrated that the synthesis of these peroxide compounds is feasible in continuous mode.

Résumé

Sébastien Leveneur

Synthèse catalytique et décomposition des acides peroxyкарбоxyliques

Thèse doctorale en cotutelle entre :

*Laboratoire de Chimie Industrielle et de Génie de la Réaction Chimique
Département de Génie Chimique
Faculté de Technologie, Åbo Akademi, 2009*

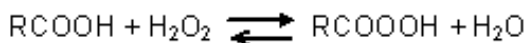
&

*Laboratoire de Sécurité des Procédés Chimiques
Institut des Sciences Nationales Appliquées de Rouen, 2009*

108 pages

Mots clés: Cinétique, catalyse homogène et hétérogène, modèle mathématique, transfert de masse, relation linéaire de l'énergie libre, calorimétrie

Les peroxydes d'acides carboxyliques sont importants d'un point de vue industriel. En effet, ils sont utilisés pour la purification de l'eau, la désinfection en alimentation et pour le blanchissement en papeterie. La synthèse d'un acide peroxyкарбоxylique à partir d'un acide carboxylique et du peroxyde d'hydrogène est décrite par l'équation ci-dessous :



La cinétique de cette réaction est lente, d'où la nécessité d'ajouter un catalyseur homogène ou hétérogène au milieu réactionnel.

Cette thèse traite de l'étude cinétique de la réaction de perhydrolyse de l'acide carboxylique en présence d'acide sulfurique. L'influence de l'eau et de la concentration en catalyseurs a été prise en compte pour développer un modèle cinétique plausible. La non-idéalité du système réactionnel est due à la présence d'un électrolyte puissant, aussi il a été nécessaire d'introduire un paramètre (δ) pour décrire ce phénomène. Les paramètres cinétiques et thermodynamiques déterminés par régression non-linéaire ont été statistiquement bien identifiés.

Une voie de synthèse plus « verte » pour cette réaction est abordée dans ce manuscrit, en testant différents catalyseurs hétérogènes. L'activité catalytique des résines échangeuse de cations sur cette réaction s'est avérée supérieure à celle des aluminosilicates.

Un modèle général, comprenant les effets cinétiques et de transfert de masse pour les particules poreuses (i.e., Amberlite IR-120) en réacteur fermé a été développé. La distribution des dimensions des particules (de catalyseurs) a été incluse dans ce modèle. À cause d'une potentielle application industrielle, la présente étude s'est focalisée sur la perhydrolyse des acides acétiques et propioniques. Les concentrations des différentes espèces dans la phase liquide et à l'intérieur du catalyseur ont été déterminées par ce modèle. Il est apparu que les catalyseurs de faible dimension opéraient en régime cinétique, alors que les catalyseurs plus larges (supérieur à 300 μm) opéraient en régime diffusionnel.

La stabilité des acides peroxyacétyliques a été étudiée afin d'évaluer les risques sur le procédé de fabrication. La décomposition de ces acides se déroule dans la phase liquide, mais certains produits de décomposition comme le dioxyde de carbone et l'oxygène sont transférés dans la phase gazeuse. Une technique d'analyse en direct a été développée pour étudier la décomposition des acides peroxyacétyliques en phase liquide en analysant les produits de décomposition en phase gazeuse, à l'aide d'un spectromètre de masse. Un modèle mathématique a été développé pour déterminer les différents paramètres influençant la décomposition. Ce modèle contient les effets cinétiques ainsi que les paramètres de transfert de masse. Les résultats estimés par ce modèle sont statistiquement satisfaisants.

Après avoir trouvé un catalyseur hétérogène adéquat et vérifier la stabilité des acides peroxyacétyliques, un réacteur à lit fixe a été construit. Les synthèses des acides peroxyacétique et peroxypropionique ont été effectuées, et il apparaît que la synthèse en continu de ces acides est possible.

LIST OF PUBLICATIONS

The thesis consists of the following publications, which are referred in the doctoral thesis by their roman numbers.

- I. S. Leveneur, T. Salmi, D. Yu. Murzin, L. Estel, J. Wärnå, N. Musakka, Kinetic Study and Modeling of Peroxypropionic Acid Synthesis from Propionic Acid and Hydrogen Peroxide Using Homogeneous Catalysts, *Industrial & Engineering Chemistry Research* 47(3) (2008) 656-664.
- II. S. Leveneur, N. Kumar, T. Salmi, D. Yu. Murzin, Stability of hydrogen peroxide during perhydrolysis of carboxylic acids on acidic heterogeneous catalysts, *Research on Chemical Intermediates*, submitted.
- III. S. Leveneur, D. Yu. Murzin, T. Salmi, J-P Mikkola, N. Kumar, L. Estel, K. Eränen, Synthesis of peroxypropionic acid from propionic acid and hydrogen peroxide over heterogeneous catalysts, *Chemical Engineering Journal* 147 (2009) 323-329.
- IV. S. Leveneur, D. Yu. Murzin, T. Salmi, Application of linear free-energy relationships to perhydrolysis of different carboxylic acids over homogeneous and heterogeneous catalysts, *Journal of Molecular Catalysis A: Chemical* 303 (2009) 148-155.
- V. S. Leveneur, J. Wärnå, T. Salmi, D. Yu. Murzin, L. Estel, Interaction of intrinsic kinetics and internal mass transfer in porous ion-exchange catalysts: green synthesis of peroxycarboxylic acids, *Chemical Engineering Science* 64 (19) (2009) 4104-4114.
- VI. S. Leveneur, T. Salmi, N. Musakka, J. Wärnå, Kinetic study of decomposition of peroxypropionic acid in liquid phase through direct analysis of decomposition products in gas phase, *Chemical Engineering Science* 62 (18-20) (2007) 5007-5012.

OTHER PUBLICATIONS RELATED TO THE TOPIC

1. S. Leveneur, T. Salmi, L. Estel, J. Wärnå, D. Yu. Murzin, "*Kinetic modelling of peroxy-carboxylic acids synthesis using heterogeneous catalysts*", 8th World Congress of Chemical Engineering, August 23rd-27th, 2009, Montréal, Canada, oral presentation.
2. S. Leveneur, J. Wärnå, D. Yu. Murzin, T. Salmi, L. Estel, "*Interaction of intrinsic kinetics and internal mass transfer in porous ion-exchange catalysts: green synthesis of peroxy-carboxylic acids*", 5th International Conference on Diffusion in Solids and Liquids, June 24th-26th, 2009, Rome, Italy, oral presentation.
3. S. Leveneur, J. Wärnå, N. Kumar, T. Salmi, L. Estel, D. Yu. Murzin, "*Synthesis of peroxy-carboxylic acids: from homogeneous to heterogeneous catalysts*", 2nd International Congress on Green Process Engineering, June 14th-17th, 2009, Venice, Italy, poster presentation.
4. S. Leveneur, J. Wärnå, D. Yu. Murzin, T. Salmi, L. Estel, "*Utilization of Taft equation: kinetic modelling of carboxylic acids perhydrolysis over heterogeneous and homogeneous catalysts*", XVIII International Conference on Chemical Reactors, September 29th - October 3rd, 2008, Malta, oral presentation.
5. S. Leveneur, T. Salmi, J. Wärnå, D. Yu. Murzin, L. Estel, "*Kinetic study and modeling of perhydrolysis of propionic acid using heterogeneous catalyst*", XVIII International Conference on Chemical Reactors, September 29th - October 3rd, 2008, Malta, poster presentation.
6. S. Leveneur, T. Salmi, D. Yu. Murzin, J. Wärnå, "*Peroxypropionic acid synthesis from propionic acid and hydrogen peroxide with homogeneous and heterogeneous catalysts*", 3rd International Conference on Green and Sustainable Chemistry, July 1st-5th, 2007, Delft, The Netherlands; Book of abstracts, poster presentation.

7. S. Leveneur, T. Salmi, D. Yu. Murzin, J. Wärnå, "*Kinetic study and modelling of peroxypropionic acid synthesis from propionic acid and hydrogen peroxide using homogeneous catalysts*", Conference on Catalysis Concept, Complexity and Diversity in Catalysis, May 12th-17th, 2007, Porquerolles, France, poster presentation.
8. S. Leveneur, N. Kumar, T. Salmi, D. Yu. Murzin, N. Musakka, "*Optimization of the synthesis of peroxypropionic acid by using zeolite and mesoporous molecular sieve catalyst*", 4th EFCATS School on catalysis, September 20th-24th, 2006, St Petersburg, Russia; Book of abstracts, poster presentation.
9. S. Leveneur, N. Musakka, J. Wärnå, T. Salmi, "*Kinetic study of decomposition of peroxypropionic acid in liquid-phase through direct analysis of decomposition products in gas-phase*", 19th International Symposium on Chemical Reaction Engineering, September 3rd-6th, 2006, Berlin, Germany; Book of abstracts, poster presentation.
10. H. Koskinen, S. Leveneur, A. Sundquist, N. Musakka, T. Salmi, I. Renvall, Functionality of Poly(α -hydroxyacrylic acid) as H₂O₂ stabilising agent, *Oxidation Communication*, accepted.

Contents

Preface	i
Abstract	v
List of publications included in the thesis	xi
Conference publications related to the topic	xii
Contents	xiv
1. Introduction	1
2. Experimental section	11
2.1 Experimental part for the synthesis	11
2.2 Catalyst characterization	12
2.3 Calorimetric measurements	13
2.4 Experimental part for the decomposition	15
2.5 Continuous reactor	17
3. Synthesis of peroxycarboxylic acids in batch mode	21
3.1 Synthesis of PCA in presence of homogeneous catalysts	21
3.1.1 Equilibrium analysis	22
3.1.2 Mechanism and kinetics equations	24
3.1.3 Modelling and statistical results	26
3.2 Synthesis of peroxycarboxylic acids over heterogeneous catalysts	30
3.2.1 Aluminosilicate materials	31
3.2.2 Ion exchange resins	32

3.3 Synthesis of peroxycarboxylic acids over Amberlite IR-120	36
3.3.1 Catalyst characterization	36
3.3.2 Equilibrium analysis	38
3.3.3 Mechanism	39
3.3.4 Kinetic expression	40
3.3.5 Modelling of mass transfer	43
3.3.6 Modelling and statistical results	46
3.4 Structure and reactivity	51
4. Calorimetry	63
5. Decomposition study	67
5.1 Mass balances for gas and liquid phases	67
5.2 Kinetic study and modelling	70
6. Continuous reactor	75
6.1 Residence time distribution	75
6.1.1 Pulse experiment	75
6.1.2 Step experiment	80
6.1.3 Comparison	81
6.2 Estimation of the pressure drop	83
6.3 Experimental results	85
6.3.1 Experiments carried out with propionic acid	85
6.3.2 Mass and heat transfer effect	88
6.4 Comparison with batch reactor	94
6.5 Comparison with acetic acid in continuous reactor	94

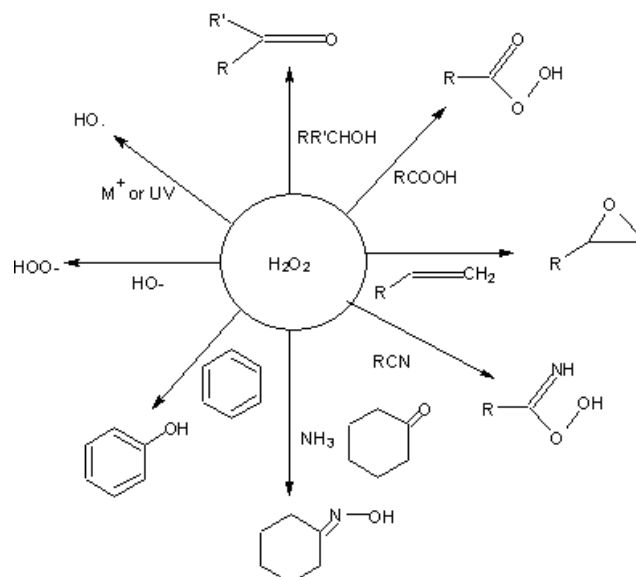
7. Conclusions	97
Notation	99
References	105
Appendix	109

Introduction

The environmental impact and the safety aspects for the production of chemicals are the two main issues to ensure the sustainability of industrial production. Preventing the formation of waste products, suppressing the energy consumption, designing safer processes, utilizing non-toxic and non-hazardous chemicals, and optimizing the productivity are the main concerns of all the chemical companies. The concept of “Green Chemistry” introduced in the 1990’s has provided methods and tools to take into account these issues for the scientific and industrial community.

Oxidation reactions are fundamental in industry, but many of these reactions are carried out by using conventional heavy-metal oxidants, which form toxic waste, application of nitric acid which form the greenhouse gas N_2O ; and utilization of molecular oxygen, which requires safety precautions and could cause over-oxidation. According to Noyori [1], an elegant way to surmount these problems is the use of aqueous hydrogen peroxide, as the oxidant hydrogen peroxide is a powerful oxidant.

The interest in hydrogen peroxide has increased in the last decade. For instance, the world production of hydrogen peroxide was around 1.9 million tonnes in 1994, and grew to 2.2 million tonnes in 2006 [2]. And about half of this world production was used for pulp- and paper-bleaching purposes. Scheme 1 illustrates the application of hydrogen peroxide in some fine chemical synthesis reactions [3].



Scheme 1. Applications of H_2O_2 in fine chemical reactions.

Among all these reactions oxidized by hydrogen peroxide, the perhydrolysis of carboxylic acid can represent a textbook example of Green Chemistry application. The reaction product is a peroxydicarboxylic acid.

The market volume can be estimated to be some 10,000 tonnes worldwide [4]. Three domains of application for peroxydicarboxylic acids can be distinguished: disinfecting agent, bleaching agent and as intermediate in fine chemistry. All these applications are based on the oxidative properties of these compounds, due to the



For instance, peroxyacetic acid (PAA) is a strong disinfectant with a wide spectrum of antimicrobial activity: bactericidal, virucidal, fungicidal, and sporicidal effectiveness. The oxidation mechanism is the transfer of electrons, therefore the stronger the oxidizer, the faster electrons are transferred to the micro-organism and the faster the micro-organism is inactivated or killed. Table 1 shows the oxidation capacity of some traditional disinfectants.

Table 1. Oxidation capacity of selected sanitizers

Sanitizer	eV
Ozone	2.07
Peroxyacetic acid	1.81
Chlorine dioxide	1.57
Sodium hypochlorite (chlorine beach)	1.36

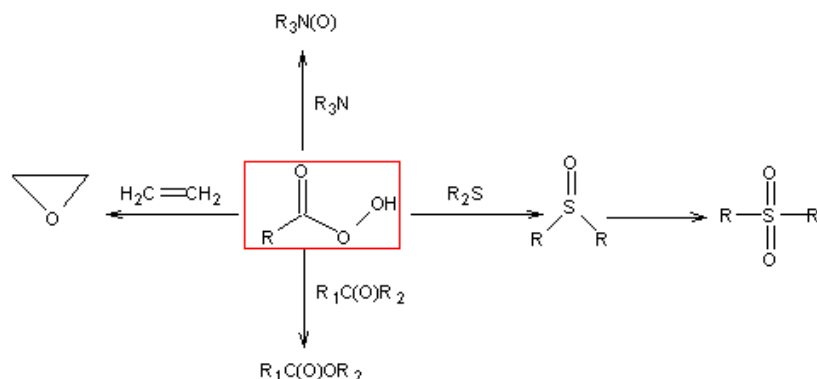
PAA has a higher oxidation potential than chlorine dioxide, which is not eco-friendly.

In medicine, this component is used to disinfect skin allograft [5] or for inactivating viruses in the context of bone tissue transplants [6]. Mixtures of PAA (2.5-10 vol.%), acetic acid (2.5-10 vol.%) and hydrogen peroxide (2.5-10 vol.%) have found a wide application in food industry as sanitizers, with various trade names (Oxonia active by Henkel-Ecolab, Oxysanitizer by Okite, Peraclean by Degussa, Proxitane and Oxystrong by Solvay). Indeed, peroxyacetic acid is ideal for clean-in-place system in such industry (dairy, livestock, beverage, fresh-cut product) [7, 8]. PAA is also used for wastewater disinfection (cooling water treatment or sewage treatment) due to the ease of implementing treatment, the broad spectrum of activity even in the presence of heterogeneous organic matter, the absence of persistent toxic or mutagenic residuals or by-products, no quenching requirement (i.e., no dechlorination), the small dependence on pH, and the short contact time required [8, 9].

PAA is also used as a decolouring or bleaching agent in textile [10] or pulp and paper industry. For instance, Kemira specializes in the production of distilled peroxyacetic acid, for the post-bleaching of pulps.

More generally, peroxycarboxylic acids are used to oxidize sulphite [11] in case of wet desulphurization or to produce ultralow-sulfur fuels [12]. Due to its capacity to oxidize sulphur components, peroxypropionic acid (PPA) is used to destroy toxic organophosphorous (paroxon) and organosulfur compounds under micellar conditions [13].

Peroxycarboxylic acids are used as oxidizing agents in fine chemical industry, for instance, in the epoxidation of olefins, Baeyer-Villiger reaction, or oxidation of thioether (Scheme 2).



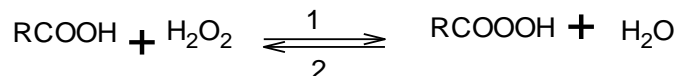
Scheme 2. Peroxycarboxylic acid in fine chemistry.

Peroxyformic or peroxyacetic acid, for instance, has been studied by Goud et al.[14] in the case of epoxidation of jatropha oil. Epoxidized fatty acid derivatives from vegetable sources can be used in various domains, for example, as stabilizers and plasticizers in polymers, as additives in lubricants, as components in plastics and urethane foams and, in general, as intermediates for a large number of commodities.

All the different applications of peroxycarboxylic acid are based on their oxidation capacity. Thus, is the use of peroxycarboxylic acids instead of hydrogen peroxide, which is more stable than PAA [8], a wise option? Hydrogen peroxide was demonstrated to be a useful alternative to PAA for isolator sterilization in hospital pharmacy or parenteral nutrition preparation unit [15]. Moreover, PAA increases the organic content in the effluent, high cost due to the limited production capacity worldwide [8]. However, PAA is more potent antimicrobial agent than hydrogen peroxide, being rapidly active at low concentrations against a wide spectrum of micro-organism. According to Pan et al. [16, 17], PAA is a better bleaching agent than hydrogen peroxide.

Min et al. [18] have studied the toxicity of peroxyacetic acid, the acute oral LD50 of PAA for mice was 1882 mg/l, which is a low toxicity. The acute inhalation toxicity LC50 was 26 g/m³ which is non-toxic. The main advantage of these chemicals is their harmless impact on the environment because of the non-toxicity of their decomposition products. Indeed, the decomposition of these compounds yield carbon dioxide, oxygen, water and carboxylic acid. However, PAA solutions exceeding 15 % begin to exhibit some degree of explosiveness, and instability [19].

Several routes of synthesis of peroxycarboxylic acids are available, oxygenation of the parent aldehyde [20] or carboxylic acid [21]. However, to use a clean oxidation process, aqueous hydrogen peroxide was selected to oxidize carboxylic acid in liquid phase:



This reaction is reversible and requires the presence of an enhancing chemical species, an acid catalyst.

The pioneering research on this reaction has begun by D'Ans et al. [22], in 1914; they studied the perhydrolysis of different carboxylic acids catalyzed by sulphuric acid, and they were able to produce concentrated peroxycarboxylic acid solutions. In 1970, Swern [23] published a book which summarized all the methods for the preparation and analysis for different organic peroxides. Several authors have noticed [24-25] that the rate of this reaction is accelerated by increasing the catalyst amount (usually mineral acids). Nevertheless, their kinetic expressions did not take into account the catalyst concentration. Zhao et al. [26], were the first to propose a complete kinetic model for the perhydrolysis of acetic acid by sulphuric acid, where the dissociation of acetic acid and concentration of the catalyst were taken into account. The first part of our work [**Publication I**] was done in order to understand the mechanism of the above reaction. A homogeneous catalyst (sulphuric acid), was used to identify the main parameters influencing the reaction rate and equilibrium. A complete kinetic model was developed by taking into account the dissociation of reacting carboxylic acid and sulphuric acid in aqueous environment at different temperature.

Due to the thermodynamic limitation, it is difficult to synthesize a pure solution of a peroxycarboxylic acid, and furthermore, there is no market for such a product. Peroxycarboxylic acid solutions contain peroxycarboxylic acids and hydrogen peroxide which behave as a redox couple. Consequently, the risk of decomposition is higher in such mixture than either component alone. For that reason, it is necessary to introduce a stabilizer agent in the solution, and the sequestrant approach is better than the scavenger approach [3]. Bewersdorf et al. [27] recommended the use of tin compounds, preferably stannates, in a range of 20-200 ppm added before the preparation. Another way of stabilization is to add pyrophosphoric acid (or an alkali metal or ammonium salt) in a range of 50-1000 ppm and a pyridinedicarboxylic acid (or an alkali metal or ammonium salt) in a range of 5-150 ppm according to Taeubl [28]. In our synthesis experiment, stabilizer

agents were not added because no spontaneous peroxo-compounds decomposition was noticed. Furthermore, a commercial aqueous hydrogen peroxide solution was used, which contains stabilizer agents.

The process for the peroxycarboxylic acid production is still industrially catalyzed by sulphuric acid [29-30], leading to several drawbacks (corrosion, catalyst separation, and threat to environment). Indeed, the homogeneous catalyst after the reaction is separated (typically by distillation) and recirculated into the process. One way to surmount these problems is to shift from homogeneous to heterogeneous catalysts following the principle of Green Chemistry. The main challenge is to discover a catalyst with a comparable acidic strength as sulphuric acid, which does not decompose peroxide species and in addition, can be re-used. Several options are available illustrated by Figure 1.

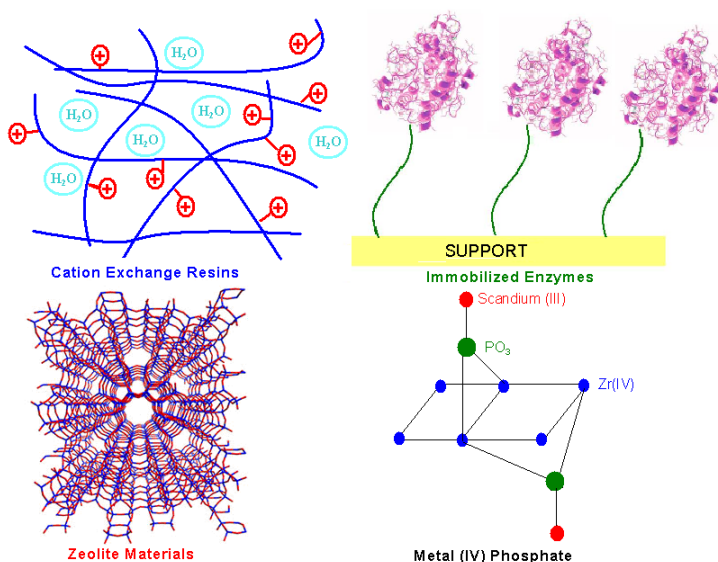


Figure 1. Potential heterogeneous catalyst for carboxylic acid perhydrolysis.

Some authors [31-32] have shown that some cation exchange resins are suitable to accelerate the rate of this reaction. Palani et al.[33] tested some aluminosilicate materials, such as zeolites and mesoporous materials. Rocha et al. [34] demonstrated that by exchanging the hydroxyl centres in amorphous α -zirconium phosphate (ZrPA) with scandium (III), the resulting solid (ScZrPA) accelerates the formation rate of peroxyacetic acid, even more than the scandium (III) ions in a homogeneous solution. Immobilized enzymes –and more precisely– immobilized lipase B from *Candida antarctica* (Novozym 435[®]) can be used as a catalyst for the perhydrolysis of different carboxylic acids (acetic, propionic, octadecanoic acid...) [35].

Our investigations have been limited to aluminosilicate materials because their use in fine chemical process are increasing, and a paper studying the stability of hydrogen peroxide toward such materials can be useful for the industrial community [Publication II]. The second screening step was to study different cation exchange resins [Publication III], which are economically more beneficial than the other ones and structurally closer to sulphuric acid. In order to prove the benefits of using these catalysts in industry, several issues were considered: catalytic comparison with sulphuric acid, deactivation behaviour and mass transfer effects.

As mentioned above, industry still uses sulphuric acid as a homogeneous catalyst, which is not economically and environmentally beneficial. However, to show the advantage to shift from a homogenous (i.e., H_2SO_4) to a heterogeneous (i.e., Amberlite IR-120) catalyst, a profound comparison between both catalysis systems has been done [Publication V]. In case of the heterogeneous catalysis system, a kinetic model taking into account the dissociation of the acids, thermodynamics as well as the mass transfer phenomena was developed.

To confirm the validity of the thermodynamic parameters estimated by our models, calorimetric measurements were performed to measure the enthalpy of perhydrolysis reaction.

The comparison based on the kinetic modelling was limited to the acetic and propionic acids, due to their potential industrial interest. In order to have a better understanding of the perhydrolysis mechanism, the influence of the alkyl group (-R) of the carboxylic acid on the kinetics was studied using linear-free energy relations [Publication IV] in homogeneously and heterogeneously catalysed systems. The basic assumption of the concept is the existence of a relation between the rate and the equilibrium constant, in other words between the Gibbs energy of activation (ΔG^\ddagger) and the Gibbs energy of the reaction (ΔG_R), as illustrated by Figure 2.

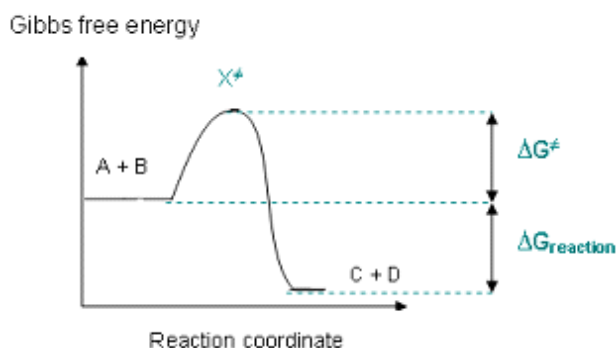


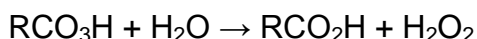
Figure 2. Potential energy diagram for the reaction $\text{A+B} \rightleftharpoons \text{C+D}$.

Furthermore, the properties of the molecule can be fine-tuned by incorporating various hydrocarbon groups (-R). This allows the industry to select the proper peroxy-carboxylic acid according to the wish of the customer, for instance, a stable peroxide with a low oxidative property or an unstable peroxide with a strong oxidative property.

After discovering the more suitable heterogeneous catalyst, elucidating the kinetics and thermodynamic of the reaction, understanding the mass transfer phenomena, the shift from batch to continuous reactor is feasible. A fixed bed reactor was chosen for the study. This shift allowed to check the validity of our kinetic model and to test the durability of the catalyst. Research efforts concerning the study of perhydrolysis reactions with a continuous reactor using heterogeneous catalyst are scarce [36].

The safety issue regarding the stability and decomposition of peroxypropionic acid was treated [**Publication VI**]. In the absence of metal impurities, decomposition of peroxy-carboxylic acids through two main mechanisms: hydrolysis and spontaneous decomposition (high temperature):

Hydrolysis:



Spontaneous decomposition:

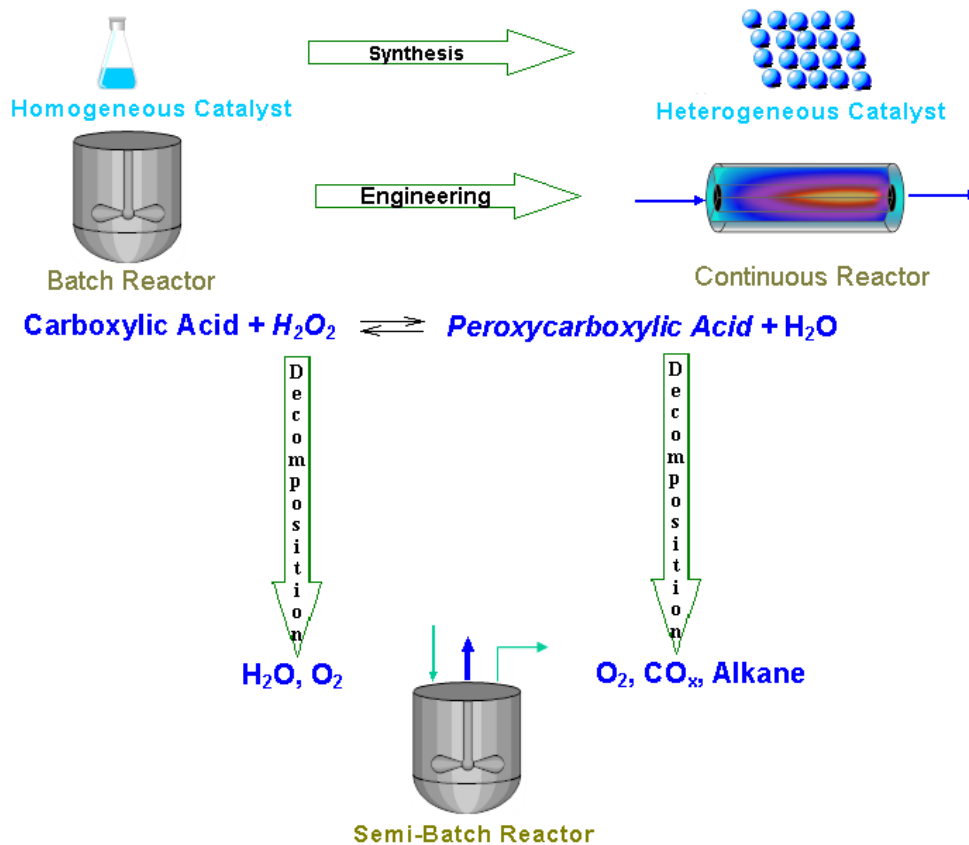


An original approach to the kinetic and mass transfer analysis developed by Musakka et al. [37] to the decomposition of peroxyacetic acid was used. Traditionally, liquid-phase decomposition kinetics is measured by analyzing the liquid phase components off-line. The method is, however, slow and cumbersome. Therefore, a rapid on-line method was developed, which is based on the analysis of the decomposition products released into the gas phase. The method utilizes on-line quadrupole mass spectrometry (MS). The kinetic model was able to quantify the decomposition of these chemicals, and to show the high stability of PPA. Spontaneous decomposition of peroxyacetic acid (PAA) in the presence of sulphuric acid at a temperature below 55°C was negligible [38].

We can summarize that the synthesis of peroxycarboxylic acids is a good example of Green Chemistry application because of

- the safety issue related to the stability of hydrogen peroxide and peroxycarboxylic acids;
- the economical and environmental issues related to necessity to shift to heterogeneous catalysts;
- the environmental issue due to the fact that peroxycarboxylic acids are eco-friendly compounds;
- the sustainable issue due to the necessity to intensify the process to separate the different organic species and the shift of the equilibrium.

The following research has been focused on the three first point of the list. Indeed, other aspect should be discussed such as the maximization of the atom economy, e.g., elimination of the water by azeotropic distillation. However, the topics covered in this thesis give a first step for a green and intensified production.



Schematic scope of the thesis

Experimental section

2.1 Experimental part for the synthesis [I-V]

The experiments were carried out in a batch reactor (Fig. 3) equipped with a mechanical stirrer and a temperature probe. On top of the reactor, a cooling condenser was placed, and adjusted at 0°C to avoid volatilization of the liquid phase compounds. In case decomposition of PCA or H₂O₂ appeared, a carrier gas (Helium) was led into the reactor through one of the necks to prevent accumulation of oxygen in the gas phase.

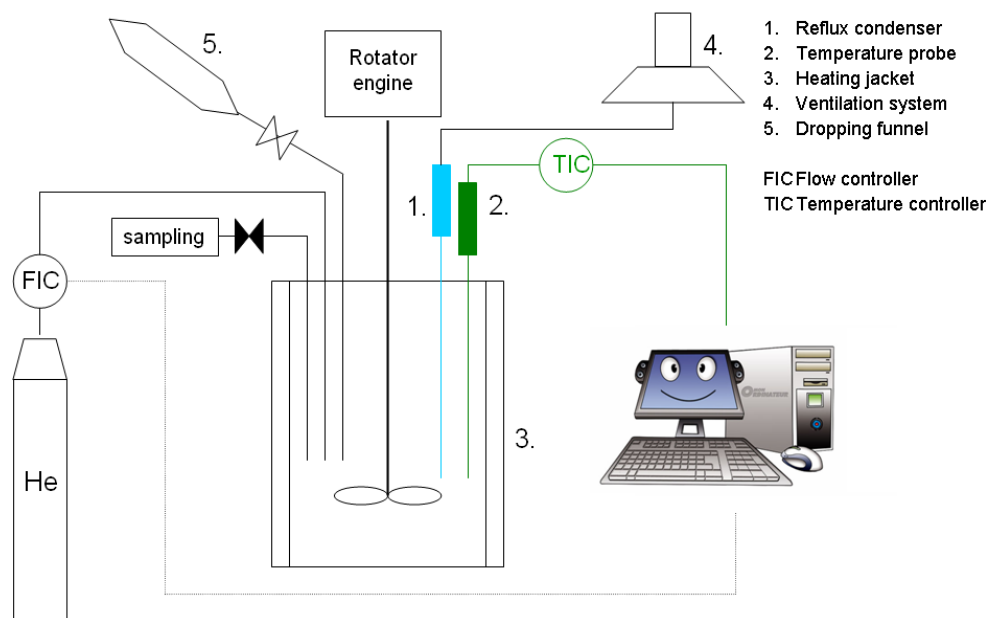


Figure 3. Schematic picture of the batch reactor.

To prevent contamination induced by alkaline and metal components, which initiate the catalytic decomposition of peroxycarboxylic acid and hydrogen peroxide, all parts of the reactor system being in contact with the reaction solution were washed with hydrochloric acid followed by another washing, with a phosphate-free detergent solution.

In the first stage, carboxylic acids, water and the catalyst were mixed together in the reactor. As the reaction temperature was reached, the hydrogen peroxide solution (30 wt.%) was added through the dropping funnel, and at time “zero” the required amount was poured into the reactor.

According to literature [39], the danger of explosion is suppressed by employing a temperature up to 60°C, a weight ratio of hydrogen peroxide-to-water up to 0.8, and a catalyst concentration of 10-40 wt.% during the reaction of hydrogen peroxide and carboxylic acid in water and in the presence of an acid catalyst. These safety issues were applied.

Table 2 introduces the experimental matrix for the synthesis in the presence of homogeneous and heterogeneous catalysts.

Table 2. Experimental matrix for synthesis in batch reactor (CA = carboxylic acid)

Reaction temperature	30-60°C
Rotation speed	200-600 rpm
[CA] ₀	5.1-9.3 mol.l ⁻¹
[H ₂ O ₂] ₀	1.9-7.5 mol.l ⁻¹
[H ₂ O] ₀	16.8-40.7 mol.l ⁻¹
[H ₂ SO ₄] ₀	0.0-1.41 mol.l ⁻¹
Amberlite loading on dry basis	0-98.8 g.l ⁻¹

2.2 Catalysts properties and characterization [II-V]

During the catalyst screening, two different heterogeneous catalysts were used: aluminosilicate materials and cation exchange resins.

Some characterization experiments were done on these solid catalysts, and particularly on the cation exchange resins. This investigation consisted essentially to determine the number of acid site (titration method), the morphology (SEM) and particle size distribution (diffraction method).

The acidic properties of the different aluminosilicate materials are summarized in Table 3. The Brønsted and Lewis acid sites were determined by FTIR by using pyridine as the probe molecule [40-43]. The specific surface area was determined by N₂ adsorption, calculated by Dubinin method for microporous materials and by BET method for the mesoporous H-MCM-41 [40-43].

Table 3. Properties of the aluminosilicate materials

	SiO ₂ /Al ₂ O ₃ mol/mol	Brønsted acid sites at 250°C μmol/g	Lewis acid sites at 250°C μmol/g
H-β-25	25	269	162
H-β-75	75	147	39
H-β-300	300	82	30
H-ZSM-5-23	23	416	36
H-ZSM-5-31	31	-	-
Al ₂ O ₃	-	7	156
H-MCM-41	40	26	40

The properties of the tested commercial cation exchange resins are listed in Table 4. Except for Smopex-101, the different cation exchange resins used were composed of similar type of matrix: styrene-divinyl benzene with sulfonic acid functional groups. The shapes of the catalysts were the same, i.e., beads. Smopex-101 (Smoptech) is a fibrous catalyst bearing sulfonic acid functional groups on poly(ethylene-graft-polystyrene). The mean particle diameter is about 0.01 mm and the average length is 4 mm [44].

Table 4. Properties of the Cation Exchange resins used

	Supplier	Polymer type	Cross linking %	Moisture content % mass	Capacity by dry weight meq/g	Native particle size range mm	Pores nm
Amberlite IR-120	Aldrich	Gel	8	45	4.4	0.3-1.2	-
Amberlyst 15	Fluka	Macroreticular	20-25	5	4.7	0.45-0.60	40-80
Dowex 50Wx2-100	Acros	Gel	2	78	4.8	0.15-0.3	-
Dowex 50Wx8-400	Sigma-Aldrich	Gel	8	54	4.8	0.04-0.08	-
Dowex 50Wx8-100	Sigma-Aldrich	Gel	8	52	4.8	0.15-0.3	-
Dowex 50Wx8-50	Fluka	Gel	8	55	4.8	0.3-0.84	-
Smopex-101	Smoptech	Fibre	2	6	2.6	-	-

2.3 Calorimetric measurements

In order to check if the estimation of the enthalpy of reaction given by our model is valid, some calorimetric measurements were carried out. Due to the low exothermicity of the chemical system, isothermal micro-calorimeter, namely C80 SETARAM, was used. This calorimeter uses the Calvet design detector in which a sample and reference cells are totally surrounded by an array of thermocouple detectors allowing for the measurement of all heat evolved. Figure 4 shows C80 SETARAM, while Figure 5 represents a schematic view of the calorimetric block.

Reversal mixing cells were used (Fig. 6) made in stainless steel. Two different compartments are separated by a lid. The measuring cell was filled with around 0.45 grams of carboxylic acid, 1 gram of an aqueous solution of hydrogen peroxide

at 50 wt.% and 0.25 grams of Amberlite IR-120. To measure only the heat flow due to the reaction of perhydrolysis catalyzed by the resins, the amount of carboxylic acid and Amberlite IR-120 was kept constant, and the aqueous solution of hydrogen peroxide was replaced by water.



Figure 4. C80 Setaram.

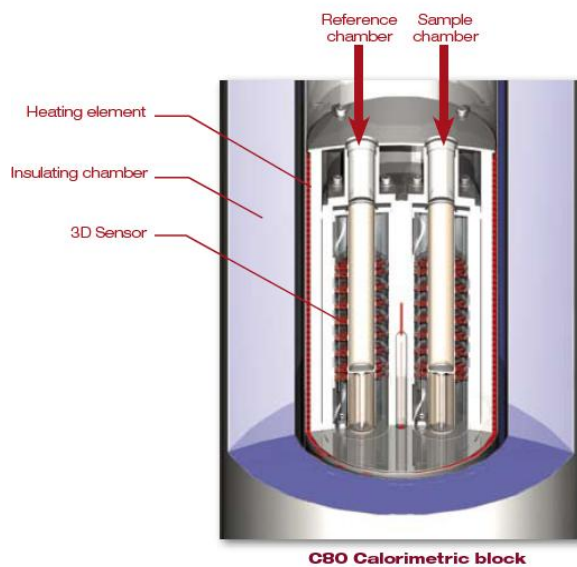


Figure 5. Schematic view of the C80 calorimetric block.

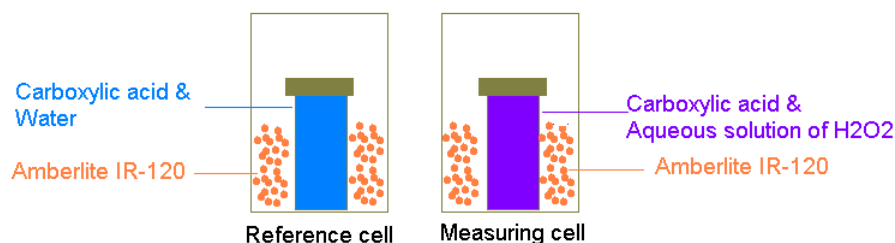


Figure 6. Schematic view of the C80 cells.

In a first stage, the cells were filled with the reactant and the catalysts. Then, they were placed in the calorimetric block. When the desired temperature was reached and the heat flow was stable, the calorimeter was switched to reversal mode.

2.4 Experimental part for the decomposition [VI]

2.4.1 Procedure

The experiment setup for the decomposition studies is described in detail in a paper of Musakka et al. [37]. A schematic experimental setup used to investigate the peroxycarboxylic acids decomposition is displayed in Figure 7.

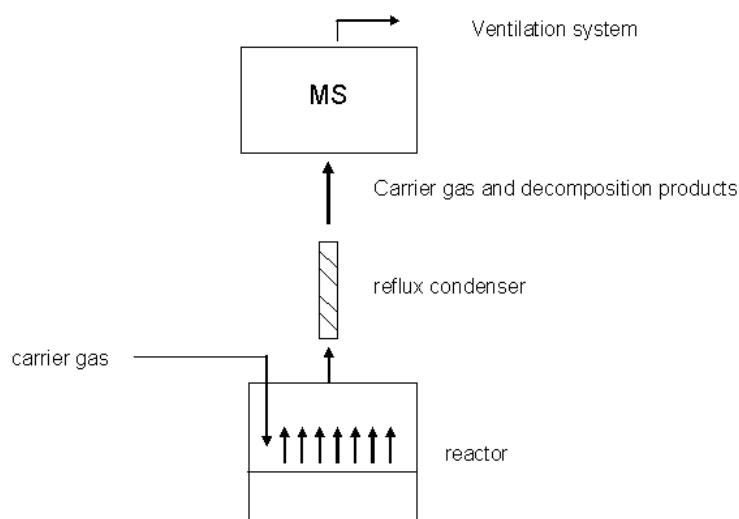


Figure 7. Schematic representation of the experimental setup used for decompositions studies.

The method is based on the on-line analysis of the decomposition products escaping to the gas phase. Quadrupole mass spectrometer (MS) (Balzers Omnistar GSD 300 O) is used as an analytical instrument.

The system consisted of two parts: the liquid phase in batch and the gas phase in continuous mode. The carrier gas (He) was fed into a 500 ml glass reactor, and it left the reactor with the gas-phase decomposition products. About 200 g of a peroxy-carboxylic acid solution was poured into the reactor, and the carrier gas flow rate was adjusted to 10 ml/min at 20°C. The temperature of the cooling condenser was adjusted to -20°C to prevent the evaporated liquid-phase components (e.g., water, carboxylic acid, peroxy-carboxylic acid) from entering the quadrupole MS. It was sufficient to apply an atmospheric pressure in the reactor to remove the decomposition product with the carrier gas.

The gas-liquid mass transfer characteristics were studied by varying the stirring rate. It was adjusted to be high enough (150 rpm) thus suppressing the liquid-gas mass transfer resistance, but avoiding vortex formation at the gas-liquid interface.

2.4.2 Analysis

The liquid phase was analyzed off-line by titration methods: Greenspan and Mackellar method [45]. The concentration of hydrogen peroxide was determined by titration using a standard solution of ammonium cerium sulfate (0.1 N). The concentrations of carboxylic and peroxy-carboxylic acids were determined by titration with an automatic titrator (Metrohm 751 GPD Titrino) using a standard solution of sodium hydroxide (0.2 N).

The mole fractions carbon dioxide, oxygen, and ethane in the gas phase were calculated from the intensities attributed to the corresponding mass numbers: 44, 32, and 27, respectively. Since some of the liquid phase components interfere with these mass numbers, we have to take into account these interferences, when calculating the mole fractions of the different gas components. The mole fraction of a component X (e.g., CO₂, O₂) was thus calculated from

$$x_X = k_X \cdot x_{cg} \cdot \left(\frac{I_X - \sum f_B \cdot I_B}{I_{cg}} \right)$$

where k_x is a calibration factor of a component x in the gas phase, x_{cg} is the mole fraction of the carrier gas, I is the intensity of a component, and f_B is the fragmentation coefficient of the liquid phase component. The fragmentation coefficients were determined by measuring the intensities of the mass numbers of the liquid-phase components present in the peroxycarboxylic acid solution.

2.4.3 Flow characteristics

The flow pattern of the gas phase was determined by tracer experiments, by introducing a pulse of another inert gas (Ar) into the main gas flow (He), and recording the pulse at the reactor outlet by MS. The tracer concentration in a tank reactor with complete mixing (CSTR) is given by the well-known expression:

$$c = c_0 \cdot e^{-\frac{t}{\tau}}$$

A straight line was obtained (Fig. 8), which implies that the gas phase of the reactor system is completely backmixed.

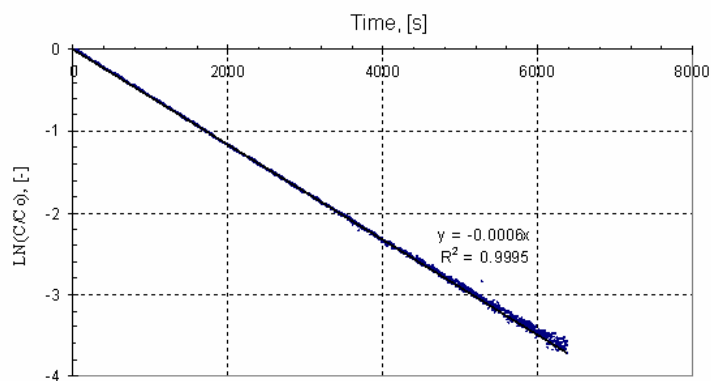


Figure 8. Calculated results from the tracer experiment.

2.5 Continuous reactor

A catalytic fixed-bed reactor functioning in upstream mode was selected to demonstrate continuous production of peroxycarboxylic acid from hydrogen peroxide and carboxylic acid. Amberlite IR-120 was used to catalyse the reaction. Figure 9 presents a schematic view of the experimental setup.

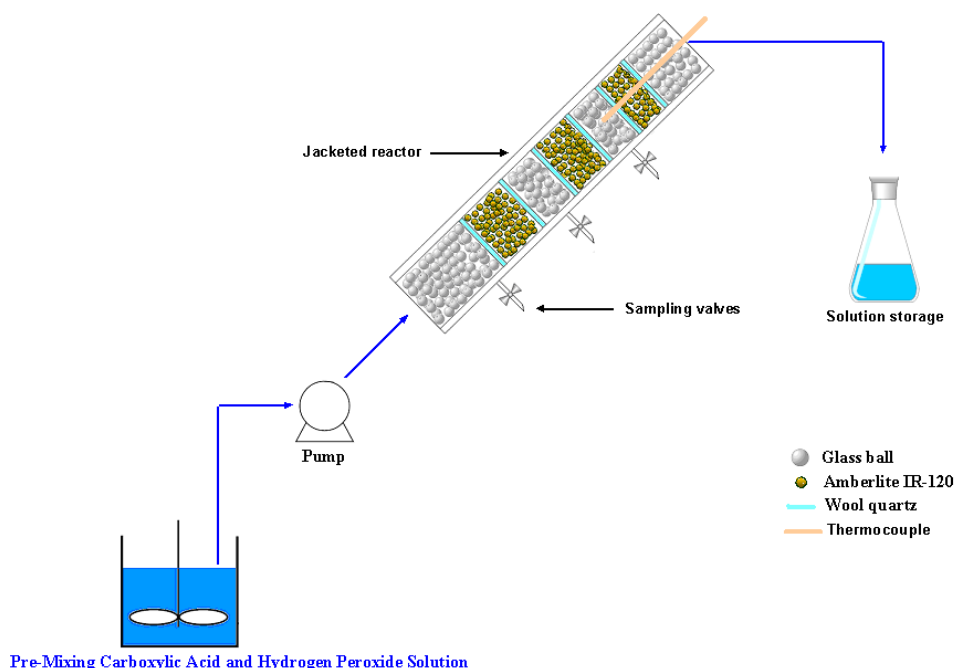


Figure. 9. Experimental scheme of the fixed-bed reactor for peroxycarboxylic acid production.

Table 5 presents the dimension characteristics of the reactor, catalyst and inert materials loading and experimental conditions.

Table 5. Reactor characteristics and experimental conditions

Reactor length [m]	0.6
Reactor diameter [m]	1.9×10^{-2}
Reactor volume [m ³]	1.7×10^{-4}
Loading of quartz ball [g]	67.4
Loading of wet Amberlite IR-120 [g]	36.3
Flow rate [ml.min ⁻¹]	0.7-2.6
Temperature [°C]	30
[CA] ₀ [mol.l ⁻¹]	5.4-5.94
[H ₂ O ₂] ₀ [mol.l ⁻¹]	6.3-6.97
[H ₂ O] ₀ [mol.l ⁻¹]	24.8-27.5

The properties of the quartz ball and Amberlite IR-120 resins are summarized in Table 6.

Table 6. Properties of quarts and catalyst materials

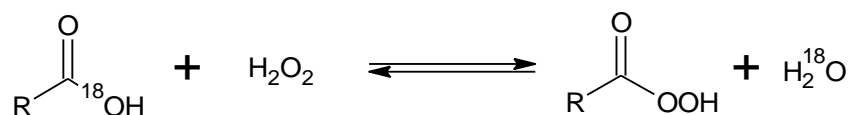
Quartz		Amberlite IR-120	
Diameter [mm]	3	Diameter [mm]	0.15-0.9
Density [kg.m ³]	2687	True density [kg.m ³]	1260
		Porosity	0.5

The native particle size distribution of Amberlite IR-120 was used during the experiments. A solution of carboxylic acids and hydrogen peroxide solution (Merck, 30 wt.%) was pre-mixed in a batch reactor, then the pre-mixed solution is pumped through the plug-flow reactor.

The residence time distribution of the fixed-bed reactor was measured by step and pulse experiments by using HCl at 0.02 M as tracers.

Synthesis of PCA in batch

By using an ^{18}O isotope label, Bunton et al. [46] have demonstrated that during the perhydrolysis, there is no dissociation of the O-O bond from H_2O_2 , but the hydroxyl group is replaced by the hydroperoxyl group,



This implies that the reaction of perhydrolysis does not involve radicals during the formation of peroxycarboxylic acids. To have a better understanding of this reaction, a kinetic study in the presence of a homogeneous catalyst is inevitable to determine the main parameters which govern the reaction system. An effort was done to discover a solid acid catalyst to surmount the problem relating to the use of homogeneous catalysts and to avoid the decomposition of peroxide species during the reaction. Linear free energy relationships were applied to understand the reaction mechanism and to establish a comparison between homogeneous and heterogeneous catalysts.

3.1 Synthesis of PCA in the presence of homogeneous catalysts [I, V]

The main goal of this part was to get reference data for the reaction kinetics and to estimate the thermodynamic parameters, such as the standard enthalpy change of reaction ΔH_r° and the heat of formation of peroxycarboxylic acid $\Delta H_f^\circ(\text{PCA})$. Indeed, it is easier to estimate these parameters by using a homogeneous catalyst than a heterogeneous catalyst, because adsorption and mass transfer phenomena are excluded. On the other hand, industrial production of peroxycarboxylic acid is, in majority, still catalyzed by homogeneous catalysts. Thus, to compare the efficiency of the two catalytic systems, it is necessary to perform a kinetic and modelling study of the synthesis of peroxycarboxylic acid by using a homogeneous catalyst.

During the modelling, the component concentrations were used instead of the activities for three reasons:

- lack of data concerning the activity coefficients of peroxide compounds,
- presence of a strong electrolyte at a non-negligible concentration, which increases the degree of complexity for the calculation of the activity coefficient of each species,
- kinetic modelling applied was able to describe the system based on concentrations.

3.1.1 Equilibrium analysis

A preliminary analysis of the experiments demonstrated that the non-ideality should be taken into account in the description of the reaction thermodynamics.

The results were analyzed with the reaction quotient defined to: $Q = \frac{[PCA]^* [H_2O]}{[CA]^* [H_2O_2]}$,

where $[H_2O]$ was determined by adding the initial water concentration and the concentration of PCA formed (the experiments were always commenced with a PCA-free solution). As the value of Q becomes constant, one can assume that the equilibrium is attained. This value is noted as K^c , because it is calculated based on concentrations, but it does not necessarily represent the true thermodynamic equilibrium constant K^T , which is based on activity.

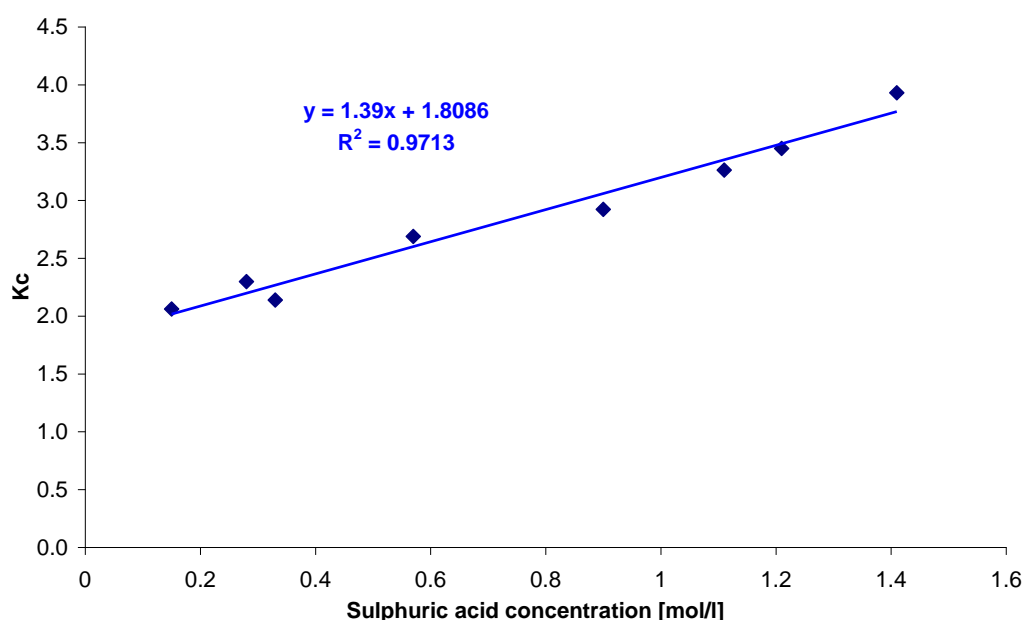


Figure 10. K^c versus sulphuric acid concentration at 40°C in case of propionic acid perhydrolysis.

As Figure 10 shows, the non-ideality of the solutions can be explained by the presence of the strong electrolyte (i.e., sulphuric acid). At infinite dilution K^c and K^T should coincide. Thus K^c is related with K^T by

$$K^c = \delta^* [H_2SO_4]_0 + K^T \quad (1)$$

where δ is a parameter which lumps the non-ideality effects of the solution.

The effect of temperature on the true thermodynamic equilibrium constant is described by the law of van't Hoff:

$$\frac{d \ln K^T}{dT} = \frac{\Delta H_r^0}{RT^2} \quad (2)$$

where ΔH_r^0 stands for the standard reaction enthalpy change. We demonstrated that this thermodynamic parameter is independent of T , and the integration of eq. (2) from a particular temperature T_{ref} to an arbitrary temperature T leads to the relation

$$\ln \frac{K^T}{K_{ref}^T} = \frac{-\Delta H_r^0}{R} \left(\frac{1}{T} - \frac{1}{T_{ref}} \right) \quad (3)$$

3.1.2 Mechanism and kinetic equations

According to the experiments, the sulphuric acid and water concentrations have an influence on the reaction velocity. Indeed, water is the solvent and the reaction product, and it has an influence on the reaction equilibrium, so its concentration should appear in the rate expression. Moreover, the proton transfer is easier from acid to water than from acid to acid according to Mohammed et al. [47]. The key issues in the mechanism are the complex protolysis equilibria of the acids being present.

The following mechanism (Fig. 11) is proposed to explain the perhydrolysis of carboxylic acid: steps I-V represent protolysis while VI-VII are reaction steps.

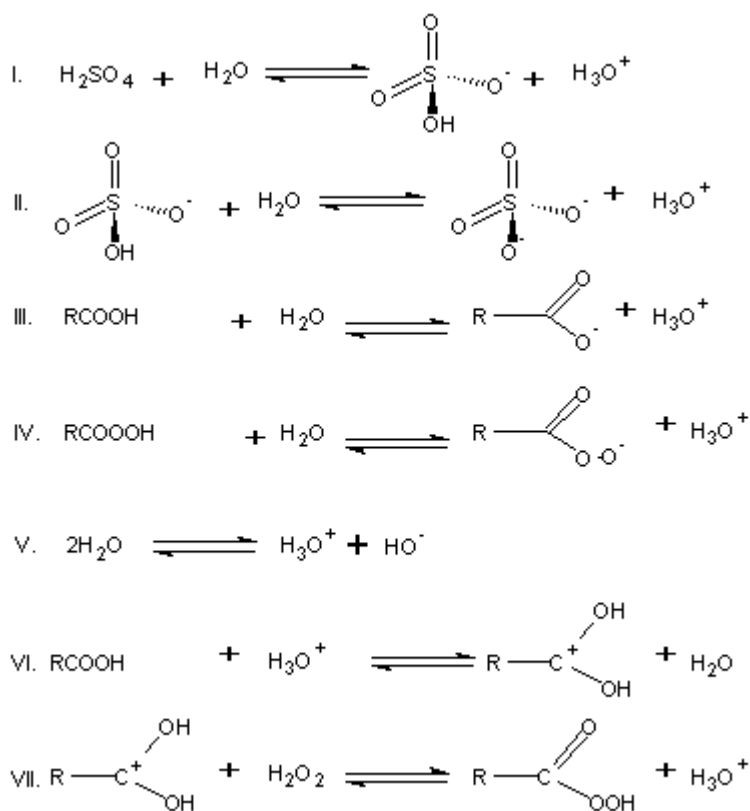


Figure 11. Simplified mechanism for PCA synthesis catalyzed by sulphuric acid in aqueous media.

One should keep in mind that several intermediates can appear during the synthesis, but to simplify the treatment, we assumed that reactions VI-VII summarize all the potential different steps for the formation of the intermediates. Reactions I to V are the hydroxonium ion sources, which is one of the key issue in

the mechanism. The proton donation steps (I-V) were assumed to be rapid compared to the synthesis steps (VI-VII).

Kinetic expressions

By applying the quasi-equilibrium hypothesis on the rapid proton transfer reaction VI and by defining reaction VII as the rate limiting one, the rate expression becomes

$$r = r_{VII} = k_{VII} * K_{VI}^c * \frac{[H_3O^+]}{[H_2O]} * \left([RCO_2H] * [H_2O_2] - \frac{1}{K_{VI}^c * K_{VII}^c} * [RCO_3H] * [H_2O] \right) \quad (4)$$

The term $K_{VI}^c * K_{VII}^c$ represents the global equilibrium constant for the reaction denoted by K_{hom}^c , which is estimated by eqs (1) and (3). The term $k_{VII} * K_{VI}^c$ is denoted by a merged constant, k_{hom} .

Finally, the reaction rate can be expressed by the following expression:

$$r = r_{VII} = k_{hom} * \frac{[H_3O^+]}{[H_2O]} * \left([RCO_2H] * [H_2O_2] - \frac{1}{K_{hom}^c} * [RCO_3H] * [H_2O] \right) \quad (5)$$

The details of the calculation of the hydroxonium ion concentrations are described in paper [II]. Based on the mass balances for the various species and the electroneutrality principle, the simplified expression for the hydroxonium concentration is

$$[H_3O^+] = \frac{1}{2} * [H_2SO_4]_0 + \sqrt{\frac{[H_2SO_4]_0^2}{4} + 2 * K_{II}^c * [H_2SO_4]_0 * [H_2O] + K_{III}^c * [H_2O] * [RCO_2H]} \quad (6)$$

where the mathematical expressions for the dissociation constants K_{II}^c and K_{III}^c were found from the literature [48-49]. Eq. (6) accounts for the catalytic effect of sulphuric acid (both protons in sulphuric acid) and the original carboxylic acid, while the catalytic effect of peroxy-carboxylic acid is neglected since it is a weaker Brønsted acid.

3.1.3 Modelling and statistical results

In order to estimate the value of ΔH_r° and K_{ref}^T , the experiments should be carried out for a long time (20-30 h) to reach the chemical equilibrium. Thus, a separate set of experiments was performed for this purpose.

The parameter estimation was carried out by a special software MODEST [50]. The objective function θ was minimized by using Simplex and Levenberg-Marquardt

algorithms. This objective function was defined as follows: $\theta = \sum \left(y_i - \hat{y}_i \right)^2$, where y_i

is the experimental concentration value, and \hat{y} is the estimated value obtained from the mathematical model. The concentrations of CA, PCA, and H_2O_2 were included in the objective function with equal weights.

The generation rates of the chemical compounds were combined to the mass balances valid for the batch reactor:

$$\begin{aligned}r_{CA} &= \frac{d[CA]}{dt} = -r_{VII} \\r_{PCA} &= \frac{d[PCA]}{dt} = +r_{VII} \\r_{H_2O_2} &= \frac{d[H_2O_2]}{dt} = -r_{VII} \\r_{H_2O} &= \frac{d[H_2O]}{dt} = r_{VII}\end{aligned}$$

These model equations were solved numerically during the parameter estimation.

Model for determination of kinetics and thermodynamic parameters close to equilibrium

In this model, four parameters were estimated: k_{ave} , Ea , ΔH_r^0 , and K_{ref}^T with the reference temperature fixed at 30°C.

The temperature dependences of the rate constant were described by a modified Arrhenius equation:

$$k = k_{ave} \exp\left(\frac{-Ea}{R} \left(\frac{1}{T} - \frac{1}{T_{ave}}\right)\right) \quad (7)$$

where $k_{ave} = Ae^{-\left(\frac{Ea}{RT_{ave}}\right)}$, T_{ave} is the average temperature of the experiments. The goal of this modification is to minimize the correlation between the frequency factor and the activation energy during the parameter estimation.

The parameter δ describing the non-ideality of the solution (eq. (1)) was assumed to be temperature independent within the temperature range 30-60°C, thus, the equilibrium constant K^C is calculated from a combination of eqs (1) and (3),

$$K^c = \delta * [H_2SO_4]_0 + K_{ref}^T * \exp\left(\frac{-\Delta H_r^0}{R} \left(\frac{1}{T} - \frac{1}{T_{ref}}\right)\right) \quad (8)$$

where T_{ref} is fixed at 30°C (303 K).

The coefficient of determination R^2 of the kinetic models is defined as follows:

$$R^2 = 1 - \frac{\sum \left(y_i - \hat{y}_i\right)^2}{\sum \left(y_i - \bar{y}_i\right)^2} \quad (9)$$

where y_i is the experimental value, \hat{y} is the estimated value and \bar{y} is the mean value of the observations.

The explanation coefficient of this model exceeded 99% in case of propionic and acetic acid perhydrolysis, which indicates a good correspondence between the experimental and calculated values. Table 7 summarizes the estimated parameters along with statistical data.

Kinetic model

According to this approach, the kinetic parameters were estimated. Eq. (5) was used for the modelling along with the modified Arrhenius equation as described previously.

Three parameters were estimated simultaneously: k_{ave} , E_a and δ , which is defined as the coefficient in eq. (1): $K^c = \delta * [H_2SO_4]_0 + K^T$

The purpose of estimating δ was to check whether this parameter correlates with the kinetic parameter. This model is more accurate for describing the kinetics, because there are more experiments with different variations included. For this model the experiments were carried out on a shorter time (4-10 hours).

The explanation coefficients of the models for acetic and propionic acid were higher than 99%. Table 7 gives the values of the estimated parameters and the statistical data.

Table 7. Summary of the estimated parameters and statistical data at $T_{ave} = 45^\circ C$ for the perhydrolysis of acetic acid (left) and propionic acid (right)

Equilibrium parameters

Parameters	Estimated	Errors (%)
$K^T(30^\circ C)$	2.39	3.4
ΔH_r° (kJ.mol ⁻¹)	-5.66	25.6

Perhydrolysis by Sulphuric Acid

Parameters	Estimated	Errors (%)
k_{ave} (l.mol ⁻¹ .s ⁻¹)	$1.70 \cdot 10^{-3}$	3.7
E_a (kJ/mol)	75.58	3.3
δ (l.mol ⁻¹)	0.40	33.2

Equilibrium parameters

Parameters	Estimated	Errors (%)
$K^T(30^\circ C)$	2.05	2.4
ΔH_r° (kJ.mol ⁻¹)	-4.17	26.9

Perhydrolysis by Sulphuric Acid

Parameters	Estimated	Errors (%)
k_{ave} (l.mol ⁻¹ .s ⁻¹)	$2.00 \cdot 10^{-3}$	3.3
E_a (kJ/mol)	44.24	6.9
δ (l.mol ⁻¹)	1.33	4.8

Figure 12 shows some modelling results for peroxypropionic acid.

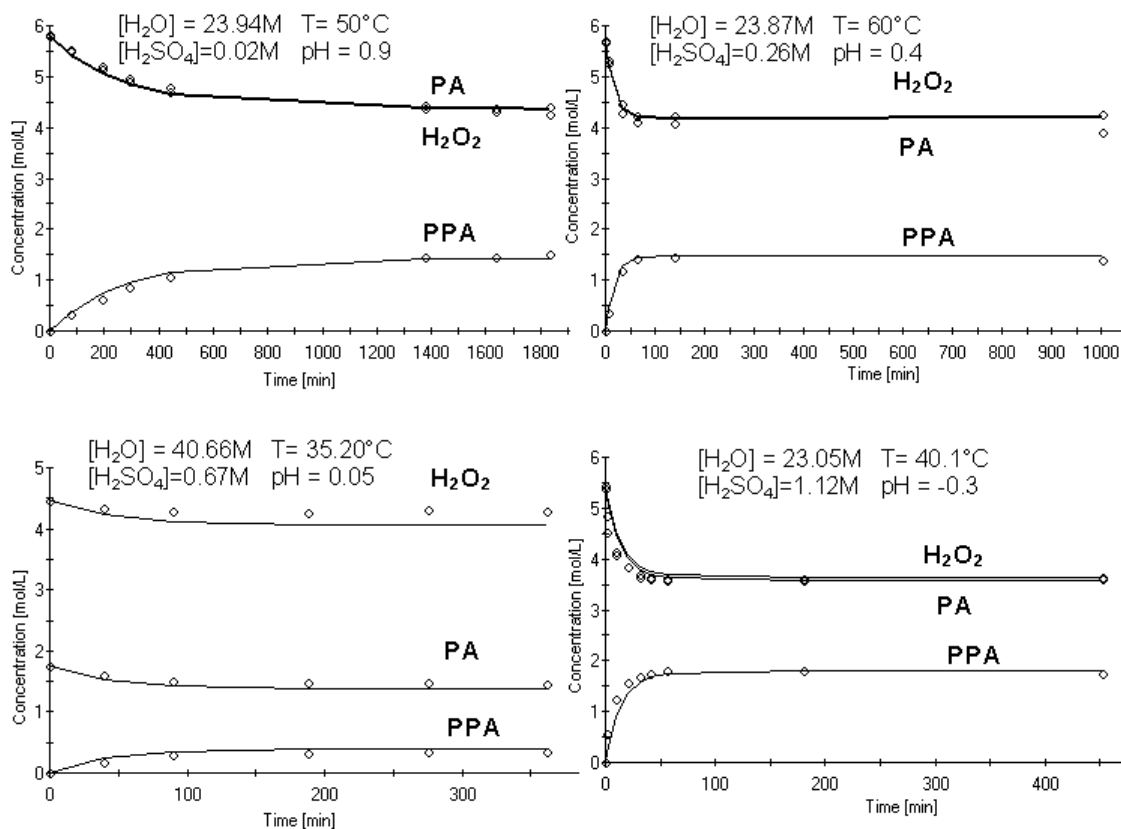


Figure 12. Fit of the model to the experiments in propionic acid perhydrolysis.

From Figure 12, it is evident that the kinetic model fits to the experimental data very well within the experimental conditions. Both the reaction kinetics and thermodynamics are well explained by the model.

3.2 Synthesis of peroxypropionic acid over heterogeneous catalysts [II, III]

The previous sections allow us to get a better understanding of the mechanism of the synthesis, to determine the thermodynamic and kinetic parameters. However, to develop a green process of peroxycarboxylic production, it is inevitable to shift to heterogeneous catalysts. The main challenge is to find a catalyst with a comparable acid strength to that of sulphuric acid, which does not decompose peroxide species; and, in addition, can be re-used. As the Figure 13 demonstrates, the synthesis of peroxypropionic acid is strongly dependent on the Brønsted acid concentration.

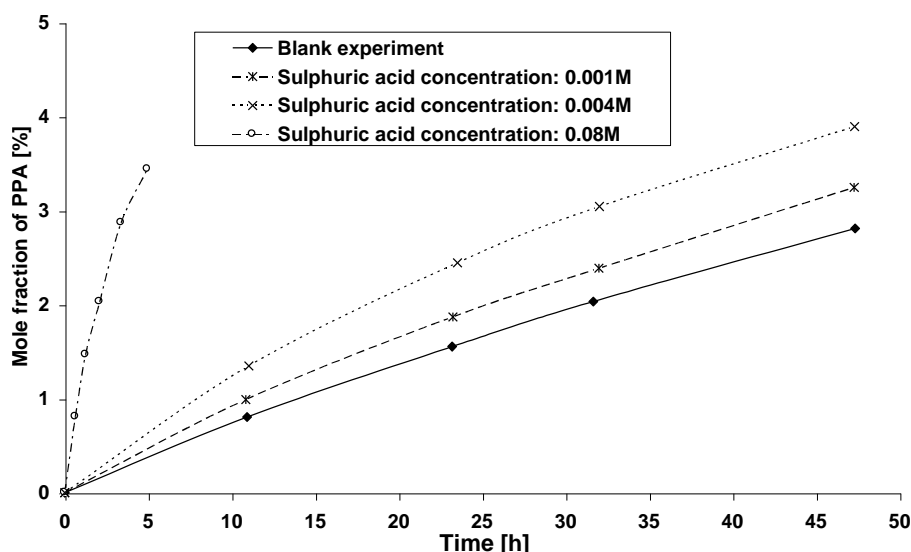


Figure 13. Mole fraction of PPA versus time at 40°C with different sulphuric acid concentrations.

Two different types of catalysts were investigated: aluminosilicate materials and cation exchange resins.

3.2.1 Aluminosilicate materials (II)

The experiments showed that aluminosilicate materials such as H- β zeolites, mesoporous material H-MCM-41 and alumina initiate the decomposition of hydrogen peroxide. The reason of the decomposition of H_2O_2 is related to the partial dealumination of these zeolites. However, in the case of experiments carried out with H-ZSM-5 zeolite catalysts, a slight catalytic effect on the perhydrolysis and no decomposition of hydrogen peroxide were noticed. In general, the use of cation exchange resins as catalysts is more kinetically beneficial than H-ZSM-5 zeolite catalysts.

Figure 14 shows that H-ZSM-5 zeolite catalyzes the perhydrolysis of propionic acid. Moreover, the activity of H-ZSM-5-23 is higher than H-ZSM-5-31, due to higher amount of Brønsted acid sites. In cases where no external catalyst is added, some perhydrolysis takes place (Fig. 14). This is due to the fact that propionic acid itself is a weak Brønsted acid having some catalytic effect.

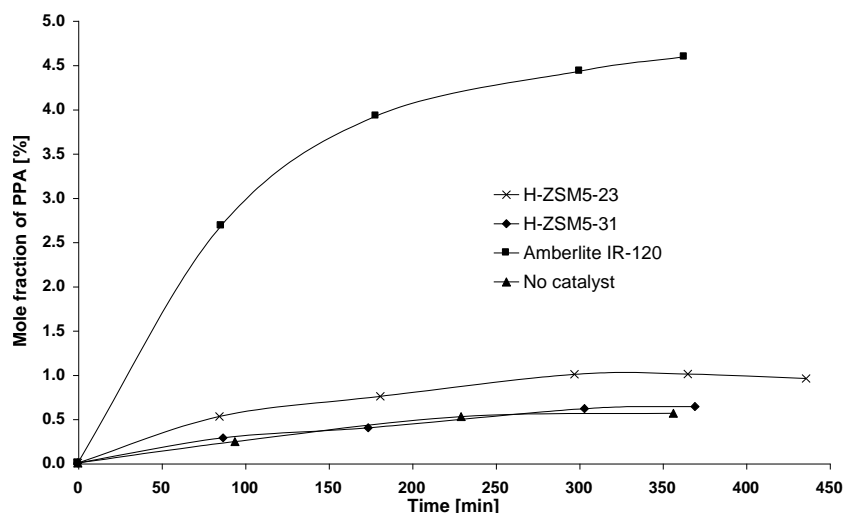


Figure 14. Formation of PPA over different catalysts at 50°C at 43.38 g/l of loading and 350 rpm.

Amberlite IR-120 catalyzes four times faster the perhydrolysis of PA than H-ZSM-5-23; for this reason, the cation exchange resins are preferred in practice.

3.2.2 Ion exchange resins (III, V)

A comparison of different cation exchange resins regarding the catalyst efficiencies, diffusion limitation and catalyst deactivation was included in the work. All of the experiments were carried out under similar conditions regarding the temperature, water amount, initial reactant concentration and apparent Brønsted acid concentration $[H^+]$. The estimation of the apparent acid concentration, $[H^+]$ (the number of Brønsted sites of the solid catalyst present per litre) was carried out on the basis of the cation exchange capacity by dry weight (meq/g) provided by the catalyst manufacturer. The amounts of the solid catalysts were fixed to a level corresponding to an apparent Brønsted acid concentration of 0.2 M on the basis of calculations. The pre-treated catalysts were dried at 70°C for 48h. After the reaction, the catalyst was washed with water and dried in an oven at 70°C for 48h.

Mass transfer effects

From the experimental data, there are no external mass transfer limitations at the stirring range 250-600 rpm. Using gelular resin with a degree of cross-linking equal to 8% (Dowex 50Wx8) for the reaction of perhydrolysis, the presence of internal mass transfer was noticed. Table 8 summarizes the values of the effectiveness factors (η) obtained at time zero and 90 minutes after the reaction in the case of experiments carried out with different particle sizes at 40°C.

Table 8. Effectiveness factor

	Dowex 50Wx8-100	Dowex 50Wx8-50	
η (with pre-treated catalyst)	1.0	0.8	0 h
η (with pre-treated catalyst)	1.00	0.95	1.5 h

The value of the initial effectiveness factor confirms that internal diffusion cannot be totally neglected in the case of native particle sizes exceeding 0.3 mm and with a degree of cross-linking at a level of 8%. Thus, for experiments carried out with Amberlite IR-120, the internal diffusion effect is present. Nevertheless, one can notice that after 1 hour and 30 minutes, there is practically no internal diffusion limitation, because the chemical equilibrium is approached and the reaction rate becomes low.

Effect of pre-treatment

The purpose of the pre-treatment was to release the water from the catalyst (Table 4). This pre-treatment improves the activity of the cation exchange resins in the gel form due to a modification of the structure, thus a modification of the diffusion properties of these materials. The differences of activity become more significant in the vicinity of the equilibrium.

Effect of cross-linking

The degree of cross-linking of the resin has a strong influence on its structure, since cross-linking controls the porosity of the resin, e.g., X8 (8% of DVB) indicates medium porosity and X2 (2% of DVB) high porosity. Dowex 50Wx8-100 and Dowex 50Wx2-100 were selected because of the similarities in their physical and chemical properties, except different degrees of cross-linking.

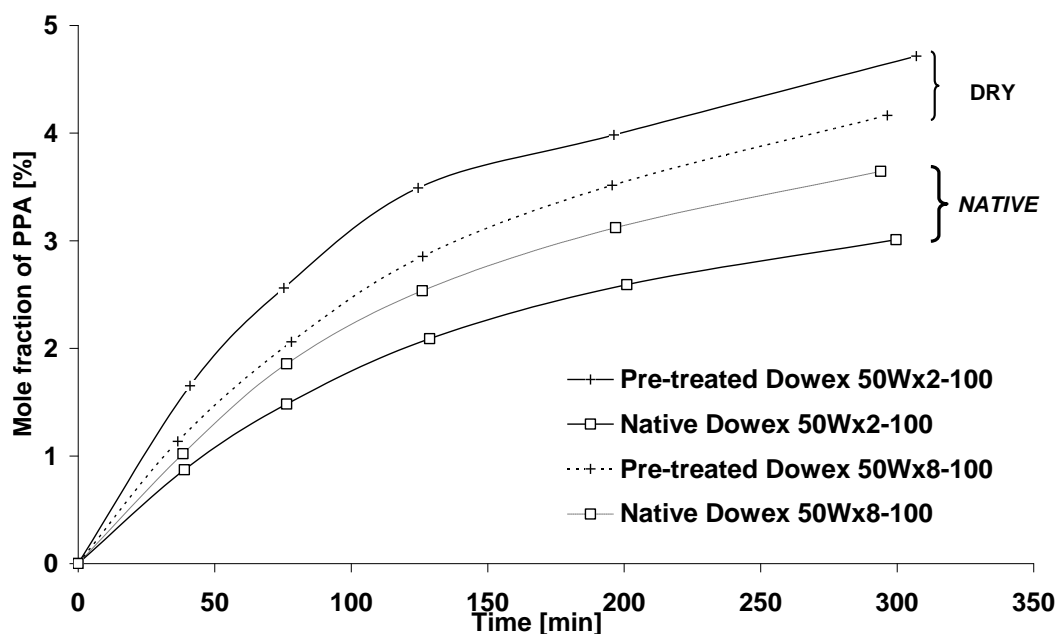


Figure 15. Effect of the degree of cross-linking on the mole fraction of PPA at 40°C.

Fig. 15 confirms the fact that there is a difference between pre-treated and native catalyst. In the case of pre-treated catalyst, the activity of Dowex 50Wx2-100 is higher than the one of Dowex 50Wx8-100. However, this phenomenon is inversed in case of experiments carried out with native catalyst.

Due to the small size of the reactants (propionic acid and hydrogen peroxide) and products (PPA and water), the porosity of these materials does not retard the diffusion process. For instance, Amberlite gel type does not have a specific or true porosity, but intramolecular distances represent a distance of around 40 Å. The pre-treatment modifies the internal structure of the matrix, and, thus, modify the tortuosity factor. One can notice that the pre-treatment improves the activity of the resins, thus, the tortuosity factor decreases. This tendency is confirmed by the fact that the active sites, i.e., sulphonic groups are located inside the particle [51]. The improvement of the tortuosity factor, by the pre-treatment, is better for the resin with low percentage of divinylbenzene. In case of a native resin, the tortuosity factor is higher with lower degree of cross-linking.

Comparison of solid catalysts with sulphuric acid

A comparison of the efficiencies of the different solid acid catalysts and the homogeneous catalyst, sulphuric acid is described in this section. Indeed, the chemical structure of the sulphonic acid group is very close to that of sulphuric acid. Figure 16 shows the mole fraction of PPA versus time for the different pre-treated catalysts.

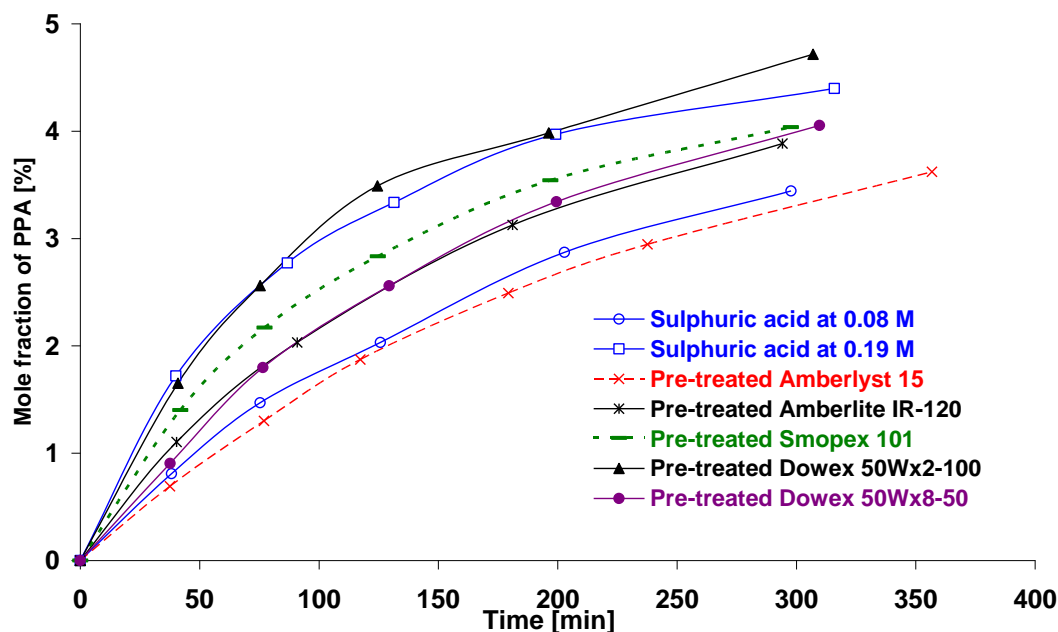


Figure 16. Synthesis of PPA over different catalysts at 40°C and 250 rpm.

As revealed by Figure 16, the efficiencies of the resins are lower than that of sulphuric acid at comparable Brønsted acid site concentration levels, in general. However, the activity of Dowex 50Wx2-100 is similar to that of sulphuric acid, at a concentration level of 0.19 M. Based on the apparent Brønsted concentration, the catalyst activity decreases in the following order: Dowex 50Wx2 > Smopex-101 > Dowex 50Wx8 \approx Amberlite IR-120 > Amberlyst 15. The highest activity of pre-treated Dowex 50Wx2 is due to its lower tortuosity factor. The diffusion process for the experiments carried out with the gelular resins is essential, and it controls the activity toward the perhydrolysis of propionic acid. The catalytic activity of Amberlyst 15 is lower than that of sulphuric acid, at a concentration level of 0.08 M. The macroreticular structure and the high level of cross-linking of this material increase the diffusion resistance, and, thus, diminish the activity. We have also noticed that the use of solid catalysts allows to decrease the acidity of the reaction medium by one pH unit compared to sulphuric acid, which could be beneficial from technological viewpoint.

Catalyst deactivation

Only few articles consider the deactivation of cation exchange resins [52-53]. Deactivation rates for Amberlite IR-120, Dowex 50Wx8-100 and Dowex 50Wx8-50 are negligible. The characteristics of these resins are: similar level of cross-linking of 8% and particles with sizes higher than 0.10 mm. Nevertheless, in the case of Dowex 50Wx8-400, Dowex 50Wx2-100 and Amberlyst 15, significant deactivation was visible.

3.3 Synthesis of peroxycarboxylic acid over Amberlite IR-120 [V]

A general model was developed, comprising the kinetic and mass transfer effects in porous particles reacting in batch reactors. The catalyst particle size distribution was included in the model. The model was applied to the synthesis of PAA and PPA. The concentrations in the bulk phase and inside the catalyst particles were predicted by the model. Amberlite IR-120 was chosen as a solid acid catalyst because it is a good compromise according to catalyst activity, deactivation and price.

3.3.1 Catalyst characterization

The concentration of the acid sites on the catalyst was determined by a conventional titration method [54], and by an elementary analysis measuring the sulphur content. The capacity value fluctuates between 4.4-4.7 meq/g (on dry basis). In the modelling work [V], the value of the capacity was assumed to be equal to 4.7 meq/g (on dry basis).

A study of the particle size distribution was done on the pre-treated resins by the classical sieving method, and on the swelled resins in water at room temperature using a Malvern 2600 model. The measurement of the particle size distribution by the Malvern instrument is based on a He-Ne laser diffraction system.

By sieving the pre-treated resin, the following distribution was found: the particle percentage with a diameter higher than 500 μm is equal to 63.6%, while the particle percentage with a diameter lower than 500 μm is equal to 36.4%.

The particle size distribution of the swelled resin in water obtained by the Malvern 2600 measurement is displayed in Figure 17.

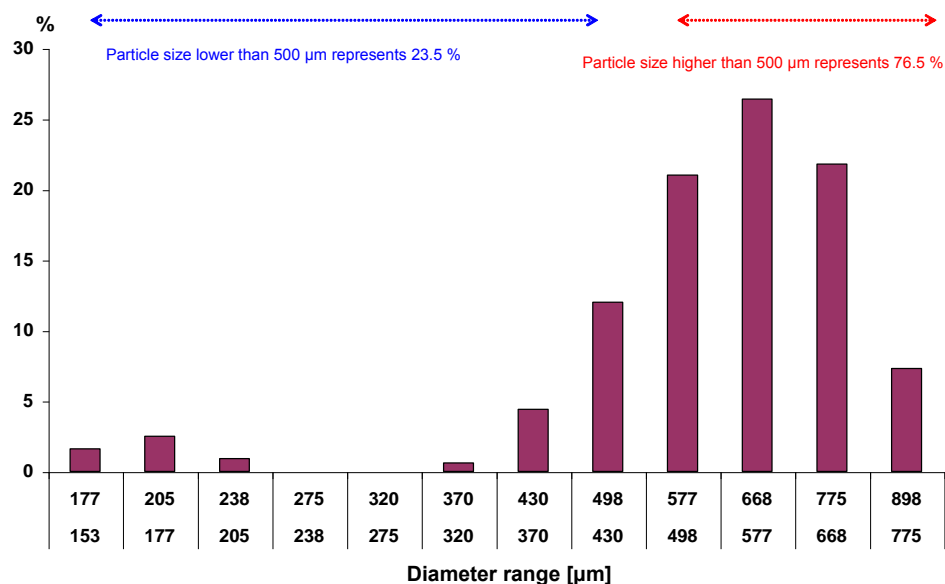


Figure 17. The particle size distribution of the Amberlite IR-120 measured by Malvern 2600.

From these results, one can notice a swelling effect when comparing the dried particles and the particles in water. The concentration of particles with diameters higher than 500 μm in water has increased by ca. 16 % compared to dry particles.

According to Musante et al. [51], in case of the perhydrolysis of acetic acid over Amberlite IR-120, water is more strongly sorbed than either acetic acid or hydrogen peroxide, and the resin swelling is thus much higher in water than in acetic acid. However, the difference in the kinetics and thermodynamics is visible only between the experiments carried out with homogeneous and heterogeneous catalysts, and when the difference in the sorption behaviour of the reactants is significant. For the sake of simplicity, the swelling effect in water is assumed to be the same as of the reaction mixture. Indeed, water was the solvent in the experimental conditions.

3.3.2 Equilibrium analysis

Figure 18 represents the reaction quotient $Q = \frac{[PPA] \cdot [H_2O]}{[PA] \cdot [H_2O_2]}$ versus time for two experiments carried out with two different catalysts loadings.

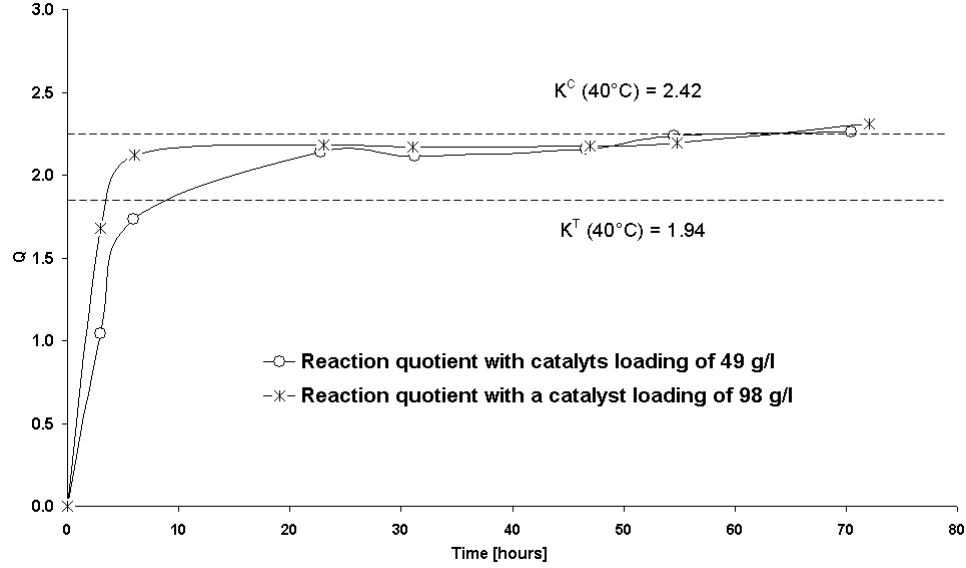


Figure 18. Equilibrium experiments for the perhydrolysis of propionic acid at 40°C.

The water concentration $[H_2O]$ was determined by adding the initial water concentration and the concentration of PPA formed (the experiments were always commenced with a PPA-free solution). The limiting value of Q obtained from the Figure 18 is 2.42. Based on eq. (3) and the data presented in article [II], the value of the true equilibrium constant at 40°C is equal to 1.94. From Figure 18, one can notice that there is a difference between the true thermodynamic constant K^T and the equilibrium constant K^C , which implies that even in presence of a solid acid catalyst, the reaction mixture is slightly non-ideal. However, the change of the catalyst loading does not affect the equilibrium constant K^C .

The equilibrium constant K^C is defined as: $K^C = \frac{K^T}{K^\gamma}$, where K^γ represents the equilibrium ratio calculated based on the activity coefficients. For the sake of simplicity, K^γ was assumed to be constant in the temperature range 30-60°C, and, the constant K^C was calculated as: $K^C = \frac{K^T}{K^\gamma} = \frac{K^T}{0.8}$, where the value of 0.8 was calculated based on Figure 18, and K^T was determined from eq. (3).

3.3.3 Mechanism

Several articles treat the carboxylic acid esterification [53, 55] or hydrolysis of esters [56] catalyzed by cation exchange resins as an Eley-Rideal mechanism. This mechanism implies that only one reactant molecule adsorbs on the surface.

According to several studies, the protonation of the carbonyl group is the key step, which it is a strong argument to assume that the carboxylic acid adsorbs on the active site, and hydrogen peroxide molecule reacts from the bulk phase. However, the protolysis of the carboxylic acid and the adsorption of water on the active sites [56] should be taken into account. The following mechanism (Figure 19) is proposed:

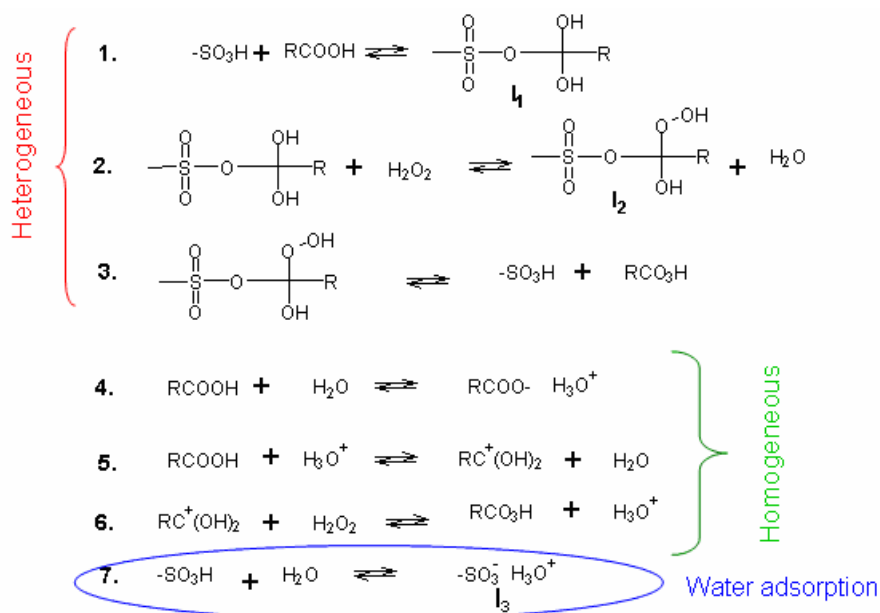


Figure 19. Simplified mechanism for peroxycarboxylic acid synthesis by Amberlite IR-120 in aqueous media.

From Figure 19, it should be noticed that the mechanism can be divided into two parts: the homogeneous part due to the protolysis of carboxylic acids producing hydroxonium ions, which act catalytically; and the heterogeneous part due the sulphonic groups on the resins. The peroxy-carboxylic acid is a much weaker acid than the corresponding carboxylic acid. Therefore, the acid-catalytic effect of the peroxy-carboxylic acid is not included in the scheme. The total rate r_{tot} of the reaction is the sum of the rates of the reactions 2 and 6, in Figure 19.

3.3.4 Kinetic expressions

For the homogeneous part of the system, the quasi-equilibrium hypothesis was applied to the reversible proton donor (reaction 5). The rate-determining step for the homogeneous system is the reversible reaction 6, and the rate r_{hom} can now be expressed as

$$\begin{aligned} r_{\text{hom}} = r_6 &= k_{+6} * [\text{RC}^+(\text{OH})_2] * [\text{H}_2\text{O}_2] - k_{-6} * [\text{RCO}_3\text{H}] * [\text{H}_3\text{O}^+] \\ &= \frac{k_{+6} * K_5^C * \sqrt{K_4^C * [\text{RCOOH}] * [\text{H}_2\text{O}]}}{[\text{H}_2\text{O}]} * \\ &\quad \left([\text{RCOOH}] * [\text{H}_2\text{O}_2] - \frac{1}{K_5^C K_6^C} * [\text{RCO}_3\text{H}] * [\text{H}_2\text{O}] \right) \end{aligned} \quad (11)$$

where the equilibrium constant K_6^C is equal to the ratio $\frac{k_{+6}}{k_{-6}}$. The products $k_{+6} * K_5^C$ and $K_5^C * K_6^C$ are denoted by the merged constants k_{hom} and K_{hom}^C , respectively. Then, eq. (11) becomes

$$r_{\text{hom}} = r_6 = \frac{k_{\text{hom}} \sqrt{K_4^C * [\text{RCOOH}] * [\text{H}_2\text{O}]}}{[\text{H}_2\text{O}]} * \left([\text{RCOOH}] * [\text{H}_2\text{O}_2] - \frac{1}{K_{\text{hom}}^C} * [\text{RCO}_3\text{H}] * [\text{H}_2\text{O}] \right) \quad (12)$$

For the heterogeneous part of the system, the quasi-equilibrium hypothesis is applied on reactions 1, 3 and 7, with the corresponding adsorption constants K_1^C , K_3^C and K_7^C . The rate-determining step for the heterogeneous system is the reversible reaction 2, and the rate(r_{het}) can be expressed as

$$r_{het} = r_2 = k_{+2} * [I_1] * [H_2O_2] - k_{-2} * [I_2] * [H_2O]$$

$$= \frac{k_{+2} * K_1^C * [-SO_3H]_0}{1 + K_1^C * [RCO_2H] + K_3^C * [RCO_3H] + K_7^C * [H_2O]} * \left([RCO_2H] * [H_2O_2] - \frac{K_3^C}{K_1^C * K_2^C} * [RCO_3H] * [H_2O] \right) \quad (13)$$

The terms $k_{+2} * K_1^C$ and $\frac{K_1^C * K_2^C}{K_3^C}$ are denoted by the lumped constants k_{het} and K_{het}^C , respectively. Then, eq. (13) becomes

$$r_{het} = r_2 = \frac{k_{het} * [-SO_3H]_0}{1 + K_1^C * [RCO_2H] + K_3^C * [RCO_3H] + K_7^C * [H_2O]} * \left([RCO_2H] * [H_2O_2] - \frac{1}{K_{het}^C} * [RCO_3H] * [H_2O] \right) \quad (14)$$

The main assumption is that the global equilibrium constants in case of the homogeneous system K_{hom}^C and in case of the heterogeneous system K_{het}^C are equal. Due to a similar structure of the peroxycarboxylic acid and the corresponding carboxylic acid, the adsorption coefficients K_1^C and K_3^C were approximated to be equal. The autoprotolysis of water was neglected.

Thus, by adding eqs. (12) and (14), the total rate combining homogeneous and heterogeneous part is:

$$r_{tot} = r_{hom} + r_{het}$$

$$= \left[\frac{k_{hom} * \sqrt{K_4^C * [RCO_2H] * [H_2O]}}{[H_2O]} + \frac{k_{het} * [-SO_3H]_0}{1 + K_1^C * ([RCO_2H] + [RCO_3H]) + K_7^C * [H_2O]} \right] * \left[[RCO_2H] * [H_2O_2] - \frac{1}{K^C} * [RCO_3H] * [H_2O] \right] \quad (15)$$

The value of k_{hom} was estimated from the kinetic model for the perhydrolysis of the carboxylic acid in the presence of sulphuric acid. The value of K_4^C was calculated based on the equation from Sue et al. [49]. The value for the adsorption coefficient of water K_7^C was calculated based on the equation developed by Altiokka [56]. In the kinetic modelling, the heterogeneous rate constant k_{het} and the adsorption coefficient K_1^C were estimated with regression analysis.

3.3.5 Modelling of mass transfer

By sieving the pre-treated Amberlite IR-120 particles into two different size fractions, i.e., lower and higher than 500 μm , the presence of internal mass transfer limitation in the beginning of the reaction was confirmed. The same phenomenon was observed with Dowex 50Wx8, which is similar to Amberlite IR-120 (regarding the acidity and the degree of cross-linking).

The mathematical treatment of the internal diffusion effect is divided into two parts: particle model and the batch reactor with the particle size distribution.

Catalyst particle model

The particle size distribution is included in the reaction-diffusion model for the porous catalyst particle. Spherical particles with the radius r_j are considered in the sequel. The heterogeneously catalyzed process appears on the acid sites of the solid catalyst, while the homogeneously catalyzed reactions take place in the pores of the catalyst.

For an infinitesimal volume element in the particle, the mass balance of a component (i) can be written as

$$(N_i A)_{\text{in}} + r_i' \Delta m + r_i \Delta V_L = (N_i A)_{\text{out}} + \frac{dn_i}{dt} \quad (16)$$

where,

r_i' is the catalytic reaction rate for the heterogeneous part in $\text{mol.s}^{-1}.\text{kg}^{-1}$,

r_i is the catalytic reaction rate for the homogeneous part in $\text{mol.s}^{-1}.\text{m}^{-3}$,

N_i is the flux of a component (i) in $\text{mol.m}^{-2}.\text{s}^{-1}$.

According to the manufacturer, the porosity ε_p of Amberlite IR-120 is medium; therefore, the value of 0.5 was applied, and the density of this material is equal to 1.26 kg.l^{-1} .

After some mathematical treatment, and by assuming a spherical shape of the catalyst particle with the radius r_j . Eq. (16) becomes

$$\frac{\partial C_{pi}}{\partial t} = \frac{r_i' \rho_p}{\varepsilon_p} + r_i - \frac{1}{\varepsilon_p r_j} \frac{\partial N_i}{\partial X} - \frac{2}{\varepsilon_p r_j X} N_i \quad (17)$$

where X denotes the dimensionless coordinate equal to r/r_j .

To describe the flux of a component (N_i), the law of Fick is used:

$$N_i = -D_{ei} \frac{\partial C_{pi}}{\partial r} = -\frac{D_{ei}}{r_j} \frac{\partial C_{pi}}{\partial X} \quad (18)$$

where D_{ei} is the effective diffusion coefficient.

Eq. (18) is inserted in eq. (17), leading to

$$\frac{\partial C_{pi}}{\partial t} = \frac{r_i \rho_p}{\varepsilon_p} + r_i + \frac{D_{ei}}{\varepsilon_p r_j^2} \left(\frac{\partial^2 C_{pi}}{\partial X^2} + \frac{2}{X} \frac{\partial C_{pi}}{\partial X} \right) \quad (19)$$

where $X \in [0, 1]$. The following boundary conditions are valid for the catalyst particle:

$$C_i(X=1) = C_{pi} \text{ in bulk phase and } \left(\frac{\partial C_{pi}}{\partial X} \right)_{X=0} = 0 \text{ for symmetry reasons.}$$

The effective diffusion coefficient is: $D_{ei} = \left(\frac{\varepsilon_p}{\eta_p} \right) D_i$, where D_i is the molecular

diffusion coefficient for a component (i), and it was determined by using Wilke-Chang equation. Eq. (19) is solved numerically for each particle size to obtain the concentration profiles in the particles. The molar volumes of the dissolved components and the liquid viscosity are included in the Wilke-Chang equation. The molar volumes were calculated from the atomic increments of Le Bas.

Batch reactor model with particle size distribution

A batchwise operating stirred tank reactor with perfect backmixing is considered. Due to vigorous stirring, the external mass transfer limitation is suppressed, and the concentration gradients in the bulk phase and in the vicinity of the catalyst particle vanish.

The size distribution of the catalysts particle is accounted for in the modelling. Thus, the mass balance of a component (i) becomes

$$\sum_j N_{ij} A_j + r_i V_L = \frac{dn_i}{dt} \quad (20)$$

In eq. (20), r_i is the homogeneous rate due to the dissociation of carboxylic acid, and A_j is the total surface area of particles with radius r_j . The total number of particles with the radius r_j is n_{pj} , thus $A_j = n_{pj} 4\pi r_j^2$. The molar amount (n_i) is expressed with concentration and volume, $n_i = C_i V_L$, where V_L is the volume of the reaction mixture and C_i the concentration in the bulk phase. The balance equation is rewritten to:

$$\frac{\partial C_i}{\partial t} = r_i + \frac{4\pi}{V_L} \sum_j n_{pj} N_{ij} r_j^2 \quad (21)$$

where N_{ij} is obtained from eq. (18) for each particle size at $X = 1$ (outer surface).

The fraction with radius r_j is denoted by y_j , i.e., $n_{pj} = y_j n_p$ where n_p is the total number of particles in the reactor. Furthermore, the average radius \bar{r} is introduced as follows $\bar{r} = \sqrt{\sum_j y_j r_j^2}$, the ratio to $\frac{A_p}{V_L}$ is denoted by a_p and $\frac{r_j}{\bar{r}} = x_j$.

The final expression equals of the mass balance equation is:

$$\frac{\partial C_i}{\partial t} = r_i + a_p \sum_j y_j N_{ij} x_j^2 \quad (22)$$

For the case of equal-sized particles $j=1$, $y_j=1$ and $x_j=1$ in eq. (22), a standard model for porous particle is obtained. Eq. (22) is valid for a discrete particle size distribution (PSD). From Figure 17, one can notice that the particle size distribution can be assumed continuous in the range 320-898 μm . However, particles with a diameter less than 238 μm represents ca. 5% of the distribution; and, furthermore, the internal mass transfer in this diameter range is absent. For that reason in the model, only particles in the range 320-898 μm were taken into account for the diffusion, the PSD can easily be replaced with a corresponding continuous distribution of particle sizes as shown below.

After some mathematical treatment [V], the mass balance including the continuous PSD becomes

$$\frac{dC_i}{dt} = r_i + 2a_p \int_0^{\frac{r_{\max}}{\bar{r}}} N_i y(x) x dx \quad (23)$$

Eqs. (19) and (23) are both coupled in order to estimate the tortuosity factor η of the resins and to get the concentration profiles in the particles. The model equations were solved numerically by discretizing the partial differential equations (PDEs) with respect to the spatial co-ordinate (X). Central finite difference formulae were used to approximate the first and second derivatives. Thus, the PDEs were transformed to ordinary differential equations (ODEs), to an initial value problem with respect to the reaction time. The ODEs were solved with the backward difference method. In practice, the discrete form of the particle size distribution was used in the numerical simulations, since the integral in eq. (23) should in any case be solved numerically. Eq. (22) represents *de facto* the discretization of eq. (23) for the numerical solution.

3.3.6 Modelling and statistical results

Two completely analogous kinetic models were used: one for the perhydrolysis of acetic acid and the other one for the perhydrolysis of propionic acid. The estimated equilibrium parameters, such as ΔH_r° and K_{ref}^T from the homogeneous model were used here, since they are of global character. However, to take into account the slight deviation from the ideality, the concentration-based equilibrium constant K^C was calculated from the relation $K^c = \frac{K^T}{K^\gamma}$.

In these models, three parameters were estimated: k_{ave} , E_a and $K(CA)$. Preliminary results from the modelling revealed that a value of 2.2 for the tortuosity factor η_p gave better statistical results. Due to the complexity to estimate this parameter with a significant statistical reliability, its value was fixed to 2.2.

Eq. (15) was used to determine the kinetic and adsorption parameters; the value of k_{hom} (which is a combination of k_{ave} and E_a according to eq. (7)) was determined from the homogeneous model.

The explanation coefficients of both models became higher than 99%. Table 10 summarizes the values of the estimated parameters and the statistical data.

The value of the adsorption coefficient for water on the resin K_7^C at 45°C is equal to 0.72 by using Altioikka equation [56]. The standard errors of the kinetic parameters, such as k_{ave} and E_a , are relatively low for both reaction systems.

However, the standard errors for the adsorption coefficients of the carboxylic acids are relatively high probably due to the statistical difficulties to determine them.

Table 10. Summary of the estimated parameters and statistical data at $T_{ave} = 45^\circ\text{C}$ for the perhydrolysis of acetic acid (left) and propionic acid (right)

Acetic acid perhydrolysis by Amberlite IR-120

Parameter	Estimated	Error (%)
$k_{ave} (\text{l.mol}^{-1}.\text{s}^{-1})$	$0.99.10^{-3}$	12.7
$E_a (\text{kJ/mol})$	42.5	7.0
$K(\text{AA}) \text{ l.mol}^{-1}$	0.89	49.1

Propionic acid perhydrolysis by Amberlite IR-120

Parameter	Estimated	Error (%)
$k_{ave} (\text{l.mol}^{-1}.\text{s}^{-1})$	$0.91.10^{-3}$	26.2
$E_a (\text{kJ/mol})$	51.4	4.6
$K(\text{PA}) \text{ l.mol}^{-1}$	1.39	80.5

Some modelling results are displayed in Figs. 20 and 21.

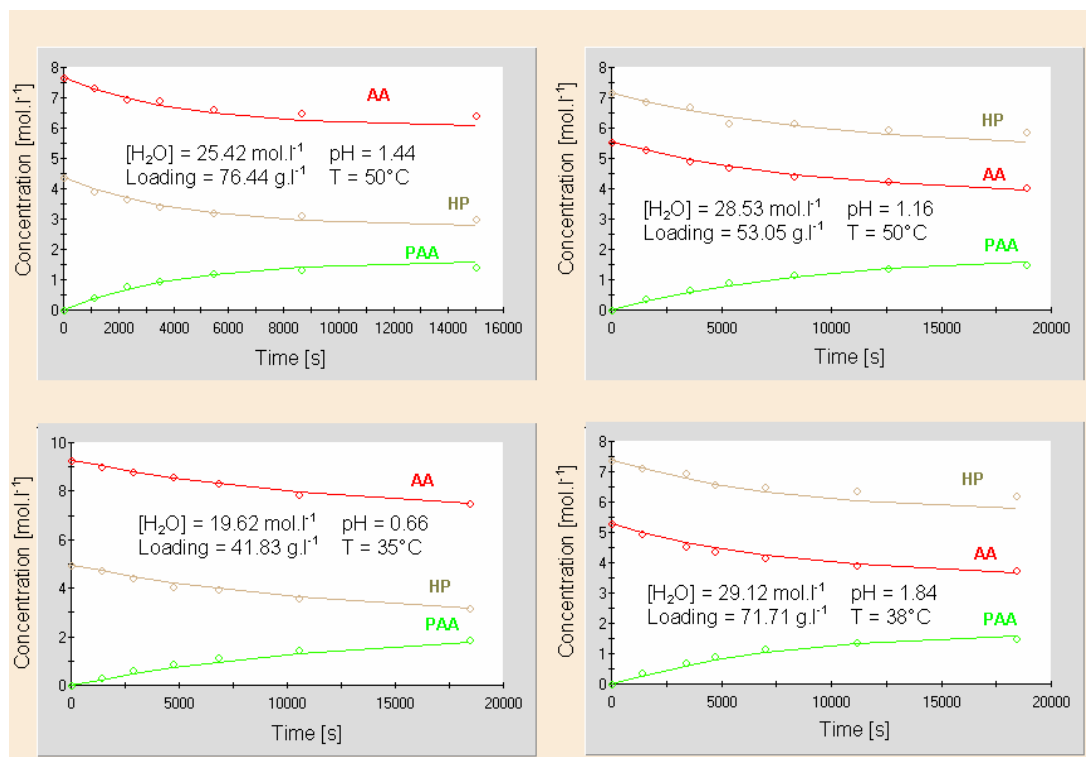


Fig. 20. Fit of the model to the experiments for the perhydrolysis of acetic acid catalyzed by Amberlite IR-120.

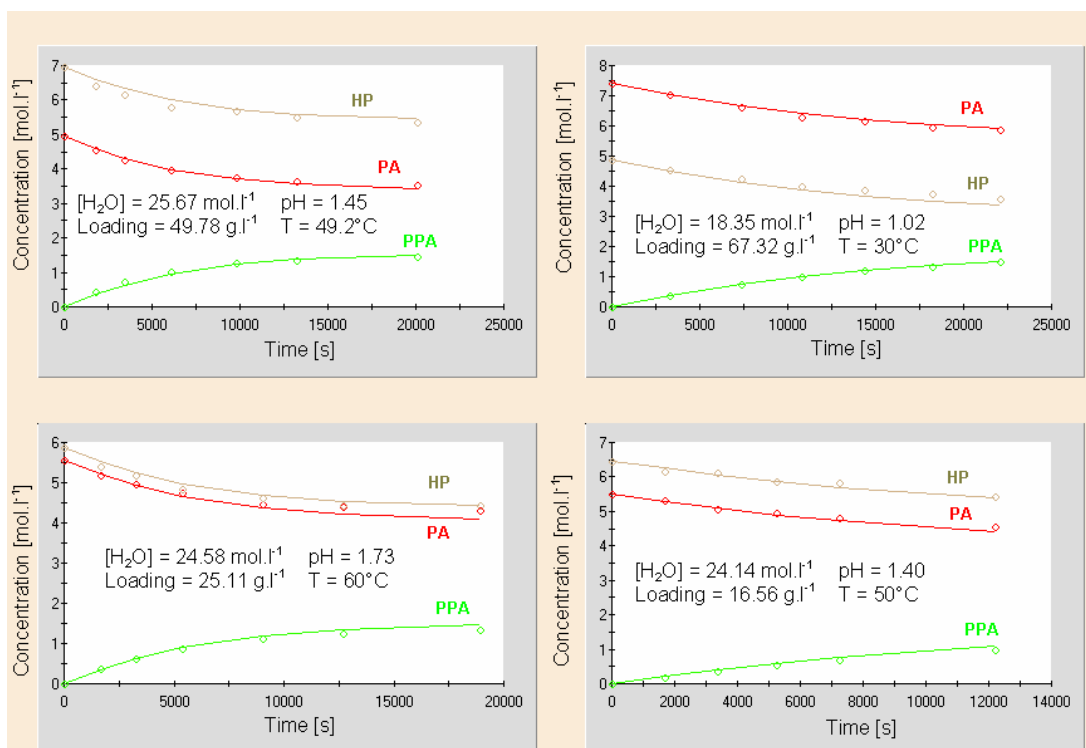


Fig. 21. Fit of the model to the experiments for the perhydrolysis of propionic acid catalyzed by Amberlite IR-120.

Figs. 20 and 21 confirm that the model describes correctly the experimental data in case of the perhydrolysis of acetic and propionic acid catalyzed by Amberlite IR-120.

Figs. 22 and 23 represent the concentration profile of peroxyacetic acid versus time and radius location in case of a particle with a diameter equal to 898 μm at 30°C and 60°C, respectively.

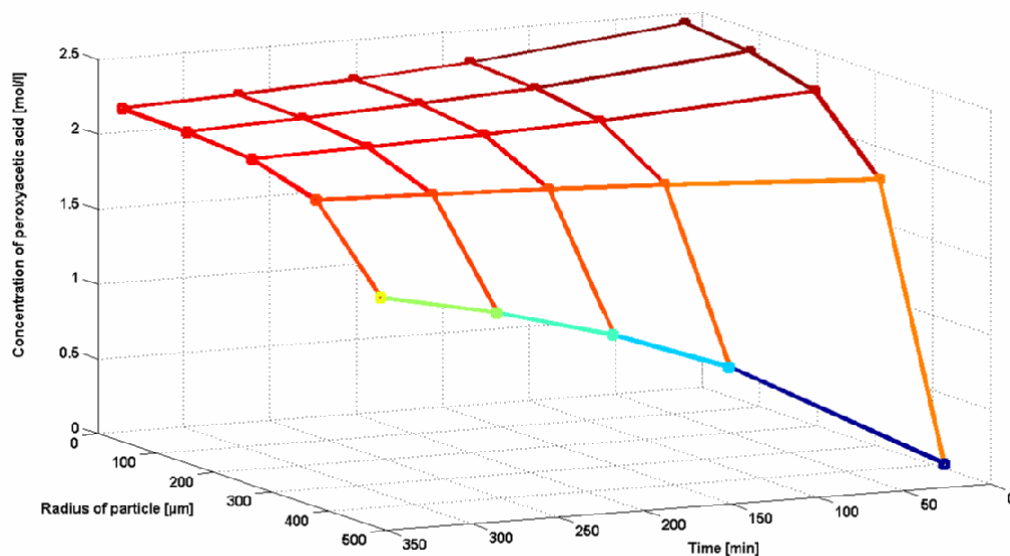


Figure 22. Concentration profile of peroxyacetic acid inside a particle of 898 μm at 30°C.

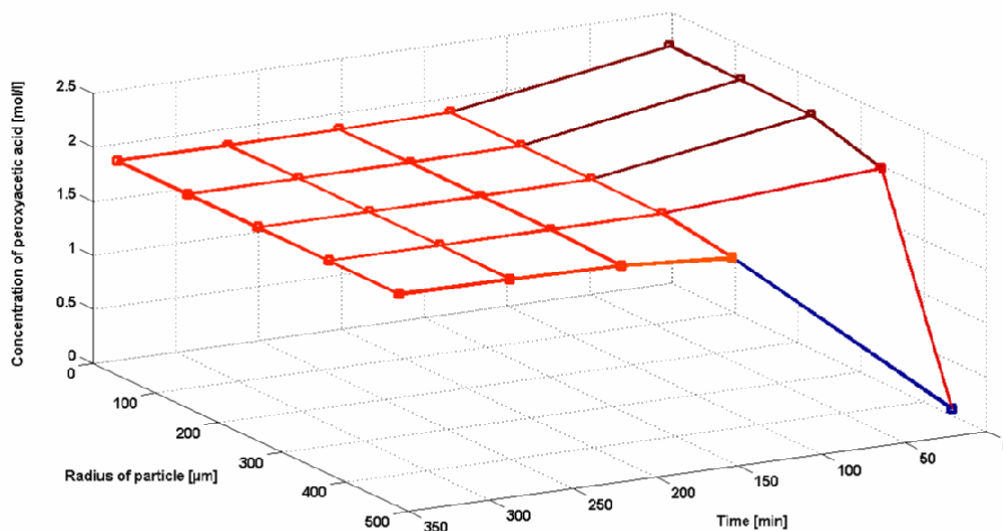


Figure 23. Concentration profile of peroxyacetic acid inside a particle of 898 μm at 60°C.

Figs. 22 and 23 were obtained by simulating the kinetic-diffusion model for an experiment of acetic acid perhydrolysis carried out at 30°C and 60°C, the catalyst loading of 57.42 g.l^{-1} and equimolar concentrations of reactant. The concentration in the bulk phase is located at 449 μm and concentration in the centre of the particle is located at 0 μm .

One can notice the presence of an internal mass transfer limitation at 30 and 60°C, Fig. 22 shows that the concentration of PAA increases from 0 to 2.43 mol.l⁻¹ when moving from the outer surface to the centre of the particle. The internal diffusion is essentially present in the beginning of the reaction, while, the concentration of PAA is uniform throughout the whole particle after 100 minutes at 60°C. As the reaction proceeds, the rate becomes slower, and the effect of diffusion is diminished.

3.4 Structure and reactivity [IV]

Linear free energy relationships (LFER) assume the existence of a correlation between the reaction kinetics and thermodynamics. These relations are strong tools for understanding the mechanism and predicting the rate and equilibrium constants of chemical reactions. The basic assumption of the concept is the existence of a relation between rate and equilibrium constant [57-58]:

$$k = \text{const} \times K^{\alpha} \quad (24)$$

Equation (24) is equivalent to a linear relationship between Gibbs energy of activation (ΔG^{\ddagger}) and Gibbs energy of the reaction (ΔG_R):

$$(\Delta G^{\ddagger}) = \alpha(\Delta G_R) + \text{const} \quad (25)$$

This approach can be established only for congeneric series of compounds, i.e., sets of compounds that share the same “functional group or reaction centre” Y (e.g., -SH, -COOH, -CO) and only have variations in the substituents R attached to this functional group. Thus, this concept implies that there is a quantitative relationship between the structural features of a molecule and its reactivity. The equation (25) is widely applied [59], although the theoretical explanation is still debated [60].

On this assumption, two types of equations have been developed: Hammett equation which describes the behaviour of meta- and para-substituted aromatic compounds; and Taft equation, which addresses the reactivity of aliphatic derivatives.

The Taft equation as applied to perhydrolysis of carboxylic acids is given by:

$$\log(k/k_o) = \delta E_s + \rho^* \zeta^* \quad (26)$$

where

- k: rate constant of a particular perhydrolysis reaction
- k_o : rate constant of acetic acid perhydrolysis
- δ : constant giving the susceptibility of a given reaction series to steric effect
- E_s : steric substituent constant

- ρ^* : constant giving the susceptibility of a given reaction series to polar substituents
- σ^* : polar substituent constant for the group R relative to the standard CH_3 group

E_s is a near-quantitative measure of the total steric effect associated with a given substituent relative to the standard of comparison. The standard of comparison in each case is the CH_3 group, δ is a reaction constant, independent of the nature of the substituent. The value of δ gives a measure of the relative susceptibility of the reaction series to the steric requirements of the substituent.

Comparison based on apparent rate constant

The perhydrolysis of formic (FA), acetic (AA), propionic (PA) and butanoic acid (BA) was investigated by homogeneously (i.e., sulphuric acid) and heterogeneously (i.e., Amberlite IR-120) catalyzed system. The comparison was based on the apparent second order rate constant k_{app} ($r \approx k_{\text{app}} [\text{CA}] [\text{H}_2\text{O}_2]$) of the reaction (Table 11).

Table 11: Apparent rate constants ($\text{l.mol}^{-1}.\text{s}^{-1}$)

	Sulphuric Acid		Pre-treated Amberlite IR-120	
	30	45	30	45
FA	2.00E-04	x	1.00E-04	x
AA	1.06E-05	1.95E-05	7.00E-06	2.23E-05
PA	7.29E-06	1.64E-05	1.16E-06	1.59E-05
BA	non-soluble	1.28E-05	non-soluble	5.00E-06

As can be noticed, the apparent rate constants decrease in the following order: k_{app} (PFA) > k_{app} (PAA) > k_{app} (PPA) > k_{app} (PBA). In addition, the apparent rate constant for the homogeneous catalyst is higher than for the heterogeneous one.

Several assumptions can be made for the cases investigated here. First of all, there is no resonance effect between the functional group and the substituent for the carboxylic acids used in these experiments. The different polar parameters σ^* can be negligible because their values are low (Table 12), and the experiments were carried out in acidic media [IV]. Indeed, Taft-Ingold and Charton have noticed that polar effect is negligible for experiments carried out in an acidic media [61]. Then, eq. (26) becomes:

$$\log \left(\frac{k}{k_o} \right) = \delta E_s \quad (27)$$

The steric parameters of Taft (E_s) for the different substituent are displayed in Table 12.

Table 12. Steric and polar parameters of Taft

Substituent	E_s	σ^*
H-COOH	1.12	0.49
CH ₃ -COOH	0.00	0.00
CH ₃ -CH ₂ -COOH	-0.08	-0.10
CH ₃ -CH ₂ -CH ₂ -COOH	-0.31	-0.12

Fig. 24 represents the application of Taft equation to the perhydrolysis of different carboxylic acids with sulphuric acid and pre-treated Amberlite IR-120 at 30 and 45°C.

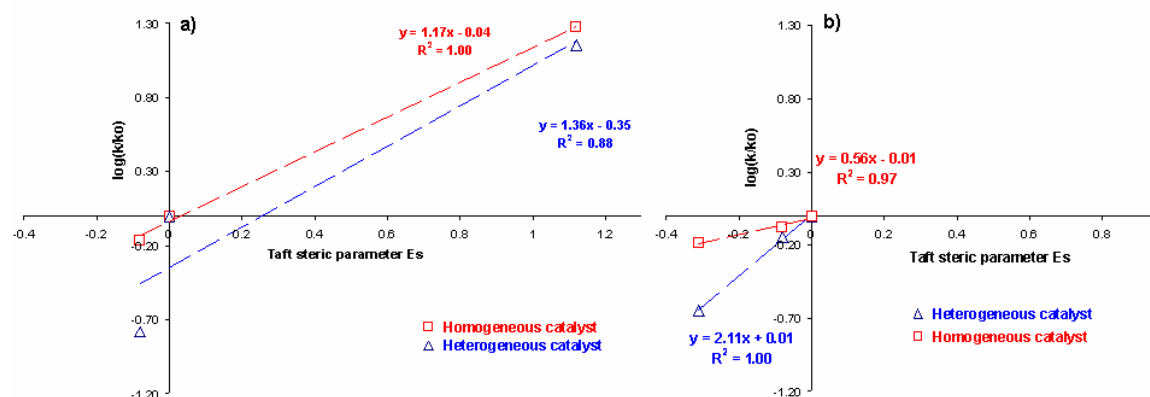


Figure 24. Taft equation (eq. (27)) for perhydrolysis of different carboxylic acids with H_2SO_4 and Amberlite IR-120 at 30°C (a) and 45°C (b).

For the sake of clarity, the values of the coefficient δ are summarized in Table 13:

Table 13. Value of coefficient δ based on k_{app}

	Coefficient δ	
	T = 30°C	T = 45°C
Homogeneous catalyst	1.17	0.56
Heterogeneous catalyst	1.36	2.11

At a first glance, Fig. 24 shows that perhydrolysis of carboxylic acids, catalyzed by an acid catalyst, follows the Taft equation by considering the steric part only. It can be concluded that the mechanism for the formation of linear carboxylic acid is the same, i.e., there is no difference between the formation of peroxyacetic and peroxybutanoic acid.

In the case of homogeneous catalysis, the apparent rate constant k_{app} can be split into two different parts associated with hydroxonium ions from the dissociation of sulphuric acid and from the dissociation of the carboxylic acid, $k_{app} = f(H_2SO_4, CA)$.

In the case of heterogeneous catalysis, the kinetics is more complex because of the adsorption phenomena. In this case, the apparent rate constant k_{app} depends on the hydroxonium ions originating from the dissociation of the carboxylic acid, the active site concentration of the heterogeneous catalyst and the adsorption term of the different species K_{ads} ; $k_{app} = f(CA, \text{Amberlite}, K_{ads})$.

The active site on Amberlite IR-120 is the functional group $-SO_3H$, which is structurally close to sulphuric acid. The apparent rate constant is proportional to the active site concentration in case of the heterogeneous catalyst and to the hydroxonium ions concentration in case of the homogeneous catalyst. However, in case of heterogeneous catalyst, the rate constant and the adsorption term are related by $k_{het} \propto \frac{1}{1 + K_{ads}}$. Thus, the main difference between the two catalytic

systems is the adsorption term, which could explain the change of the slope δ between systems catalyzed homogeneously and heterogeneously. A more detailed kinetic expression will be given in next section.

Experiments carried out at 30°C show that the slopes of the curves appear to be parallel. The accuracy of the calculated apparent rate constant for the perhydrolysis of formic acid is lower than the other rate constants. Experiments carried out at 45°C show that the slopes δ in case of homogeneous and heterogeneous catalysts are different. This difference might be certainly due to the adsorption term.

Table 12 demonstrates that the values of δ are dependent on the reaction temperature, and the nature of the catalyst at 45°C. The value of δ is positive, as in the case of the acid catalyzed hydrolysis of ethyl esters in aqueous acetone at 24.8°C, where the value of the slope δ is equal to 1.038 [62]. By comparing the slope δ from Table 12, one can notice that its value increases as the heterogeneous catalyst is used instead of the homogeneous catalyst.

kinetic equations

In case of homogeneous system, the apparent rate constant is equal to

$$k_{app}^{hom} = k_{int}^{hom} \frac{[H_3O^+]}{[H_2O]} \quad (28)$$

$$= k_{int}^{hom} \frac{1}{[H_2O]} * \left(\frac{1}{2} * [H_2SO_4]_0 + \sqrt{\frac{[H_2SO_4]_0^2}{4} + 2 * K_{II}^c * [H_2SO_4]_0 * [H_2O] + K_{III}^c * [H_2O] * [RCO_2H]} \right)$$

where k_{int}^{hom} is the intrinsic rate constant for the homogeneous system. In case of heterogeneous system, the apparent rate constant is equal to

$$k_{app}^{het} = \left(\frac{k_{int}^{het} [-SO_3H]_0}{(1 + K_{ads,CA}^c [RCOOH] + K_{ads,PCA}^c [RCO_3H] + K_{ads,water}^c [H_2O])} + \frac{k_{int}^{hom} * \sqrt{K_{RCOOH}^c [RCOOH][H_2O]}}{[H_2O]} \right) \quad (29)$$

where k_{int}^{hom} and k_{int}^{het} represent the intrinsic rate constants.

By using eqs (28) and (29), eq. (27) becomes

- In case of the homogeneous catalyst:

$$\log \left(\frac{k_{app}^{hom}(CA)}{k_{app}^{hom}(AA)} \right) = \log \left(\frac{k_{int}^{hom}(CA)}{k_{int}^{hom}(AA)} \right) + \log \left[\frac{[H_3O^+]_{CA}}{[H_3O^+]_{AA}} \right] + \text{constant} = \delta_{hom} \cdot E_S \quad (30)$$

If the water concentration is the same in both cases, then the last term of eq. (30) can be neglected. If the protolysis of the carboxylic acid is similar to the protolysis of acetic acid, then, the second term can be neglected, as well. This approximation is rather correct for acetic, propionic and butanoic acid (see Table 14). Therefore, eq. (30) becomes:

$$\log\left(\frac{k_{app}^{hom}(CA)}{k_{app}^{hom}(AA)}\right) = \log\left(\frac{k_{int}^{hom}(CA)}{k_{int}^{hom}(AA)}\right) = \log\left(\frac{A_{CA}}{A_{AA}}\right) + \frac{1}{2.3RT}(\Delta G_{AA}^{\ddagger} - \Delta G_{CA}^{\ddagger}) = \delta_{hom} \cdot E_s \quad (31)$$

Table 14. Equilibrium constant K_{III}^c

	T = 30°C	T = 45°C
Acetic acid	3.0E-07	2.8E-07
Propionic acid	2.4E-07	2.2E-07
Butanoic acid	2.6E-07	2.4E-07

By using the Arrhenius relationship, the intrinsic rate constant is expressed by:

$k_{int} = A \exp\left(\frac{-\Delta G^{\ddagger}}{RT}\right)$, where A is the pre-exponential factor, R is the gas constant,

ΔG^{\ddagger} is the Gibbs energy of activation. Equation (31) shows the linear relation between the Gibbs energy of activation ΔG^{\ddagger} and the apparent rate constant. One should keep in mind that this relation is valid only in case where the protolysis of a carboxylic acid is similar to acetic acid and the substituent has only a steric effect on the functional group.

- In a case of a heterogeneous catalyst, the following relationship is obtained:

$$\log\left(\frac{k_{app}^{het}(CA)}{k_{app}^{het}(AA)}\right) = \log\left(\frac{\frac{k_{int}^{het}[-SO_3H]_0}{(1 + K_{ads,CA}^C[RCOOH] + K_{ads,PCA}^C[RCO_3H] + K_{ads,water}^C[H_2O])} + \frac{k_{int}^{hom} * \sqrt{K_{RCOOH}^C[RCOOH][H_2O]}}{[H_2O]}}{\frac{k_{int}^{het}[-SO_3H]_0}{(1 + K_{ads,AA}^C[AcOH] + K_{ads,PAA}^C[AcOOH] + K_{ads,water}^C[H_2O])} + \frac{k_{int}^{hom} * \sqrt{K_{AcOH}^C[AcOH][H_2O]}}{[H_2O]}}\right) = \delta_{het} \cdot E_s \quad (32)$$

By neglecting the homogeneous part in eq. (32) and by assuming that the concentration of the active sites is the same for both systems, one arrives at

$$\log\left(\frac{k_{app}^{het}(CA)}{k_{app}^{het}(AA)}\right) = \log\left(\frac{k_{int}^{het}(CA)}{k_{int}^{het}(AA)}\right) + \log\left(\frac{(1 + K_{ads,AA}^C [AcOH] + K_{ads,PAA}^C [AcOOH] + K_{ads,water}^C [H_2O])}{(1 + K_{ads,CA}^C [RCOOH] + K_{ads,PCA}^C [RCO_3H] + K_{ads,water}^C [H_2O])}\right) \quad (33)$$

Applying Arrhenius law for the intrinsic rate constants, eq. (33) becomes

$$\log\left(\frac{k_{app}^{het}(CA)}{k_{app}^{het}(AA)}\right) = \log\left(\frac{A_{CA}}{A_{AA}}\right) + \frac{1}{2.3RT}(\Delta G_{AA}^\ddagger - \Delta G_{CA}^\ddagger) + \log\left(\frac{(1 + K_{ads,AA}^C [AcOH] + K_{ads,PAA}^C [AcOOH] + K_{ads,water}^C [H_2O])}{(1 + K_{ads,CA}^C [RCOOH] + K_{ads,PCA}^C [RCO_3H] + K_{ads,water}^C [H_2O])}\right) \quad (34)$$

$= \delta_{het} \cdot Es$

As can be seen, the adsorption term is taken into account in eq. (34). However, in cases where this term is negligible, e.g., adsorption phenomena are negligible, then the slope of δ_{hom} and δ_{het} can be similar. In a case where the adsorption term is similar for different carboxylic acids, then the logarithm term for the adsorption tends to zero, and, subsequently, δ_{hom} and δ_{het} can be equal.

Comparison based on the kinetic modelling

In this section, a comparison between acetic and propionic acid perhydrolysis is discussed based on the kinetic modelling results. Table 15 summarizes the kinetic and equilibrium parameters obtained in case of the perhydrolysis of acetic and propionic acids catalyzed by the homogeneous catalyst, sulphuric acid and the heterogeneous catalyst, Amberlite IR-120.

Table 15. Summary of the estimated parameters for the perhydrolysis of acetic acid (left) and propionic acid (right) for both catalytic systems

Acetic acid			Propionic acid		
Equilibrium parameters			Equilibrium parameters		
Parameters	Estimated	Errors (%)	Parameters	Estimated	Errors (%)
$K^T(30^\circ\text{C})$	2.39	3.4	$K^T(30^\circ\text{C})$	2.05	2.4
ΔH_r° (kJ.mol ⁻¹)	-5.66	25.6	ΔH_r° (kJ.mol ⁻¹)	-4.17	26.9
Perhydrolysis by Sulphuric Acid			Perhydrolysis by Sulphuric Acid		
Parameters	Estimated	Errors (%)	Parameters	Estimated	Errors (%)
k_{ave} (l.mol ⁻¹ .s ⁻¹)	$1.70 \cdot 10^{-3}$	3.7	k_{ave} (l.mol ⁻¹ .s ⁻¹)	$2.00 \cdot 10^{-3}$	3.3
Ea (kJ/mol)	75.58	3.3	Ea (kJ/mol)	44.24	6.9
δ (l.mol ⁻¹)	0.40	33.2	δ (l.mol ⁻¹)	1.33	4.8
Perhydrolysis by Amberlite IR-120			Perhydrolysis by Amberlite IR-120		
Parameters	Estimated	Errors (%)	Parameters	Estimated	Errors (%)
k_{ave} (l.mol ⁻¹ .s ⁻¹)	$0.99 \cdot 10^{-3}$	12.7	k_{ave} (l.mol ⁻¹ .s ⁻¹)	$0.91 \cdot 10^{-3}$	26.2
Ea (kJ/mol)	42.5	7.0	Ea (kJ/mol)	51.4	4.6
K(AA) (l.mol ⁻¹)	0.89	49.1	K(PA) (l.mol ⁻¹)	1.39	80.5

From Table 15, it can be noticed that the intrinsic rate constant for the synthesis of peroxyacetic acid is slightly lower than for the synthesis of peroxypropionic acid in the case of homogeneous catalysis by sulphuric acid. By comparing the kinetics of both systems within the temperature range of 20-70°C estimated from the homogeneous kinetic model (Fig. 25), it can be noticed that the estimated intrinsic kinetic rate constants are close within the temperature range of 20-50°C. Only, when the temperature of the reaction is higher than 50°C, then we observed $k_{\text{int}}(\text{AA}) > k_{\text{int}}(\text{PA})$. Due to the similarity of both molecules, it is difficult to estimate accurately the intrinsic rate constants. Even if the kinetic model for the

homogeneous catalysis system is statistically correct, it could have a tendency to underestimate the rate constant of acetic acid perhydrolysis or overestimate the rate constant of propionic acid perhydrolysis.

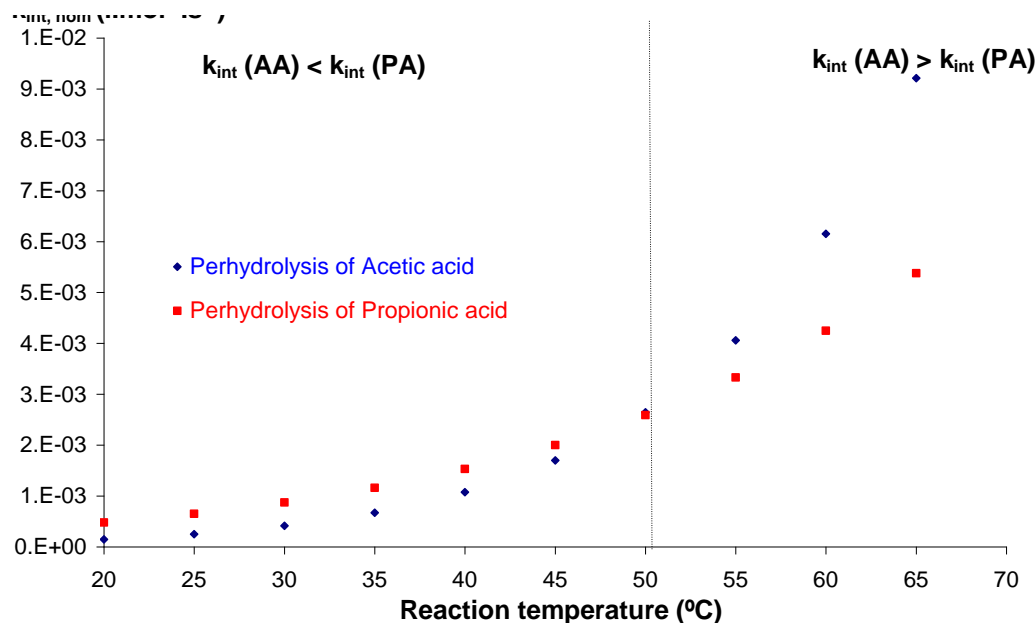


Figure 25. Intrinsic rate constant versus temperature in case of perhydrolysis catalysed by sulphuric acid.

For the intrinsic kinetic constant in case of heterogeneous catalysts (Table 15), one can notice also that the difference between acetic and propionic acid perhydrolysis is negligible, and the values of the adsorption coefficient for propionic and acetic acid estimated by the model are not statistically precise to make any accurate interpretations.

Additional kinetic study and modelling should be carried out with different carboxylic acids with higher carbon numbers. However, by increasing the carbon number, a biphasic system appears, which increases the difficulty to estimate the intrinsic rate constant. This study can represent a good start for more thorough investigations.

Perhydrolysis of fatty acids

The perhydrolysis of isobutyric and valeric acids was studied by using Amberlite IR-120 at 45°C. During the synthesis of peroxyvaleric acid, two phases were present from the beginning until the end of the reaction (around 400 min). However, in case of isobutyric acid perhydrolysis, the system was biphasic in the beginning of the reaction, but after two hours at 45°C, the system appeared to be monophasic. For the sake of simplicity, only the evolution of the peroxide organic compounds in the organic phase is displayed in Fig. 26.

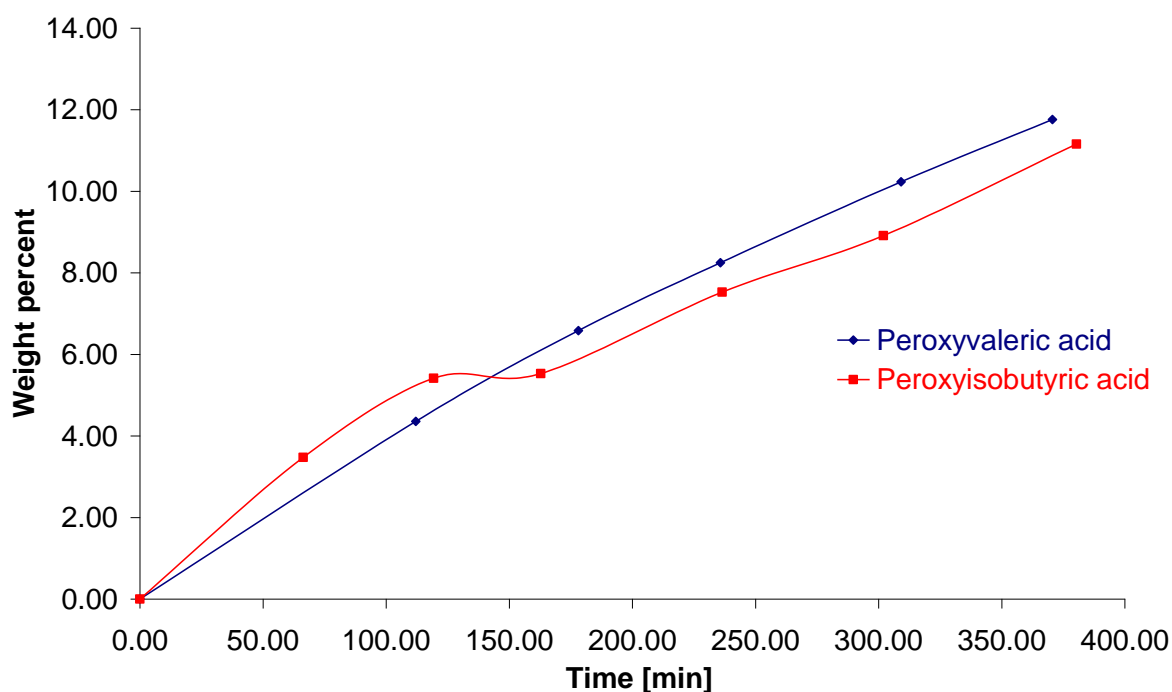


Figure 26. Synthesis of peroxyfatty acids at 45°C with Amberlite IR-120 at 50 g/l.

The aqueous phase of the experiment carried out with valeric acid was analysed and the results are displayed in Table 16. From the table 16, it can be noticed that no traces of peroxyvaleric acid was detected in the aqueous phase.

Table 16. Evolution of the compounds in the aqueous phase

	t = 0 min	t = 375 min
Valeric acid (wt.%)	3.87	3.71
Hydrogen peroxide (wt.%)	33.22	29.06
Water (wt.%)	62.91	67.22
Peroxyvaleric acid (wt.%)	0.00	0.00

Further investigation relating to the solubility, phase evolution, sampling and experimental setup is needed to propose a complete kinetic study of these peroxyfatty acids. The preliminary study reported here, however, shows that it is possible to prepare long-chain peroxydicarboxylic acids by using the heterogeneous acid catalyst.

Calorimetry

The purpose of the calorimetric measurements was to check, whether the reaction enthalpy of the perhydrolysis of acetic and propionic acids are in the same range of magnitude. The heterogeneous catalyst (Amberlite IR-120) was used instead of homogeneous catalyst for practical reasons. It is easier to fill the calorimetric cells with solid acid catalyst than with sulphuric acid (Figure 6).

Figure 27 and 28 represent the evolution of heat as a function of time in case of the perhydrolysis of acetic acid at 45°C and propionic acid at 60°C, respectively.

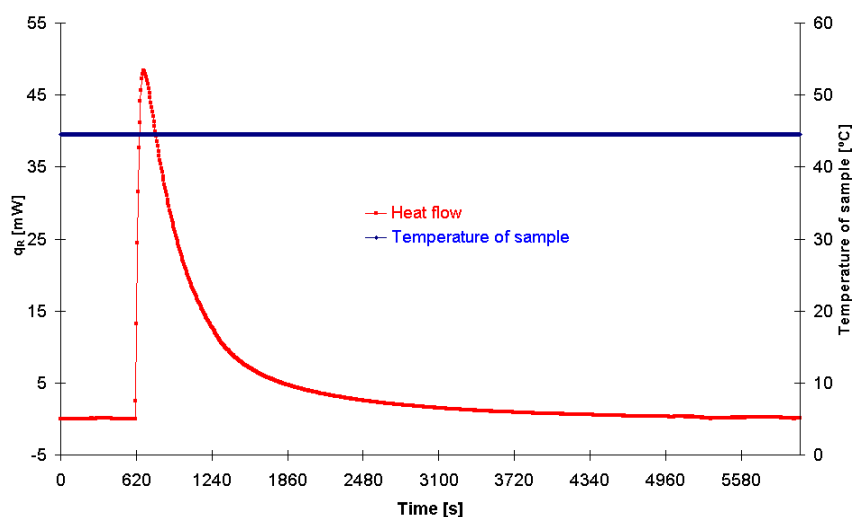


Figure 27. Heat profiles for the perhydrolysis of acetic acid at 45°C.

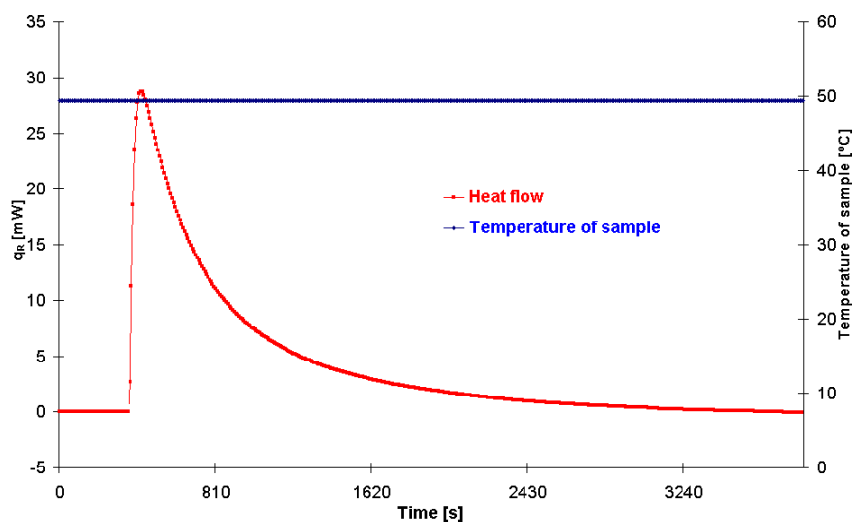


Figure 28. Heat profiles for the perhydrolysis of acetic acid at 50°C.

By integrating the graphs of the Fig. 27 and 28, one can get the amount of heat released by the reaction, Q_r (J). To get the enthalpy of reaction, one should divide Q_r by the reaction extent, ξ :

$$\Delta H_R^\circ = \frac{Q_R}{\xi} \quad (35)$$

Table 17 presents the values of the enthalpy of reaction calculated from the calorimetric experiments. Table 18 proposes a summary of the reaction enthalpies based on literature and modelling.

Table 17. Calorimetric results

	Q_R [J]	ξ [mol]	ΔH_R° [kJ/mol]
Perhydrolysis of acetic acid	-26.68	2.42E-03	-11.03
Perhydrolysis of propionic acid	-15.30	1.58E-03	-9.70

Table 18. Enthalpy of reaction for perhydrolysis of carboxylic acid

	ΔH_R° [kJ/mol]
Perhydrolysis of acetic acid [24]	-13.7
Perhydrolysis of acetic acid [63-64]	-3.62
Perhydrolysis of acetic acid [Modelling]	-5.66
Perhydrolysis of propionic acid [Modelling]	-4.17

Due to the small amount (ca. 1.45 g) of liquid solution used during the calorimetric experiment, it was difficult to estimate accurately the value of ξ . For that reason, the value of ΔH_R^0 obtained by calorimetric measurement are higher than in case of our kinetic modelling.

Dul'Neva and Moskvina [24] have estimated the value of ΔH_R^0 for the acetic acid perhydrolysis to be equal to -13.7 kJ/mol, which is higher than the results obtained by the kinetic modelling. During their study, Dul'Neva and Moskvina did not take into account the non-ideality of the reaction mixture, which could explain this overestimation.

Havel et al. [64] have measured the heat of formation of peroxyacetic acid in liquid phase, thus one can calculate the reaction enthalpy of the acetic acid perhydrolysis, which is close to the one obtained by the kinetic modelling.

The values of ΔH_R^0 obtained by kinetic modelling are more accurate because the non-ideality of the solution is taken into account. However, the results obtained by calorimetric measurements show that the value of ΔH_R^0 are of the same order of magnitude.

Decomposition of PCAs

In this chapter, a study of the stability of the PPA is reported, by using an original method described in the experimental section. The decomposition of peroxyacetic and peroxypropionic acids takes place in the liquid phase, but the main products of decomposition, CO₂, and O₂ are transferred to the gas phase. Thus, the decomposition kinetics can be determined by a rapid on-line analysis of the gas phase. The mass balances for the components in gas and liquid phase as well as the kinetic modelling are described here.

5.1 Mass balances for gas and liquid phases

The mass balance of an arbitrary component (*i*) in the liquid phase is written in a quantitative form as follows:

$$\dot{n}_{Li,in} + r_i V_{0L} = \dot{n}_{Li,out} + N_{Li} A + \frac{dn_{Li}}{dt} \quad (36)$$

The law of Fick is used to describe the interfacial component flux (N_{Li}):

$$N_{Li} = k_{Li} \cdot (c_{Li} - c_{Li}^*) \quad (37)$$

where the asterisk denotes the equilibrium concentration at the gas-liquid interface. The equilibrium concentration is *de facto* determined by the partial pressure of the component in the gas phase.

The volume of the reaction mixture can be regarded as constant. Thus the amount of substance (n_{Li}) and concentration (c_{Li}) are related by $n_{Li} = c_{Li} V$, which gives

$$\frac{dn_{Li}}{dt} = \frac{dc_{Li}}{dt} V \quad (V = \text{constant}).$$

Because the liquid phase is in batch, we get $\dot{n}_{Li,in} = \dot{n}_{Li,out} = 0$ in eq. (36). Furthermore, the mass transfer area-to-volume ratio is denoted by

$$\frac{A}{V_{0L}} = a_0 \quad (38)$$

Consequently, the mass balance of a component in the liquid phase is simplified to

$$\frac{dc_{Li}}{dt} = r_i - k_{Li} a_0 (c_{Li} - c_{Li}^*) \quad (39)$$

where the derivative dc_{Li}/dt stands for the accumulation of a component i . For non-volatile components, the mass transfer coefficient k_{Li} is zero.

The concentration at the liquid-gas interface c_{Li}^* is obtained from solubility data of gases, by using the modified Henry's law and neglecting the mass transfer

$$\text{resistance in the gas side: } K_i = \frac{c_{Gi}^*}{c_{Li}^*} \approx \frac{c_{Gi}}{c_{Li}^*}$$

The mass balance of a gas-phase component is given by

$$N_{Li} A = \dot{n}_{Gi} + \frac{dn_{Gi}}{dt} = c_{Gi} \dot{V}_G + \frac{dn_{Gi}}{dt} \quad (40)$$

According to (37) and (38), we obtain

$$k_{Li} a_0 V_{0L} (c_{Li} - c_{Li}^*) = c_{Gi} \dot{V}_G + \frac{dn_{Gi}}{dt} \quad (41)$$

Since the volume of the gas phase is constant and the relation $n_{Gi} = c_{Gi} V_G$

($V_G = \text{constant}$) is valid, we get: $\frac{dn_{Gi}}{dt} = V_G \frac{dc_{Gi}}{dt}$, which gives

$$\frac{dc_{Gi}}{dt} = \frac{k_{Li} a_0 V_{0L}}{V_G} (c_{Li} - c_{Li}^*) - \frac{c_{Gi}}{\tau_G} \quad (42)$$

where $\tau_G = \frac{V_G}{\dot{V}_G}$ and $V_G = V_{inert}$

The behaviour of a component in the liquid and gas phase is described by equations (39) and (42). For non-volatile components, $k_{Li} = 0$ and just the liquid-phase balance is needed. Other simplifications can be done, since the reactions itself are slow compared to the interfacial mass transfer in the vigorously stirred tank [37].

We can presume that the reactions take place essentially in the bulk phase and neglect reactions in the liquid film. The following simplifying notations are introduced:

$$k_{Li}a_0 = \kappa_L, \quad c_{Li} - c_{Li}^* = \Delta c \text{ and } \frac{V_{0L}}{V_G} = \alpha$$

By editing the equation (39) and (42) by the above notations we get

$$\alpha \left(\frac{dc_{Li}}{dt} \right) = (r_i - \kappa_L \Delta c) \alpha \quad (43)$$

and

$$\frac{dc_{Gi}}{dt} = \kappa_L \alpha \Delta c - \frac{c_{Gi}}{\tau_G} \quad (44)$$

After adding equations (43) and (44), we get

$$\alpha \left(\frac{dc_{Li}}{dt} \right) + \left(\frac{dc_{Gi}}{dt} \right) = \alpha r_i - \frac{c_{Gi}}{\tau_G} \quad (45)$$

Mass transfer is assumed to be rapid compared to the kinetic phenomena. Thus, the concentrations in gas and liquid bulk phases are related by the equilibrium ratio (K_i),

$$c_{Li} = \frac{c_{Gi}}{K_i}$$

This expression for c_{Li} is substituted into equation (45) giving following equation for the gas-phase concentration

$$\frac{dc_{Gi}}{dt} = \frac{\alpha r_i - \frac{c_{Gi}}{\tau_G}}{\frac{\alpha}{K_i} + 1} \quad (46)$$

where $\alpha = \frac{V_{0L}}{V_G}$ and $c_{Li} = \frac{c_{Gi}}{K_i}$ for all components in the calculation of r_i .

For the non-volatile components in liquid phase, we have:

$$\frac{dc_{Li}}{dt} = r_i \quad (47)$$

The benefit of the simplified mathematical model equations (46) - (47) is that just kinetic and equilibrium parameters are needed, but the mass-transfer parameters are excluded. The decomposition process can now be described quantitatively by assuming a kinetic model to obtain the rates (r_i).

5.2 Kinetic experiments and modelling

Figure 29 shows the decomposition of PPA versus time at different reaction temperature.

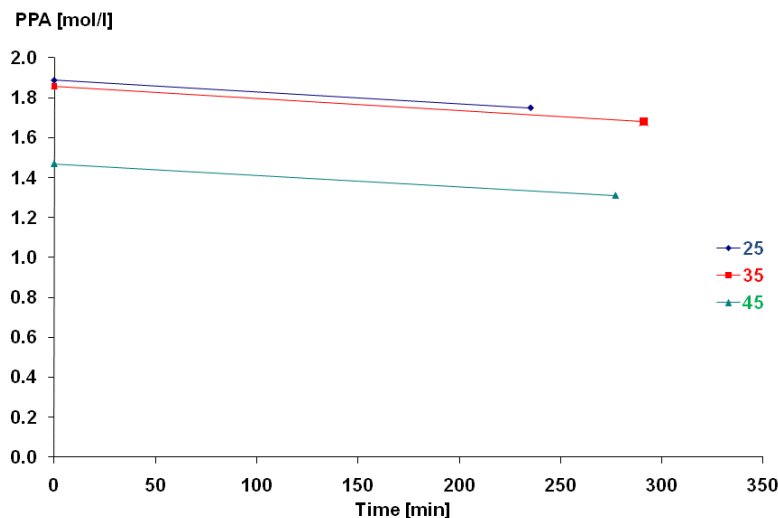
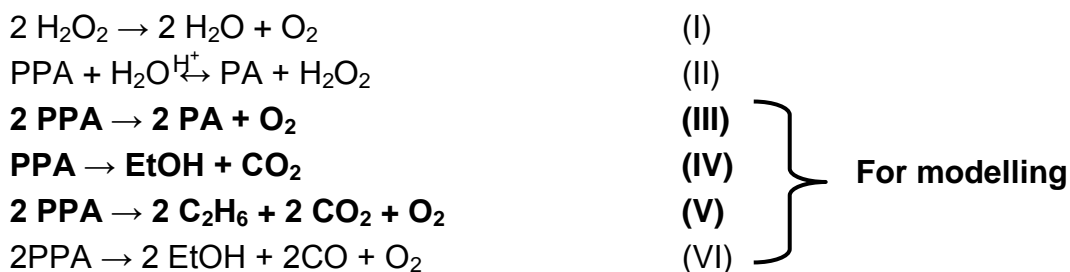


Figure 29. Evolution of peroxypropionic acid in the liquid phase.

From Figure 29, one can notice that PPA decomposes during the reaction, the initial rate of PPA decomposition was about $6 \times 10^{-4} \text{ mol.l}^{-1}.\text{min}^{-1}$, indicating a very slow reaction.

Based on our experimental data, the following overall stoichiometry was assumed in the quantitative treatment of the data:



Because equation III is a linear combination of equations I and II, the rate expression for these reactions was replaced by the rate expression of reaction III.

The overall reactions do not reflect the intrinsic reaction mechanism, because complicated radical reactions take place on the molecular level. For this reason, an empirical approach was proposed for the rate expression of the reactions, for instance:

$$R_j = \frac{k_j \cdot c_{PPA} \cdot c_{H_2SO_4}}{1 + K_{O_2} c_{O_2}} \quad (48)$$

where j represents the index of the reaction.

According to literature, molecular oxygen acts as a radical scavenger and thus retards the rates of the decomposition. The parameter K_{O_2} takes into account this effect in equation (48).

The solubility parameters K_i were determined from separate solubility measurements [65]. As previously, the temperature dependences of the rate constants were described by a modified Arrhenius equation. The parameter estimation was carried out by Modest software, by using Simplex and Levenberg-Marquardt algorithms. The ordinary differential equations (46) and (47) were solved repetitively during the parameter estimation by the backward difference method designed for stiff differential equations. For the modelling, reaction VI was ruled out because the kinetic model was better without that reaction. Only the rate constants (k_3 , k_4 and k_5 including their temperature dependencies) and the parameter K_{O_2} were estimated. The results of the modelling effort are summarized in Table 19 and some data fitting results are shown in Figure 30.

Table 19. Kinetic parameters of the model at $T_{ave} = 35^\circ\text{C}$

Parameters	Estimated	Error (%)
k_3 (l.mol ⁻¹ .s ⁻¹)	$0.172 \cdot 10^{-04}$	44.5
Ea_3 (kJ.mol ⁻¹)	132	4.6
k_4 (l.mol ⁻¹ .s ⁻¹)	$0.177 \cdot 10^{-04}$	44.9
Ea_4 (kJ/mol)	150	3.4
k_5 (l.mol ⁻¹ .s ⁻¹)	$0.677 \cdot 10^{-06}$	51.4
Ea_5 (kJ/mol)	13.9	208.1
K_{O_2}	1790	53.5

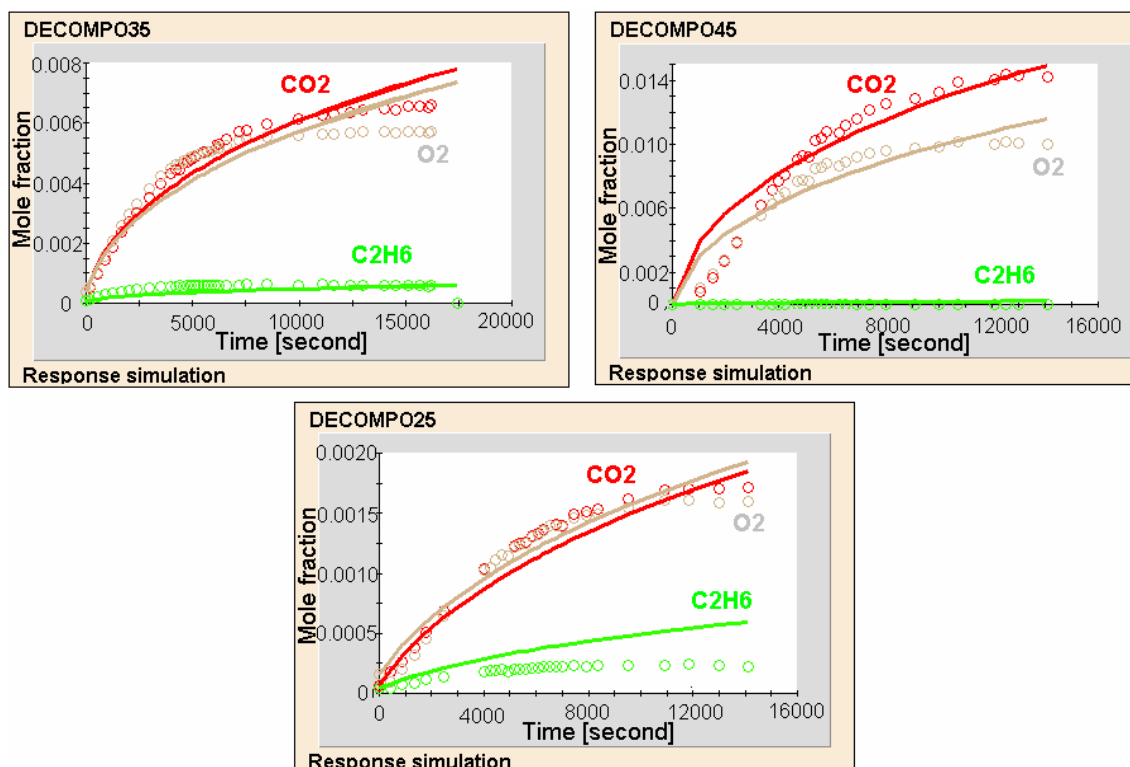


Figure 30. Fit of the model to the experiments (mole fraction versus time) carried out with 15 wt.% PPA-solutions at temperatures 25-45°C.

The coefficient of determination of this model became 99.6%, so the values calculated are statistically reliable. If we look at the estimated relative standard errors, one can see that except for the activation energy of reaction V, all of them are low. The kinetic parameters estimated indicate that reactions III and IV are the most important ones.

Comparison with decomposition of PAA

Table 20 compares the kinetics of decomposition of peroxyacetic [71] and peroxypropionic acids.

Table 20. Kinetics of decomposition of peroxycarboxylic acids at 45°C

	PAA	PPA
1) $\text{PCA} + \text{H}_2\text{O} \leftrightarrow \text{CA} + \text{H}_2\text{O}_2$ k_1 (l.mol ⁻¹ .s ⁻¹) Ea (kJ/mol)	2.45E-06 80	5.86E-04 45.39
2) $2 \text{ PCA} \rightarrow 2 \text{ CA} + \text{O}_2$ k_2 (l.mol ⁻¹ .s ⁻¹) Ea (kJ/mol)	5.19E-04 117	1.72E-05 132
3) $\text{PCA} \rightarrow \text{ROH} + \text{CO}_2$ k_3 (l.mol ⁻¹ .s ⁻¹) Ea (kJ/mol)	1.06E-04 115	1.77E-05 150
4) $2 \text{ PCA} \rightarrow 2 \text{ Alcane} + 2 \text{ CO}_2 + \text{O}_2$ k_4 (l.mol ⁻¹ .s ⁻¹) Ea (kJ/mol)	5.28E-06 117	6.77E-07 13.9

From Table 20, one can notice that the decomposition of PPA is mainly due to the equilibrium reaction (reaction 1) based on the kinetic parameters. By analysing the study done by Musakka et al. [71], the other difference is that the main decomposition products in the gas phase is oxygen in case of PAA decomposition whereas carbon dioxide is the main decomposition product in the gas phase in case of PPA decomposition. This observation might be due to the fact that the spontaneous decomposition of peroxycarboxylic acid is easier in case of PAA than PPA, due to a lower energy of activation for the reaction 2 in case of PAA than in case of PPA.

The accuracy of the kinetics parameters for reaction 2, 3 and 4 presented in Table 20 are quite poor. For that reason, this table should be used for a qualitative comparison. The purpose of this study was to show that the spontaneous decomposition of peroxyacetic and peroxypropionic acid in a temperature range 25-45°C is negligible in presence of a catalyst acid. According to Zhao et al. [38], the spontaneous decomposition of peroxyacetic acid can be assumed to be negligible at temperatures lower than 55°C.

Fixed bed reactor

The objective of this section is to demonstrate that the development of a continuous process concept based on the use of heterogeneous catalysts for manufacture of peroxy-carboxylic acids is possible, and to provide a comparison with the kinetics obtained in batch and continuous modes. However, to make this comparison, the determination of nature of the flow regime, volume of liquid phase, residence time, and diffusion phenomena is needed.

6.1 Residence time distribution

The study of the flow pattern in order to determine the residence time distribution (RTD) is one of the most important parts of this section. Indeed, to make a real comparison between batch and continuous operations, it is important to determine the mean residence time and the real volume of liquid in the system. Pulse and step experiments were used to determine the RTD and the mean residence time. The tracer molecule should have the same behaviour as the reactant and the product molecule, without interfering with the catalyst, cation exchange resin. For the sake of comparison, propionic acid, hydrogen peroxide and hydrochloric acid were used as tracer molecules.

6.1.1 Pulse experiment

Pulse experiment with HCl as a tracer molecule

HCl is a strong electrolyte and does not interact with the resins by leaching the sulphonic, which is not the case of NaCl for example. Around 1.3-1.6 gram of a solution at 0.02 M of HCl was introduced at the inlet of the tube reactor during 2-5 s. Tracer experiments were carried out at two different temperatures: 30°C and 50°C, and different flow rates. The concentration of the tracer was followed on-line by conductivity.

Due the small concentration of the HCl solution, the following relationship was used to determine the concentration,

$$\sigma = c\lambda \quad (49)$$

where σ is the measured conductivity [S.m^{-1}], c is the concentration [mol.m^{-3}] and λ [$\text{S.m}^2.\text{mol}^{-1}$] is the molar conductivity.

Figure 31 displays the E-curves registered at different flow rates. The parameter E is defined as:

$$E = \frac{C_{\text{pulse}} * F}{n_0} \quad (50)$$

where C_{pulse} is the concentration of tracer element at the outlet, F is the flow rate of the fluid and n_0 is the amount of tracer introduced in the system.

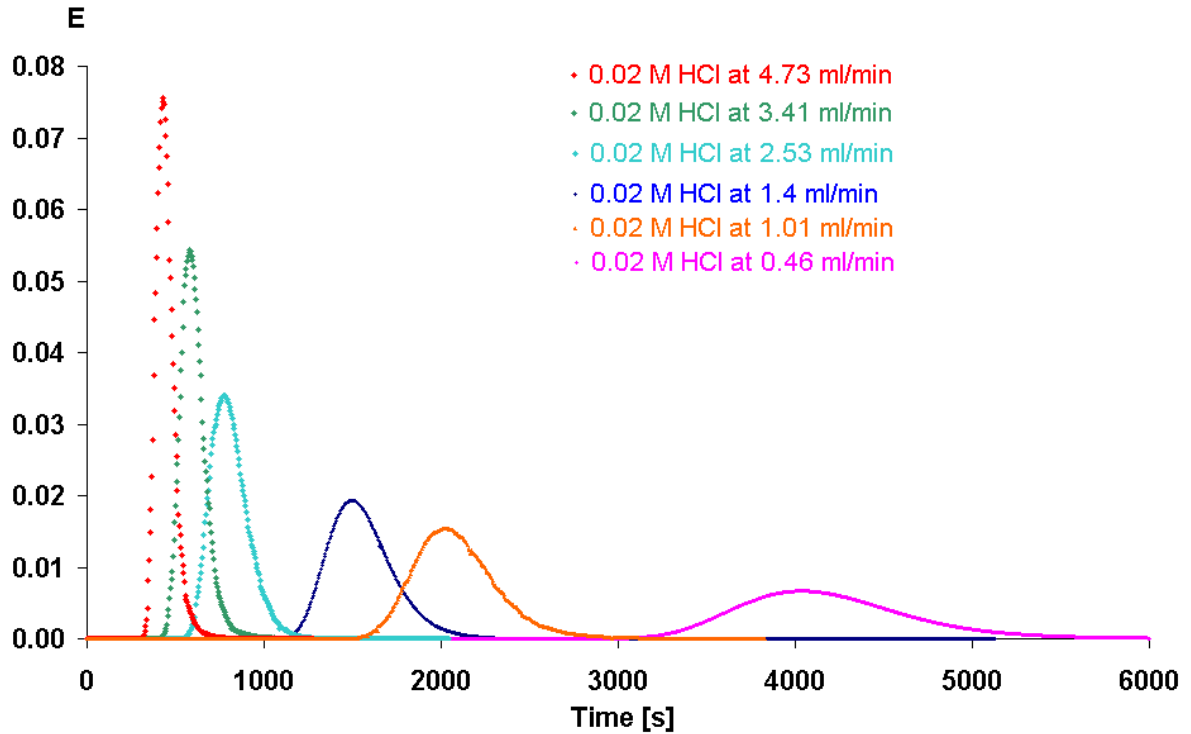


Figure 31. E-curves at 30°C by using HCl as a tracer.

One can notice that the distribution is symmetric. The interval of the measurement was the same. The mean residence time \bar{t} can be calculated from the experimental data:

$$\bar{t} = \frac{\sum_i t_i C_{\text{pulse},i} \Delta t_i}{\sum_i C_{\text{pulse},i} \Delta t_i} \quad (51)$$

The mean residence time and the flow are related by:

$$\bar{t} = \frac{V_L}{F} \quad (52)$$

where V_L represents the void volume of the tube reactor, i.e. the volume of the liquid. Figure 32 represents the flow rate versus inverse of the mean residence time at 30 and 50°C. The mean residence time was obtained from eq. (51).

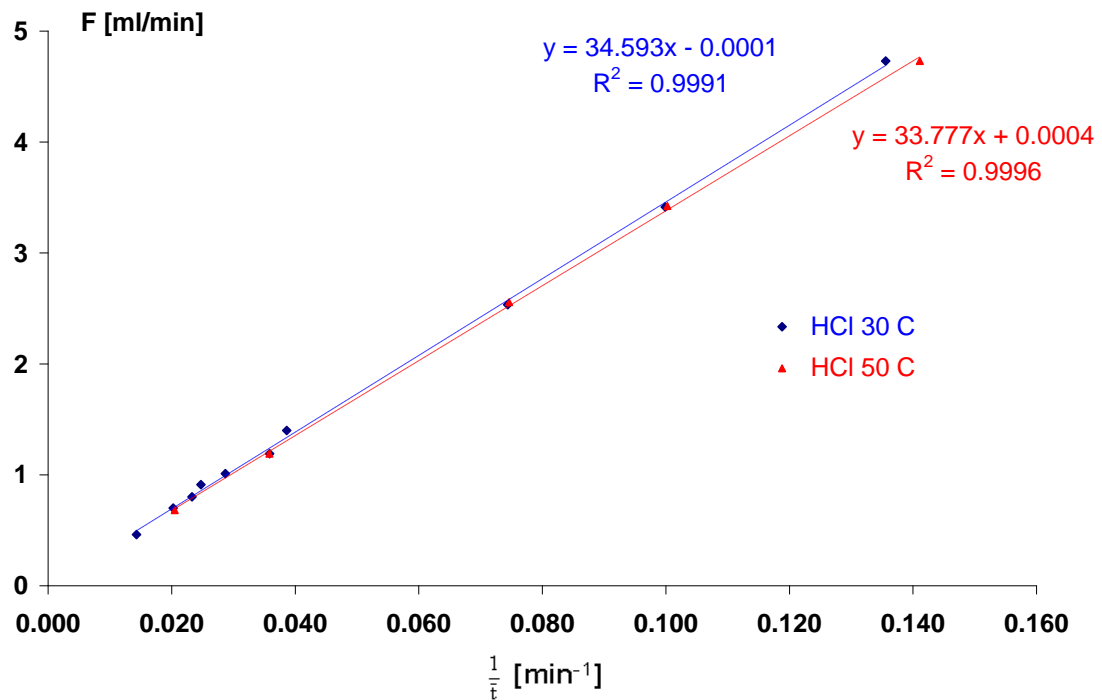


Figure 32. Flow rate versus inverse of mean residence time.

As you can notice, the flow pattern behaviour does not depend to the temperature, and the liquid volume in the reactor can be assumed to be in the range of 33.8-34.5 ml according to the pulse experiment with HCl.

Levenspiel [66] has introduced the dimensionless group $\frac{D}{uL}$, where D [$\text{m}^2.\text{s}^{-1}$] is the axial dispersion coefficient, L the length of the vessel [m] and u the superficial velocity [$\text{m}.\text{s}^{-1}$]. This parameter is called vessel dispersion number, and measures the extent of the axial dispersion. The reciprocal value of $D/(uL)$ is called Péclet number (Pe). Thus,

$\frac{D}{uL} \rightarrow 0$ negligible dispersion, hence plug flow

$\frac{D}{uL} \rightarrow \infty$ large dispersion, hence mixed flow.

Table 21 gives the value of this parameter according to the mean residence time obtained from the pulse experiment with HCl at 302 and 402 K.

Table 21. Evolution of the parameter $\frac{D}{uL}$ and Pe

Temperature [°C]	\bar{t} [min]	$\frac{D}{uL}$	Pe
30	49	0.007	143
30	29	0.008	122
30	14	0.009	116
30	10	0.007	136
30	7	0.008	130
50	50	0.006	168
50	28	0.007	138
50	13	0.008	119
50	10	0.011	91
50	7	0.011	91

From Table 21, one can notice that the value of $\frac{D}{uL}$ is low and it does not depend on the temperature or mean residence time. According to Levenspiel [66], the dispersion can be assumed to be small if the $\frac{D}{uL}$ is lower than 0.01. Thus, one can conclude that the axial dispersion is negligible in our system.

Pulse experiment carried out with propionic acid as a tracer molecule

Propionic acid was used as a tracer molecule to study the behaviour of a carboxylic acid molecule in the fixed-bed reactor. As with HCl tracer experiment, the conductivity was measured on-line. However, due to the low degree of dissociation of this molecule, a more concentrated solution was used than in the case of HCl solution and the relation (49) is not valid. Around 1.13 – 1.15 g of a solution of PA at 13.36 M was introduced at the inlet during 2-5 s.

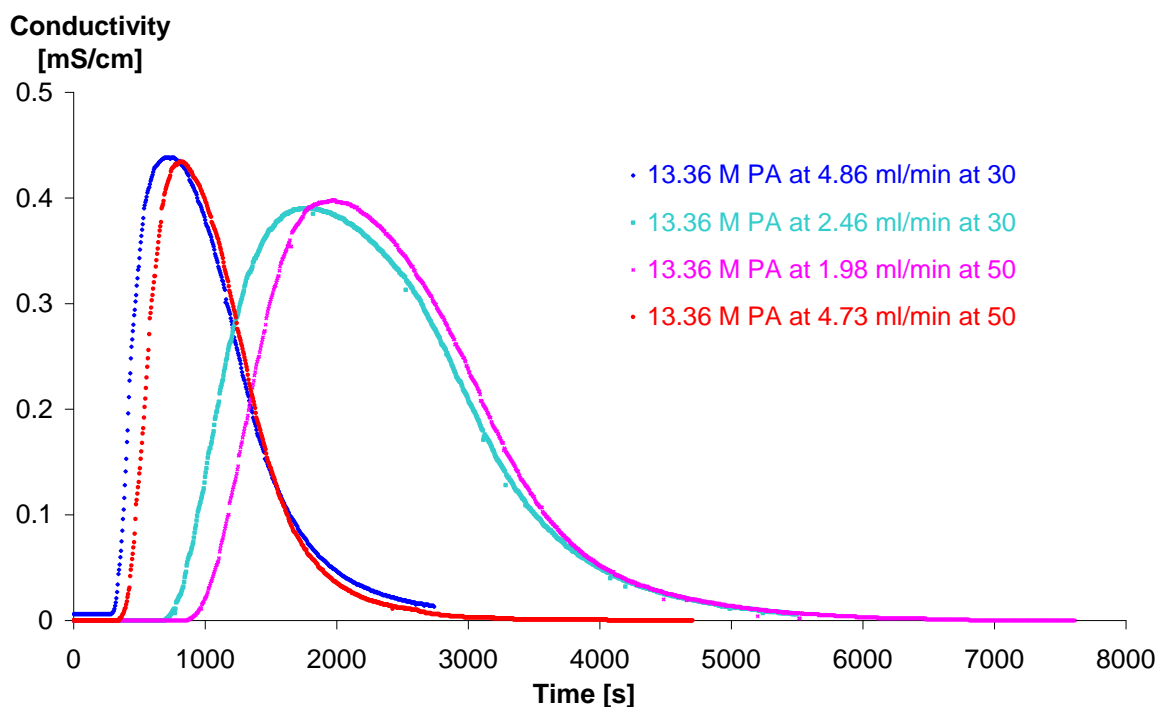


Figure. 33 Pulse curve by using propionic acid as a tracer molecule at 30°C.

The E-curve cannot be obtained with a high accuracy due to the high concentration of PA, but the determination of the volume of liquid is reachable. From Figure 33, one can notice that the curves are asymmetric, which can indicate the presence of adsorption phenomenon on the resin.

Figure 34 represents the flow rate versus the inverse of mean residence time at 30 and 50°C in case of propionic acid as a tracer.

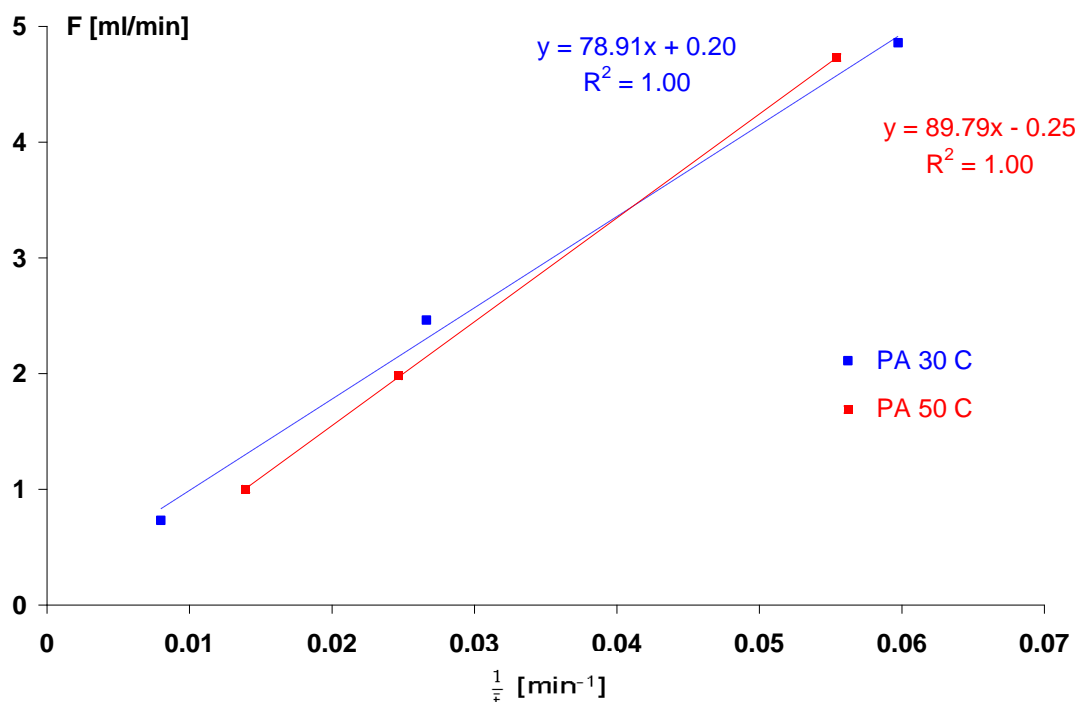


Figure 34. Flow rate versus inverse of mean residence time with propionic acid.

According to Figure 34, the flow pattern is not the same at 30 and 50°C, indeed the volume of liquid in the reactor varies between 78.9 and 89.8 ml. From this data, one can notice that PA is not an inert tracer molecule toward the resin. Compared to the HCl pulse experiment, the volume of liquid calculated is higher due to a longer residence time, which can be attributed to the adsorption of propionic acid on the sulphonic group of the resins. In this case, the vessel dispersion number was estimated to be in the range 0.04-0.09.

6.1.2 Step experiment

A solution of 32 wt.% of hydrogen peroxide was used in the step experiment carried out at 30°C. Figure 35 shows the response curves with an initial flow rate of 0.72 ml/min.

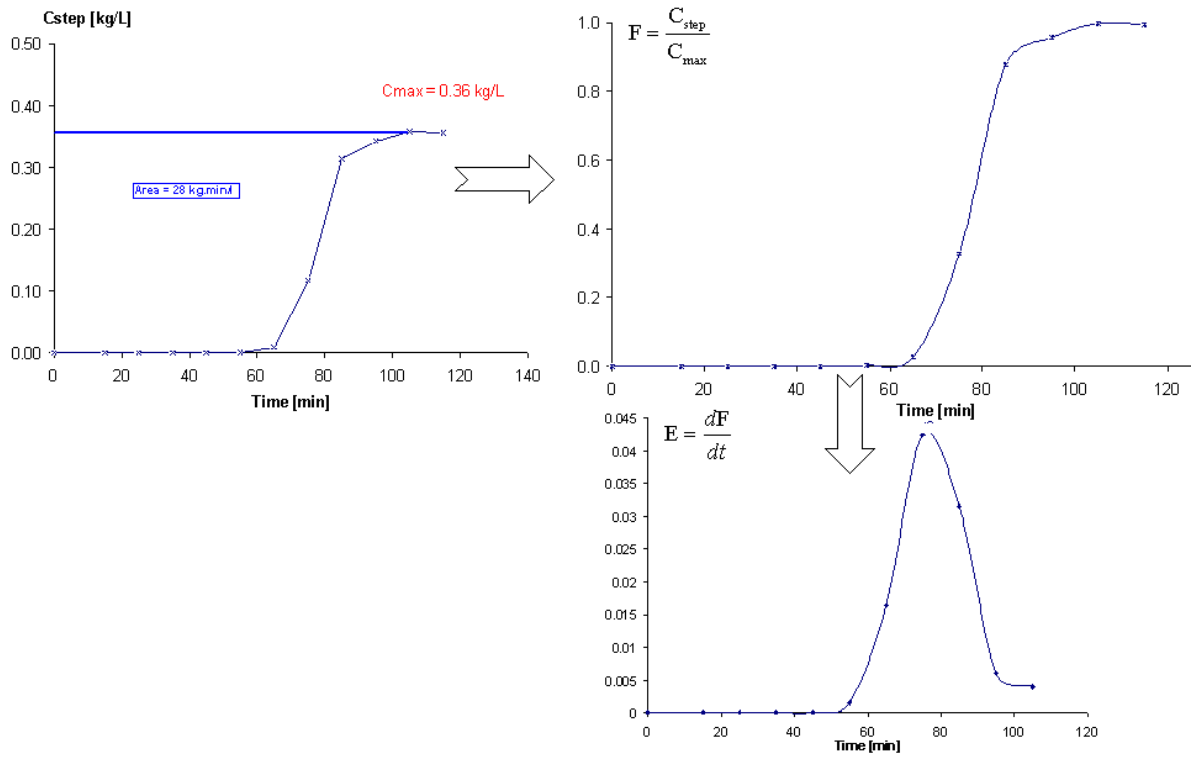


Figure 35. The experiment with C_{step} curves and transformation to F-curves and E-curves.

According to Levenspiel [66], the area is equal to:

$$A = \bar{t} * C_{\text{max}} \quad (53)$$

The E-curves obtained are more symmetrical than the ones obtained with propionic acid as a tracer molecule. The volume of the liquid phase is equal to 56 ml and the parameter $\frac{D}{uL}$ is equal to 0.007. Thus, one can notice that hydrogen peroxide has less interference with the resins than PA, and the absorption is less in that case.

6.1.3 Comparison

By taking into account the volume occupied by the glass balls, Amberlite IR-120 and its porosity in the reactor, then the volume of void should be equal to 130.6 ml. Figure 35 shows the flow rate versus the inverse mean residence time \bar{t} obtained with tracer experiments and inverse of space-time τ based on the characteristic of the reactor.

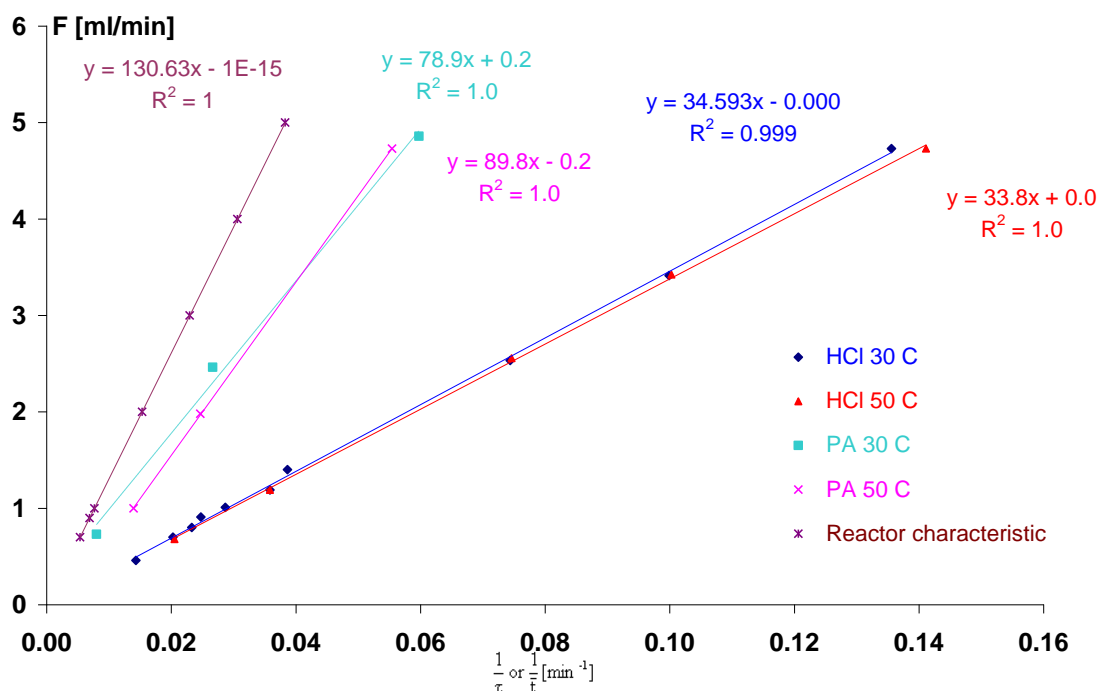


Figure 36. Flow rate versus inverse of mean residence time.

From this Figure, one can notice that the determination of the void volume depends on the nature of the tracer molecules. The difference obtained with PA is due to the adsorption of PA on the resin.

To determine the true reactor volume between the results based on the reactor characteristics and HCl pulse experiments, water was introduced at the outlet of the reactor and the volume was measured. The volume obtained by this simple method is equal to 28.24 ml, which is close to the value given by HCl pulse experiment.

Table 22. Summary

F [ml/min]	Tracer molecule	Volume of void [ml]	\bar{t} or τ [min]	$\frac{D}{uL}$
0.7	HCl	34.5	49.35	0.007
0.73	PA	91.4	125.14	0.077
0.72	Hydrogen peroxide	56.2	78.19	0.007
0.72	Based on reactor characteristic	130.6	181.43	x

Table 22 summarizes the different volume of void, mean residence time, $\frac{D}{uL}$ number. As revealed by this table, the parameter $\frac{D}{uL}$ is low, which implies that axial dispersion is negligible. The void volume is 34.5 ml, based on the pulse experiment and water measurement.

6.2 Estimation of the pressure drop [67-69]

The pressure drop for a fluid flowing through a column packed with solid particles is commonly evaluated by means of Ergun equation:

$$\frac{\Delta P}{\Delta L} = A \frac{\epsilon_{RP}^2}{(1-\epsilon_{RP})^3} \frac{\mu_f}{\bar{d}_p^2} u_f + B \frac{\epsilon_{RP}}{(1-\epsilon_{RP})^3} \frac{\rho_f}{\bar{d}_p} u_f^2 \quad (54)$$

where,

ϵ_{RP} : fraction of solid in the reactor,

$1-\epsilon_{RP}$ void fraction in reactor,

$\bar{d}_p = \frac{6\epsilon_{RP}}{A_s}$, mean diameter particle and A_s is external surface area of particle by

volume, m^2/m^3 ,

μ_f : fluid viscosity, Ns/m^2 ,

ρ_f : fluid density, kg/m^3 ,

u_f : superficial velocity, m/s .

According to Trambouze et al. [68], in case of liquid phase system, the parameters A and B could change according to the nature of the liquid. According to Villermaux [69], if $\frac{Re_p}{\epsilon_{RP}} < 500$, then A and B are equal to 150 and 1.75, respectively.

The volume of the reactor is equal to 170 ml and the volume of void is 34.5 ml, then ϵ_{RP} is equal to 0.8. Based on the characteristics of quartz and Amberlite IR-120 (Table 6) thus \bar{d}_p is equal to $7.89.10^{-4} m$.

The Reynold number is defined as:

$$Re = \frac{d_{reactor} u_f \rho_f}{\mu_f} \text{ for the reactor} \quad (55)$$

$$Re_p = \frac{\bar{d}_p u_f \rho_f}{\mu_f} \text{ for the particle} \quad (56)$$

Table 23 presents the different values of Reynolds numbers for the reactor and particles, at different flow rates.

Table 23. Reynolds numbers at 30°C

Inlet flowrate ml/min	Re	Re _P
0.84	1.2	0.1
0.71	1.1	0.0
1.15	1.7	0.1
2.63	3.9	0.2

One can notice that $\frac{Re_p}{\varepsilon_{RP}} < 500$, then A is equal to 150 and B to 1.75. Moreover, the Re number for the reactor is low, which implies that the flow is within the laminar regime. By using eq. (54), Figure 37 was plotted.

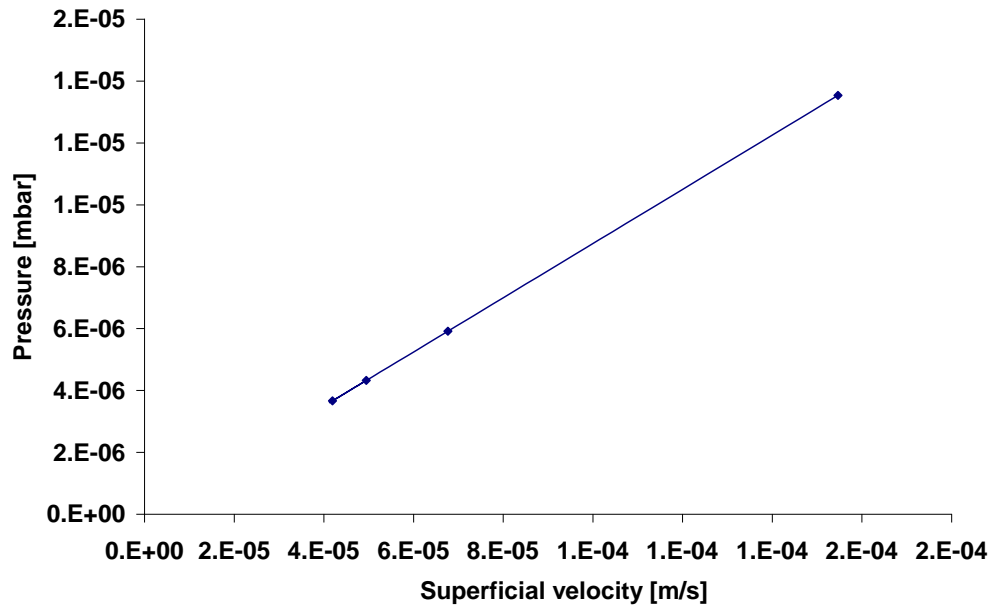


Figure 37. Results from pressure drop estimation from eq. (54).

From Figure 37, it can be observed that the pressure drop can be neglected.

6.3 Experimental results

The purpose was to verify that the synthesis of peroxycarboxylic acid through a catalytic continuous reactor is possible. A solution of carboxylic acid (propionic or acetic acid) and hydrogen peroxide were pre-mixed before entering the fixed-bed reactor at 30°C. The synthesis of peroxycarboxylic acid in the pre-mixing solution for 4.5h can be assumed negligible (i.e., conversion of PA is less than 0.7%), due to the slow kinetics in the absence of an added acid catalyst and the low temperature. Samples were withdrawn from different parts of the reactor. No decomposition of hydrogen peroxide or peroxycarboxylic acid was noticed during the experiment.

6.3.1 Experiments carried out with propionic acid

Flow rate analysis

Figure 38 depicts the flow rate of the fluid before the inlet and at the outlet at different time-on-streams.

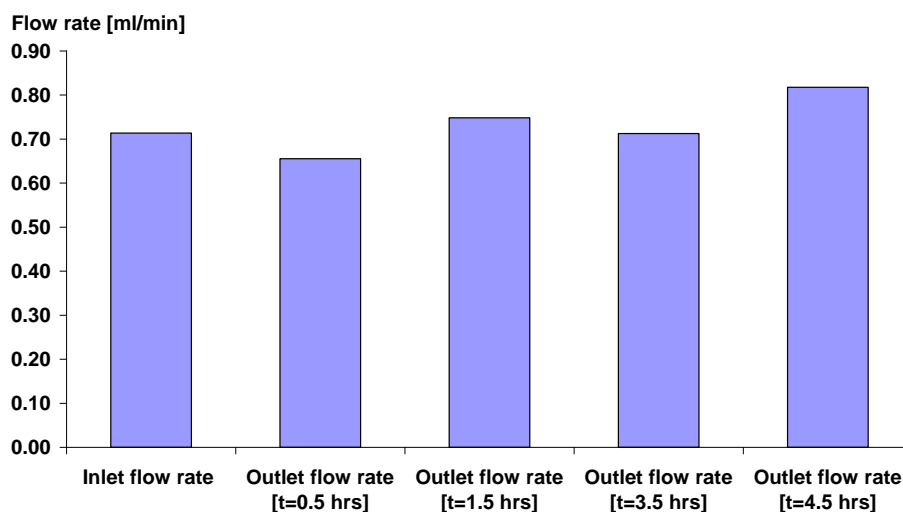


Figure 38. Evolution of the flow rate at 30°C.

From Figure 38, one can notice that the flow rate of the fluid is quite stable during the reaction.

Conversion of propionic acid

Figure 39 depicts the conversion of propionic acid along the reactor at different flow rates and at 30°C, and Figure 40 depicts the conversions of PA versus the mean residence time.

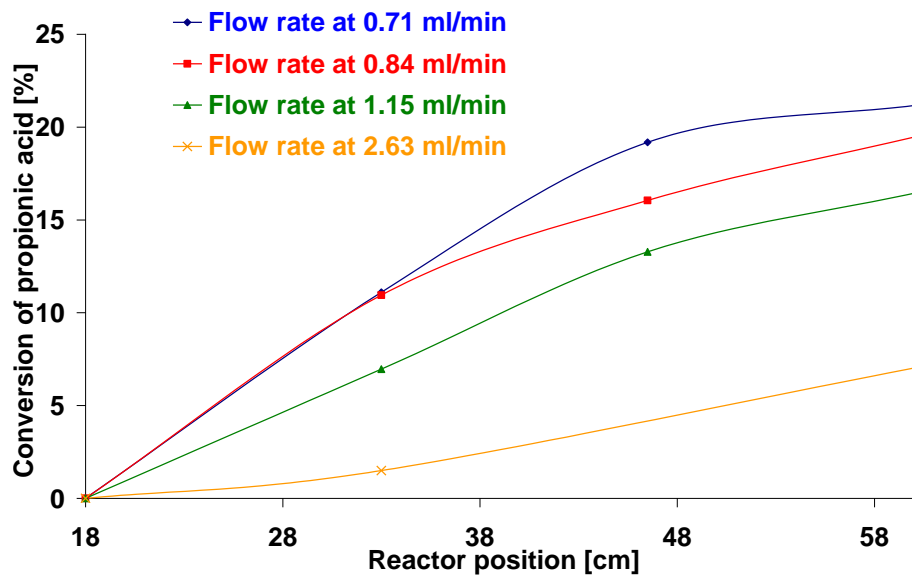


Figure 39. Conversion of propionic acid at different reactor positions and flow rates.

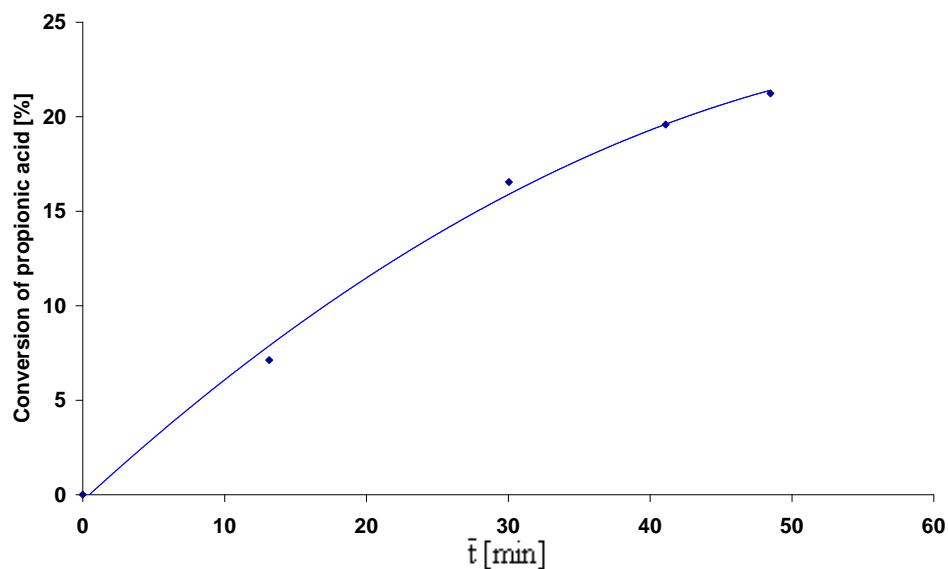


Figure 40. Conversion of propionic acid as a function of \bar{t} .

The response of the system is logical, i.e., conversion of PA is higher at low flow rate. The maximum of conversion should be at around 31% based on the equilibrium.

Study of the deactivation

Figure 41 shows the molar flow rate for propionic acid, hydrogen peroxide and peroxypropionic acid at the outlet.

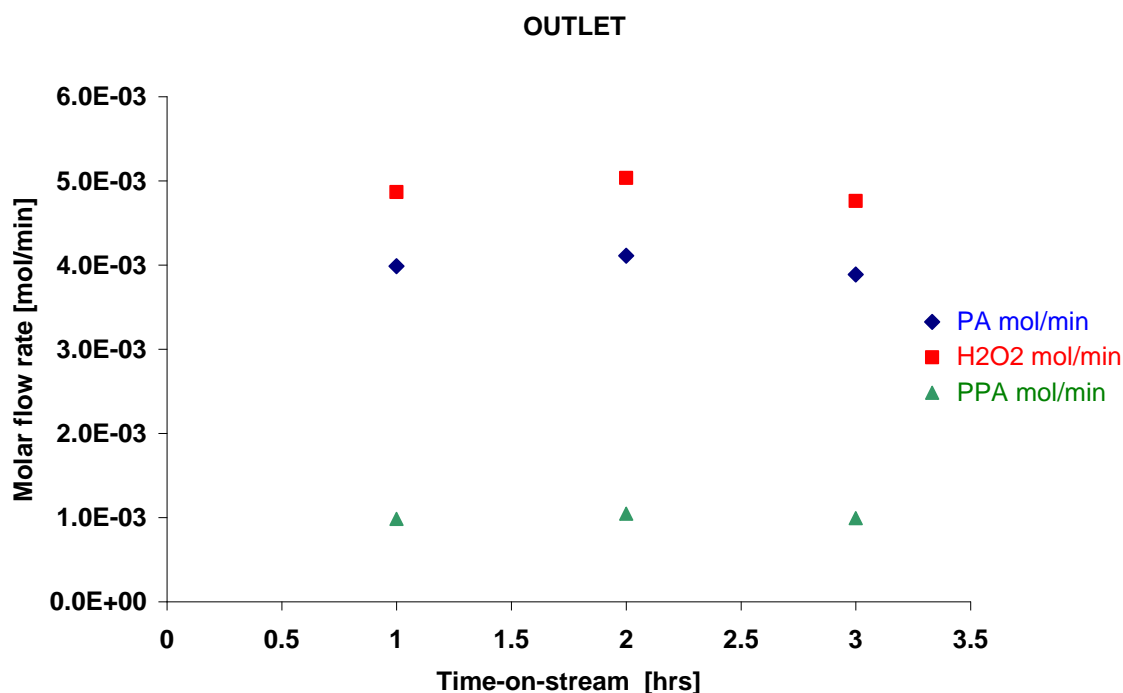


Figure 41. Outlet concentration of compounds with a flow rate of 0.84 ml^{-1} at 30°C .

Figure 41 shows that there is no catalyst deactivation during the carboxylic acid perhydrolysis.

The system studied shows a high chemical stability. To be sure that no mass and heat transfer effects interfere during the reaction, the following section comprises a study of these phenomena.

6.3.2 Mass and heat transfer effects

External and internal mass transfer effects

Several methods exist in the literature to estimate the mass transfer coefficient k_D in case of external mass transfer. The mass flux N_D between the bulk phase and the surface of the catalyst is expressed as

$$N_D = k_D(C_b - C_s) \quad (57)$$

where k_D is the mass transfer coefficient, C_b and C_s are the concentrations in the bulk and at the outer surface of the catalyst, respectively.

The coefficient k_D (m.s^{-1}) can be estimated by calculating the Sherwood number (Sh) defined as

$$\text{Sh} = \frac{k_D \bar{d}_p}{D} = 2 + 1.8 \text{Re}_p^{1/2} \text{Sc}^{1/3} \quad (58)$$

where Sc is the Schmidt number defined as

$$\text{Sc} = \frac{\mu_r}{\rho_f D} \quad (59)$$

and D is the molecular diffusion coefficient.

Villermaux [69] has defined the coefficient (f_e) to determine the influence of the external mass transfer:

$$f_e = \frac{\bar{r}L}{k_D C_b} = \frac{C_b - C_s}{C_b} \quad (60)$$

where \bar{r} is the observed reaction rate ($\text{mol.m}^{-3}.\text{s}^{-1}$), and L is defined as the ratio V_P/A_P . If f_e is less than 0.005, then the external mass transfer is negligible.

Another way to estimate the mass transfer coefficient k_D is to use the correlation proposed by Satterfield-Chilton-Colburn:

$$j_D = \frac{k_D Sc^{2/3}}{u_f} \quad (61)$$

In case of a liquid-phase reaction and if $0.006 < Re_p < 55$, the parameter j_D is defined as:

$$j_D = \frac{1.09}{(1 - \varepsilon_p) Re_p^{0.67}} \quad (62)$$

The mean diameter \bar{d}_p is equal to $7.89 \cdot 10^{-4}$ m, $\bar{r}_{obs} = 0.51 \text{ mol} \cdot \text{m}^{-3} \cdot \text{s}^{-1}$, $\mu_f = 8 \cdot 10^{-4}$ Pa.s, $L = 9.63 \cdot 10^{-5}$ m and the molecular diffusion coefficient of PPA is equal to $1.29 \cdot 10^{-9} \text{ m}^2 \cdot \text{s}^{-1}$.

Table 24 summarizes the values of the different numbers used for estimating the mass transfer coefficient k_D , and the value of f_e by using the correlation of Satterfield-Chilton-Colburn to get k_D and Sherwood number.

Table 24. External mass transfer parameters

Inlet Flow ml/min	ρ_f kg/m ³	Sc	kd from Sh m/s	fe from Sh	jd	kd from jd m/s	fe from jd
0.84	1061.47	585	0.0014	0.001	39.0	2.8E-05	0.0005
0.71	1061.81	584	0.0015	0.001	43.5	2.6E-05	0.0005
1.15	1061.53	585	0.0013	0.001	31.6	3.1E-05	0.0004
2.63	1061.68	585	0.0010	0.001	18.1	4.0E-05	0.0003

From Table 24, one can notice that f_e is less to than 0.005, thus the external mass transfer effect can be neglected.

An experimental method to determine the presence of external mass transfer is to vary the catalyst loading and keeping the same space-time. Mass transfer limitations are present if the conversion at fixed space-time depends on the flow rate. According to F. Kapteijn, G.B. Marin and J.A. Moulijn [70], this method is not a sensitive approach, because the mass transfer coefficient depends only slightly on the flow rate at the low Reynolds numbers prevailing in laboratory-scale fixed-bed reactors.

They recommend to use the Carberry number (Ca) to determine the influence of the external mass transfer. For an isothermal, n^{th} order irreversible reaction in a spherical particle, a criterion for the Carberry number can be derived, which assures that the observed rate does not deviate more than 5% from the ideal rate:

$$Ca = \frac{\bar{d}_p \bar{r}_{\text{obs}, W} \rho_P}{6k_d C_b} < \frac{0.05}{|n|} \quad (63)$$

In the present system, one can assume that perhydrolysis is an irreversible second order reaction at the beginning. Table 25 presents the result of the Carberry number from Sherwood and Satterfield-Chilton-Colburn correlations.

Table 25. Estimation of the Carberry number

Ca from Sh	Ca from jd	0.005/n
1.69E-03	5.44E-04	2.50E-03
1.79E-03	5.79E-04	2.50E-03
1.53E-03	4.91E-04	2.50E-03
1.14E-03	3.75E-04	2.50E-03

According to Table 25, the absence of external mass transfer in the system can be confirmed.

From experiments carried out in batch mode, internal mass transfer was noticed in case of perhydrolysis reaction catalyzed by Amberlite IR-120 [V]. Villermaux [69] has introduced the parameter φ'_S defined as,

$$\varphi'_S = \frac{\bar{r}L^2}{D_e C_S} \quad (64)$$

where $L = V_p/A_p$,

If φ'_S is lower than 0.1, internal mass transfer is negligible. In our case, $C_S = C_b$ because there is no external mass transfer limitation.

According to F. Kapteijn, G.B. Marin and J.A. Moulijn [70], introduction of Wheeler-Weisz modulus, and series expansion, leads to the Weisz-Prater criterion to assess the importance of internal diffusion limitations. For an irreversible n^{th} order reaction and for a spherical particle, this criterion is defined by

$$v = \frac{\bar{d}_p^2 \bar{r}_{\text{obs}, W} \rho_P}{36 D_e C_S} \left(\frac{n+1}{2} \right) < 0.15 \quad (65)$$

Table 26. Internal mass transfer effect

Coefficient from eq. (64)	Coefficient from eq. (65)
0.006	0.01
0.006	0.01
0.006	0.01
0.006	0.01

Table 26 shows that both methods indicate the absence of an internal mass transfer.

External and internal heat transfer effects

According to F. Kapteijn et al [70], if the deviation between the observed rate and the rate at the bulk temperature has to be less than 5%, the following criterion is obtained:

$$\frac{\bar{d}_p \bar{r}_{\text{obs}, W} \rho_P}{6} * \frac{(-\Delta H_r)}{h_f T_b} * \frac{E_a}{RT_b} < 0.05 \quad (66)$$

where h_f is the heat transfer coefficient of the fluid, which is mainly water in our case and R is the gas constant. From Table 11, the apparent energy of activation can be calculated and it is equal to 140 kJ/mol.

The heat transfer coefficient (h_f) was determined using Nusselt number:

$$Nu = \frac{h_f * \bar{d}_p}{\lambda_f} \quad (67)$$

$$\text{For } 0.0016 < \text{Re}_p < 55, \text{Nu} = \frac{1.31}{(1-\varepsilon_p)} * \text{Re}_p^{1/3} * \text{Pr}^{1/3}$$

where Pr is the Prater number defined as

$$\text{Pr} = \frac{\mu_f * c_{pf}}{\lambda_f} \quad (68)$$

where c_{pf} is the specific heat capacity equal to $4185 \text{ J.Kg}^{-1}.\text{K}^{-1}$, and λ_f is the thermal conductivity of the fluid, which is equal to $0.58 \text{ W.m}^{-1}.\text{K}^{-1}$. These values were obtained by assuming that the fluid is water essentially.

Table 27. Influence of the external heat transfer on perhydrolysis

\bar{r}_{obsW} mol.kg ⁻¹ _{cat} .S ⁻¹	Nu	h_f W.m ⁻² .K ⁻¹	Pr	Coefficient from eq. (66)
4.90E-04	4.31	3.17E+03	5.77	0.00002
4.90E-04	4.08	3.00E+03	5.77	0.00002
4.90E-04	4.78	3.52E+03	5.77	0.00002
4.90E-04	6.30	4.63E+03	5.77	0.00001

From Table 27, one can notice that the external heat transfer can be assumed negligible.

Concerning the internal temperature gradients, a criterion which guarantees that the deviation of the observed volumetric rate from the isothermal rate is less than 5% is given by:

$$\frac{\bar{d}_p^2 \bar{r}_{\text{obs, W}} \rho_p}{36} * \left(\frac{n+1}{2} \right) \frac{(-\Delta H_r)}{\lambda_p T_s} * \frac{\text{Ea}}{RT_s} < 0.1 \quad (69)$$

where T_s is the temperature at the surface of the catalyst, and λ_p is the thermal conductivity of the resin which can be assumed the same as polystyrene, i.e., $0.08 \text{ W.m}^{-1}.\text{K}^{-1}$.

Table 28. Influence of the internal mass transfer

\bar{r}_{obsW} mol.kg ⁻¹ _{cat} .s ⁻¹	λp W.m ⁻¹ .K ⁻¹	Coefficient from eq. (69)
4.90E-04	0.08	0.0002
4.90E-04	0.08	0.0002
4.90E-04	0.08	0.0002
4.90E-04	0.08	0.0002

From Table 28, one can notice that the internal heat transfer effects are negligible.

6.4 Comparison with batch reactor

Figure 42 displays the conversion of PA versus the parameter $\text{time} \cdot m_{\text{cat}} / [\text{PA}]_0$. The purpose of this graph is to make a plausible comparison between experiments carried out in batch and continuous reactors.

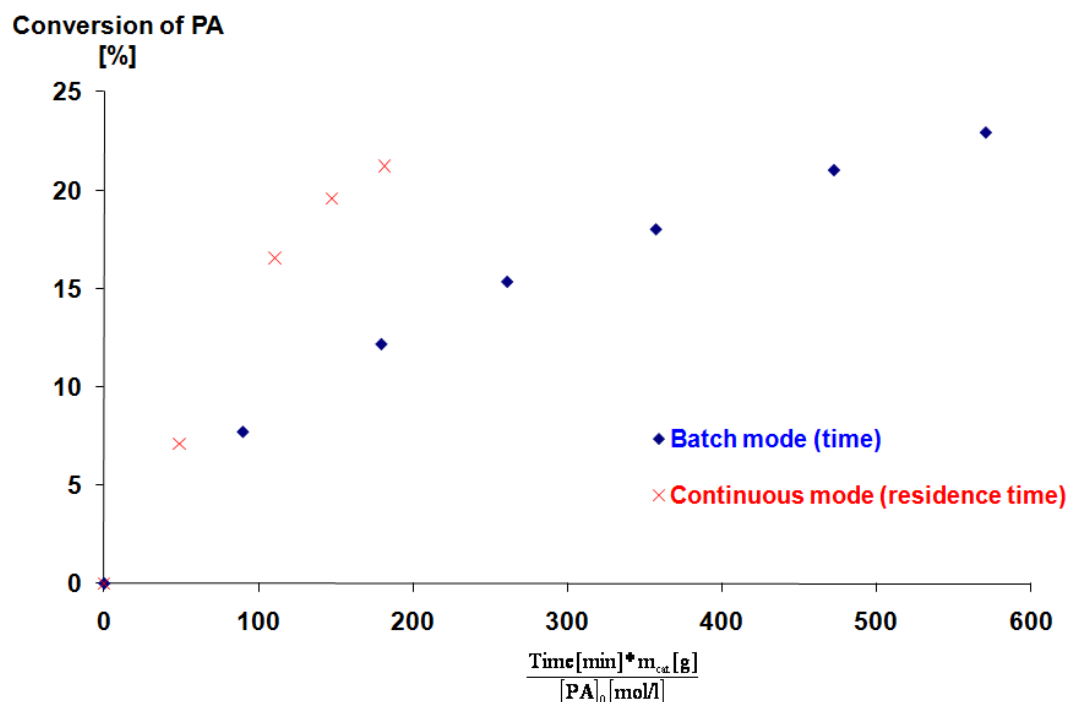


Figure 42. Evolution of the conversion of propionic acid in batch and continuous reactors at 30°C.

From Figure 42, one can notice that the conversion obtained in the continuous mode is higher than in the batch mode. Thus, the shift from batch to continuous operation is advantageous.

6.5 Comparison with acetic acid in continuous reactor

Figure 43 presents the conversion of acetic and propionic acids at different position of the continuous reactor at 30°C and with a flow rate fixed at 0.7 ml.min⁻¹.

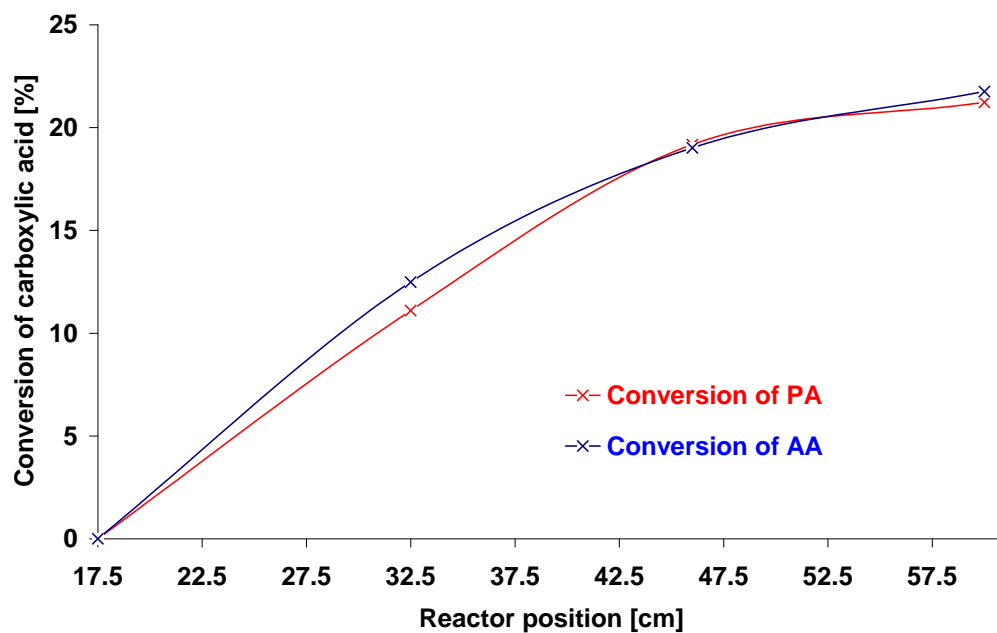


Figure 43. Conversion of carboxylic acids versus the reactor position.

From this figure, one can notice that the kinetics of formation of peroxyacetic and peroxypropionic acid are very similar.

Conclusions

The aims of this work were to identify the kinetic and thermodynamic parameters for the synthesis of peroxycarboxylic acid (PCA) from carboxylic acid (CA) and hydrogen peroxide, to propose a greener alternative route for this synthesis and to study the stability of peroxypropionic acid.

The validity of the kinetic model in the batch synthesis of PCA in the presence of sulphuric acid is correct. The non-ideality is mainly due to the presence of the homogeneous catalyst, and it can be described by an empirical equation. The standard reaction enthalpy ΔH_r° was estimated to be -5.66 and -4.17 kJ.mol⁻¹ at 30-60°C for acetic and propionic acid, respectively. This indicates that the synthesis of PAA is slightly more exothermic than the synthesis of PPA.

The synthesis of PCA with heterogeneous catalysts showed that the catalytic activity of cation exchange resins is higher compared to aluminosilicate materials. By shifting to heterogeneous catalysts, corrosion and separation problems are surmounted. The catalytic activity is higher with gelular resins with a lower cross-linking and higher cation exchange capacity. A comparison with sulphuric acid as a catalyst indicated that the catalytic activities of the resins are on a similar scale, but the resins allow the acidity of the solution to be suppressed by one pH unit.

A kinetic-diffusion model was developed in batch mode for synthesis of peroxycarboxylic acids (acetic and propionic acid) starting from the corresponding carboxylic acids and hydrogen peroxide using pre-treated Amberlite IR-120 in a temperature range 30-60°C. The models were shown to be correct in our experimental conditions. No decomposition of peroxycarboxylic acids or hydrogen peroxide was noticed.

An Eley-Rideal mechanism was applied, and the protolysis of carboxylic acid was taken into account to derive the kinetic equation for the system influenced by heterogeneous catalyst. The kinetic-diffusion modelling of the perhydrolysis of carboxylic acid by pre-treated Amberlite IR-120 shows that the energy of activation in case of acetic acid (42.5 kJ/mol) is similar to that of propionic acid (51.4 kJ/mol).

The synthesis of different peroxycarboxylic acid was treated in order to establish a relationship between the structure of carboxylic acids and their reactivity. To accomplish this goal, Linear Free-Energy Relations were used in the form of Taft correlations. A comparison between homogeneous and heterogeneous catalyst system was done by using sulphuric acid and a cation exchange resin, Amberlite IR-120. Perhydrolysis of carboxylic acids catalyzed either homogeneously or heterogeneously follows the Taft (based on the steric part) correlations, which implies that the steric effect of the substituent on the reaction centre governs the reaction, but not the polar effect.

To study of the composition of PCAs, a method was used based on on-line analysis of released gas-phase products by rapid quadrupole mass spectrometry, which is reliable for studying the kinetics of the decomposition PCA and hydrogen peroxide. The method can be applied both for qualitative and quantitative purposes. The kinetic study and modelling showed that the decomposition rates of peroxide compounds are very slow. It was shown that the PPA is more stable than PAA.

Synthesis of peroxycarboxylic acids by using a continuous reactor is feasible by using heterogeneous catalyst, namely Amberlite IR-120. By comparing batch and continuous mode, it was demonstrated that the second one is more advantageous.

Notation

A	pre-exponential factor [$\text{l.mol}^{-1}.\text{s}^{-1}$]
A	interfacial area [m^2]
A	area of liquid-gas interface [m^2]
A_s	external surface area of particule by volume, m^2/m^3
a_p	interfacial area-to-liquid volume [m^{-1}]
a_0	mass transfer-to-volume ratio [$\text{m}^2.\text{m}^{-3}$]
c	concentration [mol.L^{-1}]
c_{Pf}	specific heat capacity [$\text{J.Kg}^{-1}.\text{K}^{-1}$]
D	axial dispersion coefficient [$\text{m}^2.\text{s}^{-1}$]
D_i	molecular diffusion coefficient [$\text{m}^2.\text{s}^{-1}$]
De_i or De	effective diffusion coefficient [$\text{m}^2.\text{s}^{-1}$]
E_a	activation energy [J.mol^{-1}]
E_s	steric substituent constant
F	flow rate of the fluid [ml/min]
f_e	coefficient to determine the influence of external mass transfer
f_i	fragmentation coefficient of a component i
h	heat transfer coefficient [$\text{W.m}^{-2}.\text{K}^{-1}$]
ΔH_r°	standard enthalpy change of reaction [kJ.mol^{-1}]
ΔH_f°	heat of formation of specie [kJ/mol]
j_D	$\frac{k_D Sc^{2/3}}{u_f}$
K^c	equilibrium constant, based on concentrations
K^T	true thermodynamic constant, based on activities
K^Y	equilibrium constant, based on coefficients of activity
K	adsorption coefficient [l.mol^{-1}]
K_{O_2}	parameter for the retarding effect of oxygen

k	rate constant [$\text{l.mol}^{-1}.\text{s}^{-1}$]
k'	calibration coefficient
k_D	mass transfer coefficient [m/s]
k_{Li}	mass transfer coefficient for i in the liquid phase [m.s^{-1}]
L	length of the vessel [m]
N	flux [$\text{mol.m}^{-2}.\text{s}^{-1}$]
N_D	mass flux between the bulk phase and the surface of the catalyst [mol.m^{-2}]
n	amount of substance [mol]
n_{pi}	number of particle with radius r_i
\dot{n}	flow of the amount of substance [mol.s^{-1}]
Q	reaction quotient
Q_R	amount of heat released by the reaction [J]
R	gas constant [$\text{J.K}^{-1}.\text{mol}^{-1}$]
R	reaction rate [$\text{mol.L}^{-1}.\text{s}^{-1}$]
R^2	coefficient of explanation [%]
r	catalyst particle radius, radial coordinate
r_i	generation rate
r_j	particle radius
\bar{r}	average radius
\bar{r}_{obs}	observed reaction rate [$\text{mol.m}^{-3}.\text{s}^{-1}$]
$\bar{r}_{\text{obs, W}}$	observed specific reaction rate [$\text{mol.kg}_{\text{cat}}^{-3}.\text{s}^{-1}$]
T	temperature
u	superficial velocity [m.s^{-1}]
V	volume
y	frequency function for particle size distribution
X	dimensionless coordinate
\bar{t}	mean residence time [s]
\dot{V}	volumetric flow rate [$\text{m}^3.\text{s}^{-1}$]
x	mole fraction
y	$\frac{[H_3O]}{[H_3O^+]}$

Greek letters

α	$\frac{[H_2SO_4]_0}{[H_2O]}$
α	liquid volume-to-gas ratio
β	$\frac{[CH_3CH_2COOH]_0 - [CH_3CH_2CO_2H]}{[H_2O]}$
Δ	$C_{Li} - C_{Li}^* \quad [\text{mol.l}^{-1}]$
δ	parameter which takes into account the non-ideality of the solution
δ	constant giving the susceptibility of a given reaction series to steric effect
ϵ_{RP}	fraction of solid in the reactor
ϵ_P	porosity of particle
η	effectiveness factor
θ	objective function
κ_L	$k_{Li}.a_0 \quad [\text{s}^{-1}]$
λ	molar conductivity $[\text{S.m}^2.\text{mol}^{-1}]$
λ	thermal conductivity $[\text{W.m}^{-1}.\text{K}^{-1}]$
μ_f	fluid viscosity $[\text{Ns/m}^2]$
ξ	reaction extent $[\text{mol}]$
ρ^-	constant giving the susceptibility of a given reaction series to polar substituents
ρ_f	fluid density $[\text{kg/m}^3]$
σ^*	polar substituent constant for the group R relative to the standard CH_3 group
σ	conductivity $[\text{S.m}^{-1}]$
τ	residence time $[\text{s}]$

Subscripts and superscripts

o	initial
ref	reference state
[i]	concentration of a component i [mol.l ⁻¹]
(i)	activity of a component i [mol.l ⁻¹]
ave	average
b	bulk phase
s	surface of the catalyst
i	component index
*	interfacial (equilibrium) value
f	fluid

Abbreviations

AA	acetic acid
CA	carboxylic acid
PA	propionic acid
PAA	peroxyacetic acid
PCA	peroxycarboxylic acid
PPA	peroxypropionic acid

Dimensionless groups

Ca	Carberry number	$\frac{\bar{d}_p \bar{r}_{\text{obs}, W} \rho_P}{6k_d C_b}$
Nu	Nusselt number	$\frac{h_f * \bar{d}_p}{\lambda_f}$
Pe	(uL)/D	
Pr	Prater number	$\frac{\mu_f * c_{Pf}}{\lambda_f}$
Re	Reynold number for the reactor	$d_{\text{reactor}} u_f \rho_f / \mu_f$
Re _p	Reynold number for the particle	$d_p u_f \rho_f / \mu_f$
Sh	Sherwood number	$\frac{k_D \bar{d}_p}{D} = 2 + 1.8 \text{Re}_p^{1/2} \text{Sc}^{1/3}$
Sc	Schmidt number	$\frac{\mu_f}{\rho_f D}$
ϕ_s'		$\frac{\bar{r} L^2}{D_e C_s}$
ϕ	Weisz-Prater criterion	$\frac{\bar{d}_p^2 \bar{r}_{\text{obs}, W} \rho_P}{36 D_e C_s} \left(\frac{n+1}{2} \right)$

REFERENCES

1. R. Noyori, *Chem. Commun.* 14 (2005) 1807-1811.
2. R. Hage, A. Lienke, *Angew. Chem. Int. Ed.* 45 (2006) 206-222.
3. C.W. Jones, *Application of Hydrogen Peroxide and Derivatives*, Royal Society of Chemistry, Cambridge, 1999.
4. M. R. gen. Klaas, K. Steffens, N. Patett, *J. Mol. Catal. B-Enzym.* 19-20 (2002) 499-505.
5. R.J. Lomas, J.E. Cruse-Sawyer, C. Simpson, E. Ingham, R. Bojar, J.N. Kearney, *Burns* 29 (2003) 515-525.
6. A. Pruss, A. Hansen, M. Kao, L. Gürtler, G. Pauli, F. Benedix, R. von Versen, *Cell and Tissue Banking* 2 (2001) 201-215.
7. H. Ölmez, U. Kretzschmar, *Food Sci. Technol.* 42 (2009) 686-693.
8. M. Kitis, *Environ. Int.* 30 (2004) 47-55.
9. C. Caretti, C. Lubello, *Water Res.* 37 (2003) 2365-2371.
10. P. Polonca, P. T. Tavčer, *Color. Technol.* 124(1) (2008) 36-42.
11. L. Wang, Y. Zhao, *Chem. Eng. J.* 136 (2008) 221-226.
12. P. De Filippis, M. Scarsella, *Ind. Eng. Chem. Res.* 47 (2008) 973-975.
13. C. Lion, L. Da Conceição, G. Hecquet, C. Pralus, B. Requieme, J.-P. Schirmann, *New J. Chem.* 26 (2002) 1515-1518.
14. V.V. Goud, A.V. Patwardhan, S. Dinda, N.C. Pradhan, *Chem. Eng. Sci.* 62 (2007) 4065-4076.
15. F. Bounoure, H. Fiquet, P. Arnaud, *Am J. Health-Syst. Pharm.* 63 (2006) 451-455.
16. G.X. Pan, L. Spencer, G.J. Leary, *Holzforschung* 54 (2000) 144-152.
17. G.X. Pan, L. Spencer, G.J. Leary, *Holzforschung* 54 (2000) 153-158.
18. Z. Min, W. Jingyan, J. Xiaoguang, *Zhongguo Xiaoduxue Zazhi* 21(3) (2004) 222-224.
19. S.S. Block, *Disinfection, Sterilization, and Preservation*, 4th ed., Lea & Febiger Pubs, Philadelphia, 1991.
20. B. Phillips, P.S. Starcher, B.D. Ash, *J. Org. Chem.* 23(12) (1959) 1823-1826.
21. R. Cantieni, *Zeitschrift fuer Wissenschaftliche Photographie, Photophysik und Photochemie* 36 (1937) 90-95.
22. J. D'Ans, W. Frey, *Z. Anorg. Chem.* 84 (1914) 145-164.
23. D. Swern, *Organic Peroxides*, Wiley-Interscience, New York, 1970.
24. L.V. Dul'neva, A.V. Moskvina, *Russ. J. Gen. Chem.* 75 (2005) 1125-1130.
25. Y. Ogata, Y. Sawaki, *Tetrahedron* 21 (1965) 3381-3386.

26. X. Zhao, T. Zhang, Y. Zhou, D. Liu, J. Mol. Catal. A-Chem., 271 (2007) 246-252.
27. M. Bewersdorf, G. Goor, Preparation of stabilized peroxy-carboxylic acid solutions, No. De 4210425, 1993.
28. P. Taeubl, Stabilized percarboxylic acid solutions, No. 4317420, 1994.
29. A. Reijo, I. Renvall, Process for the preparation of peroxy acids, No. WO2007031596, 2007.
30. Zheng Xiaobing Zhou, Method for preparing peroxy acetic acid, No. CN1803771, 2006.
31. M.S. Saha, Y. Nishiki, T. Furuta, A. Denggerile, T. Ohsaka, Tetrahedron Lett. 44 (2003) 5535-5537.
32. A.T. Hawkinson, W.R. Schitz, Improvements in or relating to the oxidation of aliphatic carboxylic acids to peracids, GB776758, 1957.
33. A. Palani, A. Pandurangan, Catal. Commun. 7 (2006) 875-878.
34. G.O. Rocha, R.A.W. Johnstone, B.F. Hemming, P.J.C. Pires, J.P. Sankey, J. Mol. Catal. A : Chem. 186 (2002) 127-133.
35. M.R. gen. Klaas, K. Steffens, N. Patett, J. Mol. Catal. B : Enzym. 19-20 (2002) 499-505.
36. M. S. Saha, Y. Nishiki, T. Furuta, A. Denggeribe, T. Ohsaka, Tetrahedron Lett. 44 (2003) 5535-5537.
37. N. Musakka, T. Salmi, J. Wärnå, J. Ahlkvist, M. Piironen, Chem. Eng. Sci. 61 (2006) 6918-6928.
38. X. Zhao, K. Cheng, J. Hao, D. Liu, J. Mol. Catal. A : Chem. 284(1-2) (2008) 58-68.
39. G. Prescher, Process for preparing perpropionic acid solutions, US4088679, 1978.
40. D. Kubička, N. Kumar, P. Mäki-Arvela, M. Tiitta, V. Niemi, T. Salmi, D. Yu. Murzin, J. Catal. 222 (2004) 65-79.
41. P. Mäki-Arvela, N. Kumar, V. Nieminen, R. Sjöholm, T. Salmi, D. Yu. Murzin, J. Catal. 225 (2004) 155-169.
42. E.M. Sulman, V.V. Alferov, Yu. Yu. Kosivtsov, A.I. Sidorov, O.S. Misnikov, A.E. Afanasiev, N. Kumar, D. Kubicka, J. Agullo, T. Salmi, D. Yu. Murzin, Chem. Eng. J. 134 (2007) 162-167.
43. A. Aho, N. Kumar, K. Eränen, T. Salmi, M. Hupa, D. Yu. Murzin, Fuel 87 (2008) 2493-2501.
44. J. Lilja, D. Yu. Murzin, T. Salmi, J. Aumo, P. Mäki-Arvela, M. Sundell, J. Mol. Catal. A-Chem. 182-183 (2002) 555-563.
45. F.P. Greenspan, D.G. MacKellar, Anal. Chem. 20(11) (1948) 1061-1063.

46. C.A. Bunton, T.A. Lewis, D.L. Llewelyn, J. Am. Chem. Soc. 78(6) (1956) 1226.
47. F.O. Mohammed, D. Pines, J. Dreyer, E. Pines, E.T.J. Nibbering, Science. 310 (2005) 83-85.
48. D.A. Knopf, B.P. Luo, U.K. Krieger, T. Koop, J. Phys. Chem. A. 107 (2003) 4322-4332.
49. K. Sue, F. Ouchi, K. Minami, K. Arai, J. Chem. Eng. Data. 49 (2004) 1359-1363.
50. H. Haario, MODEST-User's Guide, Profmath Oy, Helsinki, 1994.
51. R.L. Musante, R.J. Grau, M.A. Baltanas, Appl. Catal. A 197(1) (2000) 165-173.
52. A.A. Zagorodni, D.L. Kotova, V.F. Selemenev, React. Funct. Polym., 53 (2002) 157-171.
53. M.R. Altiokka, A. Citak, Appl. Catal. A-Gen, 239 (2003) 141-148.
54. Z. P. Xu, K.T. Chuang, Chem. Eng. Sci. 52(17) (1997) 3011-3017.
55. W.-T. Liu, C.-S. Tan, Ind. Eng. Chem. Res. 40 (2001) 3281-3286.
56. M.R. Altiokka, Ind. Eng. Res. 46 (2007) 1058-1062.
57. M.I. Temkin, The kinetics of Some Industrial Heterogeneous Catalytic Reactions, Advances in Catalysis, Academic Press, New York, 1979.
58. J.N. Brønsted, Chem. Rev. 5 (1928) 231-338.
59. K.J. Laidler, Chemical Kinetics, 3rd ed., Harper & Row, New York, 1987.
60. S. Ichikawa, J. Phys. Chem. 92 (24) (1988) 6970-8.
61. R.W. Taft, Steric effect in Organic Chemistry, in: M.S. Newman (Ed.), Wiley, New York, 1956.
62. J.A. MacPhee, A. Panaye, J.-E. Dubois, Tetrahedron 34 (24) (1978) 3553-62.
63. D.R. Lide, CRC handbook of Chemistry and Physics, 75th ed., CRC Press, Boca Raton, 1995.
64. S. Havel, J. Greschner, Chem. Prum. 16 (1966) 73-78.
65. J. Ahlkvist, T. Salmi, K. Eränen, N. Musakka, Bestämning av syrets och koldioxidens löslighet i organiska vätskor, Laboratoriet för teknisk kemi, Åbo Akademi, 2003.
66. O. Levenspiel, Chemical Reaction Engineering, 3rd ed., John Wiley & Sons, Inc., New York, 1999.
67. R. Di Felice, L.G. Gibilaro, Chem. Eng. Sci. 59 (2004) 3037-3040.
68. P. Trambouze, J.-P. Euzen, Les Réacteurs Chimiques, Editions TECHNIP, Paris, 2002.
69. J. Villermaux, Génie de la Réaction Chimique, 2nd ed., Tec&Doc Lavoisier, 1993.
70. R.A. van Santen, P.W.N.M. van Leeuwen, J.A. Moulijn, B.A. Averill, Catalysis. An integrated approach, 2nd ed., Elsevier, 2000.

71. N. Musakka, Experimental study and mathematical modelling of organic decomposition reactions in liquid phase, Doctoral Thesis, Åbo Akademi, 2004.

APPENDIX

APPLIED CHEMISTRY

Kinetic Study and Modeling of Peroxypropionic Acid Synthesis from Propionic Acid and Hydrogen Peroxide Using Homogeneous Catalysts

Sébastien Leveneur,^{*,†,‡} Tapio Salmi,[†] Dmitry Yu. Murzin,[†] Lionel Estel,[‡] Johan Wärnå,[†] and Niko Musakka[†]

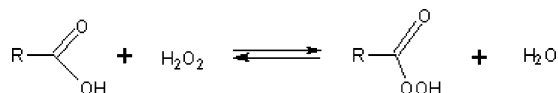
Laboratory of Industrial Chemistry, Process Chemistry Centre, Åbo Akademi, Biskopsgatan 8, FI-20500 Åbo/Turku, Finland, and LSPC-Laboratoire de Sécurité des Procédés Chimiques, INSA Rouen, Place Emile Blondel, BP8, 76131 Mont-Saint-Aignan Cedex, France

This article describes a kinetic study of the perhydrolysis of propionic acid with sulfuric acid at various molar reactant ratios (PA-H₂O₂ from 0.4 to 2.05), reaction temperatures (from 30 to 60 °C), and catalyst concentrations (from 0 to 1.41 M). The influence of water and acidic catalysts were taken into account to develop a suitable kinetic model. The system is nonideal, mainly due to the presence of the strong electrolyte (i.e., H₂SO₄), and a parameter was introduced to describe the nonideality. The kinetic and thermodynamic parameters determined by nonlinear regression analysis were statistically well identified. The standard enthalpy change of reaction was estimated to $-4.17 \text{ kJ}\cdot\text{mol}^{-1}$, and the activation energy of the reaction was estimated to $44.2 \text{ kJ}\cdot\text{mol}^{-1}$.

Introduction

Peroxy-carboxylic acids are widely applied in the industry because of its oxidative properties. Those compounds are used for disinfection in the alimentary industry, for destruction of pollutants, pesticides, bleaching agents in the paper industry, and in the manufacture of fine chemicals (Baeyer–Villiger reaction).

One way to produce peroxy-carboxylic acid is the oxidation of the parent carboxylic acid by H₂O₂ in the presence of an acidic catalyst:



This reversible reaction is named as the perhydrolysis of carboxylic acid, and it is governed by an equilibrium constant. The pioneering research on this reaction began with D'Ans et al.,¹ in 1914; they studied the perhydrolysis of different carboxylic acids, and they were able to produce concentrated peroxy-carboxylic acid. In 1970, Swern,² published a book that summarized all of the methods for the preparation and analysis of different organic peroxides.

Several authors have noticed^{5,9} that the rate of this reaction is accelerated by increasing the amount of sulfuric acid. Nevertheless, no kinetic expressions have been published that take into account the concentrations of the catalyst and water.

The goal of the present article is to determine the kinetic and thermodynamic parameters for the synthesis of peroxypropionic acid (PPA) using sulfuric acid as a homogeneous catalyst.

Experimental Section

The experiments were carried out in a batch reactor immersed in an isothermal water bath. On top of the reactor, a cooling condenser was placed and adjusted at 0 °C to avoid the loss of liquid-phase compounds. In case the decomposition of PPA or H₂O₂ appeared, carrier gas (Helium) was led into the reactor through one of the necks to avoid the accumulation of oxygen in the gas phase. The rate of mechanical agitation was adjusted to 200 rpm to avoid vortex formation. Samples were withdrawn from the liquid phase and analyzed off-line (chemical analysis and pH).

To prevent contamination induced by alkaline and metal components, which initiate the catalytic decomposition of peroxypropionic acid and hydrogen peroxide, all parts of the reactor system being in contact with the reaction solution were washed with hydrochloric acid and afterward with a phosphate free detergent solution.

In the first stage, propionic acid, water, and the catalyst were mixed together in the reactor. When the reaction temperature was reached, hydrogen peroxide solution was added through the dropping funnel, and at time zero the required amount was poured into the reactor.

Samples were withdrawn by a plastic syringe (to avoid the contamination of the solution by the trace of metals) and were analyzed by NMR spectroscopy and a Greenspan and Mackellar method.³ The concentration of hydrogen peroxide was determined by titration using a standard solution of ammonium cerium sulfate (0.1 N). The concentration of propionic and peroxypropionic acid were determined by titration with an automatic titrator (Metrohm 751 GPD Titrino) using a standard solution of sodium hydroxide (0.2 N).

According to a German patent,⁴ during the reaction of hydrogen peroxide and propionic acid in water and in the presence of an acid catalyst, the danger of explosion is

* To whom correspondence should be addressed. Tel: +358 2 215 8942; Fax: +358 2 215 4479; E-mail: sleveneu@abo.fi.

[†] Process Chemistry Centre.

[‡] INSA Rouen.

Table 1. Variation of the Parameters during the Experiments

reaction temperature [°C]	30–60
molar ratio PA/H ₂ O ₂	0.40–2.05
water concentration [mol·L ⁻¹]	16.77–40.66
sulfuric acid concentration [mol·L ⁻¹]	0–1.41

suppressed by employing a temperature up to 60 °C, a weight ratio of hydrogen peroxide/water up to 0.8, and a catalyst concentration of 10–40% by weight. These safety issues were applied in our experiments, too.

A 30 wt % of hydrogen peroxide solution was used during the experiments.

To obtain a reliable kinetic model, we varied the experimental parameters, and these variations are displayed in the Table 1.

Results and Discussions

1. Equilibrium Analysis. Preliminary analysis of experiments demonstrated that, for the description of reaction equilibrium, nonideality should be taken into account. For instance, several experiments were carried out at 40 °C with different sulfuric acid concentrations, and the values of the reaction quotient as a function of time are presented in Figure 1.

The results were analyzed by using the reaction quotient calculated as: $Q = [\text{PPA}][\text{H}_2\text{O}]/[\text{PA}][\text{H}_2\text{O}_2]$, where $[\text{H}_2\text{O}]$ was determined by adding the initial water concentration and the concentration of PPA formed (the experiments were always commenced with a PPA-free solution). As the value of Q becomes constant, one can assume that the equilibrium is attained. This value will be noted as K^c because it is calculated on the basis of concentration, but it does not represent the true thermodynamic constant K^T (which is based on activity). The development of Q is displayed in Figure 1, which clearly demonstrates the nonideality of the system because the value of Q is dependent on the catalyst concentration. By plotting K^c versus sulfuric acid concentration, a linear relationship is obtained (Figure 2).

As the Figure 2 shows, the nonideality of the solutions can be explained by the presence of the strong electrolyte (i.e., sulfuric acid). At infinite dilution, K^c and K^T should coincide. Thus, K^c is related with K^T by

$$K^c = \delta [\text{H}_2\text{SO}_4]_0 + K^T \quad (1)$$

where δ is a parameter that describes the nonideality of the solution and is equal to 1.39 with a reaction temperature of 40 °C.

The effect of temperature on the true thermodynamic equilibrium constant is described by the law of Van't Hoff

$$\frac{d \ln K^T}{dT} = \frac{\Delta H_r^0}{RT^2} \quad (2)$$

where ΔH_r^0 stands for the standard reaction enthalpy change. Assuming that ΔH_r^0 is independent of T , the integration of eq 2 from a particular temperature T_{ref} to an arbitrary temperature T leads to

$$\ln \frac{K^T}{K_{\text{ref}}^T} = \frac{-\Delta H_r^0}{R} \left(\frac{1}{T} - \frac{1}{T_{\text{ref}}} \right) \quad (3)$$

This approximation implies that a plot $\ln K^T$ versus $-1/RT$ is a straight line.

To demonstrate the temperature independence of ΔH_r^0 within the range of 30–60 °C, four experiments were carried out at 30, 40, 50, and 60 °C, and they lasted for more than 20 h to get the equilibrium composition.

Although in the Figure 3 the equilibrium constant K^c is displayed and not the true thermodynamic equilibrium constant; however, the experiments were done with the same amount of sulfuric acid, demonstrating the validity of eq 3 in the temperature range 30–60 °C.

Moreover, analyzing the data of Dul'neva et al.,⁵ for the perhydrolysis of acetic acid with low sulfuric acid concentration, the same linear relationship between $\ln(K)$ and $-1/RT$ in the temperature range 20–60 °C can be shown.

The standard enthalpy change of the reaction along K_{ref}^T of our system was estimated in a different model than for the estimation of the kinetic parameters.

The results of the modeling will be discussed in the chapter 3.

2. Influence of Sulfuric Acid Concentration on the Initial Rate. Dul'neva et al.⁵ have noticed for the perhydrolysis of acetic acid that the rate constant does not increase for experiments carried out with the concentration of sulfuric acid exceeding 5 wt %.

To control this observation, several experiments at different sulfuric acid concentrations were carried out at 40 °C.

Figure 4 displays the initial rate of PPA formation [mol⁻¹·min⁻¹] as a function of sulfuric acid concentration [mol⁻¹].

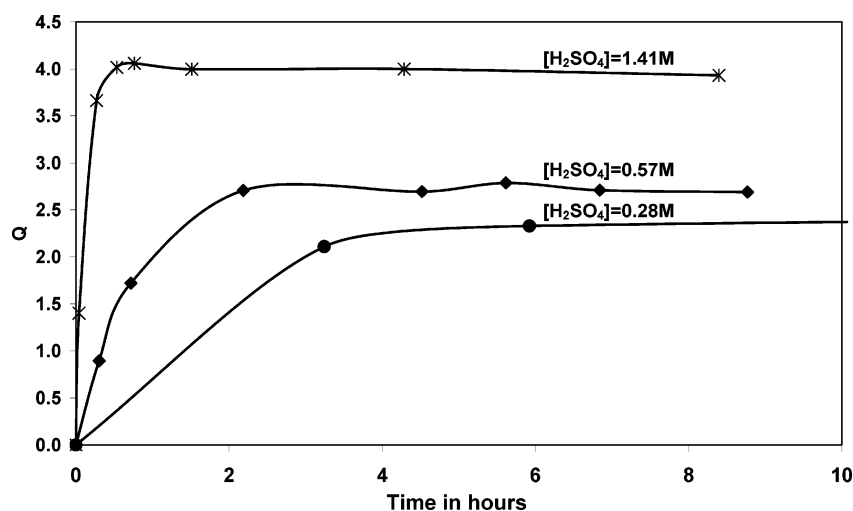


Figure 1. Reaction quotient versus time at 40 °C with different sulfuric acid concentrations.

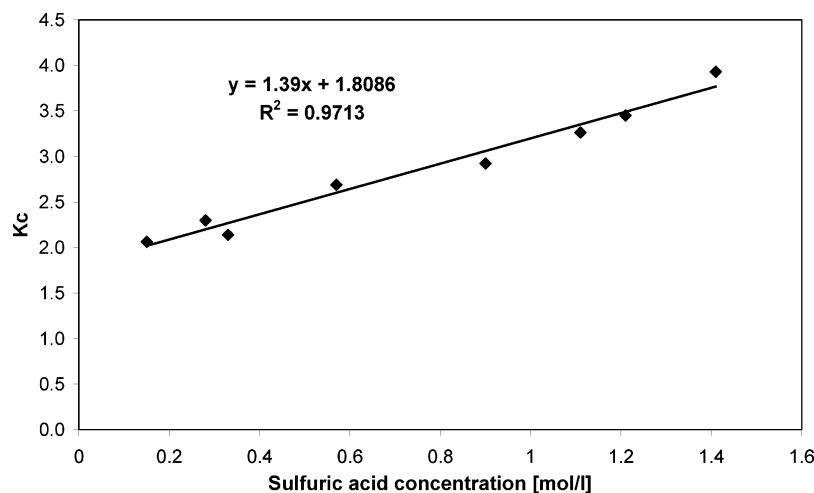


Figure 2. K^c versus sulfuric acid concentration at 40 °C.

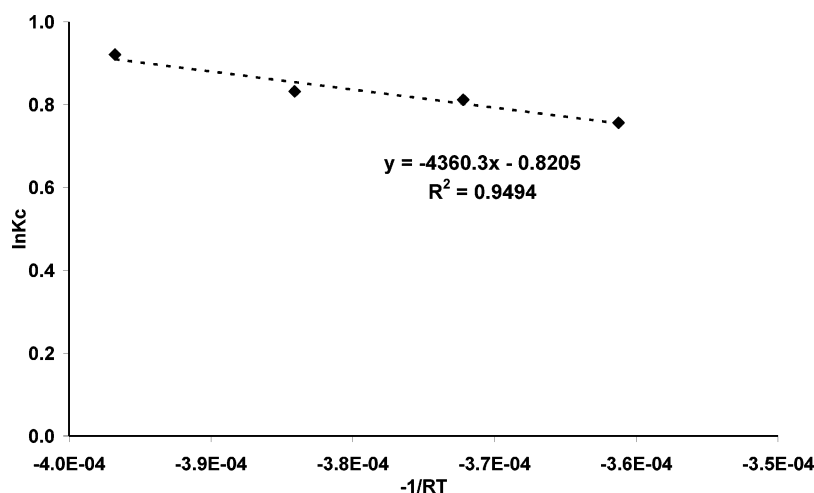


Figure 3. Plot $\ln(K^c)$ versus $-1/RT$ with $[H_2SO_4]: 0.26 \text{ mol}\cdot\text{l}^{-1}$.

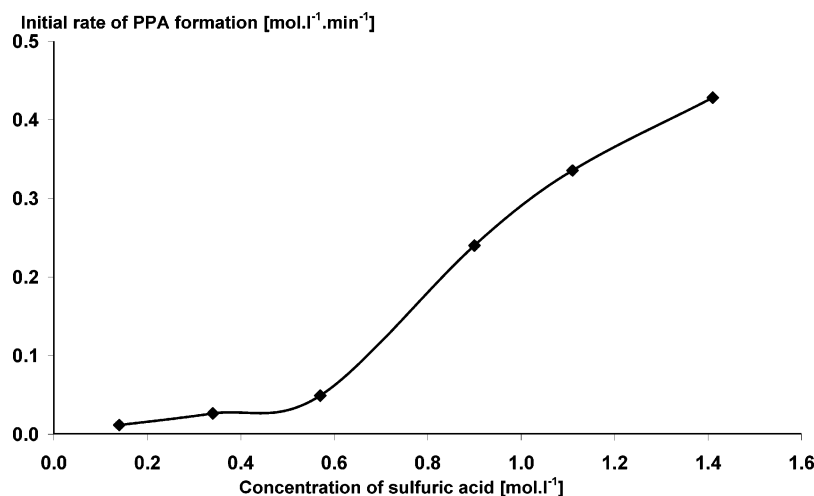


Figure 4. Initial formation rates of PPA as a function of $[H_2SO_4]$ at 40 °C.

Figure 4 demonstrates that there is no limitation of the rate by sulfuric acid in the range $0:1.41 \text{ mol}\cdot\text{l}^{-1}$ (which corresponds to $0:12.32 \text{ wt } \%$). Experiments with sulfuric acid concentration exceeding $2 \text{ mol}\cdot\text{l}^{-1}$ have not been carried out because the initial rate is too fast to be properly recorded.

3. Mechanism and Kinetics Equations. According to the experiments, sulfuric acid concentration and water have an influence on the reaction velocity. Indeed, water is the solvent and has an influence on the equilibrium constant, so its concen-

tration should appear in the rate expression. Moreover, according to Mohammed et al.⁶ the proton transfer is easier from acid to water than from acid to acid. The key issues in the mechanism are the complex protolysis equilibria of the acids being present.

Then, the following mechanism (Figure 5) is proposed to explain the perhydrolysis of propionic acid; where I–V represent protolysis steps and VI–VII reaction steps.

One should keep in mind that several intermediates can appear during the synthesis, but to simplify we assumed that the

reactions VI–VII summarize all of the potential different steps for the formation of the intermediates.

Reactions I–V are the hydroxonium ion sources, which is one of the key points in the mechanism.

Kinetic Expressions. The quasi-equilibrium hypothesis was applied to the reversible proton donor step VI, which implies that

$$k_{+VI}*(PA)*(H_3O^+) \approx k_{-VI}*(PA^+)*(H_2O) \quad (4)$$

where (PA^+) is the activity of the intermediate $CH_3CH_2C^+(OH)_2$; by noting the ratio k_{+VI}/k_{-VI} equal to K_{VI}^T .

Thus, the concentration of intermediate is

$$(PA^+) = \frac{K_{VI}^T*(PA)*(H_3O^+)}{(H_2O)} \quad (5)$$

The rate-determining step is the reversible reaction VII, and the rate can be expressed as

$$\left[\begin{aligned} r &= r_{VII} = k_{VII}*(PA^+)*(H_2O_2) - k_{-VII}*(PPA)*(H_3O^+) \\ &= (H_3O^+)*\left(k_{VII}*K_{VI}^T*\frac{(PA)*(H_2O_2)}{(H_2O)} - k_{-VII}*(PPA)\right) \\ &= k_{VII}*K_{VI}^T* \\ &\quad \frac{(H_3O^+)}{(H_2O)}*\left((PA)*(H_2O_2) - \frac{1}{K_{VI}^T*K_{VII}^T}*(PPA)*(H_2O)\right) \end{aligned} \right] \quad (6)$$

where K_{VII}^T is the equilibrium constant of the reaction VII defined as $K_{VII}^T = (PPA)*(H_3O^+)/(PA^+)*(H_2O_2) = k_{VII}/k_{-VII}$.

Finally, the rate of the system can be expressed by the following expression

$$\left[\begin{aligned} r &= r_{VII} = k_{VII}*K_{VI}^T*\frac{(H_3O^+)}{(H_2O)}*\left((PA)*(H_2O_2) - \frac{1}{K^T}*(PPA)*(H_2O)\right) \\ &= k* \\ &\quad \frac{[H_3O^+]}{[H_2O]}*\left([PA]*[H_2O_2] - \frac{1}{K^T}*[PPA]*[H_2O]\right) \end{aligned} \right] \quad (7)$$

where K^c is estimated from a different model by using the eqs 1 and 3, and the product $k_{VII}*K_{VI}^T$ is denoted by a lumped constant k .

Calculation of Hydroxonium Ions Concentration. The pH of the solution is in practice determined by the protolysis equilibrium I–III. Reaction III should be taken into account to explain the synthesis when no catalysts are used. The intermediate $CH_3CH_2C^+(OH)_2$ has a very low concentration, $CH_3CH_2CO_3H$ is a very weak acid ($pK_a = 7.74$ at $25^\circ C$), and the autoprotolysis of water is negligible. Consequently steps IV–V are ignored here.

The mass balances for the various species can be written as follows:

Sulfate species:

$$[H_2SO_4] + [HSO_4^-] + [SO_4^{2-}] = [H_2SO_4]_0 \quad (8)$$

Organic acid species:

$$[CH_3CH_2COOH] + [CH_3CH_2COO^-] + [CH_3CH_2CO_3H] + [CH_3CH_2CO_3^-] + [CH_3CH_2C^+(OH)_2] = [CH_3CH_2COOH]_0 \quad (9)$$

where $[CH_3CH_2C^+(OH)_2]$ and $[CH_3CH_2CO_3^-]$ are negligible, therefore eq 9 becomes

$$[CH_3CH_2COOH] + [CH_3CH_2COO^-] + [CH_3CH_2CO_3H] = [CH_3CH_2COOH]_0 \quad (10)$$

The electroneutrality principle gives

$$[HSO_4^-] + 2*[SO_4^{2-}] + [CH_3CH_2COO^-] = [H_3O^+] \quad (11)$$

The protolysis equilibria for the reaction I–III give

$$[HSO_4^-] = K_I^c \frac{[H_2SO_4]*[H_2O]}{[H_3O^+]} \quad (12)$$

$$[SO_4^{2-}] = K_{II}^c \frac{[HSO_4^-]*[H_2O]}{[H_3O^+]} = K_I^c*K_{II}^c \frac{[H_2SO_4]*[H_2O]^2}{[H_3O^+]^2} \quad (13)$$

$$[CH_3CH_2COO^-] = K_{III}^c \frac{[CH_3CH_2COOH][H_2O]}{[H_3O^+]} \quad (14)$$

By combining eqs 8, 12 and 13, one gets for the sulfate species

$$[H_2SO_4] = \frac{[H_2SO_4]_0}{1 + K_I^c*\frac{[H_2O]}{[H_3O^+]} + K_I^c*K_{II}^c*\frac{[H_2O]^2}{[H_3O^+]^2}} \quad (15)$$

$$[HSO_4^-] = \frac{K_I^c*\frac{[H_2O]}{[H_3O^+]}}{1 + K_I^c*\frac{[H_2O]}{[H_3O^+]} + K_I^c*K_{II}^c*\frac{[H_2O]^2}{[H_3O^+]^2}}*[H_2SO_4]_0 \quad (16)$$

$$[SO_4^{2-}] = \frac{K_I^c*K_{II}^c*\left(\frac{[H_2O]}{[H_3O^+]}\right)^2*[H_2SO_4]_0}{1 + K_I^c*\frac{[H_2O]}{[H_3O^+]} + K_I^c*K_{II}^c*\frac{[H_2O]^2}{[H_3O^+]^2}} \quad (17)$$

From eqs 10 and 14, the following expressions could be obtained

$$[CH_3CH_2COOH] = \frac{[CH_3CH_2COOH]_0 - [CH_3CH_2CO_3H]}{1 + K_{III}^c*\frac{[H_2O]}{[H_3O^+]}} \quad (18)$$

$$[CH_3CH_2COO^-] = K_{III}^c*\frac{[H_2O]}{[H_3O^+]}\frac{[CH_3CH_2COOH]_0 - [CH_3CH_2CO_3H]}{1 + K_{III}^c*\frac{[H_2O]}{[H_3O^+]}} \quad (19)$$

Finally, by applying the electroneutrality principle of eq 11, we get an implicit expression for the hydroxonium concentration:

$$\left[\begin{aligned} [H_3O^+] &= \frac{K_I^c*\frac{[H_2SO_4]_0*[H_2O]}{[H_3O^+]} + 2*K_I^c*K_{II}^c*[H_2SO_4]_0*\left(\frac{[H_2O]}{[H_3O^+]}\right)^2}{1 + K_I^c*\frac{[H_2O]}{[H_3O^+]} + K_I^c*K_{II}^c*\frac{[H_2O]^2}{[H_3O^+]^2}} \\ &\quad + \frac{K_{III}^c*\frac{[H_2O]}{[H_3O^+]}\left([CH_3CH_2COOH]_0 - [CH_3CH_2CO_3H]\right)}{1 + K_{III}^c*\frac{[H_2O]}{[H_3O^+]}} \end{aligned} \right] \quad (20)$$

By introducing the following notations

$$\alpha = \frac{[\text{H}_2\text{SO}_4]_0}{[\text{H}_2\text{O}]}; \beta = \frac{[\text{CH}_3\text{CH}_2\text{COOH}]_0 - [\text{CH}_3\text{CH}_2\text{CO}_3\text{H}]}{[\text{H}_2\text{O}]}$$

$$\text{and } y = \frac{[\text{H}_2\text{O}]}{[\text{H}_3\text{O}^+]}$$

By dividing eq 20 by water concentration, it follows,

$$1 = \frac{\alpha^2 y^2 (K_1^c + 2^* K_1^c K_{II}^c y)}{1 + K_1^c y + K_1^c K_{II}^c y^2} + \frac{K_{III}^c y^2 \beta}{1 + K_{III}^c y} \quad (21)$$

which de facto is a fourth degree polynomial, from which y can be solved iteratively.

Sulfuric acid is a strong acid, implying that the first donator step is complete, thus $K_1^c \rightarrow \infty$; we get the following simplified equation,

$$1 = \frac{\alpha^2 y^2 (1 + 2^* K_{II}^c y)}{1 + K_{II}^c y} + \frac{K_{III}^c y^2 \beta}{1 + K_{III}^c y} \quad (22)$$

which gives a third degree equation with respect to y .

An ultimate simplification is to regard HSO_4^- and PA as rather weak acids, which implies that $K_{II}^c y$ and $K_{III}^c y$ are negligible in the denominators of eq 22. Indeed, $\text{p}K_a$ values are 1.99 and 4.88, respectively, for HSO_4^- and PA (at 25 °C).

By using these simplifications in eq 22 and by resolving the second degree equation, one gets an explicit expression for the hydroxonium concentration

$$[\text{H}_3\text{O}^+] = \frac{1}{2} [\text{H}_2\text{SO}_4]_0 + \sqrt{\frac{[\text{H}_2\text{SO}_4]_0^2}{4} + 2^* K_{II}^c [\text{H}_2\text{SO}_4]_0 [\text{H}_2\text{O}] + K_{III}^c [\text{H}_2\text{O}] [\text{CH}_3\text{CH}_2\text{COOH}]} \quad (23)$$

One of the main challenges is to be able to express K_{II}^c and K_{III}^c , which are temperature dependent. The literature review regarding the dissociation of organic and inorganic acid is broad, and the protolysis equilibria are studied in dilute aqueous solution and are based on activity.

Knopf et al.⁷ have studied the dissociation reaction of the bisulfate ion; $\text{HSO}_4^- \rightleftharpoons \text{SO}_4^{2-} + \text{H}^+$ in aqueous H_2SO_4 solutions with concentrations range 0.54:15.23 mol·kg⁻¹ in the temperature range -93:200 °C using Raman spectroscopy.

They proposed that equilibrium constant K_{II} can be described by

$$\ln K_{II}^T = \ln K_{II}^O - \frac{1}{R} \left[\left(\Delta H_{II}^O - c_p^O T_O + \frac{1}{2} \frac{dc_p}{dT} T_O^2 \right) \left(\frac{1}{T} - \frac{1}{T_O} \right) - \left(c_p^O - \frac{dc_p}{dT} T_O \right) \ln \frac{T}{T_O} - \frac{1}{2} \frac{dc_p}{dT} (T - T_O) \right] \quad (24)$$

with

$$K_{II}^T = (\text{H}^+)(\text{SO}_4^{2-})/(\text{HSO}_4^-) \quad (25)$$

In the experimental conditions of Knopf et al., the sulfuric acid concentration is low; therefore, the activity coefficient of the solutions is close to unity. By dividing eq 25 with

Table 2. Experimental Conditions for Estimating K_{ref}^T and ΔH_r^O

molar ratio PA/H ₂ O ₂	[H ₂ O] [mol·l ⁻¹]	temperature [°C]	[H ₂ SO ₄] [mol·l ⁻¹]	reaction time [h]
1.00	24.00	30	0.26	72.0
0.99	23.72	40	0.26	52.7
1.01	24.00	40	0.11	73.7
1.00	24.64	50	0.26	45.6
1.00	23.87	60	0.26	23.0
1.00	23.14	55	0.57	29.5
1.01	23.94	50	0.02	46.8

Table 3. Estimated Parameters and Values of Standard Errors at $T_{\text{ave}} = 46.4$ °C

parameters	estimated parameters	estimated relative standard error (%)
k_{ave} (l·mol ⁻¹ ·s ⁻¹)	0.0015	3.2
E_a (kJ/mol)	60.4	4.8
$K_{30^\circ\text{C}}^T$	2.05	2.4
ΔH_r^O (kJ/mol)	-4.17	26.9

a concentration of water in the case of high dilution, that is, 55.5 M, we get the equilibrium constant of the reaction II

$$K_{II}^c = \frac{K_{II}^T}{55.5} \quad (26)$$

According to Sue et al.,⁸ the dissociation constant of propionic acid is correlated with the following empirical density model depending on water density, ρ , and temperature T .

$$\log_{10} K_{\text{PA}}^T = -5.427 + \frac{180.9}{T} + 10.4 \log_{10} \rho \quad (27)$$

where

$$K_{\text{PA}}^T = \frac{(\text{H}^+)(\text{CH}_3\text{CH}_2\text{COO}^-)}{(\text{CH}_3\text{CH}_2\text{COOH})} \quad (28)$$

By applying the same hypothesis as previously, the following expression is obtained

$$K_{III}^c = \frac{K_{\text{PA}}^T}{55.5} \quad (29)$$

The density of water ρ between 30 and 60 °C can be assumed constant and equal to 0.9899.

By adding eqs 7 and 23, the rate of the reaction can be expressed as

$$r = r_{\text{VII}} = \frac{k}{[\text{H}_2\text{O}]} * \left(\frac{1}{2} [\text{H}_2\text{SO}_4]_0 + \sqrt{\frac{[\text{H}_2\text{SO}_4]_0^2}{4} + 2^* K_{II}^c [\text{H}_2\text{SO}_4]_0 [\text{H}_2\text{O}] + K_{III}^c [\text{H}_2\text{O}] [\text{CH}_3\text{CH}_2\text{COOH}]} * \left([\text{PA}] [\text{H}_2\text{O}_2] - \frac{1}{K^c} [\text{PPA}] [\text{H}_2\text{O}] \right) \right) \quad (30)$$

K^c is calculated by eqs 1 and 3.

4. Modeling and Statistical Results. To estimate the value of ΔH_r^O and K_{ref}^T , the experiments should be carried out for a long time for the equilibrium to be attained. To this end, a separate set of experiments was performed (Table 2).

The parameter estimation was carried out by a special software *MODEST*.¹⁰ The objective function θ was minimized

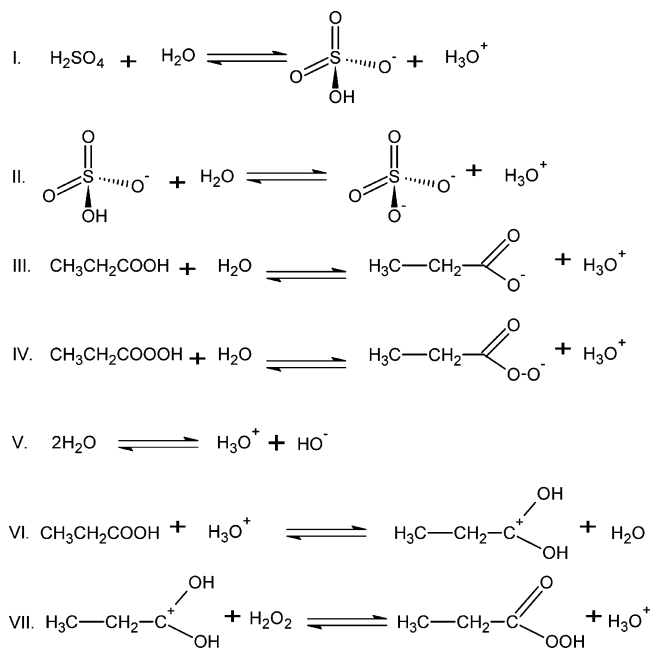


Figure 5. Simplified mechanism for peroxypropionic acid synthesis catalyzed by sulfuric acid in aqueous media.

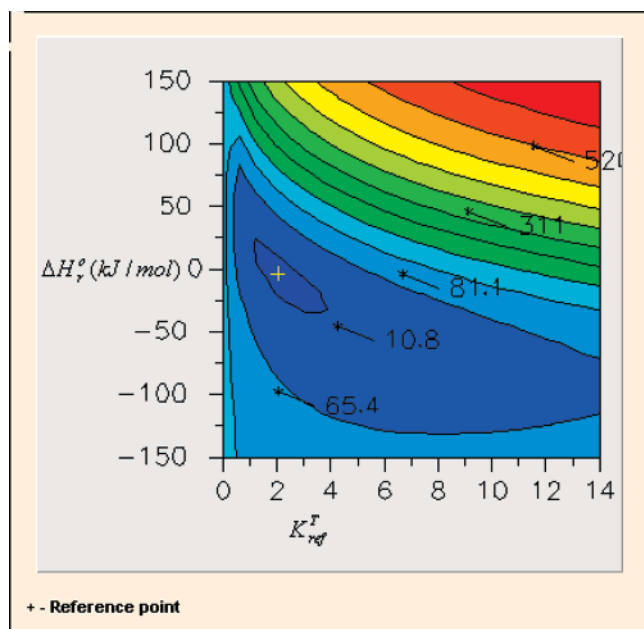


Figure 6. Contour plot of thermodynamic parameters.

Table 4. Heat of Formation of Reactants and Products in the Liquid State

	ΔH_f^o (kJ/mol)
H ₂ O	-285.8 ¹¹
H ₂ O ₂	-187.8 ¹¹
PA	-510.7 ¹¹
AA	-484.5 ¹¹
PPA	Unknown
PAA	-390.12 ¹²

by using Simplex and Levenberg–Marquardt algorithms. This objective function was defined as follows $\theta = \sum (y_i - \hat{y}_i)^2$ where y_i is the experimental value and \hat{y}_i is the estimated value. The concentration of PA, PPA, and H₂O₂ were included in the objective function with equal weight.

Model for Determination of Kinetics and Thermodynamic Parameters Close to Equilibrium. In this model, four param-

	k_{ave}	E_a	δ
k_{ave}	1.000		
E_a	0.013	1.000	
δ	-0.292	0.082	1.000

Figure 7. Correlation matrix for the kinetic model.

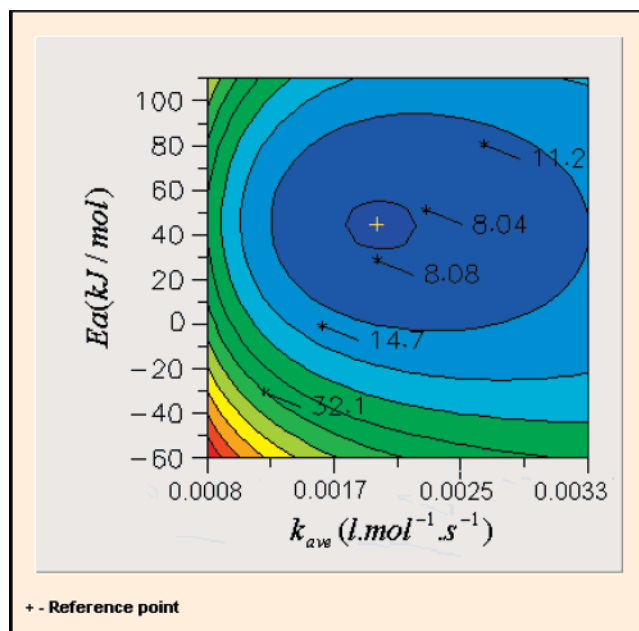


Figure 8. Contour plot of kinetic parameters.

Table 5. Estimated Parameters and Statistical Data at $T_{ave}=44.7$ °C

parameters	estimated parameters	Estimated relative standard error (%)
k_{ave} (l.mol ⁻¹ .s ⁻¹)	0.002	3.3
E_a (kJ/mol)	44.2	6.9
δ (l.mol ⁻¹)	1.33	4.8

eters were estimated: k_{ave} , E_a , ΔH_f^o , and K_{ref}^T with the reference temperature fixed at 30 °C.

The generation rates of the chemical compounds are combined to the mass balances valid for the batch reactor

$$r_{PA} = \frac{d[PA]}{dt} = -r_{VII}$$

$$r_{PPA} = \frac{d[PPA]}{dt} = +r_{VII}$$

$$r_{H_2O_2} = \frac{d[H_2O_2]}{dt} = -r_{VII}$$

$$r_{H_2O} = \frac{d[H_2O]}{dt} = r_{VII}$$

The temperature dependences of the rate constant were described by a modified Arrhenius equation

$$k = k_{ave} \exp\left(\frac{-E_a}{R} \left(\frac{1}{T} - \frac{1}{T_{ave}}\right)\right) \quad (31)$$

where $k_{ave} = Ae^{-(E_a/RT_{ave})}$ and T_{ave} is the average temperature of the experiments. The goal of this modification is to minimize the correlation between the frequency factor and the activation energy during the parameter estimation.

The parameter δ is assumed to be temperature independent within the temperature range 30–60 °C and equal to 1.39, thus

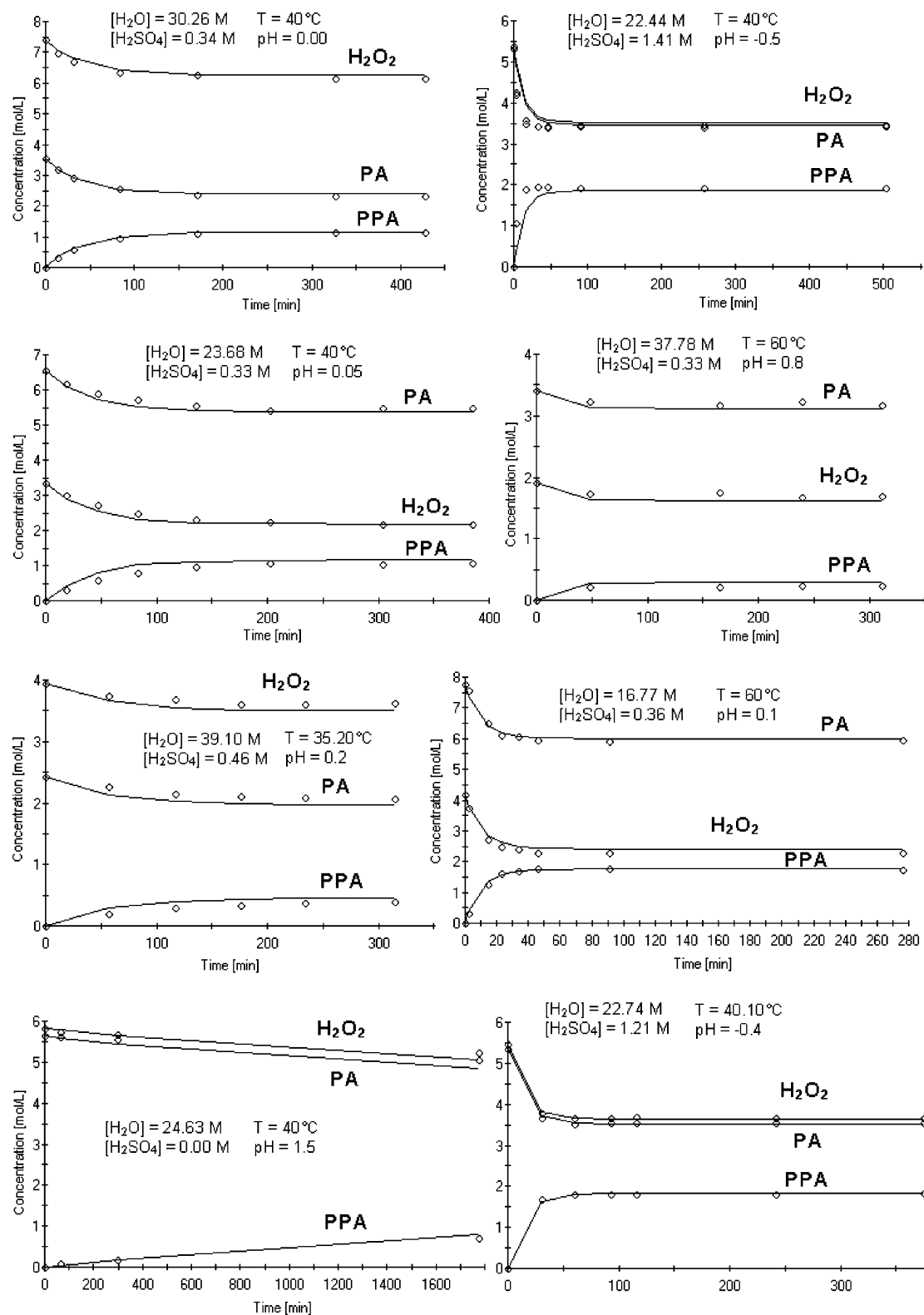


Figure 9. Fit of the model to the experiments.

the equilibrium constant K^c is calculated by

$$K^c = 1.39[\text{H}_2\text{SO}_4]_0 + K_{\text{ref}}^T \exp\left(\frac{-\Delta H^0}{R}\left(\frac{1}{T} - \frac{1}{T_{\text{ref}}}\right)\right) \quad (32)$$

where T_{ref} is fixed at 30°C in eq 32.

Equation 32 is a combination of the eqs 1 and 3.

The coefficient of determination R^2 of the kinetic models is defined as follows

$$R^2 = 1 - \frac{\sum (y_i - \hat{y}_i)^2}{\sum (y_i - \bar{y})^2} \quad (33)$$

where y_i is the experimental value, \hat{y}_i is the estimated value, and \bar{y} is the mean value of the observations.

The explanation coefficient of this model became 99.66%, which shows a good correspondence between the experimental and calculated values. Table 3 gives the estimated and statistical data for each parameter.

From Table 3 it can be concluded that, the estimated relative standard errors are low for each parameter, and, therefore, the parameters are well defined.

Figure 6 represents the contour plot of ΔH_r^0 versus K_{ref}^T , demonstrating a well-pronounced minimum, and the parameters are rather well defined.

The parameters K_{ref}^T and ΔH_r^0 were estimated to 2.05 and -4.17 kJ/mol. The main aim of this model is the achievement of those thermodynamic parameters, whereas kinetic values are only preliminary ones.

Table 4 summarizes the heat of formation ΔH_f^0 of the different species during the perhydrolysis of propionic and acetic acids.

From the literature review, no values for the heat of formation of peroxypropionic acid were found.

According to the Table 4, the heat of formation of PPA can be estimated by using the estimated value of ΔH_r^0 given by the model.

$$\Delta H_R^0 = \Delta H_f^0(\text{PPA}) + \Delta H_f^0(\text{H}_2\text{O}) - \Delta H_f^0(\text{PA}) - \Delta H_f^0(\text{H}_2\text{O}_2) \quad (34)$$

Thus, the heat of formation of PPA is equal to

$$\begin{aligned} \Delta H_f^0(\text{PPA}) &= \Delta H_R^0 - \Delta H_f^0(\text{H}_2\text{O}) + \Delta H_f^0(\text{PA}) + \Delta H_f^0(\text{H}_2\text{O}_2) \\ \Delta H_f^0(\text{PPA}) &= -416.87 \text{ kJ/mol} \end{aligned} \quad (35)$$

To check the validity of this thermodynamic parameter, one can compare the difference of the heat of formation between AA-PA and PAA-PPA.

$$\begin{aligned} \Delta H_f^0(\text{PPA}) - \Delta H_f^0(\text{PAA}) &= -26.75 \text{ kJ/mol} \\ \Delta H_f^0(\text{PA}) - \Delta H_f^0(\text{AA}) &= -26.20 \text{ kJ/mol} \end{aligned} \quad (36)$$

Because both differences are almost identical, it can be concluded that the thermodynamic parameters estimated by our model are reliable in the temperature range 25–60 °C.

Kinetic Model. In this model, only the kinetic parameters were estimated. Equation 30 was used for the modeling, and the same modified Arrhenius equation as previously was applied.

Three parameters were estimated in this model: k_{ave} , E_a , and δ , which are defined as the coefficient in the eq 1: $K^c = \delta^*[\text{H}_2\text{SO}_4]_0 + K^T$.

The purpose of the estimated δ is to check if this parameter does not correlate with the kinetic parameter.

The explanation coefficient of the model became 99.17%. Table 5 gives the value of the estimated parameters and the statistical data.

The values of k_{ave} and E_a are not far away from the previous model. This model is more accurate for describing the kinetics because there are more experiments with different variations included. In this model, the experiments were carried out on a shorter time (4–10 h).

The correlation matrix of the estimated parameters is shown in Figure 7.

From the Figure 7, one can notice that the correlation between the estimated parameters is low.

The three parameters are statistically well defined. The contour plot (Figure 8) shows that there is a clearly visible minimum for the activation energy and the rate constant k_{ave} .

In view of the journal space limitations, only some modeling results are shown in Figure 9.

From Figure 9, it is clear that the kinetic model fits the experimental data. Note, however, that in the case of the

experiment carried out with 1.41 M sulfuric acid concentration, there is a deviation of the fitting at the beginning. That deviation might be explained by the fact that the eq 1 cannot represent the nonideality at this sulfuric acid concentration.

Conclusions

The goal of this work was to establish a kinetic model in batch mode for the synthesis of peroxypropionic acid from the parent carboxylic acid and hydrogen peroxide using sulfuric acid on a temperature range 30–60 °C. The validity of this model is correct for a water concentration range of 16.77–40.66 M, a sulfuric acid concentration range of 0–1.41 M and for a molar ratio PA/H₂O₂ range of 0.40–2.05. During our experiments, the pH was rather stable.

Even if experiments at high sulfuric acid concentration seem to be impossible on an industrial scale (pH is around -0.3 at 40 °C for a sulfuric acid concentration of 1.12 M), the nonideality of the mixtures should be taken into account at lower concentration.

The nonideality is mainly due to the presence of the catalyst and can be represented by the empirical eq 1 at temperatures 30–60 °C and for [H₂SO₄] concentrations 0–1.21 M.

The standard enthalpy change of reaction ΔH_r^0 of the reaction was estimated to -4.17 kJ·mol⁻¹ in the temperature range 30–60 °C, which is substantially lower than the one for peroxyacetic synthesis (-13.7 kJ·mol⁻¹), indicating that the synthesis reaction of PPA is less exothermic than that of PAA.

In general, one can notice that the standard enthalpy change of reaction ΔH_r^0 of the perhydrolysis of acetic and propionic acid is low, which means that the true thermodynamic equilibrium constant is somewhat temperature dependent in the range 20–60 °C.

The activation energy of the system was estimated to 44.2 kJ·mol⁻¹, which is in fact the activation for the forward reaction at $T_{\text{ave}} = 44.7$ °C.

Acknowledgment

Financial support from the Åbo Akademi Forskningsinstitut and the Finnish Graduate School of Chemical Engineering (GSCE) are gratefully acknowledged. This work is part of the activities at the Åbo Akademi Process Chemistry Centre (PCC) within the Finnish Centre of Excellence Programme (2006–2011) by the Academy of Finland.

NOTATION

Q = reaction quotient
 K^c = equilibrium constant, based on concentrations
 K^T = true thermodynamic constant, based on activities
 ΔH_r^0 = standard enthalpy change of reaction [kJ·mol⁻¹]
 ΔH_f^0 = heat of formation of specie
 T = temperature
 R = gas constant (J·K⁻¹·mol⁻¹)
 k = rate constant (l·mol⁻¹·s⁻¹)
 E_a = activation energy (kJ·mol⁻¹)
 A = pre-exponential factor (l·mol⁻¹·s⁻¹)

Greek Letters

δ = parameter, which takes into account the nonideality of the solution
 α = [H₂SO₄]₀/[H₂O]
 β = [CH₃CH₂COOH]₀ - [CH₃CH₂CO₃H]/[H₂O]
 y = [H₂O]/[H₃O⁺]
 θ = objective function

Subscripts

o = initial

ref = reference state

[*i*] = concentration of a component *i* (mol·l⁻¹)(i) = activity of a component *i* (mol·l⁻¹)

ave = average

Abbreviations

PPA = peroxypropionic acid

PA = propionic acid

Literature Cited

- (1) D'Ans, J.; Frey, W. Untersuchungen über die Bildung von Persäuren aus Organischen Säuren und Hydroperoxyd. *Z. Anorg. Chem.* **1914**, *84*, 145.
- (2) Swern, D. *Organic Peroxides*; Wiley-Interscience: New York, 1970.
- (3) Greenspan, F. P.; MacKellar, D. G. Analysis of Aliphatic Peracids. *Anal. Chem.* **1948**, *20*, 1061.
- (4) Prescher, G. Process for the Preparation of Perpropionic Acid Solutions. U.S. Patent 4,088,679, 1978.
- (5) Dul'neva, L. V.; Moskvina, A. V. Kinetics of Formation of Peroxyacetic Acid. *Russ. J. Gen. Chem.* **2005**, *75*, 1125.
- (6) Mohammed, F. O.; Pines, D.; Dreyer, J.; Pines, E.; Nibbering, E. T. J. Sequential Proton Transfer Through Water Bridges in Acid-Base Reactions. *Science* **2005**, *310*, 83.
- (7) Knopf, D. A.; Luo, B. P.; Krieger, U. K.; Koop, T. Thermodynamic Dissociation Constant of the Bisulfate Ion from Raman and Ion Interaction Modeling Studies of Aqueous Sulfuric Acid at Low Temperatures. *J. Phys. Chem. A* **2003**, *107*, 4322.
- (8) Sue, K.; Ouchi, F.; Minami, K.; Arai, K. Determination of Carboxylic Acid Dissociation Constants to 350°C at 23MPa by Potentiometric pH Measurements. *J. Chem. Eng. Data.* **2004**, *49*, 1359.
- (9) Ogata, Y.; Sawaki, Y. Kinetics of the Acid-Catalysed Formation of Aliphatic Peracids from Hydrogen Peroxide and Aliphatic Acids in Dioxin. *Tetrahedron* **1965**, *21*, 3381.
- (10) Haario, H. *MODEST-User's Guide*; Profmath Oy: Helsinki 1994.
- (11) Lide, D. R. *CRC Handbook of Chemistry and Physics*, 75th edition; CRC Press: Boca Raton, FL, 1995.
- (12) Havel, S.; Greschner, J. Explosion Properties of Peroxyacetic Acid. I. Thermodynamic Calculation of the Explosion Characteristics of Peroxyacetic Acid. *Chem. Prum.* **1966**, *16*, 73.

Received for review May 11, 2007

Revised manuscript received October 9, 2007

Accepted October 16, 2007

IE070670E

Stability of hydrogen peroxide during perhydrolysis of carboxylic acids on acidic heterogeneous catalysts

Sébastien Leveneur^{a,b,}, Narendra Kumar^a, Tapio Salmi^a, Dmitry Yu. Murzin^a*

^aLaboratory of Industrial Chemistry and Reaction Engineering, Process Chemistry Centre, Åbo Akademi University, Biskopsgatan 8, FI-20500 Åbo/Turku, Finland.

Tel: +358 2 215 8942; Fax: +358 2 215 4479; E-mail: sleveneu@abo.fi

^bLSPC-Laboratoire de Sécurité des Procédés Chimiques, INSA Rouen, Place Emile Blondel, BP8, 76131 Mont-Saint-Aignan Cedex, France.

ABSTRACT

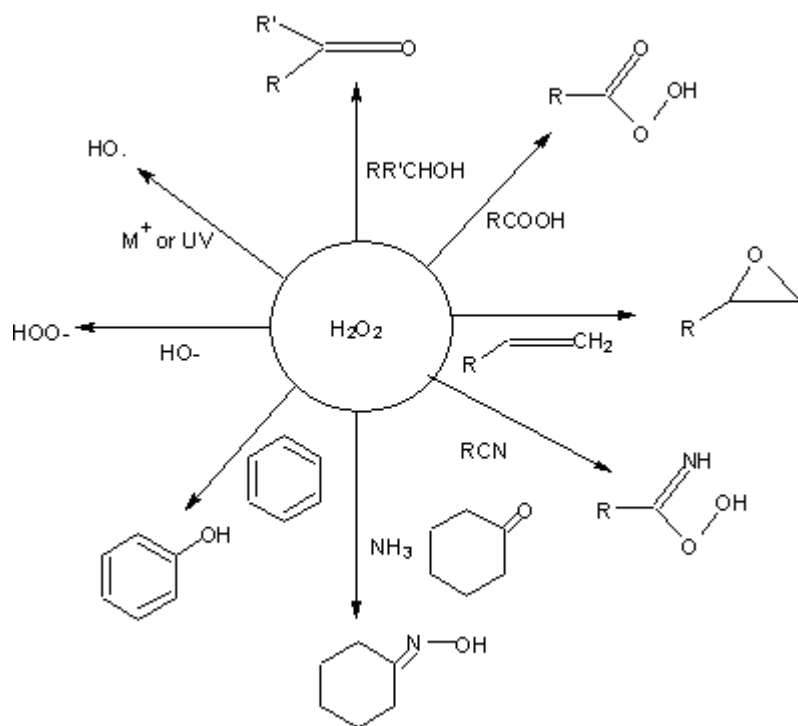
This paper describes a study of the stability of hydrogen peroxide in the presence of different aluminosilicate materials, in connection with investigation of carboxylic acid perhydrolysis. During the reaction, aluminosilicate materials such as H- β zeolites, mesoporous material H-MCM-41 and alumina initiate the decomposition of hydrogen peroxide. The reason of the spontaneous decomposition of H₂O₂ is related to the partial dealumination of these zeolites. However, in case of experiments carried out with H-ZSM-5 zeolite catalysts, a slight catalytic effect on the perhydrolysis and no spontaneous decomposition of hydrogen peroxide were noticed. The use of cation exchange resins as catalysts is more kinetically beneficial than H-ZSM-5 zeolite catalysts.

Keywords: perhydrolysis; aluminosilicate materials; decomposition; hydrogen peroxide

1. Introduction

The interest in hydrogen peroxide has increased in the last decade. For instance, the world production of hydrogen peroxide was around 1.9 million tonnes in 1994, and grew to 2.2 million tonnes in 2006 [1]. The applications of this compound are versatile: it is used as an oxidizing agent for inorganic and organic compounds, bleaching agent for textiles and wood, as an antiseptic for therapeutic use, as a disinfectant for wastewater and as a sterilizing agent.

The use of H_2O_2 as an oxidizing agent [2] in chemistry avoids the use of conventional heavy-metal oxidants which form toxic waste; application of nitric acid which form the greenhouse gas N_2O ; and utilization of molecular oxygen, which requires safety precautions. Scheme 1 illustrates the application of hydrogen peroxide in some fine chemical synthesis reactions [3].

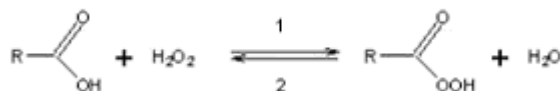


Scheme 1. Applications of H_2O_2 in fine chemical reactions

From environmental and economical point of view, these reactions should be carried out with heterogeneous catalysts, which should not decompose hydrogen peroxide.

The aim of this paper is to treat the stability issues of H₂O₂ in acidic environment over different heterogeneous catalysts, and especially aluminosilicate materials. Traditionally, synthetic aluminosilicate materials, and more particularly synthetic zeolites are widely used as catalysts in the petrochemical industry, for instance in fluid catalytic cracking and hydro-cracking. The use of zeolites for fine chemicals production is widespread: acylation, alkylation, hydroxyalkylation of aromatic and heterocyclic compounds and rearrangement reactions [4]. Selectivity (including shape selectivity), catalytic effects and environmental regulations explain the application of such materials in industry. In particular, oxidation reactions such as epoxidation of olefins, hydroxylation of arenes, oxidation of O-, S- and N- functionalities with hydrogen peroxide are conducted using Ti-zeolites. The originality of this paper is the investigation of an oxidation reaction with H₂O₂ in the presence of titanium free aluminosilicate materials.

To illustrate the stability of H₂O₂, the peroxycarboxylic acids synthesis was selected as a model reaction (Scheme 2).



Scheme 2. Synthesis of PCA from the parent carboxylic acid and hydrogen peroxide

This reaction occurs at acidic pH [5-7], and is traditionally catalyzed by sulfuric acid. This reaction was selected because spontaneous decomposition of hydrogen peroxide or peroxycarboxylic acids is negligible [8-10] in traditional experimental conditions (pH: 1-3; and temperature: 20-50°C); and configurational diffusion can be neglected because the size of the reactant molecules is smaller compared to the pore size of the materials used (Table 1). Thus, by using heterogeneous catalysts for this reaction, only decomposition due to the solid acid catalyst can occur.

Table 1. Channel structure of the tested aluminosilicate materials

Aluminosilicate materials	Channel structure
β	3-Dimensional pore system; 12-ring channel in c direction with pores 7.6 x 6.4 Å plus two 12-ring channels in a direction perpendicular to c-direction with pores 7.6 x 6.4 Å and 5.5 x 5.5 Å
ZSM-5	3-Dimensional pore system; straight 10 member-ring 5.2 x 5.7 Å channels connected by sinusoidal 5.3 x 5.6 Å channels. Intersection cavity: 9 Å
MCM-41	1-Dimensional hexagonal arrangement of uniformly open channels from 15 to 100 Å

In a previous paper, we have demonstrated that cation-exchange resins [11] are suitable heterogeneous catalysts for the carboxylic acids perhydrolysis. Our objective in the present study is to elucidate hydrogen peroxide stability towards aluminosilicate type materials, and to compare the catalytic efficiency of these aluminosilicate materials versus cation-exchange resins in such reactions.

Except the communication of Palani *et al.* [12], in which the efficacy of different zeolites and mesoporous materials was investigated, there are no other scientific papers dealing with perhydrolysis of carboxylic acids over these materials.

2. Experimental section

2.1 Apparatus and experimental procedures

All experiments were performed in a 250 ml jacketed glass reactor vessel. The reactor was equipped with a mechanical agitator and a temperature probe. Water was pumped through the outer jacket of the vessel to control the temperature of the reaction mixture. A pitched blade impeller (PTFE coated) was used to ensure a vigorous mixing during the reaction.

A reflux condenser was attached to the top of the reactor (adjusted at 0°C) to avoid loss of volatile liquid-phase compounds. In case that decomposition of peroxypropionic acid (PPA) or H₂O₂ appeared, an inert carrier gas (Helium, AGA, 99.996%) was introduced to the reactor through one of the necks to avoid the accumulation of oxygen in the gas phase.

To prevent contamination induced by alkaline and metal components, which initiate the catalytic decomposition of peroxypropionic acid and hydrogen peroxide, all parts of the reactor system being in contact with the reaction solution were washed with hydrochloric acid followed by another washing, with a phosphate-free detergent solution.

In case of experiments carried out for testing the stability of hydrogen peroxide towards zeolite, at first stage, deionized water and zeolites were mixed together in the reactor. As the desired reaction temperature was reached, the preheated hydrogen peroxide solution (Merck, 30 wt.%) was added through a dropping funnel. In fact, hydrogen peroxide was preheated at the same temperature as the reaction temperature. At the time “zero” the required amount was introduced into the reactor.

In case of experiments carried out for checking the catalytic effect of zeolites on the propionic acid perhydrolysis reaction, at the first stage, propionic acid (Acros, 99 wt.%) and the catalyst were mixed together in the reactor. Thereafter, the same protocol as described above was followed.

According to a patent [13], during the reaction of hydrogen peroxide and propionic acid in water in presence of an acid catalyst, the danger of explosion is suppressed by employing a temperature of maximum 60°C.

From our previous study [9, 11], the kinetics of propionic acid perhydrolysis is demonstrated to be dependant on the Brønsted acid sites in case of homogeneous and heterogeneous catalysis. One should keep in mind that the goal is to check the stability of hydrogen peroxide towards aluminosilicate materials in acidic environment by study the reaction of perhydrolysis. Due to the low Brønsted acid site amount of these catalysts and the difficulty to measure them in the temperature range 40-50°C, the kinetic comparisons were based on catalyst loading. Table 2 introduces the experimental matrix.

Table 2. Experimental parameters for the catalyst comparison in the batch reactor

Reaction temperature [°C]	40-50
Rotating speed [rpm]	250-350
H ₂ O ₂ [mol.l ⁻¹]	5.75-6.10
PA [mol.l ⁻¹]	5.70-5.80
H ₂ O [mol.l ⁻¹]	23.85-24.10
Catalysts loading [g.l ⁻¹]	8.26-43.40

2.2 Analytical methods

Samples were withdrawn from the reaction mixture by a plastic syringe (to avoid contamination of the solution by trace of metals) and they were analyzed by the Greenspan and Mackellar method [14]. The concentration of hydrogen peroxide was determined by titration by using a standard solution of ammonium cerium sulphate (0.1 N). The concentrations of propionic and peroxypropionic acids were determined by titration with an automatic titrator (Metrohm 751 GPD Titrino) by using a standard solution of sodium hydroxide (0.2 N).

2.3 Catalyst properties

The acidic properties of the different aluminosilicate materials are summarized in Table 3. The Brønsted and Lewis acid sites were determined by FTIR using pyridine as probe molecule [15-18]. The specific surface area was determined by N₂ adsorption, calculated by Dubinin method for the microporous materials and by BET method for the mesoporous H-MCM-41 [15-18].

Table 3. Properties of the aluminosilicate materials

	SiO₂/Al₂O₃ mol/mol	Brønsted acid sites at 523 K μmol/g	Lewis acid sites at 523 K μmol/g	Specific surface area m²/g
H-β-25	25	269	162	807
H-β-75	75	147	39	664
H-β-300	300	82	30	805
H-ZSM5-23	23	416	36	443
H-ZSM5-31	31	-	-	-
Al₂O₃	-	7	156	299
H-MCM-41	40	26	40	1242

A comparison between a cation exchange resin, i.e., Amberlite IR-120 and zeolites was carried out. The characteristics of this commercial resin are summarized in Table 4.

Table 4. Properties of Amberlite IR-120

Supplier	Aldrich
Polymer type	Gel
Cross linking %	8
Moisture content % mass	45
Capacity by dry weight meq/g	4.4
Native particle size range mm	0.3-1.2

The pretreatment of Amberlite IR-120 consisted of a drying step at 70°C for 48 h, since a higher drying temperature might affect the sulfonic acid sites on the catalyst. The parameter capacity by dry weight represents the number of Brønsted groups bearing (i.e., sulfonic group) by the resins, which is equivalent to the Brønsted acid sites of zeolites displayed in Table 3.

To dealuminate zeolite, the protocol of Marques *et al.* [19] was applied to H- β -25 zeolite, i.e., an acid treatment at 30°C by HCl (1N) for 10 min was performed.

The Al concentration in the reaction mixture was measured by ICP-OES (PerkinElmer Optima 5300DV).

3. Results and discussion

Experiments of the perhydrolysis of propionic acid over different aluminosilicate materials gave two antagonist observations: either the catalyst was active in perhydrolysis, or no formation of peroxypropionic acid was observed due to the decomposition of hydrogen peroxide over these acidic materials.

3.1. Aluminosilicate materials initiating the decomposition of hydrogen peroxide

During the reaction of perhydrolysis, decomposition of hydrogen peroxide was observed with the following materials: H- β zeolites, H-MCM-41 and alumina. For the sake of simplicity, the ratio $\frac{[H_2O_2]}{[H_2O_2]_0}$, where $[H_2O_2]_0$ is the initial concentration, was plotted versus the reaction time. An experiment with only hydrogen peroxide without any catalyst was carried out at 50°C; no spontaneous decomposition of this reactant was observed.

According to Sengupta *et al.* [20], the decomposition of hydrogen peroxide on un-impregnated silica-alumina material is dependent of the strength of acid sites. In our previous studies [9, 11] no decomposition of hydrogen peroxide was noticed due to Brønsted acidity in either sulfuric acid or sulfonic groups bearing by the resins. For that reason Lewis acid sites in such materials can be thought to be responsible for the decomposition of hydrogen peroxide.

However, Rocha *et al.* [21] have studied the kinetics of peroxyacetic acid formation from acetic acid and hydrogen peroxide in the presence of scandium (III) triflate. They have demonstrated that the use of this strong Lewis acid enhanced the reaction rate six fold compared to the catalyst absence; and no decomposition of hydrogen peroxide was reported.

Several articles treat the dealumination of H- β zeolites [22-23], or type A and Y zeolites [24] by acidic leaching. Marques *et al.* [19] have shown that treatment of HBEA zeolite (Si/Al = 12.5) with an HCl solution at 30°C causes a rapid dissolution of the extraframework Al species, especially the monomeric ones and a slow dissolution of the framework Al atoms bridging OH groups and structure defects. These Al species released in the reaction mixture could catalyze the H_2O_2 decomposition.

In this chapter, the reason of hydrogen peroxide decomposition will be discussed regarding the Lewis acid, partial dealumination and SiO_2/Al_2O_3 ratio.

Fig. 1 displays three different experiments carried out with H- β -25 zeolites.

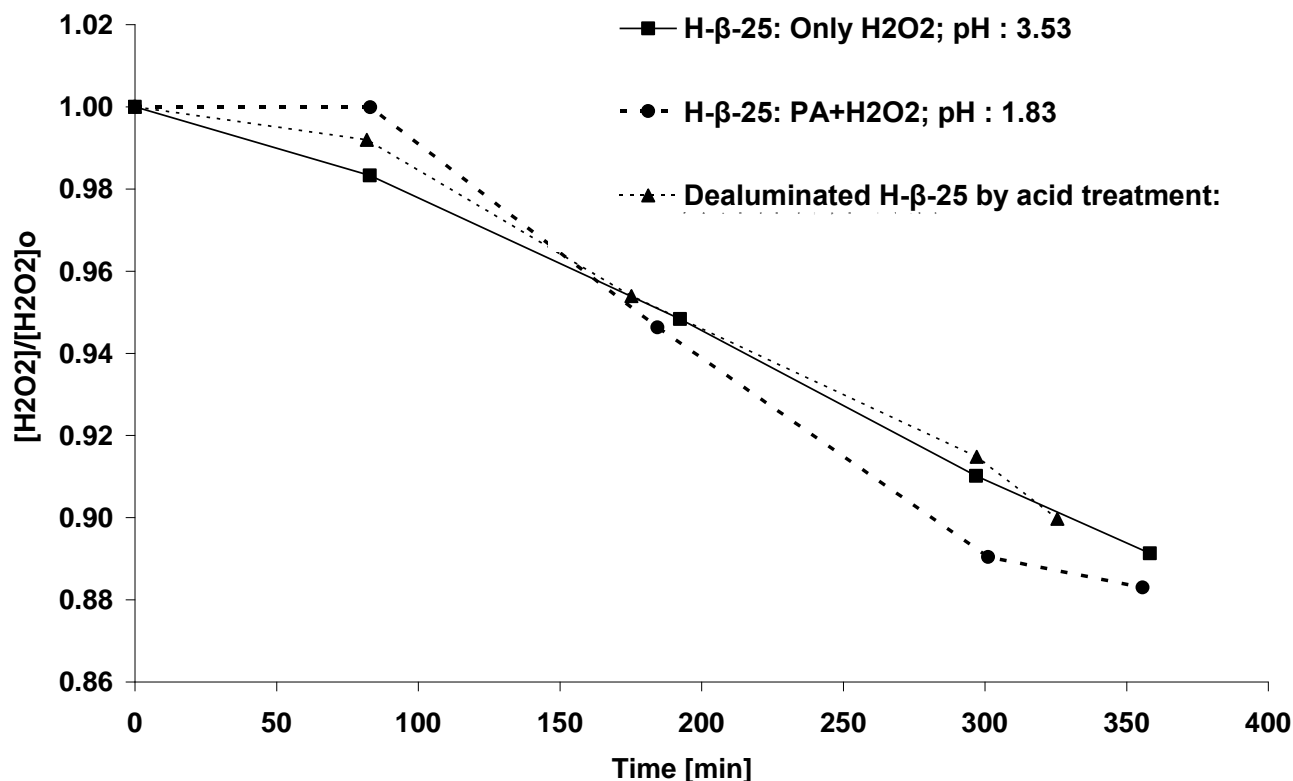


Fig. 1 Experiments carried out in the presence of H- β -25 zeolite at 50°C, at 350 rpm and loading of 18.25 g/l

The difference of pH is due to the presence of PA, which acidifies the mixture. In case of experiments carried out with a mixture PA and H₂O₂, concentration of PA remains constant. Even if the decomposition of H₂O₂ is strongly dependent on the pH, one can conclude that the production of PPA or presence of PA does not influence the kinetic of decomposition. From Fig. 1, the kinetics of hydrogen peroxide decomposition for experiments carried out with PA and H₂O₂ mixture in presence of H- β -25 and dealuminated H- β -25 by acidic treatment is similar. This observation implies that the decomposition of hydrogen peroxide is due to Al species, in particular dissolution of Al atoms from the framework of the zeolite. The difference of aluminium concentration between the end and the beginning of the experiment carried out with H- β -25 and PA and H₂O₂ mixture was measured to be equal to 181 mg.l⁻¹, which can explain the decomposition of hydrogen peroxide.

From Fig. 1, one can notice the presence of an initial retarding period, which is more significant in case of the experiment carried out with H- β -25 and PA and H_2O_2 mixture. The presence of the initial retarding effect, occurring for a long time period, during the decomposition of hydrogen peroxide is not the first observation in the literature. For instance, this phenomenon of retarding phase was noticed in case of H_2O_2 decomposition by Fe(III). De Laat *et al.* [25] had explained it by the formation of $\cdot OH$ radicals via Fenton's reaction, with duration of this phase depending on various parameters, such as the initial concentration of Fe(III). In the present case, this retarding period could be explained by the dissolution of Al. Indeed, in case of experiments carried out over dealuminated H- β -25 this retarding period seems to be shorter, because Al atoms from the extraframework have been already removed by acidic treatment.

To check if the decomposition of hydrogen peroxide in such conditions is due to the partial dissolution of Al species in the liquid phase, an experiment with aluminium oxide was carried out (Fig. 2). Alumina was chosen instead of an aluminium salt because its structure is closer to Al species present in the zeolites.

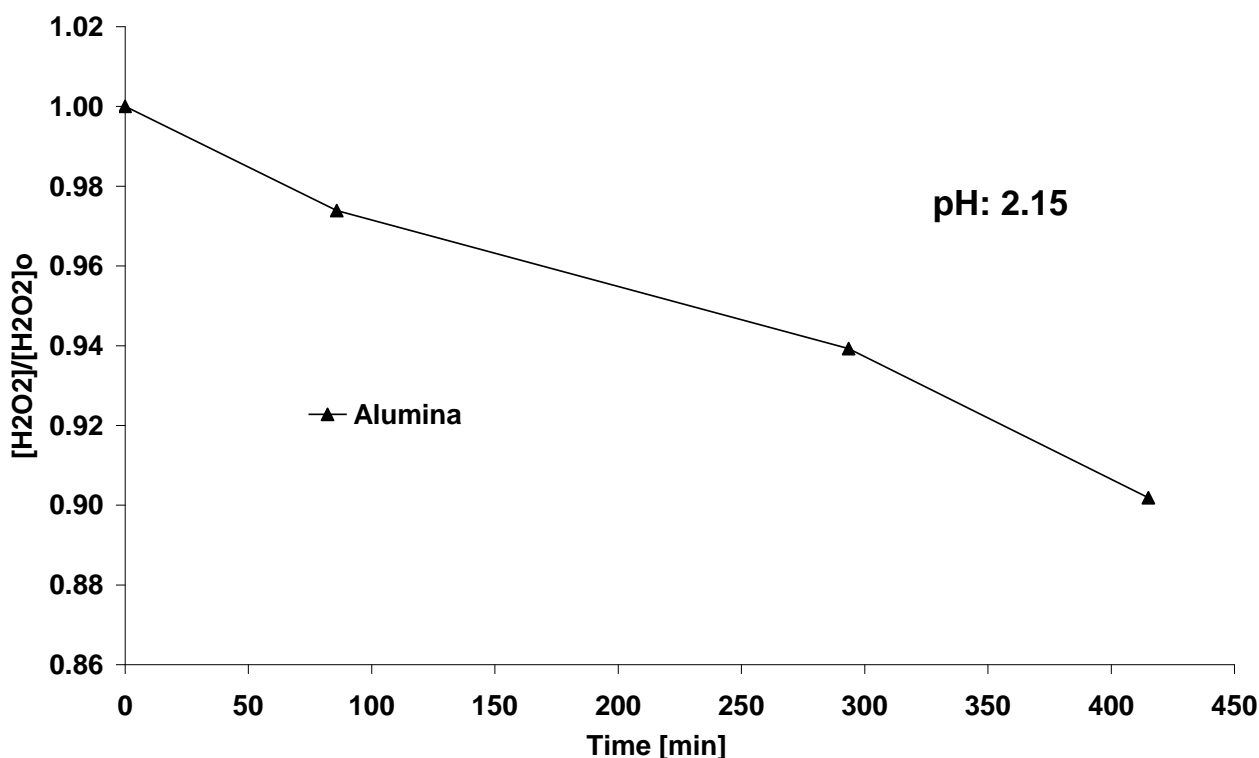


Fig. 2 Experiment carried out with a mixture of PA and H_2O_2 over alumina at 50°C, at 350 rpm and loading of 18.25 g/l

Fig. 2 shows that hydrogen peroxide decomposes over Al_2O_3 , which implies that the assumption of H_2O_2 decomposition is related to the partial dissolution of Al species is plausible. The ratio $[\text{PA}]/[\text{PA}]_0$ remained constant during this experiment.

To check if the decomposition of hydrogen peroxide is related to the ratio $\text{SiO}_2/\text{Al}_2\text{O}_3$, H- β zeolites with three different $\text{SiO}_2/\text{Al}_2\text{O}_3$ ratios were used as displayed by Fig. 3. No production of PPA was noticed, but instead, decomposition of hydrogen peroxide was observed.

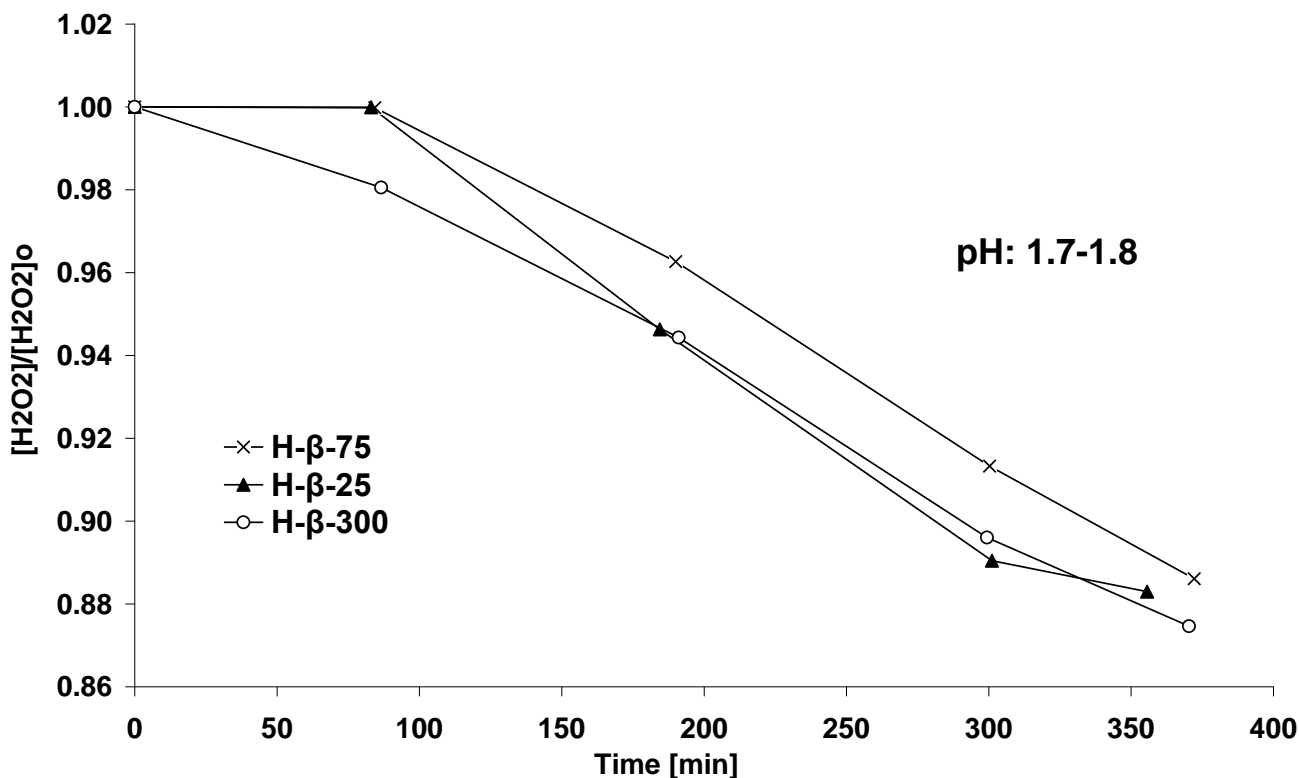


Fig. 3 Experiments carried out with a mixture of PA and H_2O_2 over H- β zeolites at 50°C , at 350 rpm and loading of 18.25 g/l

During these experiments, the concentration of PA remained constant (Fig. 3). The kinetic curves are similar, but there is an initial retarding effect during the experiments carried out with H- β -75 and H- β -25. No decomposition of hydrogen peroxide was reported in the paper of Palani *et al.* [12] during the synthesis of peroxyacetic acid using H- β with a ratio Si/Al equal to 12, catalyst loading lower than 1 g/l and at 25°C . From Fig. 3, it can be concluded that the decomposition is not directly related to the $\text{SiO}_2/\text{Al}_2\text{O}_3$ ratio.

Although, the amount of Lewis acid sites is 5 times higher in case of H- β -25 than H- β -75 or H- β -300 (Table 3), the kinetics of decomposition is similar. Thus, the Lewis acid sites bearing on these materials are not responsible for the H_2O_2 decomposition. Furthermore, the amount of Lewis acid sites in H-ZSM-5-23, which does not induce the decomposition of H_2O_2 , is on the same order of magnitude as in H- β -75, H- β -300 or H-MCM-41 (Table 3). Thus, the assumption that the decomposition of hydrogen peroxide is due to the presence of Lewis acid sites in aluminosilicate materials can be rejected.

During the experiments, the decomposition of H_2O_2 appeared only at zeolite loadings exceeding 8.26 g/l, which explains the absence of decomposition in the study of Palani *et al.* [12]. Below this catalyst loading, the perhydrolysis of propionic acid due to the protolysis of the carboxylic acids occurs [7]. The change of the catalyst loading in the range 10.24-18.25 g/l does not influence the kinetics of H_2O_2 decomposition at 50°C (Fig. 4). In both cases, there is a retarding effect; however, this induction period is longer for the experiment carried out with a loading of 18.25 g/l.

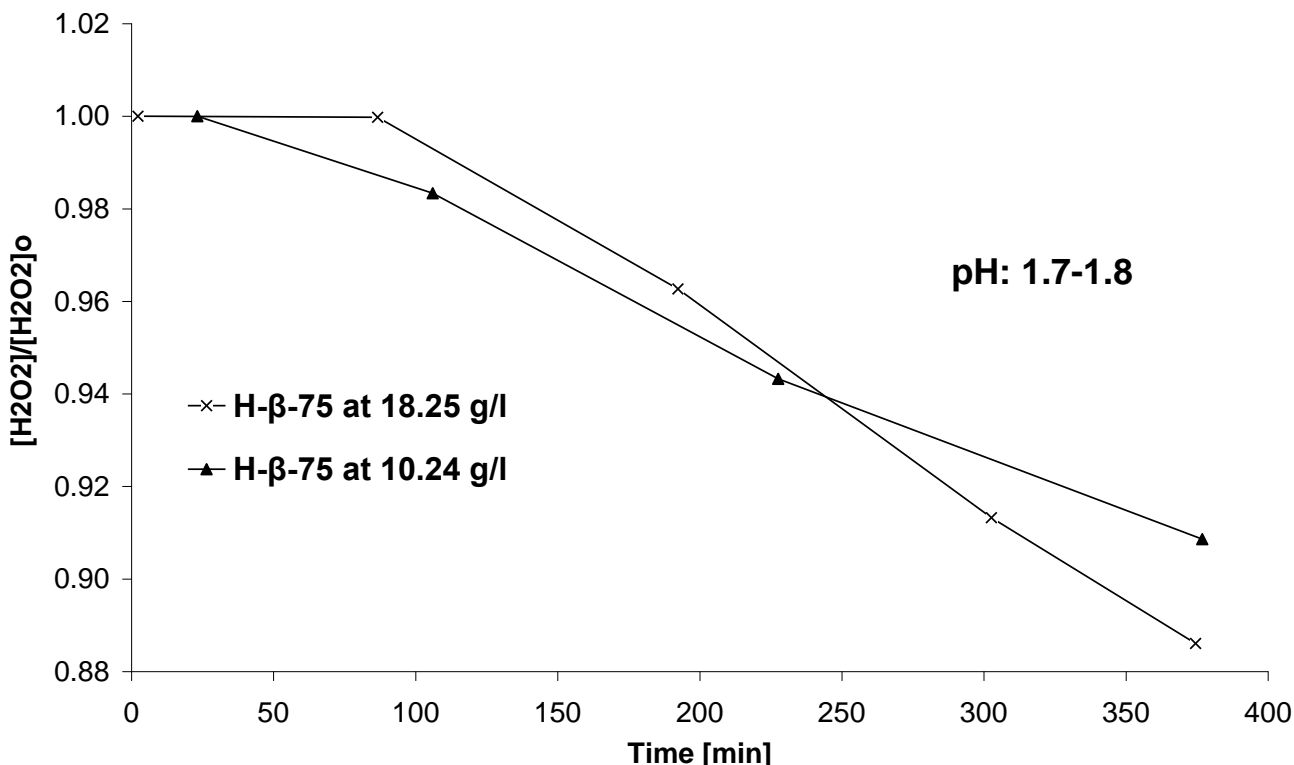


Fig. 4 Experiments carried out with a mixture of PA and H_2O_2 over H- β -75 zeolites at 50°C and at 350 rpm

A mesoporous material H-MCM-41 was used to study its behaviour in the mixture of PA and H_2O_2 . Fig. 5 displays the kinetics of H_2O_2 decomposition versus time for this mixture over H-MCM-41 and H- β -75 at 40°C. During these reactions, the concentration of PA remains constant. From Fig. 5 one can notice the same trend as with alumina or H- β materials, i.e., a decomposition phase of hydrogen peroxide. The retarding period is more pronounced at the beginning of the reaction (until 300 min) for H-MCM-41 than for H- β -75, which can be explained by the higher stability of the mesoporous material towards on acidic environment. After the induction period, the kinetics of H_2O_2 decomposition is similar in both cases.

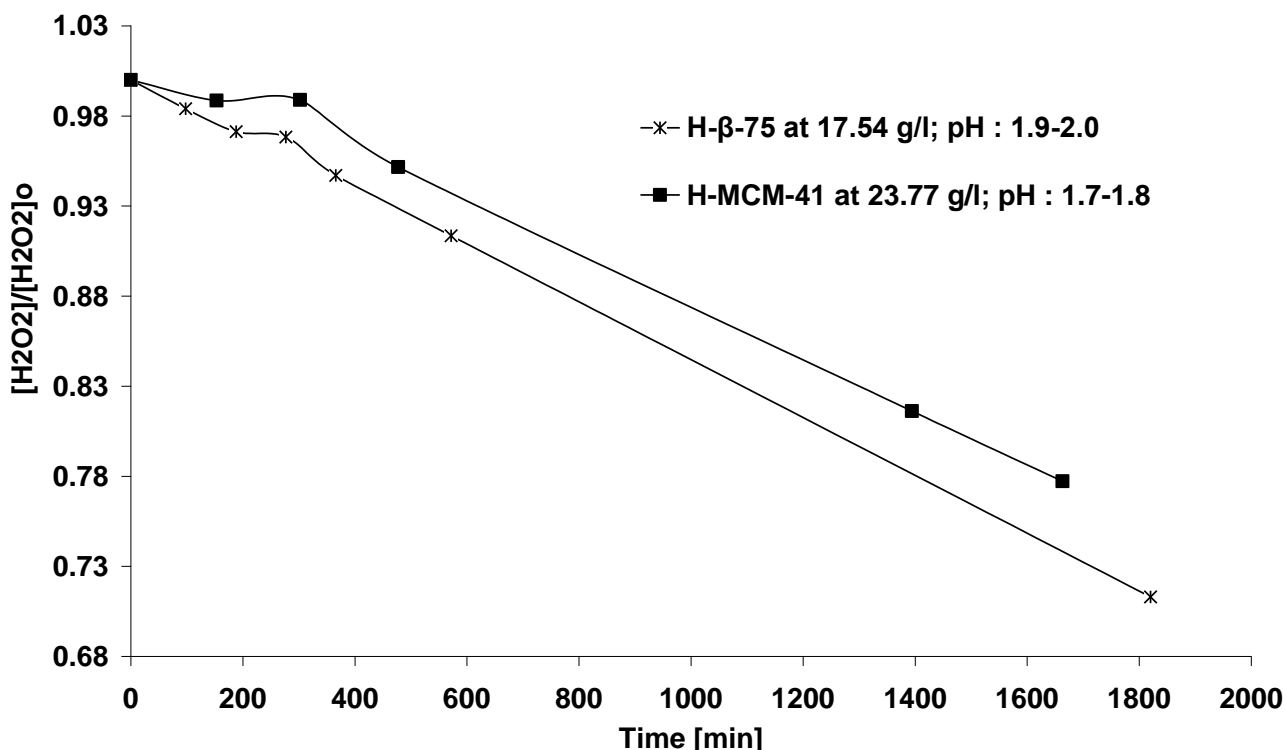


Fig. 5 Experiments carried out with a mixture of PA and H_2O_2 over H-MCM-41 and H- β -75 at 40°C and at 350 rpm

The decomposition of hydrogen peroxide is due to the presence of Al species dissolved from the framework structure of the H- β zeolites and mesoporous materials H-MCM-41. The slow kinetics of H_2O_2 is related to the fact that the dissolution of Al species from the framework is a slow phenomenon [19]. Furthermore, the Al species released are in oxide or hydroxide form, and according to Mani *et al.* [26], their catalytic activity towards hydrogen peroxide decomposition is minor.

3.2 Materials which catalyze the perhydrolysis reaction

In case of experiments carried out with H-ZSM-5 or Amberlite IR-120, no decomposition of hydrogen peroxide was noticed, while the catalytic effect on the perhydrolysis of propionic acid was visible. The purpose of this section is to propose an explanation for the selectivity of the aluminosilicate materials towards the reaction between H_2O_2 and PA, and to perform a comparative study of these materials. This comparison was based on equal catalyst loadings, and the experiments were carried out under similar conditions.

Fig. 6 shows that H-ZSM-5 zeolite catalyzes the perhydrolysis of propionic acid. Moreover, the activity of H-ZSM-5-23 is higher than H-ZSM-5-31, due to higher amount of Brønsted acid sites. In case that no external catalyst is added, some perhydrolysis takes place (Fig. 6). This is due to the fact that propionic acid itself is a weak Brønsted acid having some catalytic effect.

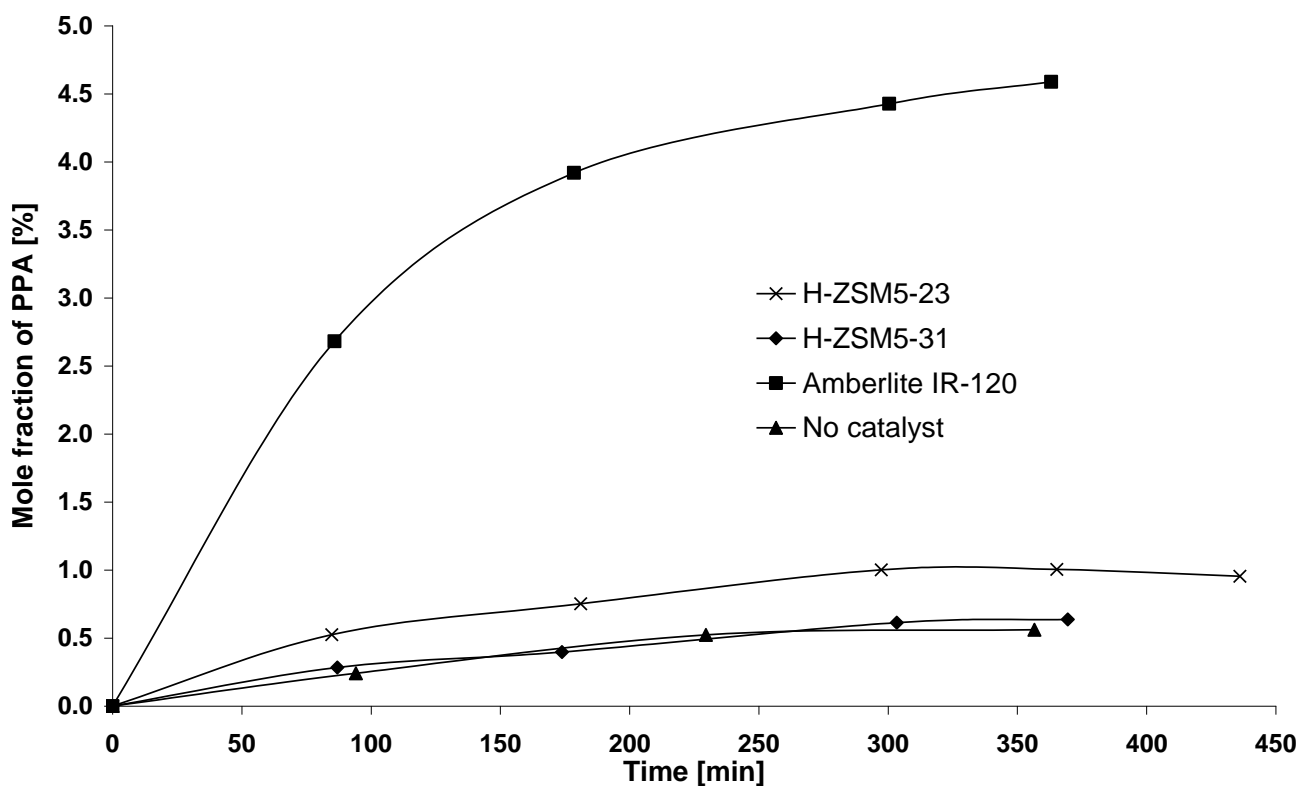


Fig. 6 Formation of PPA over different catalysts at 50°C at 43.38 g/l of loading and 350 rpm

Fig. 6 demonstrates that cation exchange resins are more beneficial than zeolites for the synthesis of peroxypropionic acid from hydrogen peroxide and propionic acid. An

estimation of the apparent second-order rate constants based on the product $[PA] \cdot [H_2O_2]$ is provided in Table 5. The apparent Brønsted acid concentration $[H^+]$ is also displayed for each catalyst (except for H-ZSM-5-31), which is the sum of the amount of Brønsted acid sites of the solid catalyst and the number of hydroxonium ions released due to the protolysis of PA present per litre of reaction mixture.

Table 5. Apparent rate constants and $[H^+]$

	$k \text{ (l.mol}^{-1} \cdot \text{s}^{-1})$	Apparent $[H^+] \text{ (mol.l}^{-1})$
H-ZSM-5-23	$5.51 \cdot 10^{-6}$	$1.80 \cdot 10^{-2}$
H-ZSM-5-31	$2.95 \cdot 10^{-6}$	-
Amberlite IR-120	$2.18 \cdot 10^{-5}$	$1.91 \cdot 10^{-1}$
Without catalyst	$1.15 \cdot 10^{-6}$	$5.64 \cdot 10^{-3}$

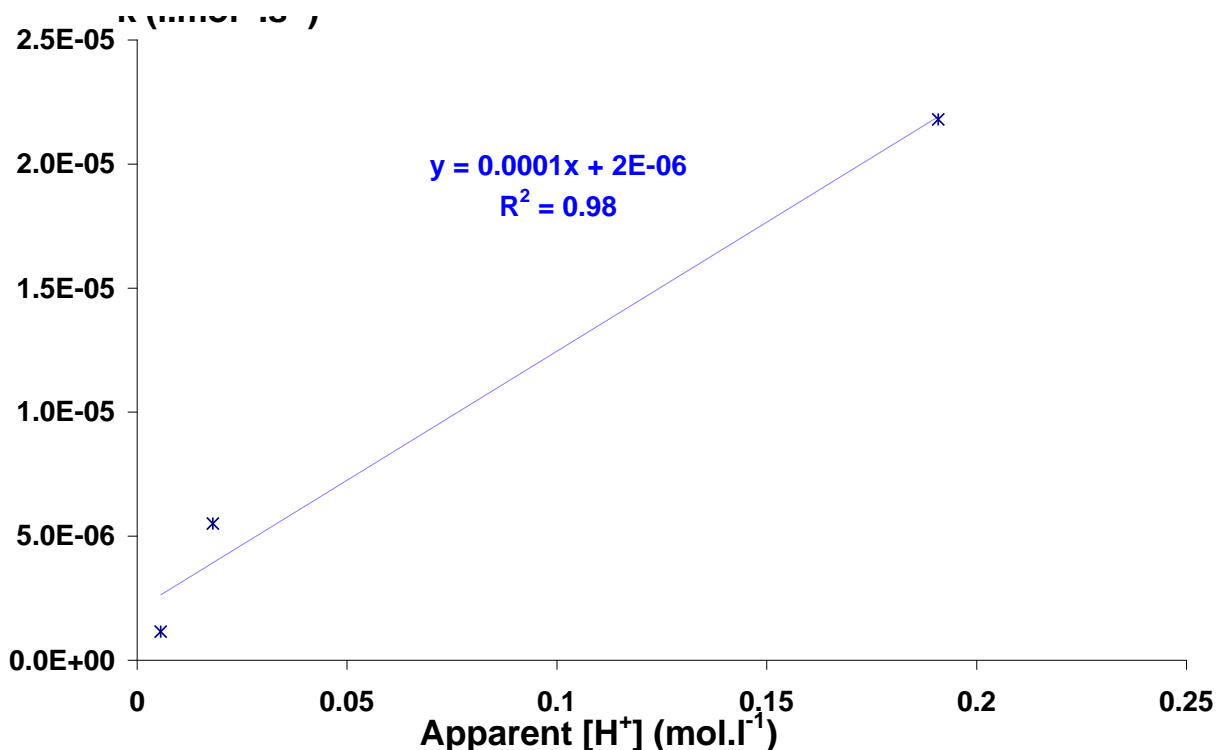


Fig. 7 Rate constants versus apparent $[H^+]$

Fig. 7 displays the rate constants versus the apparent Brønsted acid concentration $[H^+]$ for each catalyst. As can be seen the apparent rate constants are linearly proportional to $[H^+]$, which confirms the fact that the reaction of perhydrolysis is catalyzed by the Brønsted acid sites. Amberlite IR-120 catalyzes 4 times faster the perhydrolysis of PA than H-ZSM-5-23, for this reason cation exchange resins are preferred in practice.

According to Lutz *et al.* [27], the dense-structured zeolites of types ZSM-5 (MFI) are relatively stable under treatment by liquid water for 72 h up to 513 K; whereas, the open-structured zeolites of type beta (BEA) undergo strong decomposition in the same range. This statement shows that H- β zeolites are more fragile than H-ZSM-5 zeolites regarding the dealumination. In other words the dissolution of Al species is easier in the case of H- β zeolites than H-ZSM-5 zeolites.

More generally, material with a MFI structure seems to be preferably used in case of oxidation by hydrogen peroxide. For instance, titanium silicate zeolite TS-1, which has a MFI structure, is a material specifically designed for industrial oxidation reaction with hydrogen peroxide [28].

4. Conclusions

This paper describes a study of hydrogen peroxide stability over different aluminosilicate materials in the perhydrolysis of propionic acid. Several experiments were carried out in an isothermal batch reactor at temperatures 40-50°C, equimolar concentrations of the reactants and with hydrogen peroxide alone.

It was observed that some aluminosilicate materials (as H- β , H-MCM-41 or alumina oxide) decompose hydrogen peroxide, but other one (as H-ZSM-5) catalyze the perhydrolysis reaction in a moderate way.

Experiments carried out with H- β zeolites showed that the decomposition of hydrogen peroxide is not directly proportional to the ratio $\text{SiO}_2/\text{Al}_2\text{O}_3$ or to the Lewis acid site bearing by these materials. But it appears that the decomposition of hydrogen peroxide over these catalysts is related to the partial dealumination of the zeolites framework, releasing Al species in the midst which induce the decomposition mechanism. This assumption was supported by literature data, and the observation that alumina oxide material decomposes hydrogen peroxide during the propionic acid perhydrolysis reaction. A certain minimal amount of material (ca. 8.26 g/l) is needed to initiate the decomposition. The change of catalyst loading in the range 10.24-18.25 g/l does not change the kinetics of H_2O_2 decomposition.

The retarding period preceding the H_2O_2 decomposition is connected to the partial dealumination period of the zeolites. The duration of this period depends on several parameters such as: pH of the solution, catalyst loading and nature of the zeolite structure.

H-ZSM-5 does not decompose hydrogen peroxide, and in the case of a high number of Brønsted acid sites a catalytic effect on the perhydrolysis of propionic acid is observed. Amberlite IR-120 was, however even more beneficial by 4 times compared to H-ZSM-5-23.

ACKNOWLEDGEMENT

The financial support from the Åbo Akademi Forskningsinstitut and the Finnish Graduate School in Chemical Engineering (GSCE) are gratefully acknowledged. This work is part of activities at the Åbo Akademi Process Chemistry Centre (PCC) within the Finnish Centre of Excellence Programme (2006-2011) by the Academy of Finland.

REFERENCES

1. R. Hage, A. Lienke, *Angew. Chem. Int. Ed.* 45, 206 (2006).
2. R. Noyori, *Chem. Commun.* 14, 1807 (2005).
3. C.W. Jones, *Application of Hydrogen Peroxide and Derivatives*, 1st edn. (Royal Society of Chemistry, Cambridge, 1999), pp. 49-53
4. M.G. Clerici, *Top. Catal.* 13, 373 (2000).
5. L. V. Dul'neva, A.V. Moskvina, *Russ. J. Gen. Chem.* 75, 1125 (2005).
6. X. Zhao, T. Zhang, Y. Zhou, D. Liu, *J. Mol. Catal. A: Chemical* 271, 246 (2007).
7. S. Leveneur, T. Salmi, D. Yu. Murzin, L. Estel, J. Wärnå, N. Musakka, *Ind. Eng. Chem. Res.* 47, 656 (2008).
8. N. Musakka, T. Salmi, J. Wärnå, J. Ahlqvist, M. Piironen, *Chem. Eng. Sci.* 61, 6918 (2006).
9. S. Leveneur, T. Salmi, N. Musakka, J. Wärnå, *Chem. Eng. Sci.* 62, 5007 (2007).
10. X. Zhao, K. Cheng, J. Hao, D. Liu, *J. Mol. Catal. A: Chemical* 284, 58 (2008).
11. S. Leveneur, D. Yu. Murzin, T. Salmi, J.-P. Mikkola, N. Kumar, K. Eränen, L. Estel, *Chem. Eng. J.* 147, 323 (2009).
12. A. Palani, A. Pandurangan, *Catal. Commun.* 7, 875 (2006).
13. G. Prescher, O. Weiberg, H. Waldmann, H. Seifert, *International Patent US4088679* (1978).
14. F.P. Greenspan, D.G. MacKellar, *Anal. Chem.* 20, 1061 (1948).
15. D. Kubička, N. Kumar, P. Mäki-Arvela, M. Tiitta, V. Niemi, T. Salmi, D. Yu. Murzin, *J. Catal.* 222, 65 (2004).
16. P. Mäki-Arvela, N. Kumar, V. Nieminen, R. Sjöholm, T. Salmi, D. Yu. Murzin, *J. Catal.* 225, 155 (2004).
17. E.M. Sulman, V.V. Alferov, Yu. Yu. Kosivtsov, A.I. Sidorov, O.S. Misnikov, A.E. Afanasiev, N. Kumar, D. Kubicka, J. Agullo, T. Salmi, D. Yu. Murzin, *Chem. Eng. J.* 134, 162 (2007).
18. A. Aho, N. Kumar, K. Eränen, T. Salmi, M. Hupa, D. Yu. Murzin, *Fuel* 87, 2493 (2008).
19. J.P. Marques, I. Gener, P. Ayrault, J.C. Bordado, J.M. Lopes, F.R. Ribeiro, M. Guisnet, *C.R. Chimie* 8, 399 (2005).
20. P.K. Sengupta, R.N. Tiwari, S. Bhagat, *Chem. Eng. World* 32, 89 (1997).
21. G.O. Rocha, R.A.W. Johnstone, B.F. Hemming, P.J.C Pires, J.P. Sankey, *J. Mol. Catal. A: Chemical* 186, 127 (2002).
22. A.E.W. Beers, J.A van Bokhoven, K.M. de Lathouder, F. Kapteijn, J.A. Moulijn, *J. Catal.* 218, 239 (2003).
23. D.M. Roberge, H. Hausmann, W.F. Hölderich, *Phys. Chem. Chem. Phys.* 4, 3128 (2002).
24. R.L. Hartman, H.S. Fogler, *Ind. Eng. Chem. Res.* 44, 7738 (2005).
25. J. De Laat, G. T. Le, B. Legube, *Chemosphere* 55, 715 (2004).
26. B. Mani, Ch. Ravi Mohan, V. Sitakara Rao, *React. Kinet. Catal. Lett.* 13, 277 (1980).
27. W. Lutz, H. Toufar, R. Kurzhals, M. Suckow, *Adsorption* 11, 405 (2005).
28. M. Guisnet, F.R. Ribeiro, *Les zéolithes, un nanomonde au service de la catalyse*; EDP sciences (2006)



Synthesis of peroxypropionic acid from propionic acid and hydrogen peroxide over heterogeneous catalysts

Sébastien Leveneur^{a,b,*}, Dmitry Yu. Murzin^a, Tapio Salmi^a, Jyri-Pekka Mikkola^a, Narendra Kumar^a, Kari Eränen^a, Lionel Estel^b

^a Laboratory of Industrial Chemistry and Reaction Engineering, Process Chemistry Centre, Åbo Akademi, Biskopsgatan 8, FI-20500 Åbo/Turku, Finland

^b LSPC-Laboratoire de Sécurité des Procédés Chimiques, INSA Rouen, Place Emile Blondel, BP8, 76131 Mont-Saint-Aignan Cedex, France

ARTICLE INFO

Article history:

Received 17 February 2008

Received in revised form

19 November 2008

Accepted 20 November 2008

Keywords:

Peroxydicarboxylic acid

Cation exchange resin

Diffusion

Deactivation

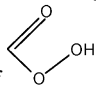
ABSTRACT

This paper proposes a study of different cation exchange resins, used as catalysts for the synthesis of peroxypropionic acid (PPA) from propionic acid and hydrogen peroxide at 40 °C, equimolar concentration of reactants and an apparent Brønsted concentration of 0.2 M. The catalytic activities of the resins are on the same scale as sulfuric acid at comparable concentration level and decrease in the order: Dowex 50Wx2 > Smopex-101 > Dowex 50Wx8 ≈ Amberlite IR-120 > Amberlyst 15. The influence of external and internal mass transfer limitation was evaluated. The experiments also demonstrated that a gelular resin with a degree of cross-linking equal to 8% and a particle size of more than 0.1 mm showed a stronger resistance to deactivation.

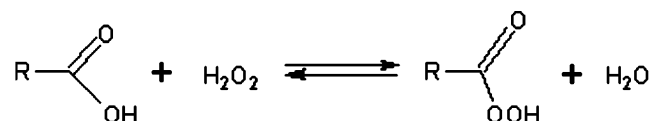
© 2008 Elsevier B.V. All rights reserved.

1. Introduction

Peroxydicarboxylic acids are widely used in industrial manufacturing although rarely as pure solutions. These chemicals are employed as disinfecting/antimicrobial agents (destruction of organophosphorus as paraoxon, control legionella bacteria) in alimentary or pharmaceutical industry; as a bleaching agent of wood pulp in paper factory, instead of ecologically non-benign chlorine dioxide; and in fine chemistry for Baeyer–Villiger reaction or olefins epoxidation. All these applications are based on the oxidative prop-

erties of peroxydicarboxylic acid, namely presence of . The main advantage of these chemicals is their harmless impact on the environment because of the non-toxicity of their decomposition products. Indeed, the decomposition of those compounds lead to carbon dioxide, oxygen, water and carboxylic acid.

Two ways of synthesis are possible for the production of peroxydicarboxylic acids: oxidation of the parent carboxylic acid by oxygen or by aqueous hydrogen peroxide. The second way of liquid phase synthesis is more safe, moreover water is an eco-friendly solvent:



Indeed, the main drawback of this reaction is the slow rate and, thus, the necessity to implement an acid catalyst. The process for peroxydicarboxylic acid production is still industrially catalyzed by sulfuric acid [1,2], leading to several drawbacks, such as corrosion, catalyst separation, and threat to environment. Indeed, after the reaction the homogeneous catalyst should be separated (typically by distillation) and recirculated to the process. One way to surmount these problems is to shift from homogeneous to heterogeneous catalysts following the principles of Green Chemistry. The main challenge is to discover a catalyst with a comparable acidic strength as sulfuric acid, which at the same time does not decompose peroxide species and in addition, can be re-used.

In Refs. [3–5], different solid acid catalysts, essentially zeolites and cation exchange resins, have been tested. Among these, cation exchange resins showed the highest catalytic efficiency. It should be noted, however, that no detail information about performance of these solid acid materials is provided, in particular impact of mass transfer, deactivation and even comparison with sulfuric acid.

In this paper we compare the efficiency of some resin catalysts with different cross-linkers and different degree of cross-linking, study the diffusion limitations and determine the deactivation rate

* Corresponding author at: Laboratory of Industrial Chemistry and Reaction Engineering, Process Chemistry Centre, Åbo Akademi, Biskopsgatan 8, FI-20500 Åbo/Turku, Finland. Tel.: +358 2 2158942; fax: +358 2 2154479.

E-mail address: sleveneu@abo.fi (S. Leveneur).

of various catalysts. It was decided to investigate the perhydrolysis of propionic acid; the choice of peroxypropionic acid is due to its higher stability compared to peroxyacetic acid. In a previous contribution [6], it was demonstrated that the kinetics of propionic acid perhydrolysis, catalyzed by sulfuric acid, is dependent on Brønsted concentration.

In order to facilitate the interpretation of the kinetic data and to make a plausible comparison of these catalysts, an isothermal batch reactor with rigorous stirring was used in the experiments.

2. Experimental

2.1. Apparatus and experimental procedures

All experiments were performed in a 250 ml jacketed glass reactor vessel. The reactor was equipped with a mechanical agitator and a temperature probe. Water was pumped through the outer jacket of the vessel to control the temperature of the reaction mixture. A pitched blade impeller (PTFE coated) was used to ensure a vigorous mixing during the reaction.

A reflux condenser was attached to the top of the reactor (adjusted to 0 °C) to avoid loss of liquid phase compounds. In case that decomposition of peroxypropionic acid (PPA) or H₂O₂ appeared, a carrier gas (Helium, AGA, 99.996%) was introduced to the reactor through one of the necks in order to avoid accumulation of oxygen in the gas phase.

To prevent contamination induced by alkaline and metal components, which initiate the catalytic decomposition of peroxypropionic acid and hydrogen peroxide, all parts of the reactor system being in contact with the reaction solution were washed with hydrochloric acid followed by another washing, with a phosphate free detergent solution.

At the first stage, propionic acid (Acros, 99 wt.%) and the catalyst were mixed together in the reactor. When the reaction desired temperature was reached, preheated hydrogen peroxide solution (Merck, 30 wt.%) was added through a dropping funnel. At the time “zero” the required amount was introduced into the reactor.

According to a patent [7], during the reaction of hydrogen peroxide and propionic acid in water and in the presence of an acid catalyst, the danger of explosion is suppressed by employing a temperature of maximum 60 °C. Thus, a compromise between rapid kinetics and the safety aspect led us to choose the reaction temperature of 40 °C.

One should keep in mind that the purpose of this paper is to compare the catalytic activity of the different resins. For this reason, all the experiments were carried out under similar conditions regarding the temperature, water amount, initial reactant concentration and apparent Brønsted acid concentration [H⁺]. The estimation of the apparent [H⁺] (the number of Brønsted sites of the solid catalyst present per liter) was carried out on the basis of the cation exchange capacity by dry weight (meq/g) provided by the manufacturer. Fur-

Table 1

Experimental parameters for catalysts comparison in the batch reactor.

Reaction temperature	40 °C
Rotation speed	250–600 rpm
[H ₂ O ₂] ₀ /[PA] ₀	0.9–1.0
[H ₂ O] ₀	21.8–26.3 mol l ⁻¹
[PA] ₀	5.5–6.4 mol l ⁻¹
Apparent [H ⁺]	0.18–0.22 mol l ⁻¹

thermore, it was assumed that the capacity remains essentially constant, even upon re-use of the catalyst. Table 1 introduces the experimental matrix.

2.2. Analytical methods and calculations

Samples were withdrawn from the reaction mixture by a plastic syringe (to avoid contamination of the solution by trace of metals) and were analyzed by the Greenspan and Mackellar method [8]. The concentration of hydrogen peroxide was determined by titration using a standard solution of ammonium cerium sulfate (0.1 N). The concentrations of propionic and peroxypropionic acids were determined by titration with an automatic titrator (Metrohm 751 GPD Titrino) using a standard solution of sodium hydroxide (0.2 N).

The mole fraction of PPA and initial turnover frequency were calculated for comparison of the experimental results.

The initial turnover frequency (T.O.F) was calculated from:

$$\text{T.O.F} = \frac{\text{Initial rate of PPA formation}}{\text{Number of Brønsted acid sites}}$$

The number of Brønsted acid sites was determined on the basis of the cation exchange capacity of the catalyst.

2.3. Catalyst properties and characterization

The properties of the tested commercial cation exchange resins are summarized in the Table 2.

Except for Smopex-101, the different cation exchange resins used were composed of similar type of matrix: styrene-divinyl benzene with sulfonic acid functional groups. The shape of the catalysts was the same, i.e. beads.

Smopex-101 (Smoptech) is a fibrous catalyst bearing sulfonic acid functional groups on poly(ethylene-graft-polystyrene). The mean particle diameter is about 0.01 mm and the average length is 4 mm [9].

A comparison was made between native catalysts (used as received) and pretreated ones. The pretreatment consisted of a drying step at 70 °C for 48 h since higher drying temperature could affect the sulfonic acid sites on the catalysts. After the reaction, the catalyst was flushed with water and dried at 70 °C for 48 h.

Scanning electron microscopy (SEM) was used to study the morphology of the resins.

Table 2

Properties of the cation exchange resins used.

	Supplier	Polymer type	Cross linking (%)	Moisture content (% mass)	Capacity by dry weight (meq/g)	Native particle size range (mm)	Pores (nm)
Amberlite IR-120	Aldrich	Gel	8	45	4.4	0.3–12	–
Amberlyst 15	Fluka	Macroreticular	20–25	5	4.7	0.45–0.60	40–80
Dowex 50Wx2-100	Acros	Gel	2	78	4.8	0.15–0.3	–
Dowex 50Wx8-400	Sigma–Aldrich	Gel	8	54	4.8	0.04–0.08	–
Dowex 50Wx8-100	Sigma–Aldrich	Gel	8	52	4.8	0.15–0.3	–
Dowex 50Wx8-50	Fluka	Gel	8	55	4.8	0.3–0.84	–
Smopex-101	Smoptech	Fibre	2	6	2.6	–	–

3. Results and discussion

3.1. Influence of sulfuric acid at low concentration on the conversion

In order to determine whether there exists a minimum in terms of proton concentration required to observe a significant enhancement of the kinetics; some experiments were carried out without sulfuric acid and with low sulfuric acid concentration. The other goal of these experiments is to establish the amount of solid acid catalyst needed to observe a significant conversion.

Fig. 1 confirms that the perhydrolysis kinetics of propionic acid in the absence of an added catalyst is slow, but propionic acid itself is able to act as a catalyst, therefore some conversion was noticeable [6]. However, one can observe that there is a significant effect of sulfuric acid even at low concentrations (0.001 and 0.004 M), implicating that there is no clear threshold value for the added catalyst concentration.

Nevertheless, to get a significant degree of conversion during a reaction time of 5 h at 40 °C, the concentration of sulfuric acid should be around 0.08 M. As the availability of the proton with sulfuric acid is, *a priori*, higher than in the case of solid acid catalysts, the amounts of solid catalysts were fixed to a level corresponding to an apparent Brønsted acid concentration of 0.2 M on the basis of calculations. During the experiments carried out with the different cation exchange resins, no side reactions such as decomposition of hydrogen peroxide were noticed.

3.2. Scanning electron microscopy

SEM was used to gain a better understanding of the morphology differences between the two cation exchange resins: Amberlite IR-120, which is a gelular or gel-type resin, and Amberlyst 15, which is a macroreticular or macroporous resin.

Prior to analysis of those materials by SEM, they were dried. Figs. 2 and 3 show an overview of the particles of Amberlyst 15 and Amberlite IR-120. At first glance, the surface of Amberlyst 15 is smoother than Amberlite IR-120. Indeed, when a gelular resin is totally dried, the polymer matrix collapses; whereas it does not collapse with macroreticular resin upon loss of water. This implies that the inner structure of the pretreated resins is different than the native one.

However, at higher magnification, one can observe the inhomogeneous surface structure of the macroporous material (Fig. 4), which consists of agglomerates of very small gelular microspheres. Fig. 5 shows a zoom of the surface of Amberlite IR-120, which has a homogeneous distribution of polymeric chains across the bead and, thus, a regular surface structure.

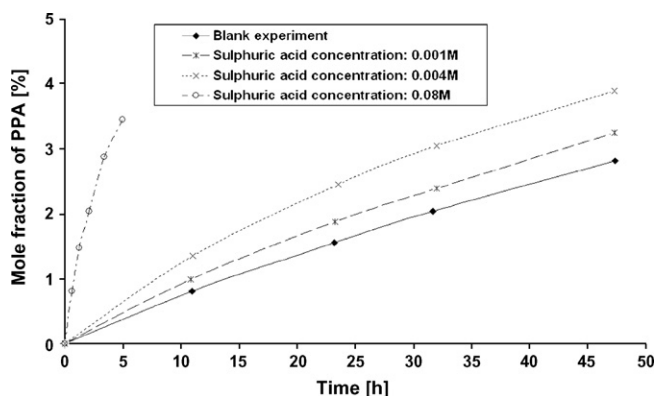


Fig. 1. Mole fraction of PPA versus time at 40 °C with different sulfuric acid concentrations.

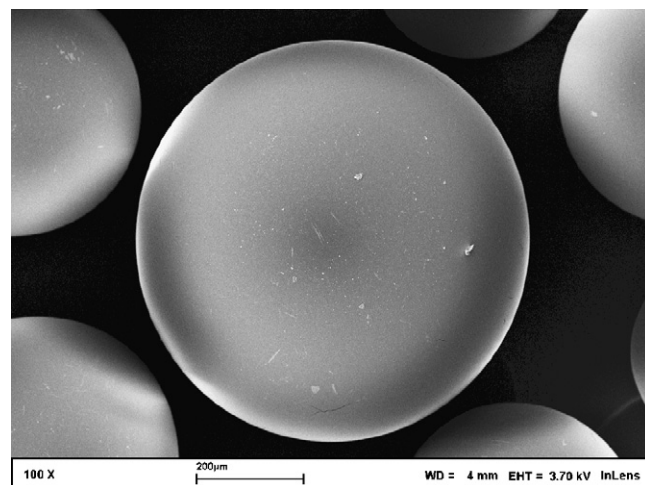


Fig. 2. SEM image of Amberlyst 15.

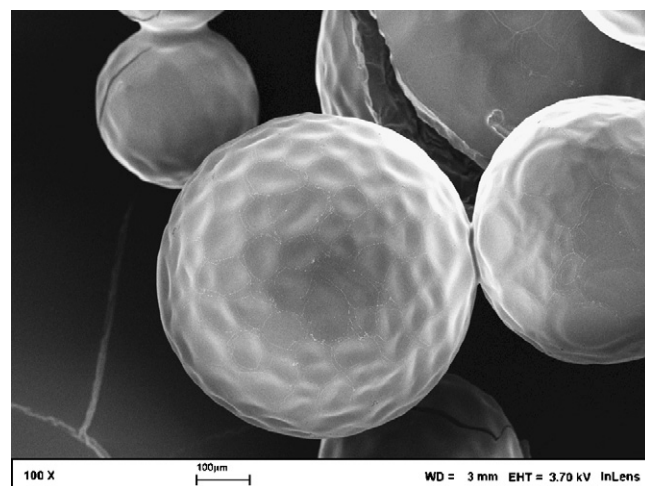


Fig. 3. SEM image of Amberlite IR-120.

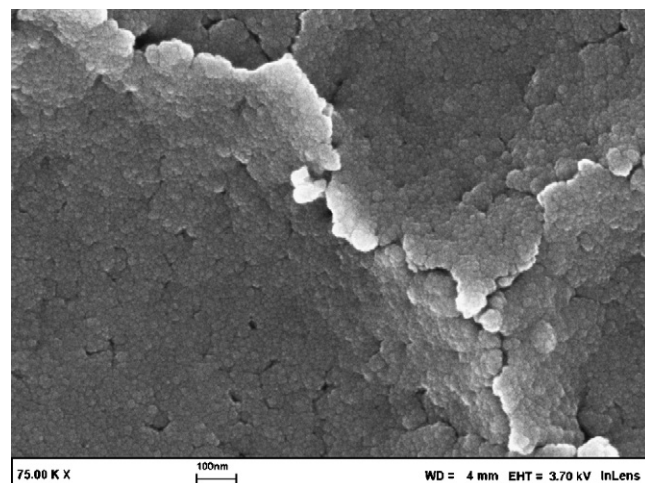


Fig. 4. SEM image of Amberlyst 15.

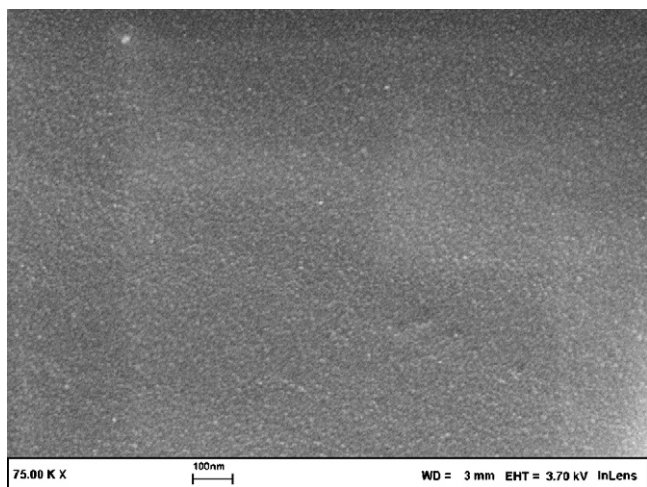


Fig. 5. SEM image of Amberlite IR-120.

3.3. Mass transfer effects

3.3.1. Effect of external mass transfer

In order to determine the influence of the external mass transfer around the catalyst particles on the kinetics, identical experiments (see Table 1) were carried out with different rotation velocities (250 and 600 rpm). This phenomenon is characterized by a liquid–solid mass transfer coefficient β_{LS} , which depends mainly on the diameter of the solid particles; consequently, particles with bigger size present stronger external mass transfer resistance. Amberlite IR-120 was selected because of its bigger particle size.

Fig. 6 illustrates the mole fraction of PPA versus time for the experiments carried out with pretreated catalyst at different stirring rates.

It is evident (Fig. 6) that there are no external mass transfer limitations in case of pretreated Amberlite IR-120 at the stirring speed range 250–600 rpm. Experiments carried out in the same conditions, but with native Amberlite IR-120 as well, show absence of external mass transfer. Thus, it can be concluded that no external mass transfer limitations prevailed in the case of other gelular resins with smaller particle size distribution than Amberlite IR-120.

3.3.2. Effect of internal mass transfer

The influence of the mass transfer inside the catalyst particles was studied with Dowex 50Wx8 with different particle size ranges. Fig. 7 illustrates the influence of the particle size distribution on the mole fraction of PPA.

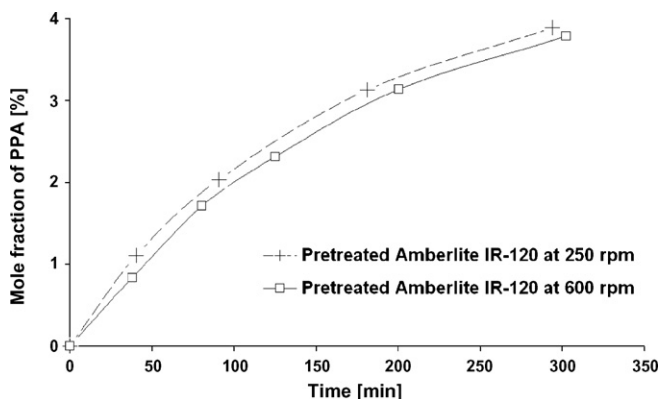


Fig. 6. Effect of the stirring on the mole fraction of PPA with pretreated catalyst at 40 °C.

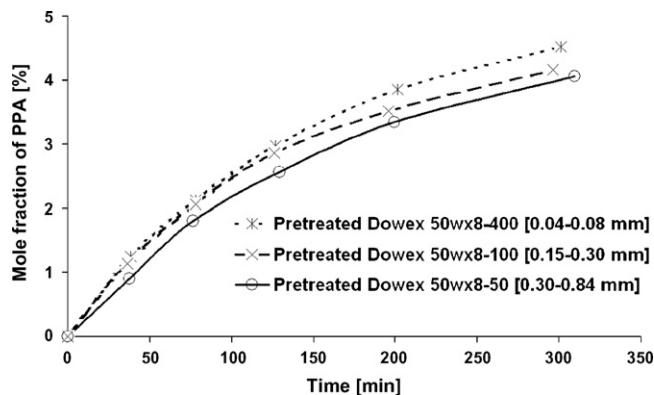


Fig. 7. Influence of internal mass transfer on the mole fraction of PPA at 40 °C and 250 rpm.

Fig. 7 displays that experiments catalyzed by the smallest particles showed rapid kinetics. The influence of the internal diffusion in the experiments carried out with Dowex 50Wx8-400 and 100 might be negligible, although there were slight deviations for the catalysts in the pretreated form. In case of an experiment carried out with native Dowex 50Wx8, the same trend was observed. Diffusion phenomenon can be observed in the case of the experiment carried out with Dowex 50Wx8-50. Assuming that no internal diffusion limitation existed in the case of the smallest particle Dowex 50Wx8-400, the effectiveness factor η can be estimated from:

$$\eta = \frac{\text{Observed rate of PPA formation}}{\text{Rate of PPA without internal diffusion}} \quad (1)$$

From Eq. (1), one can estimate the effectiveness factor for Dowex 50Wx8-100 and Dowex 50Wx8-50. Table 3 summarizes the values obtained at time zero and 90 min after the reaction.

The value of the initial effectiveness factor confirms that the internal diffusion cannot be neglected in the case of particle sizes over 0.3 mm and with a degree of cross-linking at a level of 8%, for pretreated and native resins. However, after 1 h and 30 min, the internal diffusion decreases due to the reverse reaction, which becomes more significant.

Thus, for experiments carried out with Amberlite IR-120, the internal diffusion resistances should be taken into account at the beginning of the reaction.

However, one cannot generalize those conclusions in the case of Amberlyst 15 and Dowex 50Wx2 because the degrees of cross-linking and polymer type are not the same. Indeed, the degree of cross-linkage controls the porosity of the resins, and, therefore, influences the internal diffusion.

3.4. Comparison between pretreated and native catalysts

Generally, the pretreatment of solid catalysts has been proven to be important, and have a strong influence on the activity. The main purpose of the pretreatment is to release the water from the catalyst, which represents ca. 50% of the total weight (cf. Table 2).

Table 3
Effectiveness factor.

	Dowex 50Wx8-100	Dowex 50Wx8-50
0 h		
η (with native catalyst)	0.9	0.7
η (with pretreated catalyst)	1.0	0.8
1.5 h		
η (with native catalyst)	1.00	1.00
η (with pretreated catalyst)	1.00	0.95

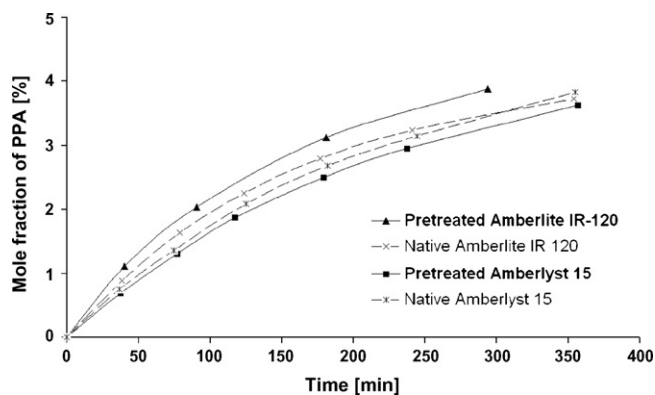


Fig. 8. Effect of the catalyst pretreatment (Amberlite IR-120 and Amberlyst 15) on the mole fraction of PPA versus time at 40 °C and 250 rpm.

One of the characteristic of polymer materials is that in contact with a liquid, they do not only adsorb the liquid, but swell as well. Ion exchange resin absorbs preferably some compounds than the others, and then, a concentration gradient can appear. Consequently, kinetics or thermodynamic parameters can change in case of experiments carried out with a cation exchange resin compared to experiments carried out with a homogeneous catalyst. According to Musante et al. [10], in case of the perhydrolysis of acetic acid by Amberlite IR-120, water is more strongly sorbed than either acetic acid or hydrogen peroxide, and the resin swelling is much higher in water than in acetic acid. However, the difference in kinetics and thermodynamic occurs only between experiments carried out with homogeneous and heterogeneous catalysts, and when the difference of sorption behavior for reactants is significant.

As illustrated by Fig. 8, the difference between pretreated and native Amberlyst 15 is negligible. Because of the macroreticular structure of Amberlyst 15, its polymer matrix is more rigid and, consequently, it does not collapse during the drying procedure. This fact is confirmed by SEM picture (Fig. 2), where one can notice that the matrix of this resin did not collapse, compared to gelular resin.

Nevertheless, the differences in activity were significant for the cation exchange resins in gel form (Figs. 8 and 9), i.e., the velocity of the reaction is higher with pretreated resins. From Fig. 3, one can notice that the structure of the resin has changed during the pretreatment. Consequently, the diffusion properties of these materials are different.

These differences become more significant in the vicinity of the equilibrium. However, according to Table 4, differences in the initial T.O.F ratio between pretreated and native catalyst are not really significant.

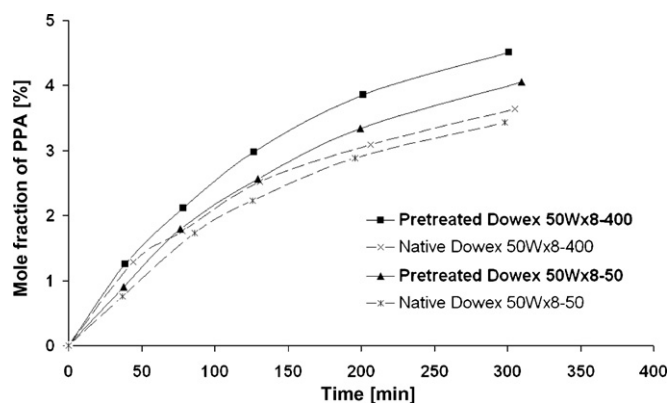


Fig. 9. Effect of the catalyst pretreatment (Dowex 50Wx8-400 and 50Wx8-50) on the mole fraction of PPA versus time at 40 °C and 250 rpm.

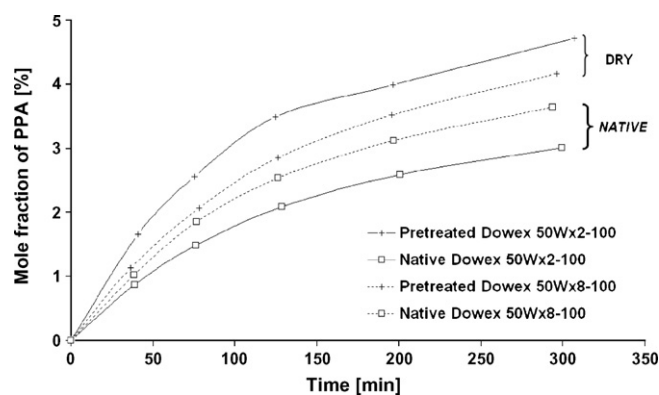


Fig. 10. Effect of the degree of cross-linking on the mole fraction of PPA at 40 °C and 250 rpm.

3.5. Effect of the cross-linking

The degree of cross-linking of the resins has a strong influence on their structures, since it controls the porosity of the resin, e.g. X8 (8%) indicates medium porosity and X2 high porosity. To have a better illustration of this effect, experiments were carried out with Dowex 50Wx8-100 and Dowex 50Wx2-100, because of the similarities in their physical and chemical properties, but different cross-linking.

Fig. 10 confirms the fact that there is a difference between pretreated and native catalyst. In the case of pretreated catalyst, the activity of Dowex 50Wx2-100 is higher than the one of Dowex 50Wx8-100. However, this phenomenon is inverted in case of experiments carried out with native catalyst.

Due to the small size of the reactants (propionic acid and hydrogen peroxide) and products (PPA and water), the porosity of these materials does not slow down the diffusion process. The pretreatment modifies the inter-structure of the matrix, and, thus, modify the tortuosity factor. One can notice that the pretreatment improves the activity of the resins, thus, the tortuosity factor decreases. This tendency is confirmed by the fact that the active sites, i.e., sulfonic groups are located inside the particle [10]. The improvement of the tortuosity factor, by the pretreatment, is better for the resin with low percentage of divinylbenzene.

In case of native resin, the tortuosity factor is higher with lower degree of cross-linking.

3.6. Comparison of the solid catalysts with sulfuric acid

A comparison of the efficiency of the different solid acid catalysts and sulfuric acid is described in this section. Indeed, the structure of the sulfonic acid group is very close to the sulfuric acid. For the sake of simplicity, only the results obtained with the pretreated catalysts are shown. All the experiments were carried out under similar conditions (see Table 1) and the speed of agitation was fixed at 250 rpm. Fig. 11 illustrates the mole fraction of PPA versus time for the different pretreated catalysts and Fig. 12 represents the T.O.F for them.

As can be seen in Fig. 11, the efficiencies of the resins are lower than for sulfuric acid at the comparable Brønsted acid concentration level, in general. However, the activity of Dowex 50Wx2-100 is similar to that of sulfuric acid, at a concentration level of 0.19 M. Based on the apparent Brønsted concentration, catalyst activity decreases in the order: Dowex 50Wx2 > Smopex-101 > Dowex 50Wx8 ≈ Amberlite IR-120 > Amberlyst 15. Fig. 12 showing the initial T.O.F for the different cation exchange resins displays the same trend.

The highest activity of pretreated Dowex 50Wx2 is because of its lower tortuosity factor. Experiments carried out with Amberlite

Table 4

Turnover frequencies data.

	T.O.F.		Ratio T.O.F (dry catalyst/native catalyst)
	Dry catalyst (s^{-1})	Native catalyst (s^{-1})	
Amberlite IR-120	6.86E-04	5.92E-04	1.16
Amberlyst 15	4.91E-04	5.12E-04	0.96
Dowex 50Wx2-100	1.01E-03	7.50E-04	1.34
Dowex 50Wx8-400	8.49E-04	7.56E-04	1.12
Dowex 50Wx8-100	8.60E-04	6.62E-04	1.30
Dowex 50Wx8-50	5.94E-04	5.70E-04	1.04

IR-120 and Dowex 50Wx8-50 (the same particle size distribution and degree of cross-linking) gave similar results to that of sulfuric acid, at a concentration level of 0.11 M. The difference of capacity between these resins (Table 2) is not significant to notice a difference in activity.

Thus, the diffusion process for experiments carried out with the gelular resins is essential, and controls the activity toward the perhydrolysis of propionic acid. The catalytic activity of Amberlyst 15 is lower than that of sulfuric acid, at a concentration level of 0.08 M. The macroreticular structure and the high level of cross-linking of this material increase the resistance against the diffusion, and, thus, diminish the activity.

The kinetic curve of Smopex-101 shows that it is possible to use other cross-linkers than divinylbenzene. However, according to our experiments and literature data [9], the swelling effect with this material is important, and strongly influences the diffusion process.

From the experiments data it follows that the pH of the solutions for experiments carried out at 40 °C in the absence of the sulfuric acid and with 0.08 M of sulfuric acid are equal to 1.3 and 0.1, respectively. In case of experiments carried out with cation exchange

resins at 40 °C with an apparent Brønsted concentration of 0.20 M, the pH range is 1.2–1.3, which implies that there is practically no formation of sulfuric acid due to a leaching of the sulfonic group or oxidation of these groups by hydrogen peroxide. Deactivation studies reported in the following section, also confirm, that the activity of cation exchange resins cannot be attributed to the oxidation of sulfonic groups with H_2O_2 , and subsequently release of sulfuric acid into the liquid milieu.

Furthermore, the decrease of the reaction medium acidity by one pH unit compared to sulfuric acid could be beneficial from technological viewpoint.

3.7. Catalyst deactivation

Only few articles consider the deactivation of cation exchange resins [11,12]. One of the main difficulties in study this phenomenon is to repeat the experiments under comparable conditions. Our goal was to find the resins which present a strong resistance toward the deactivation process.

For the sake of simplicity, only experiments showing deactivation are displayed in Figs. 13–15.

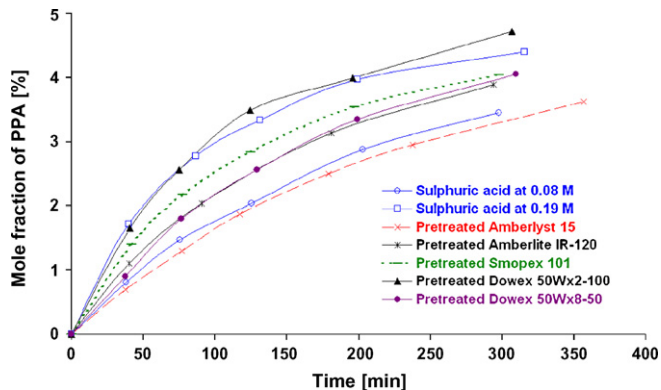


Fig. 11. Synthesis of PPA over different catalysts at 40 °C at 250 rpm.

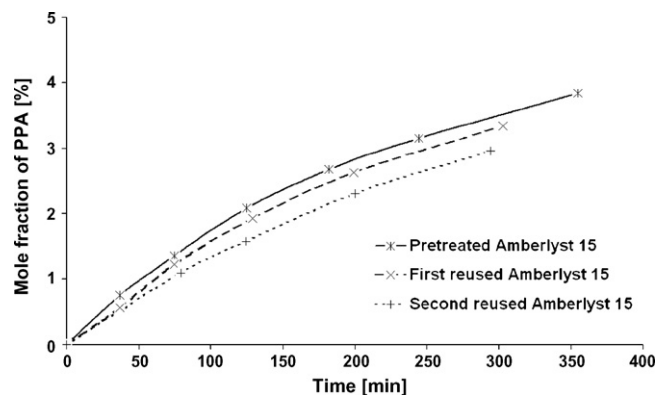


Fig. 13. Deactivation behavior for Amberlyst 15 at 40 °C and 250 rpm.

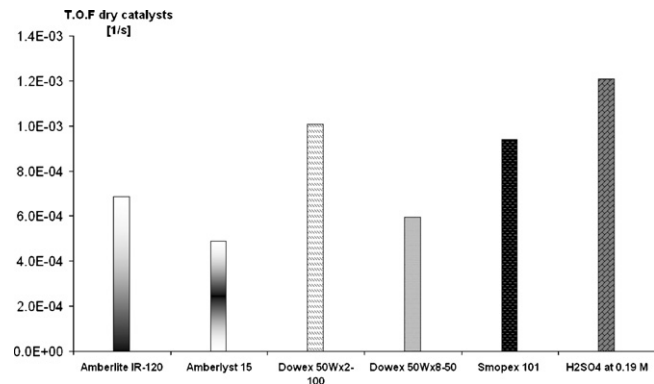


Fig. 12. Turnover frequency for the different pretreated catalysts carried out at 40 °C and 250 rpm.

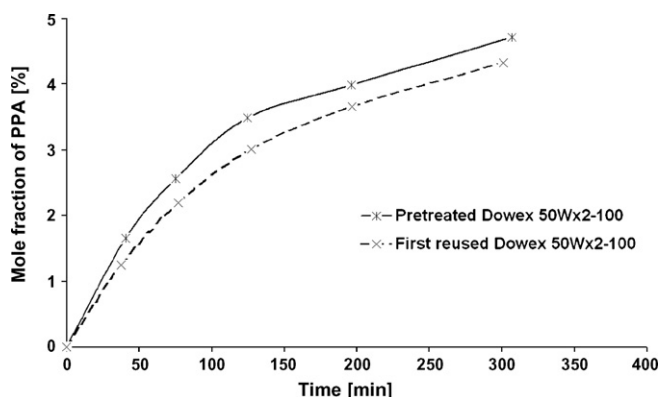


Fig. 14. Deactivation behavior for Dowex 50Wx2-100 at 40 °C and 250 rpm.

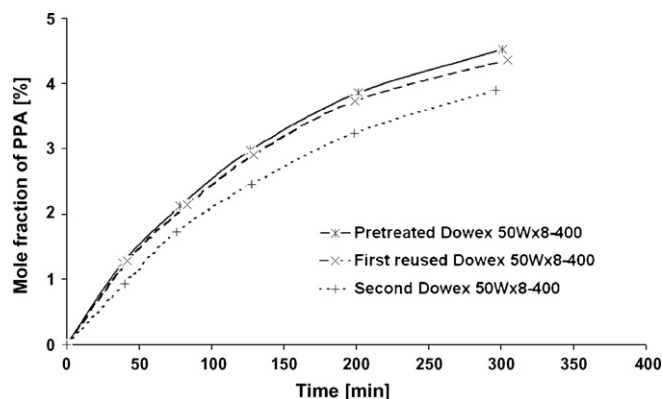


Fig. 15. Deactivation behavior for Dowex 50Wx8-400 at 40 °C and 250 rpm.

The apparent Brønsted concentration $[H^+]$ was calculated on the basis of the capacity by dry weight (meq/g) of the resins, given by the manufacturer, this capacity was assumed to remain constant from batch-to-batch.

Deactivation rates for Amberlite IR-120, Dowex 50Wx8-100 and Dowex 50Wx8-50 are negligible. The characteristics of these resins are: similar level of cross-linking of 8% and particles with sizes higher than 0.10 mm. Altiokka et al. [12] observed no deactivation for Amberlite IR-120 during the esterification of acetic acid with isobutanol.

Nevertheless, in the case of Dowex 50Wx8-400, Dowex 50Wx2-100 and Amberlyst 15, a significant level of deactivation was visible, as shown in Figs. 13–15.

The deactivation by leaching of sulfonic group is, certainly, not the reason. According to the manufacturer, sulfonic groups volatilize at a temperature of 120 °C, which were not reached during the reaction or pretreatment. Moreover, a deactivation is noticed for experiments carried out with Dowex 50Wx8-400, but not for Dowex 50Wx8-100 or 50Wx8-50 (which have the same properties, except the particle size range). Thus, deactivation by leaching of sulfonic group can be reasonably discarded. However, a more detailed study should be done; to understand deactivation phenomenon in more detail.

4. Conclusion

The goal of this work was to propose a green alternative route for catalyzing the perhydrolysis of carboxylic acid and, thus, avoided corrosive mixture and separation problems. Different cation exchange resins were evaluated. Several experiments were performed in a batch reactor at 40 °C, equimolar concentration of reactants and similar water concentration.

The pretreatment of resins is necessary since it improves the catalytic activity of the gelular resins. The catalytic activity was higher with gelular resins with lower cross-linking, due to a lower value of the tortuosity factor. A comparison with sulfuric acid indicated that the activity is on similar scale, but the resins allow the acidity to be lowered by one unit pH. Furthermore, with the heterogeneous resin catalysts, the catalyst separation problem is avoided.

The external mass transfer can be neglected in case of those experiments that were carried out at the steering speed of

250–600 rpm. However, the initial internal mass transfer was present in the case of gelular resin with a degree of cross-linking equal to 8%, essentially for pretreated catalysts with larger particles (>0.3 mm).

The use of a different cross-linker than divinylbenzene is possible, but the swelling noticed with Smopex-101, which has ethylene cross-linker, affords a stronger resistance against the diffusion.

The deactivation pattern for the resins was dependent on the degree of cross-linking and the particle size. Experiments carried out with a level of cross-linking degree of 8% and particles having sizes over 0.1 mm displayed slow deactivation. However, a better understanding about the deactivation of these materials is needed, by a kinetic modeling which takes into account this phenomenon.

To conclude, the efficiency of the resins is a compromise between their catalytic efficiency and their deactivation. Higher degree of cross-linking resulted in a slower reaction rate. Nevertheless, this relation is opposite regarding deactivation. The environmental and maintenance benefits upon use of cation exchange resins compared to sulfuric acid are important, essentially regarding the possibility to use less corrosive mixture.

Acknowledgements

The financial support from the Åbo Akademi Forskningsinstitut and the Finnish Graduate School in Chemical Engineering (GSCE) are gratefully acknowledged. This work is part of activities at the Åbo Akademi Process Chemistry Centre (PCC) within the Finnish Centre of Excellence Programme (2006–2011) by the Academy of Finland.

References

- [1] A. Reijo, I. Renvall, Process for the preparation of peroxy acids, International Patent WO2007031596 (2007).
- [2] Z.X. Zhou, Method for preparing peroxy acetic acid, International Patent CN1803771 (2006).
- [3] A. Palani, A. Pandurangan, Single pot synthesis of peroxyacetic acid from acetic acid and hydrogen peroxide using various solid acid catalysts, *Calal. Commun.* 7 (11) (2006) 875–878.
- [4] M.S. Saha, Y. Nishiki, T. Furuta, A. Denggerile, T. Ohsaka, A new method for the preparation of peroxyacetic acid using solid superacid catalysts, *Tetrahedron Lett.* 44 (29) (2003) 5535–5537.
- [5] A.T. Hawkinson, W.R. Schitz, Improvements in or relating to the oxidation of aliphatic carboxylic acids to peracids, International Patent GB776758 (1957).
- [6] S. Leveneur, T. Salmi, D.Y. Murzin, L. Estel, J. Wärnå, N. Musakka, Kinetic study and modeling of peroxypropionic acid synthesis from propionic acid and hydrogen peroxide using homogeneous catalysts, *Ind. Eng. Chem. Res.* 47 (3) (2008) 656–664.
- [7] G. Prescher, O. Weiberg, H. Waldmann, H. Seifert, Process for preparing perpropionic acid solutions, International Patent US4088679 (1978).
- [8] F.P. Greenspan, D.G. MacKellar, Analysis of aliphatic per acids, *Anal. Chem.* 20 (11) (1948) 1061–1063.
- [9] J. Lilja, D. Yu. Murzin, T. Salmi, J. Aumo, P. Maki-Arvela, M. Sundell, Esterification of different acids over heterogeneous and homogeneous catalysts and correlation with the Taft equation, *J. Mol. Catal. A: Chem.* 182–183 (2002) 555–563.
- [10] R.L. Musante, R.J. Grau, M.A. Baltanas, Kinetic of liquid-phase reactions catalyzed by acidic resins: the formation of peracetic acid for vegetable oil epoxidation, *Appl. Catal. A: Gen.* 197 (1) (2000) 165–173.
- [11] A.A. Zagorodni, D.L. Kotova, V.F. Selemenev, Infrared spectroscopy of ion exchange resins: chemical deterioration of the resins, *React. Funct. Polym.* 53 (2–3) (2002) 157–171.
- [12] M.R. Altiokka, A. Citak, Kinetics study of esterification of acetic acid with isobutanol in the presence of amberlite catalyst, *Appl. Catal. A: Gen.* 239 (1–2) (2003) 141–148.



Application of linear free-energy relationships to perhydrolysis of different carboxylic acids over homogeneous and heterogeneous catalysts

Sébastien Leveneur^{a,b,*}, Dmitry Yu. Murzin^a, Tapio Salmi^a

^a Laboratory of Industrial Chemistry and Reaction Engineering, Process Chemistry Centre, Åbo Akademi, Biskopsgatan 8, FI-20500 Åbo/Turku, Finland

^b LSPC-Laboratoire de Sécurité des Procédés Chimiques, INSA Rouen, Place Emile Blondel, BP8, 76131 Mont-Saint-Aignan Cedex, France

ARTICLE INFO

Article history:

Received 28 November 2008

Received in revised form 9 January 2009

Accepted 12 January 2009

Available online 20 January 2009

Keywords:

Taft relationship

Charton relationship

Homogeneous catalyst

Heterogeneous catalyst

Peroxydicarboxylic acids

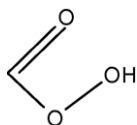
ABSTRACT

This paper describes the application of LFER to understand the mechanism of the perhydrolysis of carboxylic acids over homogeneous and heterogeneous catalysts. Several experiments were carried out with different linear carboxylic acids: formic, acetic, propionic and butyric acids; using sulfuric acid and Amberlite IR-120 as catalyst and different reaction temperatures. From the experiments, the apparent rate constants decrease in the following order: k_{app} (PFA) > k_{app} (PAA) > k_{app} (PPA) > k_{app} (PBA), in both catalytic system. Furthermore, it was found that this reaction follows Taft and Charton correlations, which implies that the steric effect of the substituent governs that reaction and the mechanism is similar between the different carboxylic acids. Comparison between homogeneous and heterogeneous catalytic system was carried out based on the analysis of the kinetic expression.

© 2009 Elsevier B.V. All rights reserved.

1. Introduction

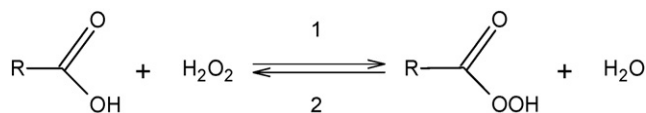
Peroxydicarboxylic acids, and mainly peroxyacetic acid, are well-known industrial chemicals. They are usually classified as eco-friendly chemical, because their decompositions do not produce toxic compounds, and their impacts on environment are harmless. They are used for their oxidative properties due to their “exotic” functional group



Those peroxydicarboxylic acids are widely used in several production technologies, as well as disinfecting and antimicrobial agents (destruction of organophosphorus as paraoxon, control legionella bacteria) in alimentary or pharmaceutical industry; as a bleaching agent of wood pulp in paper industry, instead of chlorine dioxide (which is not eco-friendly); and in fine chemistry for Baeyer–Villiger reaction or epoxidation of olefins. In industry, peroxyacetic acid is the main product used.

The nature of the substituent influences not only the oxidizing capacity of the functional group $-\text{CO}_3\text{H}$, but also the solubility and volatility of the whole molecule. For instance, Goud et al. [1] studied the epoxidation of jatropa oil with peroxyacetic and peroxyformic acid, where the peroxydicarboxylic acid synthesis occurs in the aqueous phase and the epoxidation in the organic phase. In this paper, the influence of the substituent (R) of the carboxylic acid on the synthesis of the corresponding peroxydicarboxylic acid is investigated (i.e., the influence of R on $-\text{CO}_2\text{H}$).

Several routes of peroxydicarboxylic acids synthesis are available, oxygenation of the parent aldehyde [2] or carboxylic acid [3]. In order to use a clean oxidation process, aqueous hydrogen peroxide is usually selected to oxidize carboxylic acids in liquid phase, as



The kinetics of the reaction is enhanced by an acid catalyst. In industry [4,5], the process is still catalyzed by a homogeneous catalyst (e.g., sulfuric acid) leading to several drawbacks (corrosion, catalyst separation, and threat for the environment). The use of a heterogeneous catalyst can surmount those problems.

In this work, the influence of the carbon chain length of the carboxylic acid on the perhydrolysis reaction is described. Experiments were carried out with the following carboxylic acids: formic, acetic, propionic and butanoic acid. Two different temperatures (30 and

* Corresponding author at: Laboratory of Industrial Chemistry and Reaction Engineering, Process Chemistry Centre, Åbo Akademi, Biskopsgatan 8, FI-20500 Åbo/Turku, Finland. Tel.: +358 2 215 8942; fax: +358 2 215 4479.

E-mail address: sleveneu@abo.fi (S. Leveneur).

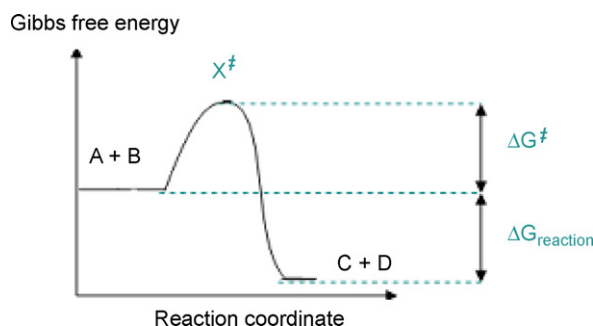


Fig. 1. Potential energy diagram for reaction $A + B = C + D$.

45 °C) and two different catalytic systems (homogeneous and heterogeneous) were applied. Our main purpose is to give a qualitative study of those effects on the kinetics of the reaction. Thus, the comparison of those experiments was based on the apparent kinetic rate constants.

2. Linear free-energy relations

Let us consider, the following reversible reaction:



For visualization of the concept of linear free-energy relationship (LFER), the potential energy diagram for this reaction is plotted in Fig. 1 (X^\ddagger is the activated complex).

The basic assumption of the concept is the existence of a relation between rate and equilibrium constant [6,7]:

$$k = \text{const} \times K^\alpha \quad (2)$$

Eq. (2) is equivalent to a linear relation between Gibbs energy of activation (ΔG^\ddagger) and Gibbs energy of the reaction (ΔG_R):

$$(\Delta G^\ddagger) = \alpha(\Delta G_R) + \text{const} \quad (3)$$

This approach can be established only for congeneric series of compounds, i.e., sets of compounds that share the same “functional group or reaction center” Y (e.g., $-\text{SH}$, $-\text{COOH}$, $-\text{CO}$) and only have variations in the substituents R attached to this functional group. Thus, this concept implies that there is a quantitative relationship between the structural features of a molecule and its reactivity. Eq. (3) is widely applied [8], although the theoretical explanation is still debated [9].

The pioneering research on this topic related to physical organic chemistry was done by Hammett, who quantified the effects of substituents in *m*- and *p*- position in benzene structure on ester hydrolysis. Taft [10] and Charton [11,12] expanded this approach to aliphatic series. Several applications of these relations can be explored such as understanding of the mechanism, prediction of the rate and equilibrium constants.

There are two different family of LFER: Hammett equation, which describes the behavior of *meta*- and *para*-substituted aromatic compounds; and Taft equation, which describes the behavior of aliphatic derivatives and *ortho*-substituted aromatic compounds. The main reason of these two different families is due to that the reaction center is close to the substituent in case of *o*-substituted aromatic and aliphatic compounds. Whereas, in case of *m*- and *p*-substituted aromatic compounds the reaction center and substituent are distant and strongly held by the benzene group.

Although the application of these equations for reactions homogeneously catalyzed is widespread in the literature, only few examples are found [13–16] for heterogeneously catalyzed reactions.

From the literature [10], three different effects of the substituent on the reaction center influence the rates or equilibria of a reaction:

- Polar interactions, which are associated with coulombic forces. The main contributors are inductive effect and the through-space electronic effect.
- Resonance interactions, which are due to the delocalization of electrons through π bond.
- Steric interactions, which result from van der Waals type forces.

Obviously, for reactions in solution, potential energies of solvation must also be considered. For that reason, experiments in this study were carried out in the same environment.

2.1. The Hammett equation

Even if the study of *m*- or *p*-substituted aromatic compounds is not treated in the experimental part, a brief description of Hammett equation is presented for the sake of clarity.

Within reaction series of the *m*- and *p*-substituted side-chain derivatives of benzene, the effect of structure on rates and equilibria is nearly always determined by a basic single factor, the polar effect of the substituent. Substituents are held rigidly at such large distances from the reaction center that no change in steric interactions occurs between the reactant and the transition state (in the rate case), or the product state (in the equilibrium case). Hammett established the following semi-empirical relationship:

$$\log \left(\frac{k}{k_0} \right) = \rho\sigma + \psi \quad (4)$$

where

- σ is a substituent constant independent of the nature of the reaction. It is a quantitative measure of the polar effect in any reaction of a given *m*- or *p*- substituent relative to hydrogen atom. Hammett selected as the standard reaction for obtaining this constant the ionization of substituted benzoic acids (K^*) in water at 25 °C:

$$\log \left(\frac{K^*}{K_0^*} \right) = \sigma \quad (5)$$

- ρ is a proportionality constant, dependent upon the nature of the reaction and the conditions. It is a measure of the susceptibility of a given reaction series to polar constituent.
- ψ is a parameter, which takes into account the resonance effects. This parameter is equal to zero if there is no resonance between the substituent in *m*- or *p*- and the rest of the molecule.
- The subscript zero in Eq. (4) refers to the unsubstituted benzene derivative.

Groups, which are electron withdrawing relative to hydrogen, are defined as having positive σ values, a reaction series in which rates or equilibria are facilitated by electron withdrawal will have a positive ρ value.

2.2. The Taft equation

Reactivity is greatly complicated in reaction series in which substituents are introduced close to the reaction center. This situation prevails in reactions involving *ortho*-substituted benzene derivatives and most aliphatic derivatives. For this reason, Taft [10] developed a different equation to explain the behavior of those compounds.

To illustrate that concept, Taft investigated the hydrolysis of esters or acid esterification. According to his conclusions, the effect of structure on equilibrium in this reaction is negligible, but both

the forward and reverse rates show very wide variations with the structure. Based on Hammett equation model, it was found that the three different effects should be taken into account, and, thus the following semi-empirical relation was developed:

$$\log \left(\frac{k}{k_0} \right) = \rho^* \sigma^* + \delta E_s + \psi \quad (6)$$

ψ is a parameter which takes into account the resonance effect between the substituent and the reaction center.

In contrast to Hammett polarity case, the relationship between the ionization of aliphatic carboxylic acids and the rate of hydrolysis or esterification is not linear. To evaluate the polar effects of substituent R on the rates of hydrolysis of esters RCOOR', Taft proposed the following relation:

$$\sigma^* = \frac{1}{2.48} \left[\log \left(\frac{k}{k_0} \right)_B - \log \left(\frac{k}{k_0} \right)_A \right] \quad (7)$$

where

- σ^* is a substituent constant dependent only upon the net polar effect of the substituent (corresponding to the rate constant k) relative to that for the standard of comparison (k_0 , R=CH₃). These values are defined as measures of the inductive electron-withdrawing power of an atom or group of atoms in a molecule.
- Subscripts B and A refer to alkaline and acidic reactions, respectively, i.e., both involving the same ester, solvent and temperature.
- The factor 2.48 is a constant introduced in an attempt to put the polar effects obtained in this manner on about the same scale as for the Hammett σ values.

ρ^* is a constant giving the susceptibility of a given reaction series to polar substituents. Its value depends upon the nature of the reaction center Y, the attacking reagent and the experimental conditions (solvent, temperature).

Except for unsaturated substituent conjugated with the carbonyl group, or for substituent which gives rise to changes in attractive interaction between reactant and transition states, e.g., internal hydrogen bonding, it has been assumed that the non-polar ($\log(k/k_0)$)_A values are near-quantitative measures of the net potential- and kinetic-energy steric effects. Again, the strongest argument in favor of this assumption is its ability to describe experimental results. In equation, this assumption is given by

$$\log \left(\frac{k}{k_0} \right)_A = E_s \quad \text{and} \quad \log \left(\frac{k}{k_0} \right)_B = 2.48 \sigma^* + E_s \quad (8)$$

E_s is a near-quantitative measure of the total steric effect associated with a given substituent relative to the standard of comparison. The standard of comparison in each case is the CH₃ group, whereas the reference group is the substituent H in the case of Hammett approach, δ is a reaction constant, independent of the nature of the substituents. The value of δ gives a measure of the relative susceptibility of the reaction series to the steric requirements of the substituents.

MacPhee et al. [17] have revisited the Taft E_s scale, by choosing as reference reaction the acid catalyzed esterification of carboxylic acids in methanol at 40 °C. In this paper, we have chosen to use this modified scale. However, for Taft σ^* values the original scale was applied.

2.3. Charton relationship

Charton [11,12] has proposed a modified Taft correlation, based on the van der Waals radii of the substituents. Indeed, the parameter E_s is linearly proportional to van der Waals radii, and, therefore it is the true measure of the steric effect. The second important conclusion was that the rates of acid-catalyzed esterification are

Table 1
Experimental matrix.

Reaction temperature	30–45 °C
Rotation speed	250 rpm
[CA] ₀	5.8–9.0 mol l ⁻¹
[H ₂ O ₂] ₀	4.3–7.5 mol l ⁻¹
[H ₂ O] ₀	17–28.2 mol l ⁻¹
[H ₂ SO ₄] ₀	0.10–0.15 mol l ⁻¹
Amberlite loading on dry basis	50.8–73.6 g l ⁻¹

solely a function of steric effects at least for the substituent studied. Thus, the following equation was established:

$$\log k = \psi v_X + h \quad (9)$$

where v_X is a steric parameter defined by the relationship $v_X = r_{v_X} - r_{v_H} = r_{v_X} - 1.2$; r_{v_X} is the van der Waals radius of the substituent X, and r_{v_H} is the van der Waals radius of the hydrogen atom.

According to MacPhee et al. [17], the scope of Eq. (9) cannot be extended to groups, which impose steric hindrance.

3. Experimental conditions

3.1. Apparatus and experimental procedures

All experiments were performed in a 250 ml jacketed glass reactor vessel. The reactor was equipped with a mechanical agitator and a temperature probe. Water was pumped through the outer jacket of the vessel to control the temperature of the reaction mixture. A pitched blade impeller (PTFE coated) was used to ensure a vigorous mixing (agitation speed was adjusted at 250 rpm) during the reaction.

A reflux condenser was attached to the top of the reactor (adjusted at 0 °C) to avoid loss of liquid phase compounds. In case that decomposition of peroxycarboxylic acid (PCA) or H₂O₂ appeared, a carrier gas (Helium, AGA, 99.996%) was introduced to the reactor through one of the necks in order to avoid accumulation of oxygen in the gas phase.

To prevent contamination induced by alkaline and metal components, which initiate the catalytic decomposition of peroxycarboxylic acid and hydrogen peroxide, all parts of the reactor system being in contact with the reaction solution were washed with hydrochloric acid followed by another washing, with a phosphate free detergent solution.

At the first stage, carboxylic acids (propionic acid: Acros, 99 wt.%, acetic acid: J.T. Baker 99–100 wt.%, butanoic acid: Fluka 98 wt.% and formic acid: J.T. Baker 98 wt.%) and the catalyst (sulfuric acid: J.T. Baker 95–97 wt.% and Amberlite IR-120 Aldrich) were mixed together in the reactor. When the reaction desired temperature was reached, preheated hydrogen peroxide solution (Merck, 30 wt.%) was added through a dropping funnel. At the time “zero” the required amount was introduced into the reactor. The experimental matrix is summarized in Table 1.

All experiments in one series were carried out at the same conditions regarding the temperature and agitation speed. However, due to the difference of molecular masses of the different acids, it is not their initial concentrations which were kept constant but their molar amounts. In other words, the initial number of moles of water, carboxylic acid, number of acid sites and hydrogen peroxide were kept constant in a reaction series (cf. Table 2).

Two series were carried out with sulfuric acid at 30 °C and 45 °C, and two series with a heterogeneous catalyst at 30 °C and 45 °C.

Table 2
Initial number of moles.

n_0 (CA)	1.1–1.2 mol
n_0 (H_2O_2)	0.8–1.1 mol
n_0 (H_2O)	3.5–4.1 mol
n_0 (H_2SO_4)	0.02 mol
n_0 (H^+) from resin	0.04–0.05 mol

3.2. Analytical methods

Samples were withdrawn from the reaction mixture by a plastic syringe (to avoid contamination of the solution by trace of metals) and were analyzed by the Greenspan and Mackellar method [18]. The concentration of hydrogen peroxide was determined by titration using a standard solution of ammonium cerium sulfate (0.1N). The concentrations of carboxylic and peroxydicarboxylic acids were determined by titration with an automatic titrator (Metrohm 751 GPD Titrino) using a standard solution of sodium hydroxide (0.2N).

3.3. Catalyst properties and characterization

The properties of the Amberlite IR-120 are summarized in Table 3. It is a cation exchange resin with a styrene-divinyl benzene matrix bearing sulfonic acid groups, which were used in the form of beads.

The Amberlite IR-120 catalyst was pre-treated before using, i.e., it was dried at 99 °C for 48 h.

The concentration of acid sites of catalyst was determined by titration [19]. Around 0.5 g of the catalyst sample was added to about 50 ml of NaCl solution (200 g/l) and stirred. The ion exchange between H^+ and Na^+ was allowed to proceed for 24 h. The mixture

Table 3
Properties of Amberlite IR-120 given by the manufacturer.

Amberlite IR-120	
Polymer type	Gel
Cross-linking (%)	8
Moisture content (% mass)	45
Capacity by dry weight (mequiv./g)	4.4
Native particle size range (mm)	0.3–1.2

was then titrated with 0.1N NaOH solution. To have a complementary method to determine the capacity of the resins, an elementary analysis of sulfur content was carried out by a ThermoQuest Flash EA1112 Series elemental.

4. Results and discussion

4.1. Catalyst characterization

The exchange capacity of the resin, determined by the titration method, is equal to 4.7 mequiv./g (on dry basis). The unit mequiv./g states for milli-equivalent per gram, which represents the number of moles of sulfonic group per gram of resins. This value is an average value of three different sets of experiments.

By assuming that all the sulfur determined by the elementary analysis corresponds to $-SO_3H$ group, the average capacity value was calculated to be equal to 4.4 mequiv./g (on dry basis).

By using titration method, Musante et al. have found a capacity equal to 4.5 mequiv./g (on dry basis) [20]. The exact value of Amberlite IR-120 capacity is difficult to determine, due to experimental errors, sensitivity of the elementary analysis and the non-ideality of the titration mixture. Moreover, the behavior of those resins in our

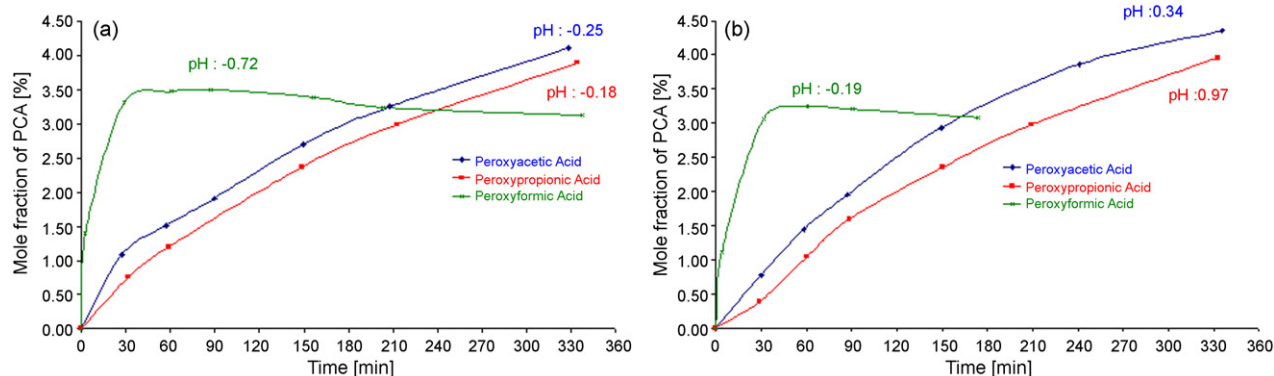


Fig. 2. Mole fraction of PCA versus time at 30 °C with sulfuric acid concentration at 0.11–0.15 M (a) and with pre-treated Amberlite IR-120 at an apparent concentration of 0.25–0.32 M (b).

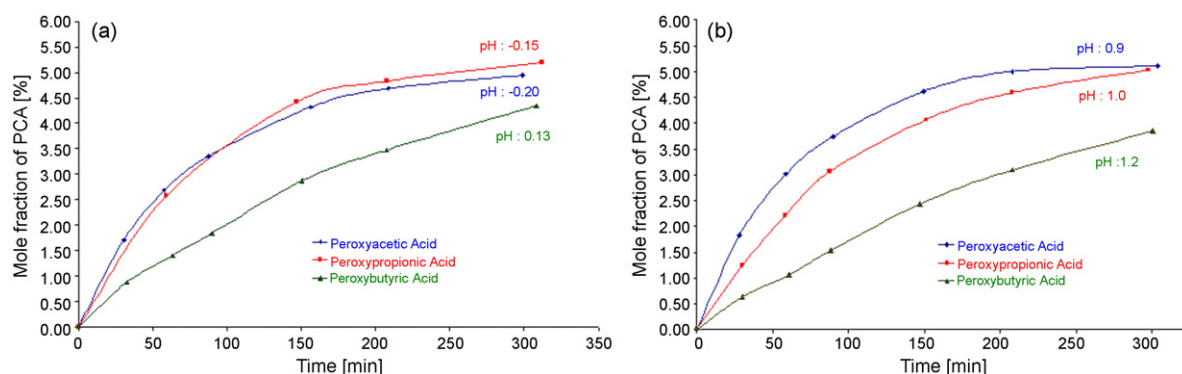


Fig. 3. Mole fraction of PCA versus time at 45 °C with sulfuric acid concentration at 0.10–0.11 M (a) and with pre-treated Amberlite IR-120 at an apparent concentration of 0.22–0.28 M (b).

reaction mixture might be different. Then, it is reasonable to assume that the capacity value fluctuates between 4.4–4.7 mequiv./g (on dry basis).

4.2. Use of linear free-energy relations

From the literature [20–23], the rate of formation of peroxy-carboxylic acid is expressed by the following relation:

$$\frac{d[\text{PCA}]}{dt} = k \left([\text{CA}][\text{H}_2\text{O}_2] - \frac{1}{K_{\text{eq}}} [\text{PCA}][\text{H}_2\text{O}] \right) \quad (10)$$

A detailed kinetic equation has been developed [21] by taking into account the effect of water and catalyst concentrations. However, the main goal of the current study is to check if the perhydrolysis of linear carboxylic acids follows the LFER, and investigate the sensitivity of the LFER parameters towards the reaction temperature and the nature of the catalyst. The apparent rate constant k_{app} was obtained by plotting the rate of formation of peroxy-carboxylic acids versus the product concentration of carboxylic acid and hydrogen peroxide:

$$\frac{d[\text{PCA}]}{dt} = k_{\text{app}} [\text{CA}][\text{H}_2\text{O}_2] \quad (11)$$

Figs. 2 and 3 show the mole fraction of peroxy-carboxylic acids as a function of time at 30 °C and 45 °C with the homogeneous and the heterogeneous catalyst.

In case of heterogeneous catalysis, the apparent $[\text{H}^+]$ concentration (the number of Brønsted sites of the solid catalyst present per liter of reaction mixture) was used. This value was calculated on the basis of the cation exchange capacity by dry weight (mequiv./g) provided by the acidity measurements.

Synthesis of peroxyformic acid was carried out only at 30 °C because of safety concerns. As can be seen from Fig. 2, peroxyformic acid is not stable. Mošovský et al. [24], have studied the synthesis of peroxyformic acid using sulfuric acid, and also noticed occurrence of this compound decomposition. For that reason, the apparent rate constant for the synthesis of peroxyformic acid was calculated before the decomposition phase starts.

No decomposition was observed for other peroxy-carboxylic acids, which is in line with our previous study [25] and literature data [26].

Synthesis of peroxybutyric acid was carried out at 45 °C because below this temperature butyric acid is not soluble in water.

Table 4 shows the apparent rate constants for the perhydrolysis of different carboxylic acids. As can be noticed, the apparent rate constants decrease in the following order: k_{app} (PFA) > k_{app} (PAA) > k_{app} (PPA) > k_{app} (PBA). Even if the apparent concentration of active site $[\text{H}^+]$ is twofold of the sulfuric acid concentration, the apparent rate constant for the homogeneous catalyst is higher than

Table 4

Apparent rate constants ($\text{l mol}^{-1} \text{s}^{-1}$).

	Sulfuric acid		Pre-treated Amberlite IR-120	
	30	45	30	45
FA	2.00E–04	–	1.00E–04	–
AA	1.06E–05	1.95E–05	7.00E–06	2.23E–05
PA	7.29E–06	1.64E–05	1.16E–06	1.59E–05
BA	Non-soluble	1.28E–05	Non-soluble	5.00E–06

Table 5

Polar and steric parameters for LFER.

Substituent	E_s	σ^*	ν_x
H–	1.12	0.49	0.00
CH ₃ –	0.00	0.00	0.52
CH ₃ –CH ₂ –	–0.08	–0.10	0.56
CH ₃ –CH ₂ –CH ₂ –	–0.31	–0.12	0.68

for the heterogeneous counterpart.

Those apparent rate constants were used in Eqs. (6) and (9) to determine the parameters dependent upon the nature of the perhydrolysis reaction (ρ^* , δ , ψ and h). The constant parameters such as steric parameter of Taft (E_s), Charton parameter (ν_x), and polar σ^* are displayed in Table 5.

From Table 5, one can notice that a high value of E_s implies a low steric hindrance; the substituent CH₃– is defined as a reference. In the case of the steric factor ν_x , it is the opposite, i.e., a high value of ν_x implies a high steric hindrance; and the substituent H– is defined as a reference. A high value of the polar parameter σ^* implies a high polar effect of the substituent, CH₃– is chosen as a reference. For instance, the value of σ^* for Cl– substituent is equal to 2.96. Note that the polar part is negligible for linear carbon chain substituent.

4.2.1. Use of Taft equation

Several assumptions can be done for the cases investigated here. First of all, there is no resonance effect between the functional group and the substituent for the carboxylic acids used in the experiments. The different polar parameters σ^* can be negligible because their values are low, and the experiments were carried out in acidic media. Indeed, Taft-Ingold and Charton have noticed that polar effect is negligible for experiments carried out in an acidic media [10]. Then, Eq. (6) becomes:

$$\log \left(\frac{k}{k_0} \right) = \delta E_s \quad (12)$$

Fig. 4 represents the application of Taft equation to the perhydrolysis of different carboxylic acids with sulfuric acid and pre-treated Amberlite IR-120 at 30 °C and 45 °C.

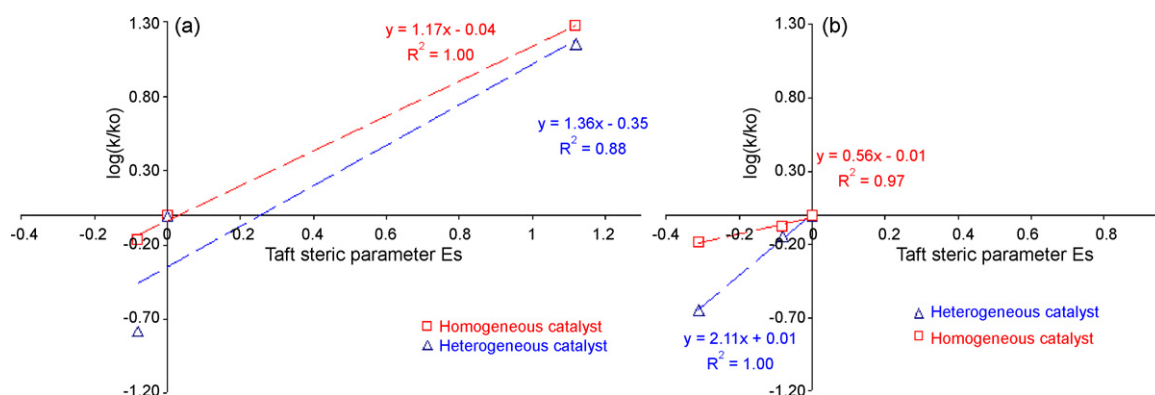


Fig. 4. Taft equation (Eq. (12)) for perhydrolysis of different carboxylic acids with H_2SO_4 and Amberlite IR-120 at 30 °C (a) and 45 °C (b).

Table 6
Value of coefficient δ .

	Coefficient δ	
	$T = 30^\circ\text{C}$	$T = 45^\circ\text{C}$
Homogeneous catalyst	1.17	0.56
Heterogeneous catalyst	1.36	2.11

For the sake of clarity, the values of the coefficient δ are summarized in Table 6.

At a first glance, Fig. 4 shows that perhydrolysis of carboxylic acids, catalyzed by an acid catalyst, follows the Taft equation by considering only the steric part. It can be concluded that the mechanism of formation of linear carboxylic acid is the same, i.e., there is no difference between the formation of peroxyacetic and peroxybutanoic acid.

In case of homogeneous catalysis, the apparent rate constant k_{app} can be split into two different parts associated with: hydroxonium ions from the dissociation of sulfuric acid and from the dissociation of carboxylic acid, respectively; $k_{\text{app}} = f(\text{H}_2\text{SO}_4, \text{CA})$.

In case of heterogeneous catalysis, kinetics is more complex because an adsorption phenomenon appears. Then, the apparent rate constant k_{app} depends on: hydroxonium ions concentration from the dissociation of carboxylic acid, active site concentration of the catalysts and the adsorption term of the different species K_{ads} ; $k_{\text{app}} = f(\text{CA}, \text{Amberlite}, K_{\text{ads}})$.

The active site of Amberlite IR-120 is the functional group $-\text{SO}_3\text{H}$, which is structurally close to sulfuric acid. The apparent rate constant is proportional to the active site concentration in case of the heterogeneous catalyst and to hydroxonium ions concentration in case of the homogeneous catalyst. However, in case of heterogeneous catalyst, the rate constant and the adsorption term are related

by $k_{\text{het}}\alpha(1/1 + K_{\text{ads}})$. Thus, the main difference between the two catalytic systems is the adsorption term, which could explain the change of the slope δ between systems catalyzed homogeneously and heterogeneously. A more detailed kinetic expression will be given below.

Experiments carried out at 30°C show that the slopes of the curves appear to be parallel. The accuracy of the calculated apparent rate constant for the perhydrolysis of formic acid is lower than the other rate constants. Experiments carried out at 45°C show that the slopes δ in case of homogeneous and heterogeneous catalysts are different. This difference might be certainly due to the adsorption term.

Table 6 demonstrates that the values of δ are dependent of the reaction temperature, and the nature of the catalyst at 45°C . The value of δ is positive, as in the case of the acid catalyzed hydrolysis of ethyl esters in aqueous acetone at 24.8°C , where the value of the slope δ is equal to 1.038 [17].

By comparing the slope δ from Table 6, one can notice that its value increases when heterogeneous catalysts are used instead of a homogeneous catalyst.

In order to check if the assumption that polar effect is negligible, the steric effect of Eq. (6) is neglected. Then, it becomes:

$$\log\left(\frac{k}{k_0}\right) = \rho^* \sigma^* \quad (13)$$

The results of this equation are shown in Fig. 5.

Fig. 5 confirms that there is no linear relation between the logarithm of the rate constant and the polar parameters.

4.2.2. Use of Charton equation

The Charton correlation takes into account only the steric effect of the substituent on the reaction center. The application of Eq. (9) to

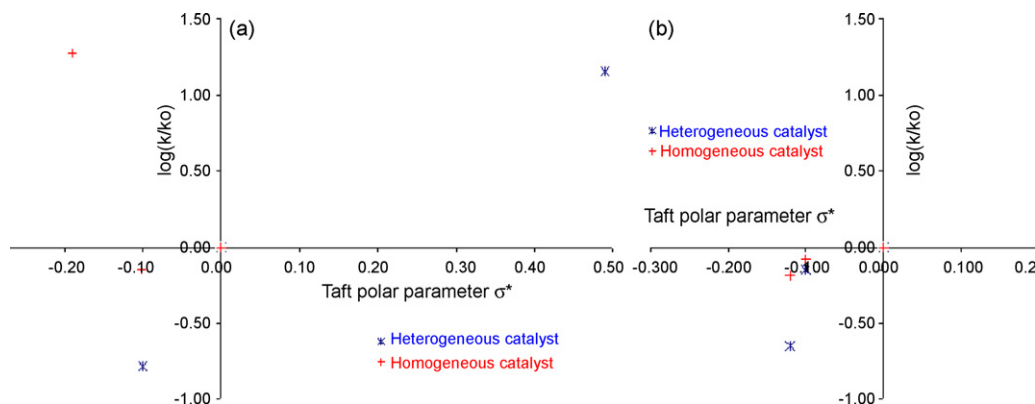


Fig. 5. Taft equation (Eq. (13)) for perhydrolysis of different carboxylic acids with H_2SO_4 and Amberlite IR-120 at 30°C (a) and 45°C (b).

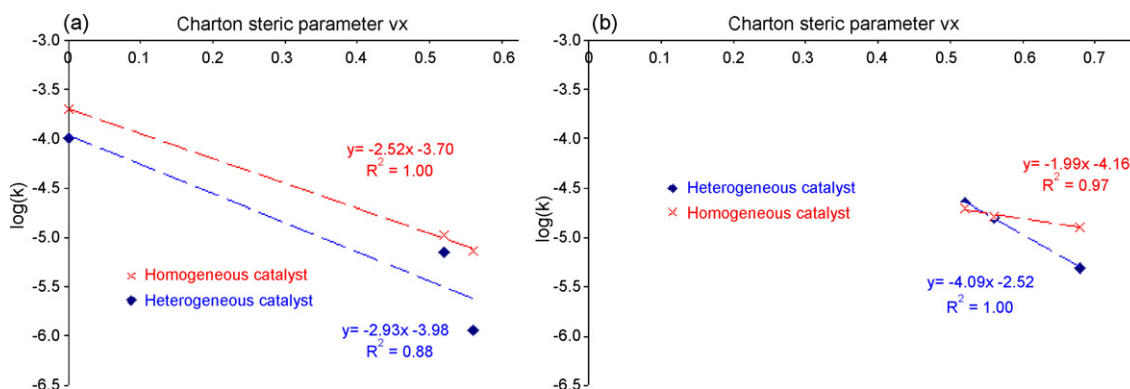


Fig. 6. Charton equation (Eq. (9)) for perhydrolysis of different carboxylic acids with H_2SO_4 and Amberlite IR-120 at 30°C (a) and 45°C (b).

Table 7
Coefficients ψ and h from Fig. 6.

	Coefficient ψ		h	
	$T = 30^\circ\text{C}$	$T = 45^\circ\text{C}$	$T = 30^\circ\text{C}$	$T = 45^\circ\text{C}$
Homogeneous catalyst	−2.52	−1.09	−3.7	−4.16
Heterogeneous catalyst	−2.93	−4.09	−3.98	−2.52

the perhydrolysis of different carboxylic acids is displayed in Fig. 6. From this figure, it is evident that the apparent rate constant for this reaction follows Charton relation, thus the polar effects are negligible for the perhydrolysis of linear carboxylic acids. The slopes for experiments carried out at 30°C are parallel. This parallelism is not due to the polar effect.

$$r_{\text{tot}} = \left(\frac{k_{\text{het}}[-\text{SO}_3\text{H}]_0}{(1 + K_{\text{ads,CA}}^{\text{C}}[\text{RCOOH}] + K_{\text{ads,PCA}}^{\text{C}}[\text{RCO}_3\text{H}] + K_{\text{ads,water}}^{\text{C}}[\text{H}_2\text{O}])} + \frac{k_{\text{hom}} \times \sqrt{K_{\text{RCOOH}}^{\text{C}}[\text{RCOOH}][\text{H}_2\text{O}]}}{[\text{H}_2\text{O}]} \right) \times \left([\text{RCOOH}][\text{H}_2\text{O}_2] - \frac{1}{K^{\text{C}}}[\text{RCO}_3\text{H}][\text{H}_2\text{O}] \right) \quad (17)$$

$$k_{\text{app}}^{\text{het}} = \left(\frac{k_{\text{int}}^{\text{het}}[-\text{SO}_3\text{H}]_0}{(1 + K_{\text{ads,CA}}^{\text{C}}[\text{RCOOH}] + K_{\text{ads,PCA}}^{\text{C}}[\text{RCO}_3\text{H}] + K_{\text{ads,water}}^{\text{C}}[\text{H}_2\text{O}])} + \frac{k_{\text{int}}^{\text{hom}} \times \sqrt{K_{\text{RCOOH}}^{\text{C}}[\text{RCOOH}][\text{H}_2\text{O}]}}{[\text{H}_2\text{O}]} \right) \quad (18)$$

For the sake of clarity, the values of the coefficient ψ and h are summarized in Table 7.

Liu et al. [15] have studied the esterification of acetic, propionic, butyric and hexanoic acid with methanol using sulfuric acid, and SAC-13 which is a Nafion/silica composite solid acid (fiber form) at 60°C . The mechanism for esterification and perhydrolysis of carboxylic acids is quite similar, therefore a qualitative comparison is possible. At the same time, the turnover frequencies were used in [15] instead of the apparent rate constant in Eq. (9), which should not, however, change qualitatively the results.

In the case of esterification, a negative value for the slope ψ was found as well with the curves, which describe homogeneous and heterogeneous catalyst systems being, however, parallel to each other.

The parallelism of the curves for perhydrolysis of carboxylic acids with homogeneous and heterogeneous catalysts (Taft or Charton correlation) is not clear. If it is genuine, further kinetic analysis is required, which is presented below.

4.2.3. Kinetic equation

In a previous paper [21], the rate of formation of peroxy-carboxylic acids using sulfuric acid is expressed:

$$r_{\text{tot}} = k \times \frac{[\text{H}_3\text{O}^+]}{[\text{H}_2\text{O}]} \times \left([\text{RCOOH}] \times [\text{H}_2\text{O}_2] - \frac{1}{K^{\text{C}}} \times [\text{RCO}_3\text{H}] \times [\text{H}_2\text{O}] \right) \quad (14)$$

The hydroxonium ions concentration was determined based on the electroneutrality principle:

$$[\text{H}_3\text{O}^+] = \frac{1}{2} \times [\text{H}_2\text{SO}_4]_0 + \sqrt{\frac{[\text{H}_2\text{SO}_4]_0^2}{4} + 2 \times K_{\text{II}}^{\text{C}} \times [\text{H}_2\text{SO}_4]_0 \times [\text{H}_2\text{O}] + K_{\text{III}}^{\text{C}} \times [\text{H}_2\text{O}] \times [\text{CH}_3\text{CH}_2\text{COOH}]} \quad (15)$$

Then, the apparent rate constant k_{app} is

$$k_{\text{app}}^{\text{hom}} = k_{\text{int}}^{\text{hom}} \frac{[\text{H}_3\text{O}^+]}{[\text{H}_2\text{O}]} \quad (16)$$

where $k_{\text{int}}^{\text{hom}}$ is the intrinsic rate constant for the homogeneous system.

In case of experiments carried out with Amberlite IR-120, an Eley-Rideal mechanism can be applied, which implies that only one reactant, is adsorbed on the surface. Due to a similarity with esterification reaction and the fact that it is the protonation of the carbonyl group which is a key step; only carboxylic acid is assumed to be adsorbed.

The protolysis of carboxylic acid and the adsorption of water on the active sites should be taken into account in the reaction rate (Eq. (17)):

Then, the apparent rate constant k_{app} is

$$k_{\text{app}}^{\text{het}} = \left(\frac{k_{\text{int}}^{\text{het}}[-\text{SO}_3\text{H}]_0}{(1 + K_{\text{ads,CA}}^{\text{C}}[\text{RCOOH}] + K_{\text{ads,PCA}}^{\text{C}}[\text{RCO}_3\text{H}] + K_{\text{ads,water}}^{\text{C}}[\text{H}_2\text{O}])} + \frac{k_{\text{int}}^{\text{hom}} \times \sqrt{K_{\text{RCOOH}}^{\text{C}}[\text{RCOOH}][\text{H}_2\text{O}]}}{[\text{H}_2\text{O}]} \right) \quad (18)$$

where $k_{\text{int}}^{\text{hom}}$ and $k_{\text{int}}^{\text{het}}$ represent the intrinsic rate constants.

Note that Eq. (6) in principle should be used for an elementary reaction. By using Eqs. (16) and (18), Eq. (12) becomes:

- In case of the homogeneous catalyst:

$$\log \left(\frac{k_{\text{app}}^{\text{hom}}(\text{CA})}{k_{\text{app}}^{\text{hom}}(\text{AA})} \right) = \log \left(\frac{k_{\text{int}}^{\text{hom}}(\text{CA})}{k_{\text{int}}^{\text{hom}}(\text{AA})} \right) + \log \frac{[\text{H}_3\text{O}^+]_{\text{CA}}}{[\text{H}_3\text{O}^+]_{\text{AA}}} + \text{const} = \delta_{\text{hom}} \cdot E_s \quad (19)$$

If the water concentration is the same or similar in both cases, then the last term of Eq. (19) can be neglected. If the protolysis of the carboxylic acid is similar to the protolysis of acetic acid, then, the second term can be neglected, as well. Therefore, Eq. (19) becomes:

$$\log \left(\frac{k_{\text{app}}^{\text{hom}}(\text{CA})}{k_{\text{app}}^{\text{hom}}(\text{AA})} \right) = \log \left(\frac{k_{\text{int}}^{\text{hom}}(\text{CA})}{k_{\text{int}}^{\text{hom}}(\text{AA})} \right) = \log \left(\frac{A_{\text{CA}}}{A_{\text{AA}}} \right) + \frac{1}{2.3RT} (\Delta G_{\text{AA}}^\ddagger - \Delta G_{\text{CA}}^\ddagger) = \delta_{\text{hom}} \cdot E_s \quad (20)$$

By using the Arrhenius relationship, the intrinsic rate constant is expressed by: $k_{\text{int}} = A \exp(-\Delta G^\ddagger / RT)$, where A is the pre-exponential factor, R is the gas constant, ΔG^\ddagger is the Gibbs energy of activation.

Eq. (20) shows the linear relation between the Gibbs energy of activation ΔG^\ddagger and the apparent rate constant. One should keep

in mind that this relation is valid only in case where the protolysis of a carboxylic acid is similar to acetic acid and the substituent has only a steric effect on the functional group.

- In a case of a heterogeneous catalyst, one gets:

$$\log \left(\frac{k_{\text{app}}^{\text{het}}(\text{CA})}{k_{\text{app}}^{\text{het}}(\text{AA})} \right) = \log \left(\frac{(k_{\text{int}}^{\text{het}}[-\text{SO}_3\text{H}]_0)/(1 + K_{\text{ads,CA}}^{\text{C}}[\text{RCOOH}] + K_{\text{ads,PAA}}^{\text{C}}[\text{RCO}_3\text{H}] + K_{\text{ads,water}}^{\text{C}}[\text{H}_2\text{O}]) + \left(k_{\text{int}}^{\text{hom}} \times \sqrt{K_{\text{RCOOH}}^{\text{C}}[\text{RCOOH}][\text{H}_2\text{O}]} \right) / [\text{H}_2\text{O}]}{k_{\text{int}}^{\text{het}}[-\text{SO}_3\text{H}]_0/(1 + K_{\text{ads,AA}}^{\text{C}}[\text{AcOH}] + K_{\text{ads,PAA}}^{\text{C}}[\text{AcOOH}] + K_{\text{ads,water}}^{\text{C}}[\text{H}_2\text{O}]) + \left(k_{\text{int}}^{\text{hom}} \times \sqrt{K_{\text{AcOH}}^{\text{C}}[\text{AcOH}][\text{H}_2\text{O}]} \right) / [\text{H}_2\text{O}]} \right) = \delta_{\text{het}} \cdot E_s \quad (21)$$

By neglecting the homogeneous part in Eq. (21) and by assuming that the concentration of the active sites is the same for both systems, one arrives at

$$\log \left(\frac{k_{\text{app}}^{\text{het}}(\text{CA})}{k_{\text{app}}^{\text{het}}(\text{AA})} \right) = \log \left(\frac{k_{\text{int}}^{\text{het}}(\text{CA})}{k_{\text{int}}^{\text{het}}(\text{AA})} \right) + \log \left(\frac{1 + K_{\text{ads,AA}}^{\text{C}}[\text{AcOH}] + K_{\text{ads,PAA}}^{\text{C}}[\text{AcOOH}] + K_{\text{ads,water}}^{\text{C}}[\text{H}_2\text{O}]}{1 + K_{\text{ads,CA}}^{\text{C}}[\text{RCOOH}] + K_{\text{ads,PAA}}^{\text{C}}[\text{RCO}_3\text{H}] + K_{\text{ads,water}}^{\text{C}}[\text{H}_2\text{O}]} \right) \quad (22)$$

Applying Arrhenius law for the intrinsic rate constants Eq. (22) becomes

$$\log \left(\frac{k_{\text{app}}^{\text{het}}(\text{CA})}{k_{\text{app}}^{\text{het}}(\text{AA})} \right) = \log \left(\frac{A_{\text{CA}}}{A_{\text{AA}}} \right) + \frac{1}{2.3RT} (\Delta G_{\text{AA}}^{\ddagger} - \Delta G_{\text{CA}}^{\ddagger}) + \log \left(\frac{1 + K_{\text{ads,AA}}^{\text{C}}[\text{AcOH}] + K_{\text{ads,PAA}}^{\text{C}}[\text{AcOOH}] + K_{\text{ads,water}}^{\text{C}}[\text{H}_2\text{O}]}{1 + K_{\text{ads,CA}}^{\text{C}}[\text{RCOOH}] + K_{\text{ads,PAA}}^{\text{C}}[\text{RCO}_3\text{H}] + K_{\text{ads,water}}^{\text{C}}[\text{H}_2\text{O}]} \right) = \delta_{\text{het}} \cdot E_s \quad (23)$$

As can be seen, the adsorption term is taken into account in Eq. (23). However, in case when this term is negligible, e.g., adsorption phenomena are negligible, then the slope of δ_{hom} and δ_{het} can be similar. In case that the adsorption term is constant with the different carboxylic acids, then the logarithm term for the adsorption tends to zero, and, subsequently, δ_{hom} and δ_{het} can be similar.

5. Conclusions

The synthesis of different peroxy-carboxylic acid was treated in order to establish a relationship between the structure of carboxylic acids and their reactivity. To accomplish this goal Linear Free-Energy Relations were used in the form of Taft and Charton correlations. A comparison between homogeneous and heterogeneous catalyst system is done by using sulfuric acid and a cation exchange resin Amberlite IR-120.

Based on the experiments, the apparent rate constants decreased in the following order: $k_{\text{app}}(\text{PFA}) > k_{\text{app}}(\text{PAA}) > k_{\text{app}}(\text{PPA}) > k_{\text{app}}(\text{PBA})$ in both catalytic systems, which demonstrates the importance of steric hindrance. The catalytic activity in case of the homogeneous system is higher than in case of the heterogeneous one.

Perhydrolysis of carboxylic acids catalyzed either homogeneously or heterogeneously follows the Taft (based on the steric part) and Charton correlations, which implies that the steric effect of the substituent on the reaction center governs the reaction, but not the polar effect. It was found that the parameters δ or ψ are temperature dependent.

The difference between δ_{hom} and δ_{het} or ψ_{hom} and ψ_{het} allows to elucidate the importance of the adsorption.

The major problem with experiments carried out with formic acid is the instability of the formed peroxy-carboxylic acid, and the importance of the self-catalytic effect of formic acid on the perhydrolysis reaction. These two phenomena prevent very accurate measurements of the apparent rate constant.

Semi-empirically equations used in this study, even if they do not show a clear dependence between the Gibbs energy of activation and the Gibbs energy of reaction, are excellent tools to elucidate the mechanism and predict the reaction rates.

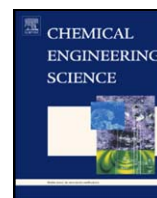
Acknowledgements

The financial support from the Åbo Akademi Forskningsinstitut and the Finnish Graduate School in Chemical Engineering (GSCE) are gratefully acknowledged. This work is part of activities at the

Åbo Akademi Process Chemistry Centre (PCC) within the Finnish Centre of Excellence Programme (2006–2011) by the Academy of Finland.

References

- [1] V.V. Goud, A.V. Patwardhan, S. Dinda, N.C. Pradhan, Chem. Eng. Sci. 62 (15) (2007) 4065.
- [2] B. Phillips, P.S. Starcher, B.D. Ash, J. Org. Chem. 23 (1958) 1823.
- [3] R. Cantieni, Zeitschrift fuer Wissenschaftliche Photographie, Photophysik und Photochemie 36 (1937) 90.
- [4] A. Reijo, I. Renvall, Patent No. WO2007031596 (2007).
- [5] X. Zheng, X. Zhou, J. Zhu, Z. Xu, Z. Ye, Patent No. CN1803771 (2006).
- [6] M.I. Temkin, The Kinetics of Some Industrial Heterogeneous Catalytic Reactions, Advances in Catalysis, Academic Press, New York, 1979, p. 173.
- [7] J.N. Brønsted, Chem. Rev. 5 (1928) 231–338.
- [8] K.J. Laidler, Chemical Kinetics, Third ed., Harper&Row, New York, 1987.
- [9] S. Ichikawa, J. Phys. Chem. 92 (24) (1988) 6970–6978.
- [10] R.W. Taft, in: M.S. Newman (Ed.), Steric Effect in Organic Chemistry, Wiley, New York, 1956, p. 556.
- [11] M. Charton, J. Am. Chem. Soc. 97 (6) (1975) 1552–1556.
- [12] M. Charton, J. Org. Chem. 41 (12) (1976) 2217–2220.
- [13] J. Lilja, D.Y. Murzin, T. Salmi, J. Aumo, P. Maki-Arvela, M. Sundell, J. Mol. Catal. A 182–183 (2002) 555–563.
- [14] A. Finiels, P. Geneste, C. Moreau, J. Mol. Catal. A 107 (1–3) (1996) 385–391.
- [15] Y. Liu, E. Lotero, J.G. Goodwin, J. Catal. 243 (2) (2006) 221–228.
- [16] T. Bligaard, J.K. Nørskov, S. Dahl, J. Matthiesen, C.H. Christensen, J. Sehested, J. Catal. 224 (2004) 206–217.
- [17] J.A. MacPhee, A. Panaye, J.-E. Dubois, Tetrahedron 34 (24) (1978) 3553–3562.
- [18] F.P. Greenspan, D.G. Mackellar, Anal. Chem. 20 (1948) 1061–1063.
- [19] Z.P. Xu, K.T. Chuang, Chem. Eng. Sci. 52 (17) (1997) 3011–3017.
- [20] R.L. Musante, R.J. Grau, M.A. Baltanas, Appl. Catal. A 197 (1) (2000) 165–173.
- [21] S. Leveneur, T. Salmi, D.Y. Murzin, L. Estel, J. Wärnå, N. Musakka, Ind. Eng. Chem. Res. 47 (3) (2008) 656–664.
- [22] L.V. Dul'neva, A.V. Moskvina, J. Gen. Chem. 75 (7) (2005) 1125–1130.
- [23] X. Zhao, T. Zhang, Y. Zhou, D. Liu, J. Mol. Catal. A 271 (2007) 246–252.
- [24] V. Mošovský, Z. Cvengrosová, A. Kaszonyi, M. Kralík, M. Hronec, Collect. Czech. Chem. C 61 (10) (1996) 1457–1463.
- [25] S. Leveneur, T. Salmi, N. Musakka, J. Wärnå, Chem. Eng. Sci. 62 (18–20) (2007) 5007–5012.
- [26] X. Zhao, K. Cheng, J. Hao, D. Liu, J. Mol. Catal. A 284 (1–2) (2008) 58–68.



Interaction of intrinsic kinetics and internal mass transfer in porous ion-exchange catalysts: Green synthesis of peroxydicarboxylic acids

Sébastien Leveneur^{a,b,*}, Johan Wärnå^a, Tapio Salmi^a, Dmitry Yu. Murzin^a, Lionel Estel^b

^aLaboratory of Industrial Chemistry and Reaction Engineering, Process Chemistry Centre, Åbo Akademi University, Biskopsgatan 8, FI-20500 Åbo/Turku, Finland

^bLSPC-Laboratoire de Sécurité des Procédés Chimiques, INSA Rouen, Place Emile Blondel, BP8, 76131 Mont-Saint-Aignan Cedex, France

ARTICLE INFO

Article history:

Received 24 February 2009

Received in revised form 8 May 2009

Accepted 15 May 2009

Available online 25 June 2009

Keywords:

Kinetics

Internal mass transfer

Particle size distribution

Mathematical modelling

Peroxydicarboxylic acids

Catalysis

ABSTRACT

Description of the interactions between intrinsic kinetics and internal mass transfer is one of the central issues in chemical reaction engineering. A general model was developed, comprising the kinetic and mass transfer effects in porous particles reacting in batch reactors. The catalyst particle size distribution was included in the model. A numerical algorithm and software was developed to solve the model for simulation and parameter estimation purposes. The model was applied to an industrially relevant case of green chemistry: synthesis of peroxydicarboxylic acids from dicarboxylic acids and hydrogen peroxide. Due to the potential industrial applications, the present study was focused on the acetic and propionic acid perhydrolysis. The concentrations in the bulk phase and inside the catalyst particles were predicted by the model. It turned out that the smallest ion-exchange resin particles operated under kinetic control, whereas the largest particles (higher than 300 µm) are influenced by diffusional limitation. Thus the combined effect of reaction and diffusion along with the particle size distribution are essential ingredients in the model.

© 2009 Elsevier Ltd. All rights reserved.

1. Introduction

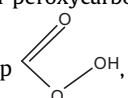
The environmental impact and the safety aspects for the production of chemicals are the two main issues to ensure the sustainability of industrial production. Preventing the formation of waste products, suppressing the energy consumption, designing safer process, utilizing non-toxic and non-hazardous chemicals, and optimizing the productivity are the main concerns of all the chemical companies. The concept of “Green Chemistry” introduced in the 1990s has provided methods and tools to take into account these issues for the scientific and industrial community. Synthesis of peroxydicarboxylic acid can be regarded as a textbook example of the philosophy.

The pioneering research of the laboratory-scale synthesis of peroxydicarboxylic acids began by D'Ans and Frey (1914), and the industrial production started around 75 years ago. However, since that time, the patents concerning the production of peracids still recommended homogeneous catalysts, such as sulphuric acid; which is recirculated to the process. The consequences of using sulphuric acid are corrosion of the equipment, setup of an energy-consuming

distillation system for the catalyst separation, and threat to the environment. In addition, impurities of the feed are enriched in the recycling catalyst solution.

The application of peroxydicarboxylic acids (Kitis, 2004) as a disinfectant is widely spread in different industries: alimentary manufactures, pharmaceutical industry, dairy manufacture and in sewage treatment to disinfect wastewaters. Peroxydicarboxylic acids are used as oxidizing agents in fine chemical industry for instance in epoxidation of olefins, Baeyer–Villiger reaction, or oxidation of thioether. Another area of application is in textile, pulp and paper industries as a decoloring agent.

The properties of peroxydicarboxylic acids are based on their ex-

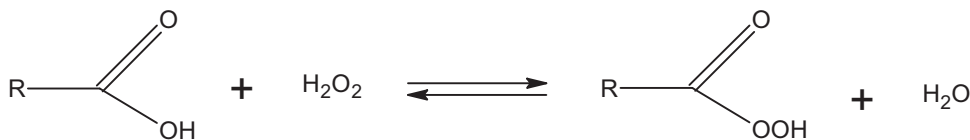
otic functional group , which gives them their oxidative

power. Furthermore, the decomposition products of the compounds are eco-friendly (Musakka et al., 2006; Leveneur et al., 2007; Zhao et al., 2008). For instance, the use of peroxyacetic acid for the bleaching of wood pulp assures a total chlorine-free process. From the viewpoint of safety, an advantage is that peroxydicarboxylic acids can be produced on-site, and the handling of them is convenient.

Several routes for peroxydicarboxylic acids (PCA) synthesis are available: oxidation of the parent aldehyde (Phillips et al., 1958) or carboxylic acid (Cantieni, 1937). In this study, a “green” oxidation of the parent carboxylic acid with aqueous hydrogen peroxide is used,

* Corresponding author at: Laboratory of Industrial Chemistry and Reaction Engineering, Process Chemistry Centre, Åbo Akademi University, Biskopsgatan 8, FI-20500 Åbo/Turku, Finland. Tel.: +358 2215 8942; fax: +358 2215 4479.

E-mail address: sleveneu@abo.fi (S. Leveneur).



Scheme 1. Synthesis of PCA from the corresponding carboxylic acid and hydrogen peroxide.

following the recommendation of Noyori (2005). Scheme 1 represents the reversible reaction of perhydrolysis of carboxylic acid.

Due to a slow kinetics, an acid catalyst is needed to increase the velocity of this reaction. Sulphuric acid is the most common mineral acid used. A greener way is to utilize heterogeneous catalysts, e.g., cation exchange resins. Based on the previous paper from our group (Leveneur et al., 2009), the use of Amberlite IR-120, as a heterogeneous catalyst, is a feasible alternative to homogeneous catalysis.

Few articles deal with the kinetics (Dul'neva and Moskvin, 2005) and modelling (Zhao et al., 2007) of peroxyacetic or peroxypropionic acid synthesis (Leveneur et al., 2008) catalyzed by sulphuric acid. Kinetic modelling of peroxyacetic acid catalyzed by Amberlite IR-120 was carried out by Musante et al. (2000). The objective of the present communication is to provide a comparison between homogeneous and heterogeneous catalysis system. To quantify this comparison by determining the parameters which govern the process, kinetic models corresponding for both catalytic systems were developed.

Because of the industrial practise and potential applications, two different peroxycarboxylic acids were studied: peroxyacetic acid (PAA) and peroxypropionic acid (PPA). Indeed, peroxyacetic acid is the most common peroxycarboxylic acids used industrially. However, PPA is more stable than PAA; and, furthermore propionic acid is less volatile ($t_B = 141^\circ\text{C}$) than acetic acid ($t_B = 118.1^\circ\text{C}$). The shortest chain peroxycarboxylic acid, peroxyformic acid is used to epoxidize unsaturated vegetable oils, but this compound should be prepared in situ for safety reasons.

Kinetic modelling of the carboxylic acids perhydrolysis reaction by using a homogeneous catalyst was inspired from the previous study (Leveneur et al., 2008). In case of heterogeneous catalysis, the particle size distribution (PSD) of the catalysts was included in the kinetic model to take into account the internal diffusion phenomenon, as Wärnå et al. (2002) has done previously.

2. Experimental section

2.1. Apparatus and experimental procedures

All experiments were performed in a 250 ml jacketed glass reactor vessel. The reactor was equipped with a mechanical agitator and a temperature probe. Water was pumped through the outer jacket of the vessel to control the temperature of the reaction mixture. A pitched blade impeller (PTFE coated) was used to ensure vigorous mixing (the agitation speed was adjusted at 250 rpm) during the reaction.

A reflux condenser was attached to the top of the reactor (adjusted at 0°C) to avoid the loss of volatile liquid-phase compounds. In case that decomposition of peroxycarboxylic acid or H_2O_2 might appear, an inert gas (Helium, AGA, 99.996%) was introduced to the reactor through one of the necks in order to avoid accumulation of oxygen in the gas phase.

To prevent the contamination induced by alkaline and metal components, which initiate the catalytic decomposition of peroxycarboxylic acid and hydrogen peroxide, all parts of the reactor system being in contact with the reaction solution were washed with hydrochloric acid followed by another washing, with a phosphate-free detergent solution.

Table 1

Experimental matrix for the homogeneous catalysis system.

Reaction temperature	30–60 °C
Rotation speed	250 rpm
[AA] ₀	5.15–9.00 mol l ^{−1}
[PA] ₀	1.80–6.50 mol l ^{−1}
[H ₂ O ₂] ₀	1.95–7.00 mol l ^{−1}
[H ₂ O] ₀	16.80–40.70 mol l ^{−1}
[H ₂ SO ₄] ₀	0.0–1.41 mol l ^{−1}

Table 2

Experimental matrix for the heterogeneous catalysis system.

Reaction temperature	30–60 °C
Rotation speed	250 rpm
[AA] ₀	5.60–9.30 mol l ^{−1}
[PA] ₀	4.95–7.40 mol l ^{−1}
[H ₂ O ₂] ₀	4.40–7.40 mol l ^{−1}
[H ₂ O] ₀	18.35–29.10 mol l ^{−1}
Catalyst (Amberlite) loading on dry basis	0.00–98.75 g l ^{−1}

At the first stage, carboxylic acids (propionic acid: Acros, 99 wt% and acetic acid: J.T.Baker 99–100 wt%) and the catalyst (sulphuric acid: J.T.Baker 95–97 wt% or Amberlite IR-120 Aldrich) were mixed together in the reactor. As the desired reaction temperature was reached, preheated hydrogen peroxide solution (Merck, 30 wt%) was added through a dropping funnel. At the time “zero” the required amount was introduced into the reactor.

To obtain a reliable kinetic model for the perhydrolysis of carboxylic acids, the experimental parameters in case of the homogeneous (Table 1) and heterogeneous catalyst (Table 2) were used.

2.2. Analytical methods

Samples were withdrawn from the reaction mixture (around 2.4 g) with a plastic syringe (to avoid contamination of the solution by trace of metals) and were analysed by the method of Greenspan and Mackellar (1948). The change of the liquid volume was taken into account, since the liquid volume was diminished during the reaction because of sampling. The concentration of hydrogen peroxide was determined by titration with a standard solution of ammonium cerium sulphate (0.1 N). The concentrations of carboxylic and peroxycarboxylic acids were determined by titration with an automatic titrator (Metrohm 751 GPD Titrino) using a standard solution of sodium hydroxide (0.2 N).

2.3. Catalyst properties and characterization

The properties of the Amberlite IR-120 are summarized in Table 3. It is a cation exchange resin with a styrene-divinyl benzene matrix bearing sulphononic acid groups, which were used in the form of beads.

Different pretreatments of Amberlite IR-120 were carried to check their potential influence on the kinetics of the reaction, namely drying at 70 and 90 °C for 48 h in an oven, and at 70 °C under vacuum (16 mbar) for 48 h.

The concentration of the acid sites on the catalyst was determined by a conventional titration method (Xu and Chuang, 1997).

Around 0.5 g of the catalyst sample was added to about 50 ml of NaCl solution (200 g/l) and stirred. The ion exchange between H^+ and Na^+ was allowed to proceed for 24 h. The mixture was then titrated with a 0.1 N NaOH solution. To have a complementary method to determine the capacity of the resins, an elementary analysis of the sulphur content was carried out by a ThermoQuest Flash EA1112 Series elemental, which oxidizes the sample and measures the gas as a gas chromatography.

A study of the particle size distribution was done on the pretreated resins (dried at 99°C) by the classical sieving method, and on the swelled resins in water at room temperature using a Malvern 2600 model. The measurement of the particle size distribution by the Malvern instrument is based on a He–Ne laser diffraction system.

3. Catalyst characterization results

3.1. Particle size distribution

The exchange capacity of the resin, determined by the titration method, is equal to 4.7 meq/g (on dry basis). This value is an average value of three different measurements.

By assuming that all the sulphur determined by the elementary analysis corresponds to the $-SO_3H$ group, the average capacity value was calculated to be equal to 4.4 meq/g (on dry basis).

By using the titration method, Musante et al. (2000) have found a capacity equal to 4.5 meq/g (on dry basis). The exact value of the Amberlite IR-120 capacity is difficult to determine, due to experimental errors, the sensitivity of the elementary analysis and the non-ideality of the titration mixture. Moreover, the behaviour of these resins in our reaction mixture might be different. Then, it is

reasonable to assume that the capacity value fluctuates between 4.4 and 4.7 meq/g (on dry basis). In the modelling, the value of the capacity was assumed to be equal to 4.7 meq/g (on dry basis).

By sieving the pretreated resin, the following distribution was found:

- the particle percentage with a diameter higher than 500 μm is equal to 63.6%, while
- the particle percentage with a diameter lower than 500 μm is equal to 36.4%.

The particle size distribution of the swelled resin in water obtained by the Malvern 2600 measurement is displayed in Fig. 1.

From these results, one can notice a swelling effect between the dried particles and the particles in water. The concentration of particles with a diameter higher than 500 μm in water has increased by ca. 16% compared to dry particles.

According to Musante et al. (2000), in case of the perhydrolysis of acetic acid over Amberlite IR-120, water is more strongly sorbed than either acetic acid or hydrogen peroxide, and the resin swelling is thus much higher in water than in acetic acid. However, the difference in the kinetics and thermodynamic occurs only between the experiments carried out with homogeneous and heterogeneous catalysts, and when the difference in the sorption behaviour of the reactants is significant.

For the sake of simplicity, the swelling effect in water is assumed to be the same as of the reaction mixture. Indeed, water is the solvent in the experimental condition.

3.2. Influence of the pretreatment of Amberlite IR-120

The main purpose of the pretreatment of the commercial Amberlite IR-120 is to release the native water from the resins. Amberlite IR-120 resins pretreated at different temperatures and pressures were tested. The aim was to inspect, whether the internal structure of the resin varies with different pretreatment methods.

From Fig. 2 one can notice that there is no influence of the nature of the pretreatment on the kinetics of propionic acid perhydrolysis, which implies that the different pretreatments modify the internal

Table 3

Properties of Amberlite IR-120 given by the manufacturer.

Amberlite IR-120	
Polymer type	Gel
Cross linking, %	8
Moisture content, % mass	45
Capacity by dry weight, meq/g	4.4
Native particle size range, mm	0.3–1.2

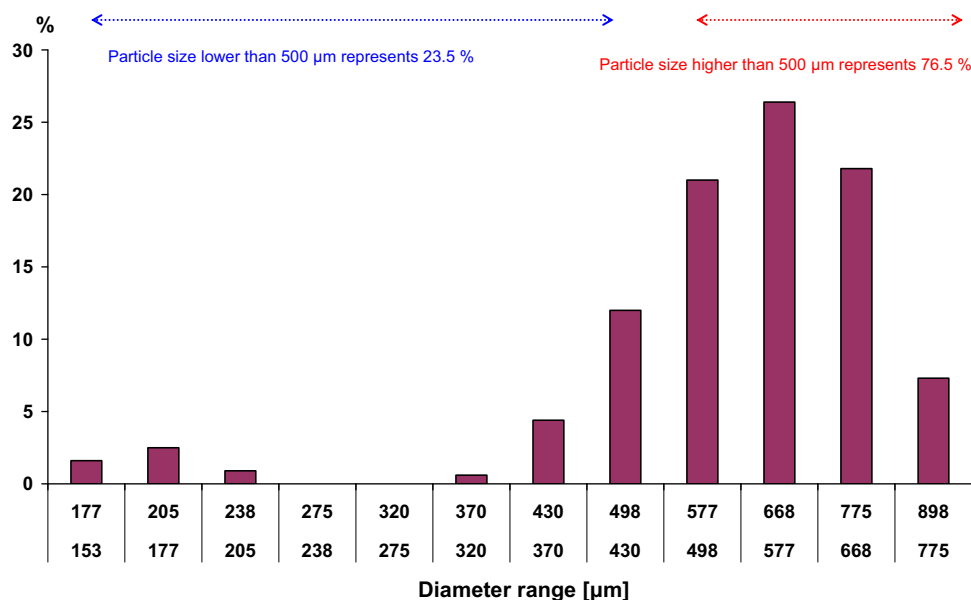


Fig. 1. The particle size distribution of the Amberlite IR-120 measured by Malvern 2600.

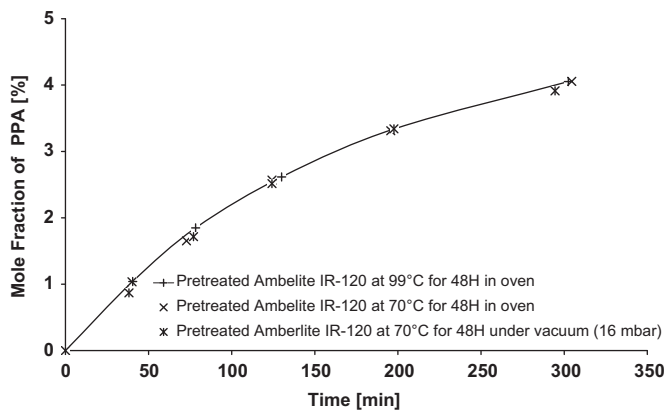


Fig. 2. The influence of the catalyst (Amberlite IR-120) pretreatment on the mole fraction of peroxypropionic acid at 40 °C and catalyst loading of 49 g l⁻¹.

catalyst structure in the same way. From a previous study (Leveneur et al., 2009), it was found that there is a difference in the kinetics for the experiments carried out with native Amberlite IR-120 and pretreated Amberlite IR-120.

4. Equilibrium analysis

4.1. Homogeneous catalysis

The non-ideality in the propionic acid perhydrolysis catalyzed by sulphuric acid was described previously (Leveneur et al., 2008). This non-ideality is mainly due to the presence of the strong electrolyte; therefore, a parameter δ was introduced to describe it.

A linear relationship between K^C (defined as the concentration ratio $[PCA]_{eq}[H_2O]_{eq}/[CA]_{eq}[H_2O_2]_{eq}$) and $[H_2SO_4]_0$ was established as

$$K^C = \delta^* [H_2SO_4]_0 + K^T \quad (1)$$

The true thermodynamic constant K^T follows the law of Van't Hoff:

$$\frac{d \ln K^T}{dT} = \frac{\Delta H_r^0}{RT^2} \quad (2)$$

where ΔH_r^0 stands for the standard reaction enthalpy change. Assuming that ΔH_r^0 is independent of T , integration of Eq. (2) from a particular temperature T_{ref} to an arbitrary temperature T leads to

$$\ln \frac{K^T}{K_{ref}^T} = \frac{-\Delta H_r^0}{R} \left(\frac{1}{T} - \frac{1}{T_{ref}} \right) \quad (3)$$

To determine the standard reaction enthalpy change ΔH_r^0 of the acetic acid perhydrolysis reaction, the protocol described in the previous article (Leveneur et al., 2008) was applied. The standard enthalpy change of the reaction (ΔH_r^0) and K_{ref}^T were estimated separately, namely these thermodynamic parameters were determined by carrying out some experiments for longer reaction times (around 20 h) to reach the equilibrium composition. The results of the modelling will be discussed in Section 7.1.

4.2. Heterogeneous catalysis

Fig. 3 represents the reaction quotient $Q = [PPA] * [H_2O]/[PA] * [H_2O_2]$ versus time for two experiments carried out with two different catalysts loadings.

The water concentration $[H_2O]$ was determined by adding the initial water concentration and the concentration of PPA formed (the

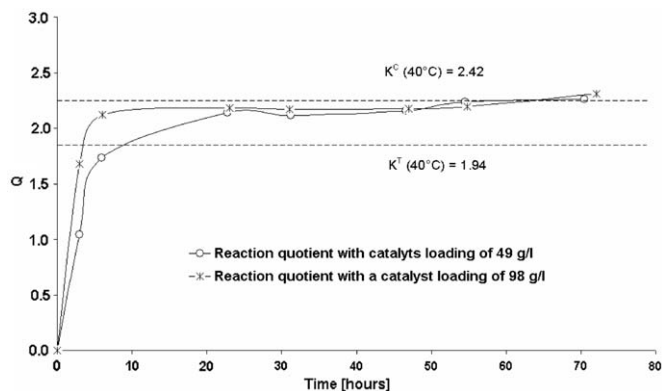


Fig. 3. Equilibrium experiments for the perhydrolysis of propionic acid at 40 °C.

experiments were always commenced with a PPA-free solution). The limiting value of Q obtained from Fig. 3 is 2.42.

Based on Eq. (3) and the data from the previous article (Leveneur et al., 2008), the value of the true equilibrium constant at 40 °C is equal to 1.94.

From Fig. 3, one can notice that there is a difference between the true thermodynamic constant K^T and the equilibrium constant K^C , which implies that even in presence of a solid acid catalyst, the reaction mixture is slightly non-ideal. However, the change of the catalyst loading does not affect the equilibrium constant K^C .

The equilibrium constant K^C is defined as: $K^C = K^T/K^\gamma$, where K^γ represents the equilibrium constant calculated based on the activity coefficients. For the sake of simplicity, K^γ was assumed to be constant in the temperature range 30–60 °C, and, the constant K^C was calculated as

$$K^C = \frac{K^T}{K^\gamma} = \frac{K^T}{0.8}$$

where the value of 0.8 was calculated based on Fig. 3, and K^T was determined from Eq. (3).

5. Mechanism and kinetic equations

5.1. Homogeneous catalysis

A detailed description of the kinetic equations can be found in the previous paper (Leveneur et al., 2008). Based on the experimental results, the following simplified mechanism was proposed (Fig. 4). Protolysis equilibria play a central role in the mechanism. The last steps (VI–VII) describe the synthesis reaction itself.

By applying the quasi-equilibrium hypothesis on the rapid proton transfer reaction VI and by defining reaction VII as the rate limiting, the rate expression becomes:

$$r = r_{VII} = k_{VII} * K_{VI}^C * \frac{[H_3O^+]}{[H_2O]} * \left([RCOOH] * [H_2O_2] - \frac{1}{K_{VI}^C * K_{VII}^C} * [RCO_3H] * [H_2O] \right) \quad (4)$$

The term $K_{VI}^C * K_{VII}^C$ represents the global equilibrium constant for the reaction denoted by K_{hom}^C , which is estimated by Eqs. (1) and (3). The term $k_{VII} * K_{VI}^C$ is denoted by a merged constant k_{hom} .

Finally, the reaction rate can be expressed by the following expression:

$$r = k_{hom} * \frac{[H_3O^+]}{[H_2O]} * \left([CA] * [H_2O_2] - \frac{1}{K_{hom}^C} * [PCA] * [H_2O] \right) \quad (5)$$

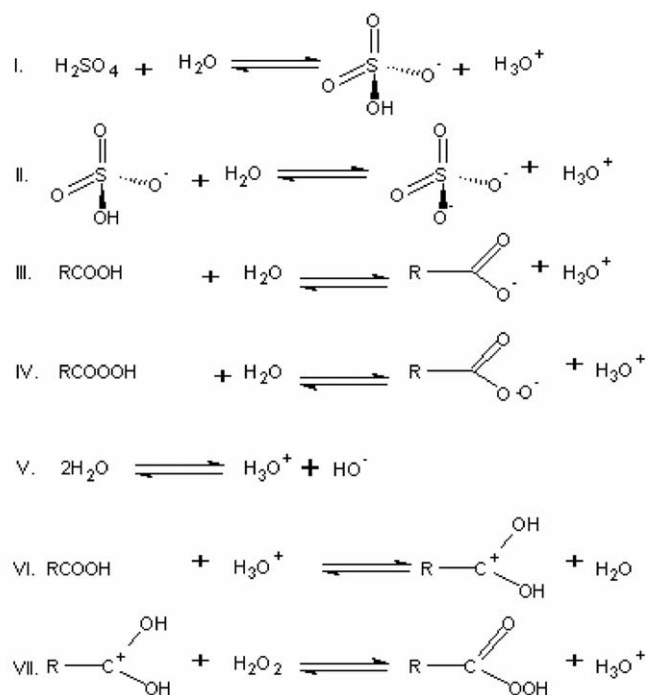


Fig 4. Simplified mechanism for peroxycarboxylic acid synthesis by sulphuric acid in aqueous media.

The hydroxonium ion concentration $[\text{H}_3\text{O}^+]$ was determined based on the electroneutrality principle and the protolysis equilibria, and after some simplifications, the concentration can be calculated from:

$$[\text{H}_3\text{O}^+] = \frac{1}{2} * [\text{H}_2\text{SO}_4]_0 + \sqrt{\frac{[\text{H}_2\text{SO}_4]_0^2}{4} + 2 * K_{\text{II}}^C * [\text{H}_2\text{SO}_4]_0 * [\text{H}_2\text{O}] + K_{\text{III}}^C * [\text{H}_2\text{O}] * [\text{CA}]}$$

(6)

where the mathematical expressions for the dissociation constants K_{II}^C and K_{III}^C were found from the literature (Knopf et al., 2003; Sue et al., 2004).

5.2. Heterogeneous catalysis

Several articles treat the carboxylic acid esterification (Altiokka and Çitak, 2003; Liu and Tan, 2001) or hydrolysis of esters (Altiokka, 2007) catalyzed by cation exchange resins as an Eley–Rideal mechanism. This mechanism implies that one reactant molecule adsorbs on the surface.

According to several studies (Dul'neva and Moskvina, 2005; Zhao et al., 2007; Leveneur et al., 2008; Musante et al., 2000), the protonation of the carbonyl group is the key step, which it is a strong argument to assume that the carboxylic acid adsorbs on the active site, and hydrogen peroxide molecule reacts from the bulk phase. However, the protolysis of the carboxylic acid and the adsorption of water on the active sites (Altiokka, 2007) should be taken into account. The following mechanism (Fig. 5) is proposed.

From Fig. 5, it should be noticed that the mechanism can be divided into two different parts: the homogeneous part due to the protolysis of carboxylic acids producing hydroxonium ions, which act catalytically; and the heterogeneous part due to the sulphonic groups on the resins. The peroxycarboxylic acid is a much weaker

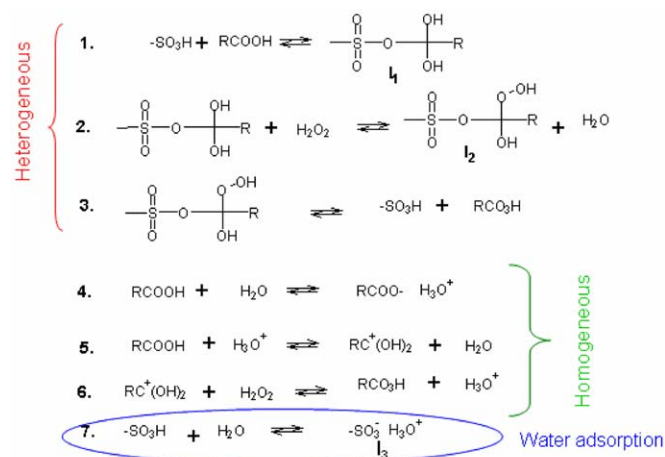


Fig 5. Simplified mechanism for peroxycarboxylic acid synthesis by Amberlite IR-120 in aqueous media.

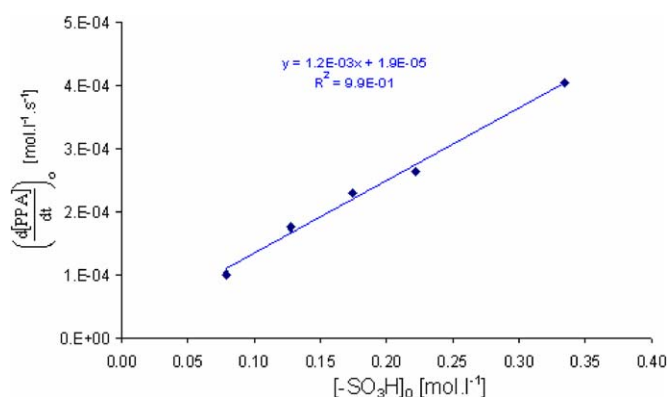


Fig 6. Influence of the loading catalyst on the perhydrolysis of propionic acid at 50 °C.

acid than the corresponding carboxylic acid. Therefore, the acid-catalytic effect of the peroxycarboxylic acid is not included in the scheme. The total rate r_{tot} of the reaction is the sum of the rates of the reactions 2 and 6, in Fig. 5.

Fig. 6 represents the initial rates of peroxypropionic acid formation ($d[\text{PPA}]/dt)_0$ plotted versus the active site concentration $[-\text{SO}_3\text{H}]_0$ (mol.l^{-1}), which is the apparent Brønsted acid concentration, i.e., the number of sulphonic groups bearing by the solid catalyst present per litre of solution. From the kinetic model for the synthesis of peroxypropionic acid using the homogeneous catalyst (Leveneur et al., 2008), in the absence of sulphuric acid the initial rate of formation of PPA is equal to $2.15 \times 10^{-5} \text{ mol.l}^{-1} \text{ s}^{-1}$ at 50 °C, which is closer to $1.87 \times 10^{-5} \text{ mol.l}^{-1} \text{ s}^{-1}$ given by Fig. 6.

5.3. Kinetic expressions for heterogeneous catalysis (Amberlite IR-120)

For the homogeneous part of the system, the quasi-equilibrium hypothesis was applied to the reversible proton donor (reaction 5). By noting the ratio k_{+5}/k_{-5} equal to K_5^C , the concentration of the intermediate $\text{RC}^+(\text{OH})_2$ is obtained from

$$[\text{RC}^+(\text{OH})_2] = \frac{K_5^C * [\text{RCOOH}] * [\text{H}_3\text{O}^+]}{[\text{H}_2\text{O}]}$$

(7)

Concentrations of carboxylate anions and hydroxonium ions are equal; then, the concentration of $[H_3O^+]$ can be obtained from

$$[H_3O^+] = \sqrt{K_4^C [RCOOH] [H_2O]} \quad (8)$$

The rate-determining step for the homogeneous system is the reversible reaction 6, and the rate r_{hom} can now be expressed as

$$\begin{aligned} r_{\text{hom}} = r_6 &= k_{+6} * [RC^+(OH)_2] * [H_2O_2] - k_{-6} * [RCO_3H] * [H_3O^+] \\ &= \frac{k_{+6} * K_5^C * \sqrt{K_4^C * [RCOOH] * [H_2O]}}{[H_2O]} \\ &\quad * \left([RCOOH] * [H_2O_2] - \frac{1}{K_5^C K_6^C} * [RCO_3H] * [H_2O] \right) \end{aligned} \quad (9)$$

where the equilibrium constant K_6^C is equal to the ratio k_{+6}/k_{-6} . The products $k_{+6} * K_5^C$ and $K_5^C * K_6^C$ are denoted by the merged constants k_{hom} and K_{hom}^C , respectively. Then, Eq. (9) becomes:

$$\begin{aligned} r_{\text{hom}} = r_6 &= \frac{k_{\text{hom}} \sqrt{K_4^C * [RCOOH] * [H_2O]}}{[H_2O]} \\ &\quad * \left([RCOOH] * [H_2O_2] - \frac{1}{K_{\text{hom}}^C} * [RCO_3H] * [H_2O] \right) \end{aligned} \quad (10)$$

For the heterogeneous part of the system, the quasi-equilibrium hypothesis is applied on reactions 1, 3 and 7, with the corresponding adsorption constants K_1^C , K_3^C and K_7^C . Then, the concentration of sulphonic group can be expressed as

$$[-SO_3H] = \frac{[-SO_3H]_0}{1 + K_1^C * [RCO_2H] + K_3^C * [RCO_3H] + K_7^C * [H_2O]} \quad (11)$$

where $[-SO_3H]_0$ is the initial sulphonic group concentration.

The rate-determining step for the heterogeneous system is the reversible reaction 2, and the rate r_{het} can be expressed as

$$\begin{aligned} r_{\text{het}} = r_2 &= k_{+2} * [I_1] * [H_2O_2] - k_{-2} * [I_2] * [H_2O] \\ &= \frac{k_{+2} * K_1^C * [-SO_3H]_0}{1 + K_1^C * [RCO_2H] + K_3^C * [RCO_3H] + K_7^C * [H_2O]} \\ &\quad * \left([RCO_2H] * [H_2O_2] - \frac{K_3^C}{K_1^C * K_2^C} * [RCO_3H] * [H_2O] \right) \end{aligned} \quad (12)$$

The terms $k_{+2} * K_1^C$ and $K_3^C/K_1^C * K_2^C$ are denoted by the lumped constants k_{het} and K_{het}^C , respectively. Then, Eq. (12) becomes:

$$\begin{aligned} r_{\text{het}} = r_2 &= \frac{k_{\text{het}} * [-SO_3H]_0}{1 + K_1^C * [RCO_2H] + K_3^C * [RCO_3H] + K_7^C * [H_2O]} \\ &\quad * \left([RCO_2H] * [H_2O_2] - \frac{1}{K_{\text{het}}^C} * [RCO_3H] * [H_2O] \right) \end{aligned} \quad (13)$$

By adding Eqs. (10) and (13), the total rate combining homogeneous and heterogeneous part is

$$\begin{aligned} r_{\text{tot}} = r_{\text{hom}} + r_{\text{het}} &= \left[\frac{k_{\text{hom}} * \sqrt{K_4^C * [RCOOH] * [H_2O]}}{[H_2O]} \right. \\ &\quad \left. + \frac{k_{\text{het}} * [-SO_3H]_0}{1 + K_1^C * ([RCO_2H] + [RCO_3H]) + K_7^C * [H_2O]} \right] \\ &\quad * \left[[RCO_2H] * [H_2O_2] - \frac{1}{K^C} * [RCO_3H] * [H_2O] \right] \end{aligned} \quad (14)$$

The main assumption is that the global equilibrium constants in case of the homogeneous system K_{hom}^C and in case of the heterogeneous

system K_{het}^C are equal. Due to a similar structure of the peroxy-carboxylic acid and the corresponding carboxylic acid, the adsorption coefficients K_1^C and K_3^C were approximated to be equal.

The values of k_{hom} were estimated in the previous work (Leveneur et al., 2008) for the perhydrolysis of propionic acid, and estimated by the kinetic model for the perhydrolysis of acetic acid by sulphuric acid. The value of K_4^C was calculated based on the equation from Sue et al. (2004). Altiokka (2007) has investigated the kinetics of benzaldehyde dimethyl acetal hydrolysis over Amberlite IR-120, which is the same catalyst as used in this study. The adsorption equilibrium constant related to water was calculated to be $K_{\text{water}} = \exp(1296/T - 4.4)$. The value for the adsorption coefficient of water K_7^C was calculated based on the equation developed by Altiokka (2007). In the kinetic modelling, the heterogeneous rate constant k_{het} and the adsorption coefficient K_1^C were estimated with regression analysis.

6. Mass transfer effect in case of the heterogeneous catalyst

6.1. Experimental verification of mass transfer

From a previous study (Leveneur et al., 2009), it has been demonstrated that there is no external mass transfer limitation in the range 250–600 rpm for the perhydrolysis of propionic acid catalyzed by pretreated Amberlite IR-120.

However, by sieving the pretreated Amberlite IR-120 particles into two different size fractions, i.e., lower and higher than 500 μm ; the presence of internal mass transfer limitation in the beginning of the reaction was confirmed (Fig. 7 and Table 4). One should keep in mind that the particle diameter (d_p) corresponds to the dried particles, and not the swollen particles in the reaction mixture.

In a previous study (Leveneur et al., 2009), by using similar resins (Dowex 50W \times 8) but with different sizes, the presence of internal mass transfer was noticed. Indeed, initial internal mass transfer limitation was present in the case of gelular resins with a degree of cross-linking equal to 8%, essentially for pretreated catalysts with larger particles. In order to take into account this effect to determine the kinetic parameters, the following mathematical expressions were derived.

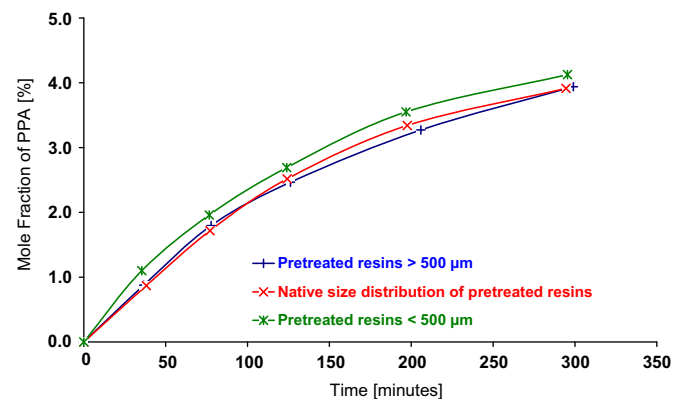


Fig. 7. The influence of the particle size distribution on the perhydrolysis of propionic acid at 40 °C and with a catalyst loading of 49 g l⁻¹.

Table 4
Effectiveness factor.

	$d_p < 500 \mu\text{m}$	Native distribution	$d_p > 500 \mu\text{m}$
$\eta(t = 0 \text{ min})$	1.00	0.76	0.79
$\eta(t = 77 \text{ min})$	1.00	1.00	0.98
$\eta(t = 195 \text{ min})$	1.00	0.96	0.97

6.2. Mathematical model of the batch reactor

The methodology to take into account the mass transfer phenomena on the kinetics is similar to the one developed by Silva and Rodrigues (2006), however, it is applied to a different system and moreover the particle size distribution is considered in the present study. The mathematical treatment of the diffusion phenomenon is divided into two parts: particle model and the batch reactor with the particle size distribution. For the sake of simplicity, the most important derivations will be presented in this chapter. More details can be found in Appendix A.

6.2.1. Catalyst particle model

The particle size distribution is included in the reaction–diffusion model for the porous catalyst particle. Spherical particles with the radius r_j are considered in the sequel. The heterogeneously catalyzed process appears on the acid sites of the solid catalyst, while the homogeneously catalyzed reactions take place in the pores of the catalyst.

For an infinitesimal volume element in the particle, the mass balance of a component (i) can be written as

$$(N_i A)_{in} + r'_i \Delta m + r_i \Delta V_L = (N_i A)_{out} + \frac{dn_i}{dt} \quad (15)$$

where r'_i is the catalytic reaction rate for the heterogeneous system in $\text{mol s}^{-1} \text{kg}^{-1}$, r_i is the catalytic reaction rate for the homogeneous part in $\text{mol s}^{-1} \text{m}^{-3}$, N_i is the flux of a component (i) in $\text{mol m}^{-2} \text{s}^{-1}$.

According to the manufacturer, the porosity ε_p of Amberlite IR-120 is medium, then the value of 0.5 was applied; and the density of this material is equal to 1.26 kg l^{-1} .

After some mathematical treatments, and by considering the spherical shape of the catalyst particles with a radius r_j . Eq. (15) becomes:

$$\frac{\partial C_{pi}}{\partial t} = \frac{r'_i \rho_p}{\varepsilon_p} + r_i - \frac{1}{\varepsilon_p r_j} \frac{\partial N_i}{\partial X} - \frac{2}{\varepsilon_p r_j X} N_i \quad (16)$$

X is a dimensionless coordinate equal to r/r_j .

To calculate the flux of a component (N_i), the law of Fick is used:

$$N_i = -D_{ei} \frac{\partial C_{pi}}{\partial r} = -\frac{D_{ei}}{r_j} \frac{\partial C_{pi}}{\partial X} \quad (17)$$

where D_{ei} is the effective diffusion coefficient.

Eq. (17) is inserted in Eq. (16), leading to

$$\frac{\partial C_{pi}}{\partial t} = \frac{r'_i \rho_p}{\varepsilon_p} + r_i + \frac{D_{ei}}{\varepsilon_p r_j^2} \left(\frac{\partial^2 C_{pi}}{\partial X^2} + \frac{2}{X} \frac{\partial C_{pi}}{\partial X} \right) \quad (18)$$

where $X \in [0, 1]$. The following boundary conditions are valid: $C_i(X=1) = C_{pi}$ in bulk phase and $(\partial C_{pi}/\partial X)_{X=0} = 0$ for symmetry reasons.

The effective diffusion coefficient D_{ei} is defined as: $D_{ei} = (\varepsilon_p/\tau_p) D_i$, where D_i is the molecular diffusion coefficient for a component (i), and was determined by using Wilke–Chang equation. Eq. (18) is solved numerically for each particle size to obtain the concentration profiles in the particles. The molar volumes of the dissolved components and the liquid viscosity are included in the Wilke–Chang equation. The molar volumes were calculated from the atomic increments of Le Bas.

Typical values of the diffusion coefficient D_i at 45°C are listed in Table 5.

6.2.2. Batch reactor model with particle size distribution

A batchwise operating stirred tank reactor is considered. Due to vigorous stirring, external mass transfer is suppressed, and concentration gradients in the bulk phase vanish (Leveneur et al., 2009).

Table 5

Diffusion coefficient values of the different species at 45°C

	Molecular diffusion coefficient ($\text{m}^2 \text{s}^{-1}$)
PA	1.82×10^{-9}
AA	2.23×10^{-9}
PPA	1.68×10^{-9}
PAA	1.85×10^{-9}
Water	4.68×10^{-9}
Hydrogen peroxide	4.22×10^{-9}

The size distribution of the catalysts particle is accounted for in the modelling. Thus, the balance of a component (i) becomes:

$$\sum_j N_{ij} A_j + r_i V_L = \frac{dn_i}{dt} \quad (19)$$

In Eq. (19), r_i is the homogeneous rate due to the dissociation of carboxylic acid, and A_j is the total surface area of particles with radius r_j . The total number of particles with radius r_j is n_{pj} , thus $A_j = n_{pj} 4\pi r_j^2$. The molar amount (n_i) is expressed with concentration and volume, $n_i = C_i V_L$, where V_L is the volume of the reaction mixture and C_i the concentration in the bulk phase. The balance equation is rewritten to

$$\frac{\partial C_i}{\partial t} = r_i + \frac{4\pi}{V_L} \sum_j n_{pj} N_{ij} r_j^2 \quad (20)$$

where N_{ij} is obtained from Eq. (17) at $X = 1$ (outer surface).

The fraction with radius r_j is denoted by y_j , i.e., $n_{pj} = y_j n_p$ where n_p is the total number of particles in the reactor. Furthermore, the approximate average radius \bar{r} is introduced as follows $\bar{r} = \sqrt{\sum_j y_j r_j^2}$,

the ratio to A_p/V_L is denoted by a_p and $r_j/\bar{r} = x_j$.

The final expression equals of the mass balance equation is

$$\frac{\partial C_i}{\partial t} = r_i + a_p \sum_j y_j N_{ij} x_j^2 \quad (21)$$

For the case of equal-sized particles $j = 1$, $y_j = 1$ and $x_j = 1$ in Eq. (21), a standard model for porous particle (PSD) is obtained. Eq. (21) is valid for a discrete particle size distribution. From Fig. 1, one can notice that the particle size distribution can be assumed continuous in the range $320\text{--}898 \mu\text{m}$. However, particles with a diameter lower than $238 \mu\text{m}$ represents ca. 5% of the distribution; and, furthermore, the internal mass transfer in this diameter range is absent. For that reason in the model, only particles in the range $320\text{--}898 \mu\text{m}$ were taken into account for the diffusion, the PSD can easily be replaced with a corresponding continuous distribution of particle sizes as shown below.

After some mathematical treatments, the mass balance including the continuous PSD becomes:

$$\frac{dC_i}{dt} = r_i + 2a_p \int_0^{r_{\max}/\bar{r}} N_i y(x) x dx \quad (22)$$

Eqs. (18) and (22) are both coupled in order to estimate the tortuosity factor τ of the resins and to get the concentration profiles in the particles. The model equations were solved numerically by discretizing the partial differential equations (PDEs) with respect to the spatial co-ordinate (X). Central finite difference formulae were used to approximate the first and second derivatives. Thus, the PDEs were transformed to ordinary differential equations (ODEs). The ODEs were solved with the backward difference method. In practice, the discrete form of the particle size distribution was used in numerical simulations, since the integral in Eq. (22) should in any case be solved numerically. Eq. (21) represents *de facto* the discretization of Eq. (22) for the numerical solution.

7. Kinetic modelling and results

7.1. Homogenous catalysis

The values of ΔH_r^0 and K_{ref}^T were estimated from separate experiments carried out for a long time until the chemical equilibrium was reached. The parameter ΔH_r^0 stands for the standard reaction change enthalpy of the perhydrolysis reaction, and K_{ref}^T is the true equilibrium constant at a particular temperature. The parameter estimation was carried out by a special software Modest (Haario, 2001). The objective function θ was minimized by using Simplex and Levenberg–Marquardt algorithms. This objective function was defined as follows $\theta = \sum (y_i - \hat{y}_i)^2$ where y_i is the experimental value and \hat{y}_i is the estimated value. The concentrations of CA, PCA and H_2O_2 were included in the objective function with equal weights. In this section, the results obtained by the kinetic model of the perhydrolysis of acetic acid catalyzed by sulphuric acid will be presented.

7.1.1. Determination of kinetics and thermodynamic parameters close to equilibrium

In this model, four parameters were estimated: k_{ave} , E_a , ΔH_r^0 and K_{ref}^T with the reference temperature fixed at 30 °C. The temperature dependence of the rate constant was described by a modified Arrhenius equation:

$$k = k_{\text{ave}} \exp \left(\frac{-E_a}{R} \left(\frac{1}{T} - \frac{1}{T_{\text{ave}}} \right) \right) \quad (23)$$

where $k_{\text{ave}} = Ae^{-(E_a/RT_{\text{ave}})}$, T_{ave} is the average temperature of the experiments. The goal of this modification is to minimize the correlation between the frequency factor and the activation energy during the parameter estimation.

The parameter δ (Eq. (1)) was assumed to be temperature independent within the temperature range 30–60 °C and equal to 0.35 (based on our previous experimental observations). Thus the equilibrium constant K^C is calculated from

$$K^C = 0.35 * [\text{H}_2\text{SO}_4]_0 + K_{\text{ref}}^T \exp \left(\frac{-\Delta H_r^0}{R} \left(\frac{1}{T} - \frac{1}{T_{\text{ref}}} \right) \right) \quad (24)$$

Table 6
Heat of formation of reactants and products in the liquid state.

	ΔH_f^0 (kJ/mol)
H_2O	−285.8
H_2O_2	−187.8
AA	−484.5
PAA	−390.1

Table 7
Summary of the estimated parameters and statistical data at $T_{\text{ave}} = 45^\circ\text{C}$ for the perhydrolysis of acetic acid (left) and propionic acid (right) for both catalytic systems.

Parameters	Estimated	Errors (%)	Parameters	Estimated	Errors (%)
<i>Equilibrium parameters</i>			<i>Equilibrium parameters</i>		
K^T (30 °C)	2.39	3.4	K^T (30 °C)	2.05	2.4
ΔH_r^0 (kJ mol ^{−1})	−5.66	25.6	ΔH_r^0 (kJ mol ^{−1})	−4.17	26.9
<i>Perhydrolysis by sulphuric acid</i>			<i>Perhydrolysis by sulphuric acid</i>		
k_{ave} (l mol ^{−1} s ^{−1})	1.70×10^{-3}	3.7	k_{ave} (l mol ^{−1} s ^{−1})	2.00×10^{-3}	3.3
E_a (kJ mol ^{−1})	75.58	3.3	E_a (kJ mol ^{−1})	44.24	6.9
δ (l mol ^{−1})	0.40	33.2	δ (l mol ^{−1})	1.33	4.8
<i>Perhydrolysis by Amberlite IR-120</i>			<i>Perhydrolysis by Amberlite IR-120</i>		
k_{ave} (l mol ^{−1} s ^{−1})	0.99×10^{-3}	12.7	k_{ave} (l mol ^{−1} s ^{−1})	0.91×10^{-3}	26.2
E_a (kJ mol ^{−1})	42.5	7.0	E_a (kJ mol ^{−1})	51.4	4.6
$K(\text{AA})$ (l mol ^{−1})	0.89	49.1	$K(\text{PA})$ (l mol ^{−1})	1.39	80.5

where T_{ref} is fixed at 30 °C in Eq. (24). Eq. (24) is a combination of Eqs. (1) and (3).

The coefficient of explanation R^2 of the kinetic models is defined as follows:

$$R^2 = 1 - \frac{\sum (y_i - \hat{y}_i)^2}{\sum (y_i - \bar{y})^2} \quad (25)$$

where y_i is the experimental value, \hat{y}_i is the estimated value and \bar{y} is the mean value of the observations.

The explanation coefficient of this model became 99.41%, which shows a good agreement between the experimental and calculated values.

The kinetic parameters k_{ave} and E_a obtained with this model are estimated to be 1.80×10^{-3} l mol^{−1} s^{−1} and 69.94 kJ mol^{−1}. These parameters were used as initial ones for the more detailed kinetic model. Table 7 summarizes the estimated values of parameters and their respective statistical data.

From Table 7 it can be concluded that the estimated relative standard error are low for each parameter, and, therefore the parameters are well defined. The parameters K_{ref}^T and ΔH_r^0 were estimated to be 2.39 and −5.66 kJ/mol. It should be emphasized that the main aim of this model is the achievement of these thermodynamic parameters, while the values of the kinetic parameters are only preliminary ones.

Table 6 summarizes the heat of formation ΔH_f^0 of the different reactants and products during the perhydrolysis of acetic acid; where the values of $\Delta H_f^0(\text{AA})$, $\Delta H_f^0(\text{H}_2\text{O})$ and $\Delta H_f^0(\text{H}_2\text{O}_2)$ were obtained from Lide (1995), and $\Delta H_f^0(\text{PAA})$ was measured by Havel and Greschner (1966).

By using the value of the heat of formation from Table 6, the standard enthalpy of reaction for the perhydrolysis of acetic acid is equal to −3.62 kJ mol^{−1}, which is close to the estimated value. However, from the study of Dul'neva and Moskvina (2005), this value is equal to −13.7 kJ mol^{−1}, which is higher than the two previous values. This difference can be explained by the difficulty to establish when the equilibrium is reached and the non-ideality of the solution in the presence of sulphuric acid.

7.1.2. Kinetic model

In this model, only the kinetic parameters were estimated. Eq. (5) was used for the modelling and the modified Arrhenius equation was applied.

Three parameters were estimated in this model: k_{ave} , E_a and δ which is defined as the coefficient in Eq. (1): $K^C = \delta * [\text{H}_2\text{SO}_4]_0 + K^T$. The explanation coefficient of the model became 99.41%. Table 7 gives the value of the estimated parameters and the statistical data.

The values of k_{ave} and E_a are rather similar to those from the preliminary model. The present model is more accurate for

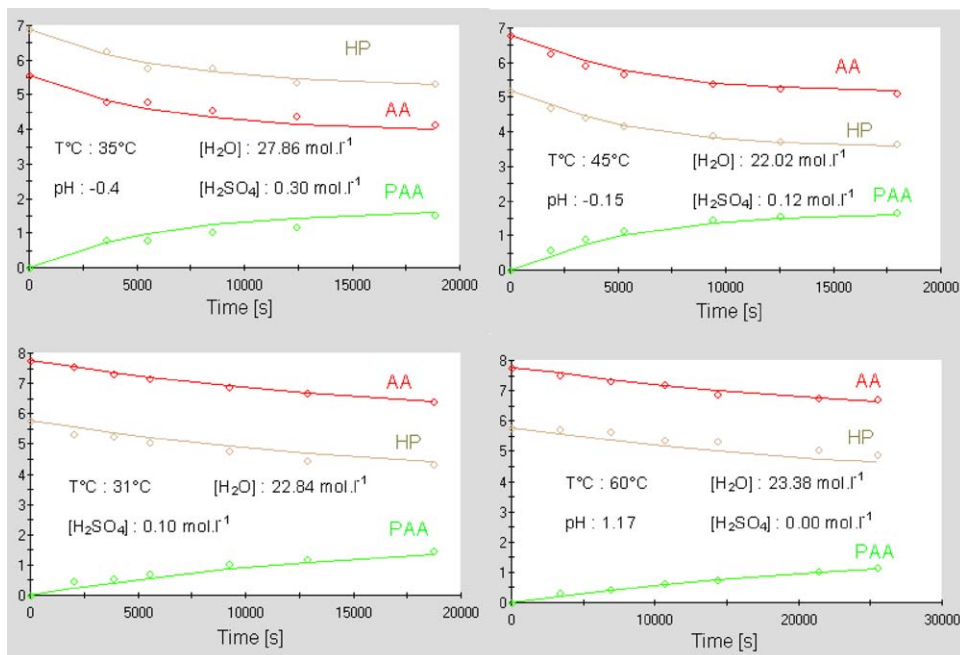


Fig. 8. Fit of the model to the experiments for the perhydrolysis of acetic acid catalyzed by sulphuric acid.

describing the kinetics, because there are more experiments with different variations included. In this model the experiments were carried out on a shorter reaction time (3–6 h). Examples of the modelling results are illustrated by Fig. 8.

Fig. 8 confirms in an unequivocal manner that the kinetic model fits correctly the experimental data.

7.2. Heterogeneous catalysis

Two analogous kinetic models were developed: one for the perhydrolysis of acetic acid and the other one for the perhydrolysis of propionic acid. The estimated equilibrium parameters such as ΔH_f^0 and K_{ref}^T from the homogeneous model were used here, since they are of global character. However, to take into account the slight deviation from the ideality, the concentration-based equilibrium constant K^C was calculated from

$$K^C = \frac{K^T}{K^T} \quad (26)$$

where K^T is the parameter including the activity coefficients. As noticed in Section 4.2, this constant was not estimated in the model but used from the experimental data by assuming that its value is constant over the temperature 30–60 °C.

In these models, three parameters are estimated: k_{ave} , E_a and $K(CA)$. Preliminary results from the modelling have shown that a value of 2.2 for the tortuosity factor τ_p gave better statistical results. Due to the complexity to estimate this parameter with a significant statistical reliability, the value of 2.2 was used in this model.

Eq. (14) was used to determine the kinetic and adsorption parameters; the value of k_{hom} (which is a combination of k_{ave} and E_a according to Eq. (23)) was determined by the homogeneous model.

The correlation matrix of the estimated parameters is shown on Fig. 9. From Fig. 9, one can notice that the correlations between the estimated parameters are low, indicating that the parameters are well identified.

K(AA)				K(PA)			
k	1	Ea	K(AA)	k	1	Ea	K(PA)
Ea	0.40	1		Ea	0.01	1	
K(AA)	0.97	0.25	1	K(PA)	0.99	-0.03	1

Fig. 9. Correlation matrix for the kinetic model.

The explanation coefficients of both models became higher than 99%. Table 7 gives the values of the estimated parameters and the statistical data.

The value of the adsorption coefficient for water on the resin K_7^C at 45 °C is equal to 0.72 by using Altioikka (2007) equation. The standard errors of the kinetic parameters, such as k_{ave} and E_a , are relatively low in both reaction systems. However, the standard error for the adsorption coefficient of the carboxylic acids is relatively high probably due to the fact that in the modelling it was assumed to be temperature independent.

Some modelling results are displayed in Figs. 10 and 11.

Figs. 10 and 11 confirm that the model fits correctly the experimental data in case of the perhydrolysis of acetic and propionic acid catalyzed by Amberlite IR-120.

Figs. 12 and 13 represent the concentration profile of peroxyacetic acid versus time and radius location in case of a particle with a diameter equal to 898 μm at 30 and 60 °C, respectively.

Figs. 12 and 13 were obtained by simulating the kinetic-diffusion data for an experiment of acetic acid perhydrolysis carried out at 30 and 60 °C, the catalyst loading of 57.42 g l^{-1} and equimolar concentrations of reactant. The concentration at the bulk is located at 449 μm and concentration in the centre of the particle is located at 0 μm .

One can notice the presence of an internal mass transfer limitation at 30 and 60 °C, Fig. 12 shows that the concentration of PAA increases from 0 to 2.43 mol l^{-1} when moving from the outer surface to the centre of the particle. The internal diffusion is essentially present at the beginning of the reaction, while, the concentration of PAA is uniform throughout the whole particle after 100 min at 60 °C. As the reaction proceeds, the rate becomes slower, and the effect of diffusion is diminished.

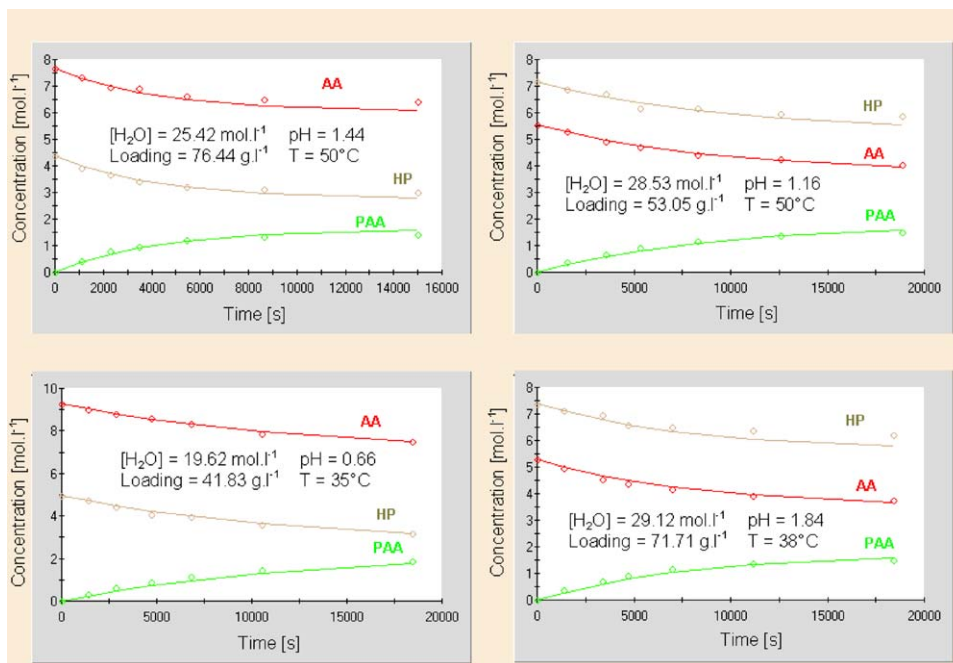


Fig 10. Fit of the model to the experiments for the perhydrolysis of acetic acid catalyzed by Amberlite IR-120.

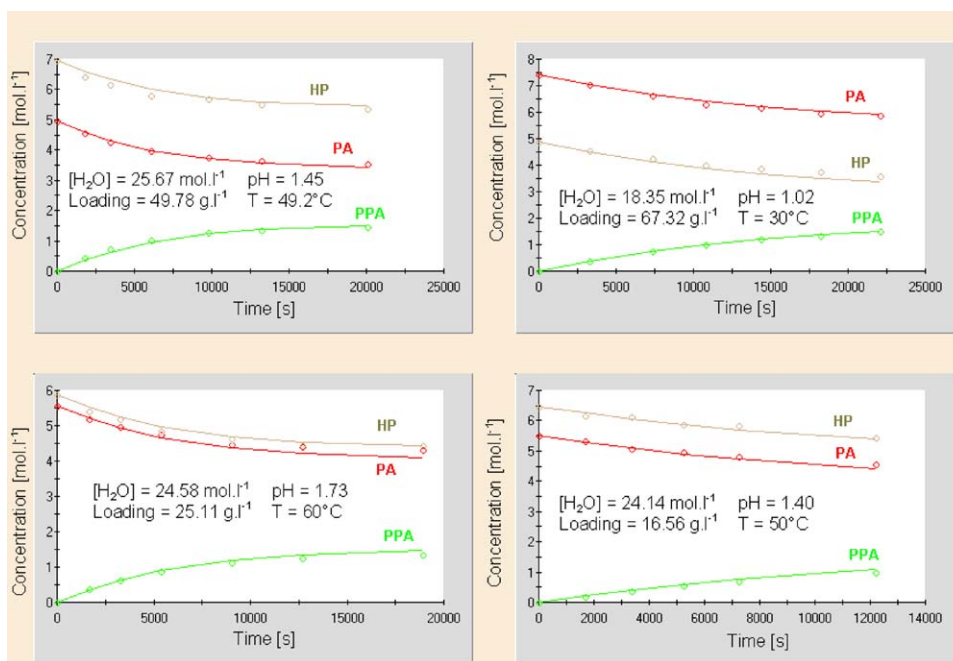


Fig 11. Fit of the model to the experiments for the perhydrolysis of propionic acid catalyzed by Amberlite IR-120.

7.3. Comparison of two catalytic systems

Table 7 summarizes the kinetic, equilibrium, and mass transfer parameters obtained in case of the perhydrolysis of acetic and propionic acid catalyzed by the homogeneous catalyst, sulphuric acid and the heterogeneous catalyst, Amberlite IR-120.

Table 7 reveals that the standard errors for the estimation of the equilibrium parameters are low. The absolute value of the enthalpy of reaction and equilibrium constant are higher in case of experiments

carried out with acetic acid, which imply that the energy amount released by this reaction is higher.

The standard errors for the parameters in perhydrolysis of carboxylic acids with sulphuric acid are low, which confirm the validity of the estimation. The higher energy of activation in case of the perhydrolysis of acetic acid reaction implies that to reach the transition state, more energy is required than for propionic acid. However, the rates of formation of peroxyacetic and peroxypropionic acids are similar. The value of the parameter δ , which describes the

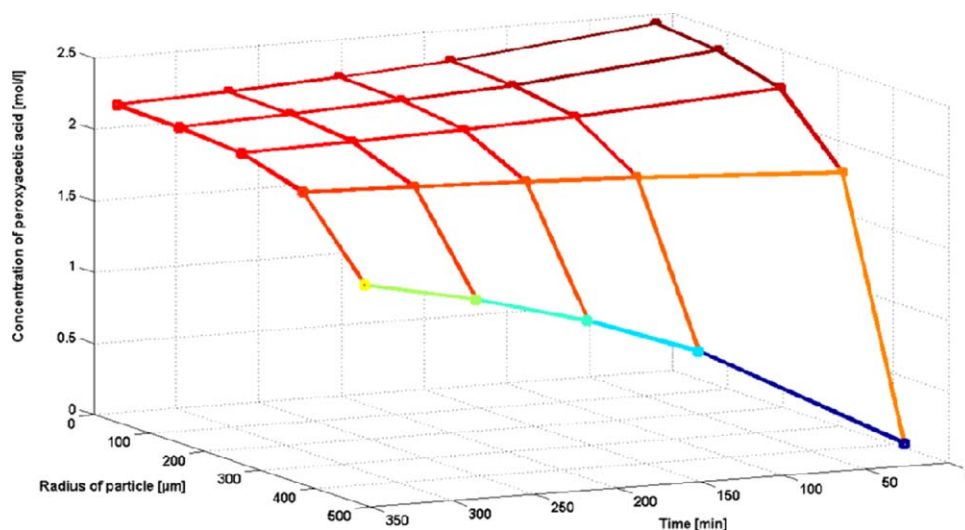


Fig 12. Concentration profile for peroxyacetic acid inside a particle of 898 μm at 30 $^{\circ}\text{C}$.

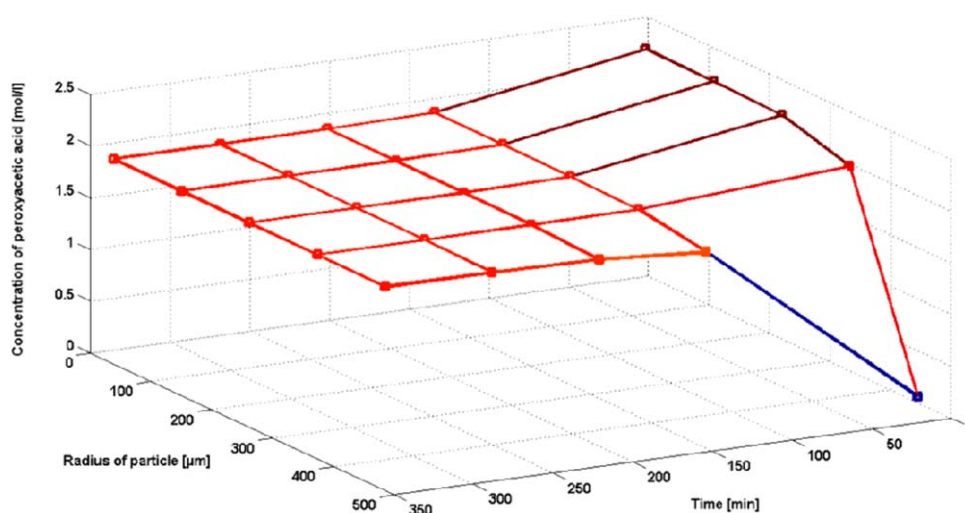


Fig 13. Concentration profile for peroxyacetic acid inside a particle of 898 μm at 60 $^{\circ}\text{C}$.

non-ideality of the solution, in the case of experiments carried out with acetic acid is lower than propionic acid. This means that the non-ideality due to sulphuric acid is lower for peroxyacetic than for peroxypropionic acid solution.

In case of perhydrolysis by Amberlite IR-120, the estimated kinetic parameters are similar for acetic and propionic acid, with low values of the standard errors. Based on the model, a value of 2.2 for the tortuosity factor gives better statistical response.

By comparing the kinetics parameters for the perhydrolysis of carboxylic acid catalyzed by sulphuric acid and by Amberlite IR-120, one can notice that these values are on the same order of magnitude. Obviously, the presence of internal mass transfer limitations in the beginning of the reaction slows down the heterogeneous system. However, this effect should be taken into account when real intrinsic kinetics is pursued, and also in the development of a continuous process since large particles are typically preferred in a continuous fixed bed to suppress the pressure drop.

8. Conclusions

A kinetic-diffusion model was developed in batch mode for synthesis of peroxycarboxylic acids (acetic and propionic acid) start-

ing from the corresponding carboxylic acids and hydrogen peroxide using sulphuric acid and pretreated Amberlite IR-120 in a temperature range 30–60 $^{\circ}\text{C}$. The models were shown to be correct for a water concentration range of 17–40 M, sulphuric acid concentration of 0–1.41 M and for a reactant concentration range of 2–8 M. No decomposition of peroxycarboxylic acids or hydrogen peroxide was noticed.

Pretreatment of resins at different temperature and pressure did not have any influence on the kinetics of the perhydrolysis reaction.

Particle size distribution of the catalyst was determined in water, and it was noticed that the fraction of particles with a diameter higher than 500 μm was increased by ca. 16% compared to dry particles. The swelling effect can be concluded to be negligible. The presence of an internal mass transfer limitation in the beginning of the reaction was noticed by using different particle sizes. This internal mass transfer effect was taken into account in the kinetic model by using the particle size distribution of Amberlite IR-120, and the tortuosity factor was estimated to be 2.2.

Based on the equilibrium analysis, the solution of perhydrolysis of carboxylic acid catalyzed by sulphuric acid was shown to be non-ideal, and this non-ideality was quantified by the factor δ . The standard enthalpy change of reaction ΔH_r^0 of the perhydrolysis of acetic

acid was estimated to be $-5.66 \text{ kJ mol}^{-1}$, which is lower than the one for the perhydrolysis of propionic acid reaction, $-4.17 \text{ kJ mol}^{-1}$, indicating that the synthesis of PAA is slightly more exothermic than the synthesis of PPA.

In case of the experiments carried out with pretreated Amberlite IR-120, a minor deviation from the ideality was noticed, but the amount of catalyst does not influence the chemical equilibrium. Kinetic modelling of carboxylic acids perhydrolysis with sulphuric acid showed that the energy of activation in case of acetic acid ($75.58 \text{ kJ mol}^{-1}$) is higher than for propionic acid ($44.24 \text{ kJ mol}^{-1}$).

An Eley–Rideal mechanism was applied, and the protolysis of carboxylic acid was taken into account to derive the kinetic equation for the system influenced by heterogeneous catalyst. The kinetic-diffusion modelling of the perhydrolysis of carboxylic acid by pretreated Amberlite IR-120 shows that the energy of activation in case of acetic acid (42.5 kJ mol^{-1}) is similar to that of propionic acid (51.4 kJ mol^{-1}). The adsorption coefficients of the carboxylic and peroxyarboxylic acid were supposed to be equal, due to their similar structures, and they were estimated to be in the range of $0.90\text{--}1.40 \text{ l mol}^{-1}$.

The values of kinetic parameters (k_{ave} and E_a) for sulphuric acid and pretreated Amberlite IR-120 catalyst are close (see Table 7). Thus, production of these peroxyarboxylic acids via heterogeneous catalysis is feasible, and could avoid the drawbacks associated with the use of sulphuric acid. Kinetic modelling for the synthesis of PPA and PAA shows that the estimated parameters were similar in both cases. The kinetic model and the diffusion model can be used for the design of batch reactors, and they can be easily extended to continuous fixed bed reactors.

Notation

a_p	interfacial area-to-liquid volume, m^{-1}
D_{ei}	effective diffusion coefficient, $\text{m}^2 \text{s}^{-1}$
D_i	molecular diffusion coefficient, $\text{m}^2 \text{s}^{-1}$
E_a	activation energy, kJ mol^{-1}
ΔH_f^0	heat of formation of specie, kJ mol^{-1}
ΔH_r^0	standard enthalpy change of reaction, kJ mol^{-1}
k	rate constant, $\text{l mol}^{-1} \text{s}^{-1}$
K	adsorption coefficient, l mol^{-1}
K^C	equilibrium constant, based on concentrations
K^T	true thermodynamic constant, based on activities
K'	equilibrium constant, based on coefficients of activity
n	amount of substance, mol
n_{pj}	number of particle with radius r_j
N	flux, $\text{mol m}^{-2} \text{s}^{-1}$
Q	reaction quotient
r	catalyst particle radius, radial coordinate
\bar{r}	average radius
r_i	generation rate
r_j	particle radius
R	gas constant, $\text{J K}^{-1} \text{mol}^{-1}$
R^2	coefficient of explanation, %
T	temperature, K
V	volume
X	dimensionless coordinate
y	frequency function for particle size distribution

Greek letters

δ	parameter which takes into account the non-ideality of the solution
ε_p	porosity of particle

η	effectiveness factor
θ	objective function
ρ_p	density of particle
τ_p	tortuosity of particle

Subscripts

ave	average
eq	equilibrium
het	heterogeneous catalytic system
hom	homogeneous catalytic system
i	component i
j	particle size fraction
ref	reference state
0	initial

Abbreviations

AA	acetic acid
CA	carboxylic acid
PA	propionic acid
PAA	peroxyacetic acid
PCA	peroxycarboxylic acid
PPA	peroxypropionic acid
PSD	particle size distribution

Acknowledgements

The financial support from the Åbo Akademi Forskningsinstitut and the Finnish Graduate School in Chemical Engineering (GSCE) are gratefully acknowledged. This work is part of activities at the Åbo Akademi Process Chemistry Centre (PCC) within the Finnish Centre of Excellence Programme (2006–2011) by the Academy of Finland. The authors express their gratitude to M.Sc. Krister Steinby for his help with the particle size distribution measurement.

Appendix A

A.1. Catalyst particle model

For an infinitesimal volume element in the particle, the mass balance of a component (i) can be written as

$$(N_i A)_{\text{in}} + r'_i \Delta m + r_i \Delta V_L = (N_i A)_{\text{out}} + \frac{dn_i}{dt} \quad (\text{A.1})$$

where, r'_i is the catalytic reaction rate for the heterogeneous system in $\text{mol s}^{-1} \text{kg}^{-1}$, r_i is the catalytic reaction rate for the homogeneous part in $\text{mol s}^{-1} \text{m}^{-3}$, N_i is the flux of a component (i) in $\text{mol m}^{-2} \text{s}^{-1}$.

The relation Δm , ΔV_L and n_i can be expressed as $\Delta m = \rho_p \Delta V$ in kg, $\Delta V_L = \varepsilon_p \Delta V$ in m^3 , $n_i = c_{pi} \Delta V_L = c_{pi} \varepsilon_p \Delta V$ in mol.

By including these relations in Eq. (A.1), the balance is transformed to

$$\frac{\Delta(N_i A)}{\Delta V} + \varepsilon_p \frac{dc_{pi}}{dt} = r'_i \rho_p + r_i \varepsilon_p \quad (\text{A.2})$$

For a spherical particle with radial coordinate (r), the area (A), the volume (V) and the volume element (ΔV) are: $A = 4\pi r^2$, $V = 4/3\pi r^3$ and $\Delta V = 4\pi r^2 \Delta r$. The derivative becomes:

$$\frac{\Delta(N_i A)}{\Delta V} = \frac{\Delta(N_i 4\pi r^2)}{4\pi r^2 \Delta r}$$

and by letting $\Delta r \rightarrow 0$, we get

$$\frac{\Delta(N_i A)}{\Delta V} = \frac{dN_i}{dr} + \frac{2}{r} N_i$$

After introducing the dimensionless coordinate $X = r/r_j$, where r_j is the particle radius, and letting $\Delta V \rightarrow 0$, the differential Eq. (A.2) becomes:

$$\frac{\partial C_{pi}}{\partial t} = \frac{r'_i \rho_p}{\varepsilon_p} + r_i - \frac{1}{\varepsilon_p r_j} \frac{\partial N_i}{\partial X} - \frac{2}{\varepsilon_p r_j X} N_i \quad (\text{A.3})$$

To calculate the flux of a component (N_i), the law of Fick is used:

$$N_i = -D_{ei} \frac{\partial C_{pi}}{\partial r} = -\frac{D_{ei}}{r_j} \frac{\partial C_{pi}}{\partial X} \quad (\text{A.4})$$

where D_{ei} is the effective diffusion coefficient.

Eq. (A.4) is inserted in Eq. (A.3), leading to

$$\frac{\partial C_{pi}}{\partial t} = \frac{r'_i \rho_p}{\varepsilon_p} + r_i + \frac{D_{ei}}{\varepsilon_p r_j^2} \left(\frac{\partial^2 C_{pi}}{\partial X^2} + \frac{2}{X} \frac{\partial C_{pi}}{\partial X} \right) \quad (\text{A.5})$$

where $X \in [0, 1]$. The following boundary conditions are valid: $C_i(X = 1) = C_{pi}$ in bulk phase and $(\partial C_{pi} / \partial t)_{X=0} = 0$ for symmetry reasons.

The effective diffusion coefficient D_{ei} is defined as: $D_{ei} = (\varepsilon_p / \tau_p) D_i$, where D_i is the molecular diffusion coefficient for a component (i), and was determined by using Wilke–Chang equation.

A.2. Batch reactor with PSD

A batchwise operating stirred tank reactor is considered and the external mass transfer is neglected.

The size distribution of the catalysts particle is accounted for in the modelling. Thus, the balance of a component (i) becomes:

$$\sum_j N_{ij} A_j + r_i V_L = \frac{dn_i}{dt} \quad (\text{A.6})$$

In Eq. (A.6), r_i is the homogeneous rate due to the dissociation of carboxylic acid, and A_j is the total surface area of particles with radius r_j . The total number of particles with radius r_j is n_{pj} , thus $A_j = n_{pj} 4\pi r_j^2$. The molar amount (n_i) is expressed with concentration and volume, $n_i = C_i V_L$, where V_L is the volume of the reaction mixture. The balance equation is rewritten to

$$\frac{\partial C_i}{\partial t} = r_i + \frac{4\pi}{V_L} \sum_j n_{pj} N_{ij} r_j^2 \quad (\text{A.7})$$

where N_{ij} is obtained from Eq. (A.4) at $X = 1$ (outer surface).

The second term on the right-hand side in Eq. (A.7) requires further consideration. The fraction with radius r_j is denoted by y_j , i.e., $n_{pj} = y_j n_p$ where n_p is the total number of particles in the reactor. Furthermore, the approximate average radius \bar{r} is introduced as follows:

$$A_p = n_p 4\pi \bar{r}^2 = \sum_j n_{pj} 4\pi r_j^2$$

gives $\bar{r} = \sqrt{\sum_j y_j r_j^2}$.

The balance Eq. (A.7) can be now rewritten to

$$\frac{\partial C_i}{\partial t} = r_i + \frac{4\pi \bar{r}^2 n_p}{V_L} \sum_j y_j N_{ij} \left(\frac{r_j}{\bar{r}} \right)^2 \quad (\text{A.8})$$

The ratio $n_p 4\pi \bar{r}^2 / V_L$ equals to A_p / V_L which is denoted by a_p and $r_j / \bar{r} = x_j$.

The final expression equals of the mass balance equation is

$$\frac{\partial C_i}{\partial t} = r_i + a_p \sum_j y_j N_{ij} x_j^2 \quad (\text{A.9})$$

For the case of equal-sized particles $j = 1$, $y_j = 1$ and $x_j = 1$ in Eq. (A.9) and a standard model for porous particle (PSD) is obtained. Eq. (A.9) is valid for a discrete particle size distribution.

The frequency function $y(x)$ is introduced and one gets $\sum_j y_j N_{ij} x_j^2$, where $x_j = x_j^2$. By assuming the PSD continuous, then, $y_j x_j$ can be diminished to $\Delta(y_j x_j)$, an infinitesimal fraction.

The term $\sum_j y_j N_{ij} x_j^2$ of Eq. (A.9) becomes $\sum_j N_{ij} \Delta(y_j x_j)$, which is equivalent to $\int N_i y(x') dz$, where $z = x^2$ and $dz = 2x' dx'$.

Thus, $\sum_j N_{ij} y_j x_j^2$ approaches to $2 \int N_i y(x) x' dx'$ as the continuous particle size distribution is approached. The mass balance including the continuous PSD becomes

$$\frac{dC_i}{dt} = r_i + 2a_p \int_0^{r_{\max}/\bar{r}} N_i y(x) dx \quad (\text{A.10})$$

The flux (N_i) at the outer of the surface is obtained from the solution of the particle model, according to Eq. (A.4), giving

$$N_i = -\frac{D_{ei}}{r_j} \left(\frac{dC_i}{dX} \right)_{X=1}$$

References

- Altioikka, M.R., Çitak, A., 2003. Kinetics study of acetic acid with isobutanol in the presence of amberlite catalyst. Appl. Catal. A Gen. 239, 141–148.
- Altioikka, M.R., 2007. Kinetics of hydrolysis of benzaldehyde dimethyl acetal over Amberlite IR-120. Ind. Eng. Res. 46, 1058–1062.
- Cantieni, R., 1937. Photochemical peroxide formation. VII. Oxidation of acetic, propionic, butyric and isovaleric acids by means of molecular oxygen in ultraviolet light. Z. Wiss. Photogr. Photophys. Photochem. 36, 90–95.
- D'Ans, J., Frey, W., 1914. The formation of per-acids from organic acids and hydrogen peroxide. Z. Anorg. Chem. 84, 145–164.
- Dul'neva, L.V., Moskvina, A.V., 2005. Kinetics of formation of peroxyacetic acid. J. Gen. Chem. 75 (7), 1125–1130.
- Greenspan, F.P., Mackellar, D.G., 1948. Analysis of aliphatic per acids. Anal. Chem. 20, 1061–1063.
- Haario, H., 2001. MODEST-User's Guide. Profmath Oy, Helsinki.
- Havel, S., Greschner, J., 1966. Explosion properties of peroxyacetic acid. I. Thermodynamic calculation of the explosion characteristics of peroxyacetic acid. Chem. Prum. 16, 73–78.
- Kitis, M., 2004. Disinfection of wastewater with peracetic acid: a review. Environ. Int. 30, 47–55.
- Knopf, D.A., Luo, B.P., Krieger, U.K., Koop, T., 2003. Thermodynamic dissociation constant of the bisulfate ion from Raman and ion interaction modeling studies of aqueous sulfuric acid at low temperatures. J. Phys. Chem. A 107, 4322–4332.
- Leveneur, S., Salmi, T., Musakka, N., Wärnå, J., 2007. Kinetic study of decomposition of peroxypropionic acid in liquid phase through direct analysis of decomposition products in gas phase. Chem. Eng. Sci. 62 (18–20), 5007–5012.
- Leveneur, S., Salmi, T., Murzin, D.Yu., Estel, L., Wärnå, J., Musakka, N., 2008. Kinetic study and modeling of peroxypropionic acid synthesis from propionic acid and hydrogen peroxide using homogeneous catalysts. Ind. Eng. Chem. Res. 47 (3), 656–664.
- Leveneur, S., Murzin, D.Yu., Salmi, T., Mikkola, J.-P., Kumar, N., Eränen, K., Estel, L., 2009. Synthesis of peroxypropionic acid from propionic acid and hydrogen peroxide over heterogeneous catalysts. Chem. Eng. J. 147, 323–329.
- Lide, D.R., 1995. CRC Handbook of Chemistry and Physics. seventy-fifth ed. CRC Press, Boca Raton.
- Liu, W.-T., Tan, C.-S., 2001. Liquid-phase esterification of propionic acid with *n*-butanol. Ind. Eng. Chem. Res. 40, 3281–3286.
- Musakka, N., Salmi, T., Wärnå, J., Ahlqvist, J., Piironen, M., 2006. Modelling of organic liquid-phase decomposition reactions through gas-phase product analysis: model systems and peracetic acid. Chem. Eng. Sci. 61 (21), 6918–6928.
- Musante, R.L., Grau, R.J., Baltanas, M.A., 2000. Kinetic of liquid-phase reactions catalyzed by acidic resins: the formation of peracetic acid for vegetable oil epoxidation. Appl. Catal. A 197 (1), 165–173.
- Noyori, R., 2005. Pursuing particle elegance in chemical synthesis. Chem. Commun. 14, 1807–1811.
- Phillips, B., Starcher, P.S., Ash, B.D., 1958. Preparation of aliphatic peroxyacids. J. Org. Chem. 23, 1823–1826.
- Silva, V.M.T.M., Rodrigues, A.E., 2006. Kinetics studies in a batch reactor using ion exchange resin catalysts for oxygenates production: role of mass transfer mechanisms. Chem. Eng. Sci., 316–331.

- Sue, K., Ouchi, F., Minami, K., Arai, K., 2004. Determination of carboxylic acid dissociation constants to 350 °C at 23 MPa by potentiometric pH measurements. *J. Chem. Eng. Data* 49, 1359–1363.
- Wärnå, J., Rönnholm, M.R., Salmi, T., Keikko, K., 2002. Influence of intraparticle reaction–diffusion in a catalytic reactor. *Chem. Eng. J.* 90, 209–212.
- Xu, Z.P., Chuang, K.T., 1997. Effect of internal diffusion on heterogeneous catalytic esterification of acetic acid. *Chem. Eng. Sci.* 52 (17), 3011–3017.
- Zhao, X., Zhang, T., Zhou, Y., Liu, D., 2007. Preparation of peracetic acid from hydrogen peroxide, part I: kinetics for peracetic acid synthesis and hydrolysis. *J. Mol. Catal. A Chem.* 271, 246–252.
- Zhao, X., Cheng, K., Hao, J., Liu, D., 2008. Preparation of peracetic acid from hydrogen peroxide, part II: kinetics for spontaneous decomposition of peracetic acid in the liquid phase. *J. Mol. Catal. A Chem.* 284 (1–2), 58–68.

Kinetic study of decomposition of peroxypropionic acid in liquid phase through direct analysis of decomposition products in gas phase

Sébastien Leveneur^{a,b,*}, Tapio Salmi^a, Niko Musakka^a, Johan Wärnå^a

^aLaboratory of Industrial Chemistry, Process Chemistry Centre, Åbo Akademi, FI-20500 Åbo/Turku, Finland

^bLRCP-Laboratoire des Risques Chimiques et Procédés, INSA Rouen, Place Emile Blondel, BP8, 76131 Mont-Saint-Aignan Cedex, France

Received 16 June 2006; received in revised form 7 December 2006; accepted 10 December 2006

Available online 29 December 2006

Abstract

Decomposition of peroxypropionic acid (PPA) takes place in the liquid phase, but the main products of decomposition, carbon dioxide and oxygen are transferred to gas phase. An analytical method was developed to determine the decomposition of PPA in liquid phase by means of chemical analysis of gas phase. The method is based on on-line mass spectroscopy (MS). A mathematical model for the semi-batch gas–liquid system was developed. The model comprised both kinetic and mass transfer effects. A comparison between experimental results and results predicted from the mathematical model revealed that the model can describe the essential effects of decomposition kinetics.

© 2007 Elsevier Ltd. All rights reserved.

Keywords: Kinetics; Mass transfer; Mathematical modelling

1. Introduction

Peroxypropionic acid (PPA) has potential importance from an industrial viewpoint. Because of its oxidative properties, it can be used in the destruction of organophosphorus (as paraoxon) and sulfurated pollutants. However, like many peroxy-compounds, it decomposes in the liquid phase.

Traditionally, liquid-phase decomposition kinetics is measured by analyzing the liquid-phase components off-line. The method is, however, slow and cumbersome. Therefore, we developed a rapid on-line method, which is based on the analysis of the decomposition products released into the gas phase. The method is based on quadrupole mass spectrometry (MS). The experimental system consists of a semi-batch reactor coupled to an online-MS. Reactor modelling aspects are considered.

2. Experimental setup

The experiment setup is described in detail in the doctoral thesis of Musakka (2004). A schematic experimental setup

used to investigate the PPA decomposition is displayed in Fig. 1.

The system consisted of two parts: the liquid phase in batch and the gas phase in continuous mode. The carrier gas was fed into a 500 ml glass reactor and leaves the reactor with the gas-phase decomposition products. About 200 g of a PPA solution was poured into the reactor, the carrier gas flow rate was adjusted to 10 ml min^{−1} at 20 °C. Temperature of the cooling condenser was adjusted to −20 °C to avoid the evaporated liquid-phase components (e.g. water, propionic acid, PPA) to enter the MS. It is sufficient to apply an atmospheric pressure in the reactor to remove the decomposition product; helium is used as a carrier gas. In the purpose of preventing any metal contamination, each part of the reactor was cleaned by a phosphate-free detergent (Deconex^R 22PF).

The gas–liquid mass transfer characteristics were studied by varying the stirring rate. It was adjusted to be high enough (150 rpm) thus suppressing the liquid–gas mass transfer resistance, but avoiding vortex formation at the gas–liquid interface.

3. Chemical analysis

The liquid phase was analyzed offline by titrations and NMR-spectroscopy. For measuring the PPA and hydrogen peroxide

* Corresponding author. Laboratory of Industrial Chemistry, Process Chemistry Centre, Åbo Akademi, FI-20500 Åbo/Turku, Finland.
Tel.: +358 2 215 4983; fax: +358 2 215 4479.

E-mail address: sleveneu@abo.fi (S. Leveneur).

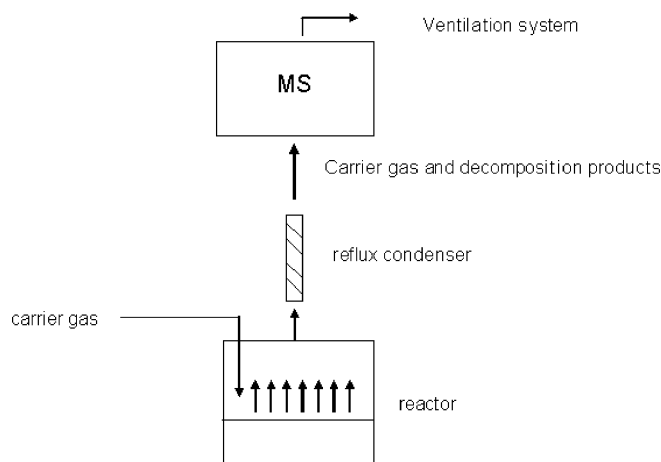


Fig. 1. Schematic representation of the experimental setup used for decompositions studies.

concentrations, the Greenspan and MacKellar (1948) method was used. Propionic acid was titrated with sodium hydroxide.

The mole fractions of carbon dioxide, oxygen and ethane were calculated from the intensities attributed to their mass numbers: 44, 32 and 27, respectively. Since liquid-phase components interfere with these mass numbers, we have to take into account these interferences when calculating the mole fractions of the different gas components. The mole fraction of a component X (e.g. CO_2 , O_2) was calculated from

$$x_X = k_X \cdot x_{cg} \left(\frac{I_X - \sum f_B I_B}{I_{cg}} \right),$$

where f_B is the fragmentation coefficient of the liquid phase component. The fragmentation coefficients were determined by measuring the intensities of the mass numbers of the liquid phase components present in the peroxypropionic acid solution.

4. Characterization of flow characteristics

The flow pattern of the gas phase was determined by tracer experiments, by introducing a pulse of another inert gas (here: Ar) into the main inert gas flow (here: He) and recording the pulse at the reactor outlet by MS. The tracer concentration in a tank reactor with complete backmixing (CSTR) is given by the well-known expression

$$c = c_0 e^{-t/\bar{t}}. \quad (1)$$

The straight line in the logarithmic plot (Fig. 2) implies that the gas phase of the reactor system is completely backmixed.

5. Mass balances for gas and liquid phases

In this work, a tank reactor with a continuous flow out from the reactor is considered. The gas outflow contained the decomposition products and helium, which was used as a carrier gas. Under the present circumstances, the vapor pressure of the liquid phase was negligible (the outlet gas was fed through the reflux condenser, Fig. 1).

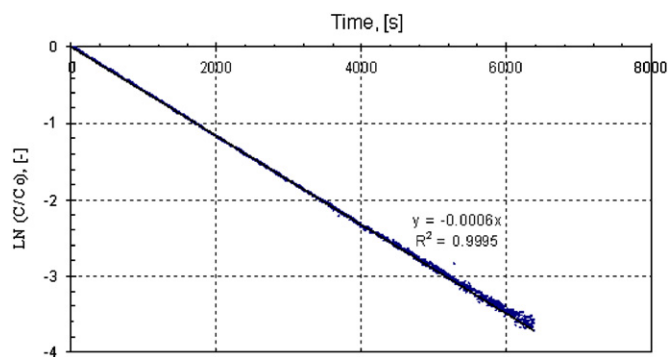


Fig. 2. Calculated results from the tracer experiment.

The mass balance of an arbitrary component (i) in the liquid phase is written in a quantitative form as follows:

$$\dot{n}_{Li,in} + r_i V_{0L} = \dot{n}_{Li,out} + N_{Li} A + \frac{dn_{Li}}{dt}. \quad (2)$$

For the simplest approach, the interfacial component flux (N_{Li}) is expressed by the law of Fick:

$$N_{Li} = k_{Li}(c_{Li} - c_{Li}^*), \quad (3)$$

where the asterisk denotes the equilibrium concentration at the gas–liquid interface. The equilibrium concentration is de facto determined by the gas solubility.

The volume of the reaction mixture can be regarded as constant. Thus the amount of substance (n_{Li}) and concentration (c_{Li}) are related by $n_{Li} = c_{Li} V$, which gives

$$\frac{dn_{Li}}{dt} = \frac{dc_{Li}}{dt} V \quad (V = \text{constant}).$$

Because the liquid phase is in batch, we get $\dot{n}_{Li,in} = \dot{n}_{Li,out} = 0$. Furthermore, the mass transfer area-to-volume ratio is denoted by

$$\frac{A}{V_{0L}} = a_0. \quad (4)$$

Consequently, the balance is simplified to

$$\frac{dc_{Li}}{dt} = r_i - k_{Li} a_0 (c_{Li} - c_{Li}^*), \quad (5)$$

where the derivative dc_{Li}/dt stands for the accumulation of a component i . For non-volatile components, the mass transfer coefficient k_{Li} is zero.

The concentration at the liquid–gas interface c_{Li}^* is obtained from solubility data of gases, by using the modified Henry's law: $K_i = c_{Gi}^*/c_{Li}^* \approx c_{Gi}/c_{Li}^*$.

The mass balance of a gas-phase component is

$$N_{Li} A = \dot{n}_G + \frac{dn_{Gi}}{dt} = c_{Gi} \dot{V}_G + \frac{dn_{Gi}}{dt}. \quad (6)$$

According to (3) and (4), we obtain

$$k_{Li} a_0 V_{0L} (c_{Li} - c_{Li}^*) = c_{Gi} \dot{V}_G + \frac{dn_{Gi}}{dt}. \quad (7)$$

Table 1
Behavior of liquid-phase components in the decomposition of PPA

	Reaction temperature (°C)	Reaction time (min)	Initial concentration (mol L ⁻¹)	Final concentration (mol L ⁻¹)
Hydrogen peroxide	25	235	4.41	4.39
PPA	25	235	1.89	1.75
Propionic acid	25	235	3.64	3.64
Sulfuric acid	25	235	0.36	0.36
Hydrogen peroxide	35	291	4.29	4.47
PPA	35	291	1.86	1.68
Propionic acid	35	291	3.70	3.87
Sulfuric acid	35	291	0.41	0.41
Hydrogen peroxide	45	277	3.41	3.57
PPA	45	277	1.47	1.31
Propionic acid	45	277	3.04	3.15
Sulfuric acid	45	277	0.31	0.31

Since the volume of the gas phase is constant and the relation $n_{Gi} = c_{Gi} V_G$ ($V_G = \text{constant}$) is valid, we get: $dn_{Gi}/dt = V_G dc_{Gi}/dt$, which gives

$$\frac{dc_{Gi}}{dt} = \frac{k_{Li} a_0 V_{0L}}{V_G} (c_{Li} - c_{Li}^*) - \frac{c_{Gi}}{\tau_G}, \quad (8)$$

where $\tau_G = V_G/\dot{V}_G$ and $V_G = V_{\text{inert}}$.

The behavior of a component in the liquid and gas phase is described by the Eqs. (5) and (8). For non-volatile components, $k_{Li} = 0$ and just the liquid-phase balance is needed. Other simplifications can be done, since the reactions itself are slow compared to the interfacial mass transfer in the vigorously stirred tank.

5.1. Simplified mass balances

The derivatives dc_i/dt are low, so the kinetics of the decomposition is slow. We can presume that reactions occur essentially in the bulk phase and neglect reactions in the liquid film (see also Table 1 and discussion thereafter).

The following simplifying notations are introduced:

$$k_{Li} a_0 = \kappa_L, \quad c_{Li} - c_{Li}^* = \Delta c \quad \text{and} \quad \frac{V_{0L}}{V_G} = \alpha.$$

By editing Eqs. (5) and (8) by the above notations we get

$$\alpha \left(\frac{dc_{Li}}{dt} \right) = (r_i - \kappa_L \Delta c) \alpha \quad (9)$$

and

$$\frac{dc_{Gi}}{dt} = \kappa_L \alpha \Delta c - \frac{c_{Gi}}{\tau_G}. \quad (10)$$

After adding Eqs. (9) and (10), we get

$$\alpha \left(\frac{dc_{Li}}{dt} \right) + \left(\frac{dc_{Gi}}{dt} \right) = \alpha r_i - \frac{c_{Gi}}{\tau_G}. \quad (11)$$

Mass transfer is assumed to be rapid compared to the kinetic phenomena. Thus the concentrations in gas and liquid bulk

phases are related by the equilibrium ratio (K_i):

$$c_{Li} = \frac{c_{Gi}}{K_i}.$$

This expression for c_{Li} is substituted into Eq. (11) giving the following equation:

$$\frac{dc_{Gi}}{dt} = \frac{\alpha r_i - c_{Gi}/\tau_G}{\alpha/K_i + 1}, \quad (12)$$

where $\alpha = V_{0L}/V_G$ and $c_{Li} = c_{Gi}/K_i$ for all components in the calculation of r_i .

Eq. (12) is valid for gas-phase components.

For non-volatile components in liquid phase, we have

$$\frac{dc_{Li}}{dt} = r_i. \quad (13)$$

The benefit of the simplified mathematical model equations (12) and (13) is that just kinetic and equilibrium parameters are needed, but mass-transfer parameters are discarded.

6. Results and discussion

6.1. Experimental data

The experiments were carried out with a solution containing (wt%): 25% of propionic acid, 15% of PPA, 3% of sulphuric acid, 15% of hydrogen peroxide and water. The graphs obtained from on-line MS analysis show the experimental data (Fig. 3).

CO₂ and O₂ were the main products detected in the gas phase and the amount of carbon dioxide was always higher than the amount of oxygen. Carbon monoxide and ethane were detected, too. Their amounts decreased as the temperature increased.

The graph O₂ versus CO₂ shows that there is a linear relationship between these components. For lower temperatures, the molar ratios were $x_{\text{CO}_2} \approx x_{\text{O}_2}$ but at 45 °C the ratio became $x_{\text{CO}_2} \approx 2x_{\text{O}_2}$. The results indicate that parallel reactions take place and the importances of some reactions depend on the temperature.

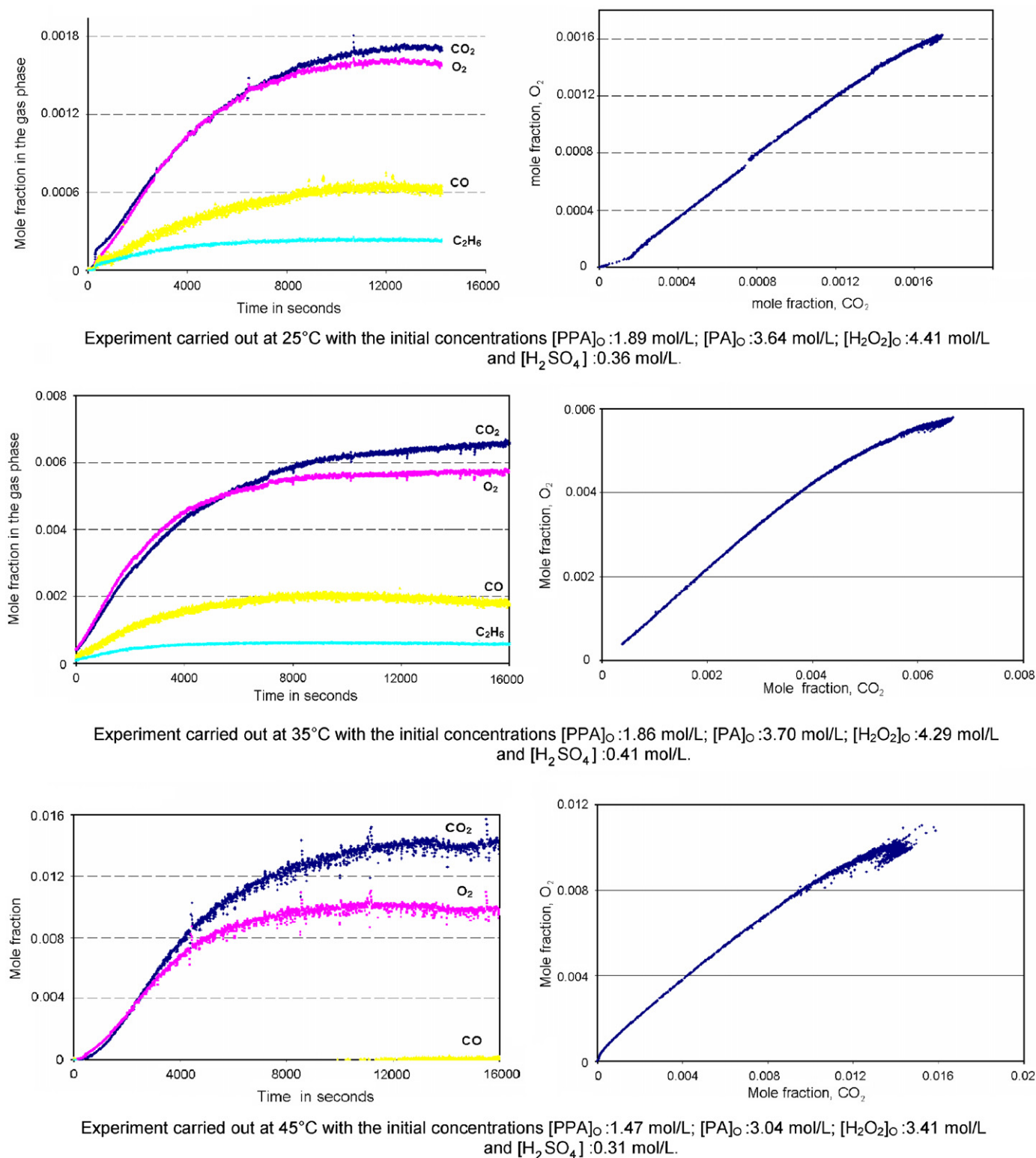


Fig. 3. Decomposition products at different temperatures.

Table 1 shows the concentration evolution for each component during the reactions in the liquid phase.

One can notice that the liquid-phase variations are small. Indeed, the concentrations of propionic acid and hydrogen

peroxide increase slightly during reaction, whereas one can notice that the decomposition of PPA decreases. From Table 1 it can be evaluated that the initial rate of PPA decomposition was about $6 \times 10^{-4} \text{ mol L}^{-1} \text{ min}^{-1}$, indicating a very slow reaction.

Table 2
Kinetic parameters of the model

Parameter	Estimated parameters	Estimated std. error	Est. relative std. error (%)	Parameter/std. error
Rate constant of the reaction (III), k_3 (L mol ⁻¹ s ⁻¹)	$0.172 \cdot 10^{-04}$	$0.766 \cdot 10^{-05}$	44.5	2.2
Activation energy of reaction (III), E_{a3} (J mol ⁻¹)	$0.132 \cdot 10^{+06}$	$0.608 \cdot 10^{+04}$	4.6	21.8
Rate constant of the reaction (IV), k_4 (L mol ⁻¹ s ⁻¹)	$0.177 \cdot 10^{-04}$	$0.796 \cdot 10^{-05}$	44.9	2.2
Activation energy of reaction (IV), E_{a4} (J mol ⁻¹)	$0.150 \cdot 10^{+06}$	$0.518 \cdot 10^{+04}$	3.4	29.0
Rate constant of the reaction (V), k_5 (L mol ⁻¹ s ⁻¹)	$0.677 \cdot 10^{-06}$	$0.348 \cdot 10^{-06}$	51.4	1.9
Activation energy of reaction (V), E_{a5} (J mol ⁻¹)	$0.139 \cdot 10^{+05}$	$0.290 \cdot 10^{+05}$	208.1	0.5
Retarding effect of oxygen, K_{O_2}	$0.179 \cdot 10^{+04}$	$0.960 \cdot 10^{+03}$	53.5	1.9

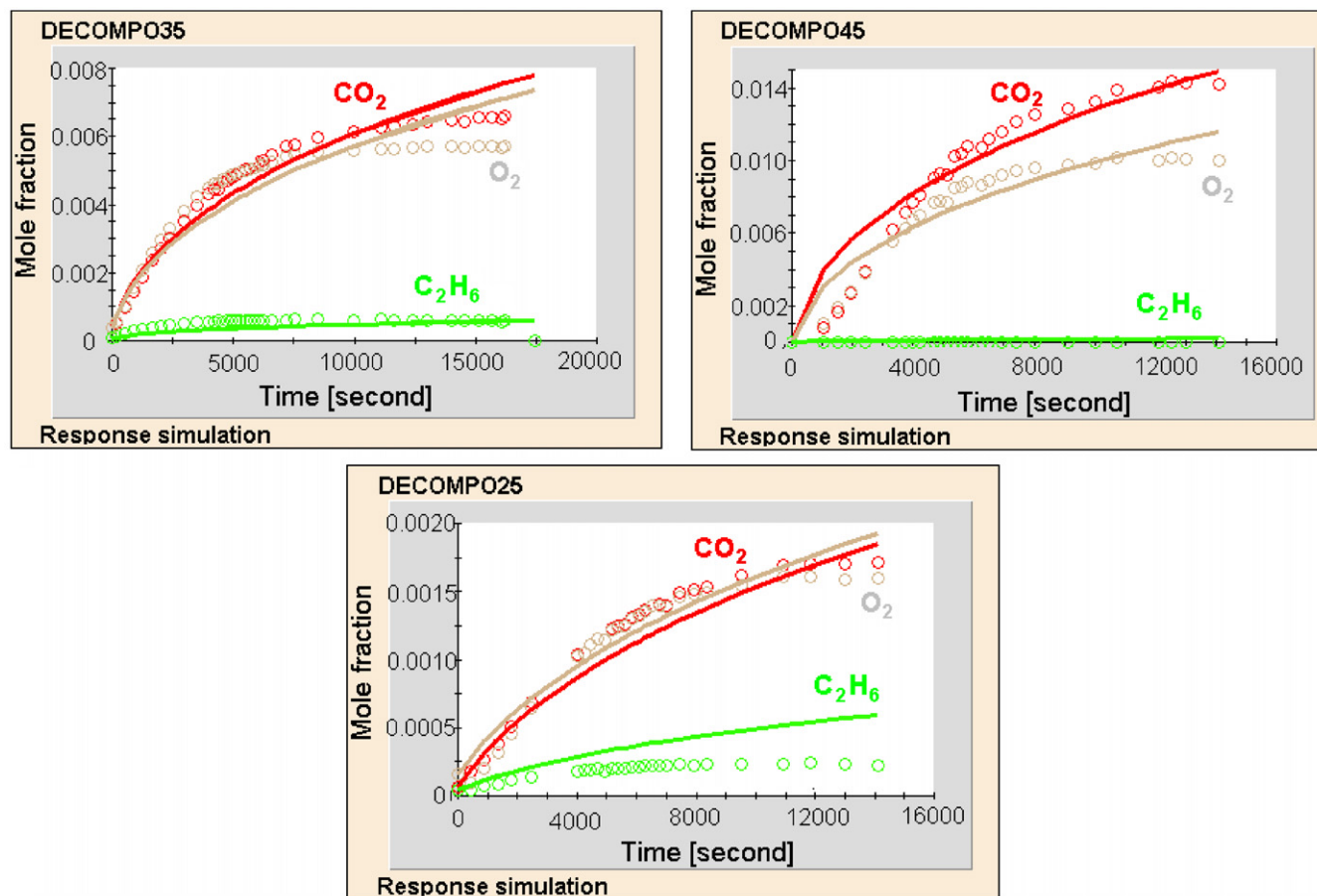
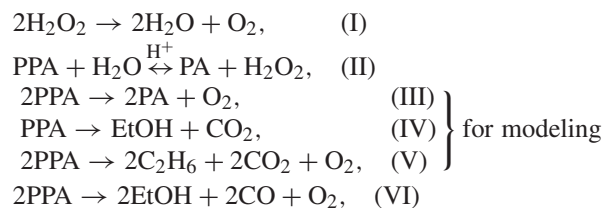


Fig. 4. Fit of the model to the experiments (mole fraction versus time) carried out with 15%PPA solutions at temperatures 25–45 °C.

6.2. Data fitting

Based on our experimental data, the following stoichiometry was assumed in the quantitative treatment of the data:



where PA is propionic acid. Because Eq. (III) is a linear combination of Eqs. (I) and (II), the rate expression for these reactions will be replaced by the rate expression of reaction (III).

The overall reactions do not reflect the intrinsic reaction mechanism, because complicated radical reactions take place. For this reason, an empirical approach is proposed for the rate expression of the reactions, for instance,

$$R_j = \frac{k_j c_{\text{PPA}} c_{\text{cat}}}{1 + K_{\text{O}_2} c_{\text{O}_2}},$$

where j resents the index of the reaction.

According to literature, molecular oxygen acts as a radical scavenger and thus retards the rates of the decomposition. The parameter K_{O_2} takes into account this effect.

The solubility parameters K_i were determined from separate solubility measurements (Ahlgvist et al., 2003). The

temperature dependences of the rate constants are described by a modified Arrhenius equation:

$$k = k_{\text{ref}} \exp \left(-\frac{E_a}{R} \left(\frac{1}{T} - \frac{1}{T_{\text{ref}}} \right) \right),$$

where $k_{\text{ref}} = A e^{-(E_a/RT_{\text{ref}})}$, T_{ref} is the reference temperature, typically the average temperature of the experiments. The goal of this modification is to minimize the correlation between the frequency factor and the activation energy during the parameter estimation.

The parameter estimation was carried out by Modest software (Haario, 1994), by using Simplex and Levenberg–Marquardt algorithms. The ordinary differential equations (12) and (13) were solved repetitively during the parameter estimation by the backward difference method designed for stiff differential equations.

For the modelling, reaction (VI) was ruled out. Only the rate constants (k_3 , k_4 and k_5 including their temperature dependencies) and the parameter K_{O_2} were estimated. The results from the modeling are summarized in Table 2 and some data fitting is shown in Fig. 4.

The coefficient of determination of this model is 99.6%, so the values calculated are statistically reliable. If we look the estimated relative standard error, one can see that except for the activation energy of reaction (V), all of them are low. The kinetic parameters estimated indicate that reactions (III) and (IV) are the most important.

7. Conclusion

The proposed method based on on-line analysis of released gas-phase products by rapid quadrupole mass spectrometry is reliable for studying the kinetics of the decomposition reactions. The method can be applied both for qualitative and quantitative purposes. It is useful as the effect of temperature, concentration, pressure, impurities and stabilizers can be studied on the percarboxylic acid decomposition kinetics. In addition, the method can be used to determine the kinetic parameters quantitatively. A detailed modelling of the reactor system and well-defined flow conditions are required. A more detailed approach to understand the decomposition mechanism of perpropionic acid and the formation of carbon monoxide is required in future.

Notation

a_0 mass transfer-to-volume ratio, $\text{m}^2 \text{m}^{-3}$
 A area of liquid–gas interface, m^2

c concentration, mol L^{-1}
 E_a activation energy, J mol^{-1}
 f_i fragmentation coefficient of a component, i
 I_i intensity of a component i , A
 k rate constant, $\text{L mol}^{-1} \text{s}^{-1}$
 k' calibration coefficient
 k_{Li} mass transfer coefficient for i in the liquid phase, m s^{-1}
 K equilibrium parameter
 K_{O_2} parameter for the retarding effect of oxygen
 n amount of substance, mol
 \dot{n} flow of the amount of substance, mol s^{-1}
 N flux, $\text{mol m}^{-2} \text{s}^{-1}$
 R reaction rate, $\text{mol L}^{-1} \text{s}^{-1}$
 t time, s
 \bar{t} mean residence time, s
 V volume, m^3
 \dot{V} volumetric flow rate, $\text{m}^3 \text{s}^{-1}$
 x mole fraction

Greek letters

α liquid volume-to-gas ratio
 Δ $C_{Li} - C_{Li}^*$, mol L^{-1}
 κ_L $k_{Li} \cdot a_0$, s^{-1}
 τ residence time, s

Subscripts and superscripts

* interfacial (equilibrium) value
 cat catalyst
 cg carrier gas
 i component index

References

- Ahlkvist, J., Salmi, T., Eränen, K., Musakka, N., 2003. Bestämning av syrets och koldioxidens löslighet i organiska vätskor, Laboratoriet för teknisk kemi, Åbo Akademi.
- Greenspan, F.P., MacKellar, D.G., 1948. Analysis of aliphatic per acids. *Analytical Chemistry* 20 (11), 1061–1062.
- Haario, H., 1994. MODEST—User's Guide. Profmath Oy, Helsinki.
- Musakka, N., 2004. Experimental study and mathematical modelling of organic decomposition reactions in liquid phase. Doctoral Thesis, Åbo Akademi.